Edinburgh Wave Power Project

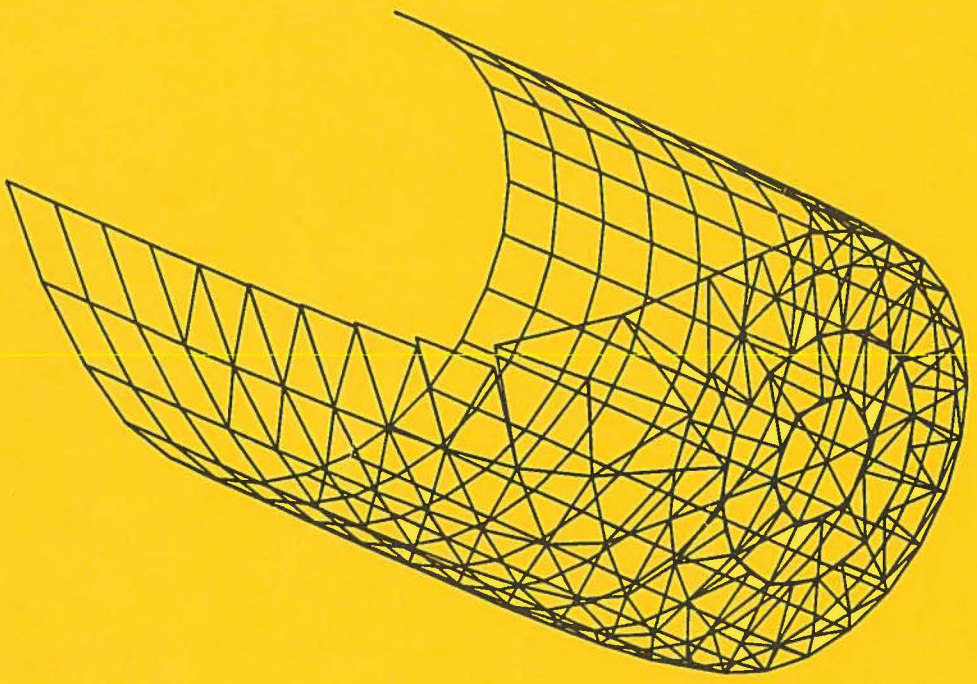

NUMERICAL MODELS

1994

Numerical Modelling of Wave Energy Absorbers

David Pizer

September 1994

The work described in this report was carried out at the University of Edinburgh wave energy project with support from the U.K. Department of Trade and Industry under contract number V/03/00172/00/00 and was co-ordinated by John Robertson at the Energy Technology Support Unit, Harwell.

Summary

This work is a continuation of a previous DTI project on "The Numerical Prediction of the Performance of a Solo Duck". Results of the previous study are extended by computing the reactive powers required to attain the optimal complex control.

Results are also presented for the optimal real control for cases in which power is absorbed in one degree of freedom. This corresponds to a pure damping control force, ie with no reactive power.

The equations for optimal power absorption under an amplitude constraint have been reformulated to permit non-absorbing (ie uncontrolled) degrees of freedom. The effect of releasing a degree of freedom is investigated.

The properties of heaving and surging devices are studied by considering a 20 metre diameter hemisphere. Power absorption through inclined degrees of freedom is also considered. The effect of device geometry is investigated by simple volume-conserving transformations of the hemisphere.

Results are presented for the solo duck considered in the previous project in all possible configurations of a) surge, heave and pitch system, and b) fore, aft and pitch system. Results are also presented for three widths of a rounded solo duck.

Cooperative research with the European Commission JOULE programme is described.

Contents

1 Introduction

Large amounts of power exist in the oceans in the form of wave energy. Many devices have been proposed for converting wave energy into electricity. At present, most of the converters that have been built are shoreline oscillating water-column devices. However, by the time an ocean wave reaches the shoreline, most of its energy has been dissipated during its passage through shallow coastal waters. For the generation of large amounts of power, offshore conversion is desirable.

Theoretical and experimental studies over the last 20 years have identified important principles of offshore conversion. Many of the offshore designs exploit one or more of these principles to enhance power absorption. However, at present no specific design has emerged to be a clear favourite.

Theoretical studies have the limitations of over-simplifying assumptions (such as an idealised geometry), where as experimental studies have the drawback of being expensive and time-consuming. Numerical studies enable a wider range of investigations than purely theoretical studies, in a small fraction of the time it would take to perform experiments.

Of course, it is still important to develop theoretical methods to identify fundamental concepts. Also experimental work will be needed to verify the numerical models, and to produce results beyond their limitations.

An important fundamental concept of three-dimensional power absorption is the *point absorber effect.* It occurs when the width of a device is less than the width of sea which contains the same power as is being absorbed. In other words, a three-dimensional device can absorb power from outside its own width. Most numerical studies to date have been in two-dimensions, which is of little use in investigating the point absorber effect.

The present work is a continuation of the previous DTI research contract: "The Numerical prediction of the performance of a Solo Duck". This is described in the corresponding report, [1], which is reproduced here as appendix B.

1.1 The Previous Project

A linear three-dimensional numerical method was adopted to investigate the performance of a solo duck device. The program models the interaction of a water wave with a floating body of arbitrary geometry. The numerical method was verified by comparison with theoretical results for a hemisphere, and model experiments on a solo duck.

Efficiency calculations were performed for various power take-off configurations. In order to attain the maximum point absorber effect, the excursions of the device became very large. It soon became apparent that an amplitude constraint had to be imposed if the linear assumption was to remain valid.

Even with realistic excursion constraints a significant point absorber effect was predicted: the Solo Duck was able to absorb as much power than is in a wave twice its width.

In head-on waves the difference in productivity between a duck using any two degrees of freedom was found to be only a little below (about 10 %) that achieved by using all three degrees of freedom. This suggests that an optimal design may absorb power in a reduced number of degrees of freedom.

It was found that the solo-duck performed *better* in oblique seas than in head-on seas. This suggests that the performance of the duck may be improved by modifying its geometry.

1.2 The Present Project

The numerical methods have been extended in the current research programme to investigate three dimensional power absorption in more detail.

The feasibility of achieving the sophisticated *complex* control (considered in the previous project) is investigated by calculating the amounts of reactive power required. A less sophisticated *real* control is also formulated. The advantages of the more sophisticated control is assessed.

In the previous project it was assumed that power was absorbed through all the degrees of freedom. In the present study non-absorbing degrees of freedom are also considered.

The theory of wave power absorption is presented in section 3. The latest version of the linear diffraction program has been installed and a geometry-viewing program has been written in order to provide a visual check on geometry discretisations, see section 4.

In section 5 the properties of translating devices are investigated by considering a 20 metre diameter hemisphere. Power absorption calculations are performed for surge and heave configurations as well as for inclined fore and aft configurations. The effect of varying the mass and the amplitude constraint is first studied. The effect of variations in geometry is also investigated by performing simple volume-conserving stretches, squashes and shears.

In section 6 the solo duck considered in the previous project is investigated further. Calculations are performed for all 19 possible power absorption configurations in each of the surge-heave-pitch and the fore-aft-pitch systems. Three widths of a rounded solo duck are considered in section 7.

Cooperation with the European JOULE 2 programme is described in section 8. Other research teams have been provided with numerical data on hydrodynamic coefficients and power absorption for the floats used in the programme.

2 Conclusions

Over 150 power absorption calculations have been performed, covering a variety of geometries, power absorption configurations and control strategies. Such comprehensive studies would be difficult to perform experimentally. The following general conclusions can be drawn.

2.1 General Conclusions

1. Two control strategies are considered: i)complex control, corresponding to applying optimal damping and reactive forces; ii)real control, corresponding to applying optimal damping only.

2. It is important to design the device so that its natural period corresponds to the significant wave period.

   (a) Away from resonance complex control requires large reactive forces. This implies that large amounts of power are being put into and taken out of the motion of the float, compared with the relatively small time-averaged power absorbed. In these cases large losses will result in the power exchange mechanisms and the predicted power absorption levels will be unattainable.

   Away from resonance real control results in small device motions, and power absorption levels are low.

   (b) Near resonance the optimal complex control is achieved with acceptable reactive forces. Complex control absorbs roughly twice as much power as real control and the point absorber effect becomes important.

   (c) At resonance the complex control real control are equivalent since the complex control does not require a reactive force to produce the desired motion. The calculations generally predict very good power absorption, corresponding to a large point absorber effect.

3. Inclined degrees of freedom are often advantageous.

   (a) The angle of inclination may be chosen to tune the natural period of the device to the wave period.

   (b) The asymmetric radiation pattern associated with an inclined motion enables higher efficiencies in seas with directionality.

4. It was thought that an uncontrolled degree of freedom would result in less power being absorbed than if it were fixed. However, in the present study many cases exhibit sufficient coupling between controlled and uncontrolled degrees of freedom. This allows significant absorption via the released degree of freedom. In these cases releasing a degree of freedom results in *more* power being absorbed.

2.2 Specific Conclusions

1. The properties of translating devices are investigated by considering a half-buoyant 20 metre diameter hemisphere with an excursion constraint of 5 metres. The conclusions for heaving and/or surging systems are:

   (a) Relative capture widths significantly greater than one are attainable with complex control in surge and/or heave, although large reactive powers are required.

   (b) Real control produces only small amounts of power.

   (c) Complex control with a reduced excursion constraint produces significantly more power than real control, and with an acceptable reactive power requirement.

   (d) For complex control in surge a theoretically massless hemisphere requires less reactive power than the half-buoyant case. In heave a neutrally buoyant hemisphere requires less reactive power. For complex control in two degrees of freedom, a device is proposed which is effectively massless in surge and neutrally buoyant in heave.

   Power absorption in inclined degrees of freedom is also considered. The main conclusions are:

   (a) For a single inclined degree of freedom the natural period can be chosen to be within the wave periods of interest. At resonance the optimal complex control is achieved with zero reactive power (ie its equivalent to real control).

   (b) In the region of the natural period large amounts of power are absorbed with either real or complex control. Complex control is achieved with acceptable levels of reactive powers, producing twice as much power as real control in many cases.

   (c) The best single degree of freedom is an elevation of 30 degrees from the horizontal in the direction of wave propagation (60 degree fore case). At short periods this single degree of freedom produces as much power as the optimal two degree of freedom case.

   (d) Results are presented for absorption in one inclined degree of freedom, with the perpendicular degree of freedom released (ie uncontrolled). Releasing a degree of freedom need not necessarily decrease the power absorbed. In some cases resonance is induced in the released degree of freedom resulting in large excursions. Coupling with the controlled degree of freedom is sufficient to absorb large amounts of power from the released degrees of freedom.

   The effect of variations in geometry is investigated by considering simple volume-conserving transformations (stretches and shears) of the hemisphere.

   (a) For degrees of freedom with a vertical component (ie not surge), increasing the water-plane area increases power absorption.

   (b) For all degrees of freedom, increasing the width while conserving the volume generally increases power absorption.

(c) At low periods the positive shear gives reduced power absorption in surge and aft degrees of freedom, but increased power for heave and fore degrees of freedom. The negative shear does not affect power absorption in surge and heave, gives more power for aft cases and less power for fore cases.

(d) Combining the best stretch with the best shear gives a geometry which performs better than both the best stretched case and the best sheared case.

2. The solo duck studied in the previous research project in investigated further. Results are presented for all 19 power absorption configurations of the surge-heave-pitch system. The main conclusions are

   (a) Power absorption in a single degree of freedom can attain relative capture widths up to 1.3 with acceptable levels of reactive power. Releasing heave or pitch increases power absorption in surge. For power absorption in heave or pitch, releasing a degree of freedom reduces power absorption.

   (b) Power absorption in 2 degrees of freedom gives relative capture widths of up to 1.7 with with acceptable levels of reactive power. Releasing the third degree of freedom results in a loss of power. This loss is fairly small for pitch and heave released, but quiet large with surge released.

   (c) Power absorption in all three degrees of freedom provides at least as much power as any other configuration. In the region of 7 seconds the three degrees of freedom case produces the same amount of power as each of the two degree of freedom cases. This is due to the singularity in the damping matrix, as discussed in [1].

   19 power absorption configurations are also investigated for the 45 degree inclined system (fore-aft-pitch).

   (a) Fore is the best single degree of freedom case, giving a relative capture width of 1.5 .

   (b) Releasing a fore or aft degree of freedom results in large motions in the released degree of freedom. Surprisingly the released motions increases the power absorbed. Pitch has smaller motions when released and results in small power losses for absorption in fore, but larger losses for aft.

   (c) Power absorption in 2 degrees of freedom gives relative capture widths of up to 1.8 with with acceptable levels of reactive power. Releasing the third degree of freedom need not necessarily result in a loss of power. With fore or aft released large motions can increase power absorption.

3. Solo ducks 19m, 29m and 49m wide are studied with complex control in all three degrees of freedom. It is found that a wider duck gives at least as much power as a shorter duck. It is interesting to note that there are regions in which ducks of different widths give the same power. It is thought that this is due to the singularities in the damping matrices at around 8s.

2.3 Recommendations for Further Study

1. Due to the large number of variables in the design of a wave power device, only a very limited optimisation of geometry has been possible in the present study. An automated optimisation procedure should be implemented for the geometry and the power absorption configurations in order to find optimal designs.

2. The software should be extended to study multi-body devices, such as the hose-pump and the IPS buoy.

3. The prediction of the performance of an array of devices requires knowledge of hydrodynamic interaction between devices. The optimal spacings and geometries should be investigated.

4. Statistical predictions using realistic sea spectra are required in order to obtain accurate estimates of power output.

5. Experimental studies should be performed to investigate the non-linear effects at various wave amplitudes.

3 Theory of 3-D Power Absorption

The theoretical fundamentals of wave power absorption appeared in 1976 with independent publications by Evans [4] , Mei [5] and Newman [6]. These works consider simple cases of axi-symmetric bodies and small bodies in the context of linear wave theory to derive important principles of power absorption. A review of the key 3-D results is given in [1]. A brief reminder of the essential facts follows.

3.1 Linear Wave Diffraction Theory

It is assumed that the fluid flow is irrotational, incompressible, inviscid and undergoes only small displacements from its static equilibrium position. Equating quantities which are linearly dependent on the wave amplitude gives a linear theory which has proven highly successful in predicting the motions of ships and offshore structures, even in relatively severe environments.

A detailed description of the linear (and second-order) formulation for the interaction of a water-wave with a floating body is presented in [9]. A less detailed account is presented in [8]. The final linear expressions for the excitation forces and moments and the equations of motion are given here in Appendix A.

It is assumed throughout this study that all time-dependence is harmonic with circular frequency ω. The time-dependence of a quantity $V(t)$ is then removed by the introduction of the complex variable U:

$$V(t) = Re\{Ue^{-i\omega t}\}$$

Here we consider n degrees of freedom where $1 \leq n \leq 6$. The relevant equations of motion in Appendix A may then be expressed as a single complex $n \times n$ matrix equation:

$$\mathbf{F}_C = \mathbf{ZU} - a\mathbf{X} \tag{1}$$

where $\mathbf{F}_C$ is a complex n-vector denoting the control forces and moments, $\mathbf{X}$ denotes the the excitation forces and moments for a wave of unit amplitude, a is the wave amplitude, $\mathbf{U}$ is the body velocity vector and $\mathbf{Z}$ is the impedance matrix which contains terms due to mass, added mass, damping, hydrostatic restoring terms, and gravity restoring terms.

3.2 Power Absorption

The power extracted from the body is the scalar product of the control force with the device velocity:

$$P(t) = -\mathbf{U}(t) \cdot \mathbf{F}_C(t) = -\sum_{k=1}^{n} U_k(t) F_{Ck}(t) \tag{2}$$

In complex form this is written as:

$$P(t) = -\tfrac{1}{2}\sum_{k=1}^{n} Re\{F_{Ck}U_k e^{-2i\omega t} + F_{Ck}U_k^*\} \tag{3}$$

where * denotes the complex conjugate.

It is seen that the instantaneous power through each degree of freedom may be expressed as a steady component and a double frequency component.

The complex power, P_k, is defined as:

$$P_k = -\tfrac{1}{2}F_{Ck}U_k^* \tag{4}$$

The real power, $Re\{P_k\}$, is the time averaged power absorbed; and the hypotenuse power, $|P_k|$, is the amplitude of the double frequency component.

The total power absorbed is then given by:

$$P = \sum_{k=1}^{n} Re\{P_k\} \tag{5}$$

3.2.1 Imaginary Power

The double frequency component makes no contribution to the time averaged power absorbed. It represents the power being put into and taken out of the body through a particular degree of freedom over a cycle. If this is large compared to the time average power, a small inefficiency in the power exchange mechanism will result in a loss of a large fraction of the useful power absorbed. Since $|P_k|^2 = Re\{P_k\}^2 + Im\{P_k\}^2$, the relative size of the imaginary power is a measure of how inefficiencies in each degree of freedom will be amplified.

3.2.2 Hypotenuse Power Ratio

The hypotenuse power ratio (HPR) is defined as:

$$\frac{1}{P}\sum_{k=1}^{n} |P_k| \tag{6}$$

and is a non-dimensional measure of how inefficiencies in the power exchange mechanism are amplified due to large imaginary powers. Clearly HPR ≥ 1, and HPR $= 1$ only if $Im\{P_k\} = 0$ for all k=1,..,n .

It is thought that an efficient single degree of freedom power exchange system will be capable of operating at HPRs up to about two. For larger values it is expected that time average power losses become large.

Multi-degree of freedom power exchange systems are more difficult to asses since power may also be exchanged from one degree of freedom to another. In such cases the HPR, as defined above, is a very crude measure of how efficiencies may be amplified.

3.2.3 Relative Capture Width

The capture width, l, of a device is defined as the width of sea which contains the same power as is being absorbed by the device.

$$l = \frac{P}{P_w} \tag{7}$$

The efficiency of a 3-D device is expressed in terms of its relative capture width η. This is defined as the capture width divided by the device width, W:

$$\eta = \frac{l}{W} \tag{8}$$

Hence, a relative capture width greater than 1 means that the device is absorbing more power than is in the width of sea it occupies. In theory values as high as 20 or more can apparently be achieved by small devices in long waves, but only with such large amplitudes of motion that linear assumptions will be hopelessly invalid. Practical relative capture widths of 2 to 3 are more realistic.

3.3 Control Strategies

It is important to apply a suitable control force in order to maximise power absorption and ensure that the excursions of the body do not exceed engineering constrains and/or the limitations of the linear theory.

In the previous study the optimal control force was computed for a multi degree of freedom system with a global motion constraint. However this optimal control often required large imaginary powers and consequently large losses would result in the power exchange systems. We therefore also consider the optimal real control, for which the imaginary powers are zero.

3.3.1 Control Matrix

It is assumed that the control force vector is proportional to the velocity vector:

$$\mathbf{F}_C = -\mathbf{C}\mathbf{U} \tag{9}$$

where $\mathbf{C}$ is the complex control matrix. The real part of $\mathbf{C}$ represents the damping behaviour of the control force, and the imaginary part represents its spring behaviour.

Then from equation (2) the complex power is

$$P = \frac{1}{2}\mathbf{U}^*\mathbf{C}^*\mathbf{U} \tag{10}$$

Hence the time average power absorbed is

$$P = \frac{1}{4}\mathbf{U}^*(\mathbf{C} + \mathbf{C}^*)\mathbf{U} \tag{11}$$

3.3.2 Real Control in One Degree of Freedom

The case $n = 1$ and C real is described in [7]. This corresponds to the control force being pure damping only and is the sub-optimal control to ensure zero imaginary powers away from resonance. Equation (1) may be used to express the power in the form:

$$P = \frac{a^2|X|^2}{4(B + |Z|)}\left(1 - \frac{(C - |Z|)^2}{|C + Z|^2}\right) \tag{12}$$

showing that

$$P_{max} = \frac{a^2|X|^2}{4(B + |Z|)} \tag{13}$$

when

$$C = |Z| \tag{14}$$

Then

$$U = U_o \equiv \frac{aX}{(|Z| + Z)} \tag{15}$$

The control may require modification to ensure that the excursions of the body do not exceed a specified constraint. Let γ be the maximum velocity permitted. If $|U_o| \leq \gamma$ then $U = U_o$ gives the maximum power. However, if $|U_o| > \gamma$ the control (damping) must be increased until $|U| = \gamma$. This is achieved when:

$$C = -B + A\sqrt{1/\nu^2 - 1} \tag{16}$$

where $Z = B + iA$, and $\nu = \frac{\gamma A}{a|X|}$ and is the ratio of the mass, added mass and spring forces, with the wave excitation force.

Using equation (15) this may be written in the form:

$$C = -B + \sqrt{||Z| + Z|^2(\frac{|U_o|^2}{\gamma^2} - 1) + (|Z| + B)^2} \tag{17}$$

from which it is clear that C is continuous at $|U_o| = \gamma$.

Thus, when $|U_o| > \gamma$ the optimal velocity satisfying the constraint is given by:

$$U = \frac{\gamma X}{|X|}[\sqrt{1 - \nu^2} - i\nu] \tag{18}$$

3.3.3 Complex Control in One Degree of Freedom

The case $n = 1$ and C complex is also described in [7]. Equation (1) may be used to express the power in the form:

$$P = \frac{a^2|X|^2}{8B}\left(1 - \frac{|C - Z^*|^2}{|C + Z|^2}\right) \tag{19}$$

showing that:

$$P_{max} = \frac{a^2|X|^2}{8B} \tag{20}$$

when

$$C = Z^* \tag{21}$$

Note that when Z is real (ie, at resonance) C is also real and P_{max} is in agreement with equation (13).

The optimal complex control with a constraint on the excursions is attained by increasing the real part of the control (ie increasing the damping), see the multi-degree of freedom case below.

3.3.4 Complex Control in Two or More Degrees of Freedom

The optimal control for a multi-degree of freedom system, subject to a *weighted global* motion constraint, was evaluated in the previous study. The detailed formulation is given in [2] and [3].

It is assumed that the constraint imposed on $\mathbf{U}$ is of the form:

$$\mathbf{U}^*\mathbf{\Gamma}^{-2}\mathbf{U} \leq 1 \qquad \text{i.e.} \qquad \sum_{k=1}^{n} \frac{|U_k|^2}{{\gamma_k}^2} \leq 1 \tag{22}$$

where $\mathbf{\Gamma}$ is a diagonal matrix with elements γ_k. This constraint confines the system to an ellipsoid in the complex n-dimensional $\mathbf{U}$-space. This is equivalent to Evans' *global* constraint if all the γ_k have the same value and are proportional to a.

Note that for many devices a more realistic engineering constraint would be of the form $|U_k| \leq \gamma_k$. For $n > 1$ this is a weaker condition than (22) and would therefore give larger efficiencies, especially for large n. However $|U_k| \leq \gamma_k$ is more difficult to implement since it requires numerical optimisation techniques . The *weighted global* constraint is probably more appropriate as a linearity constraint.

Equation (1) may be used to express the power in the form:

$$P = \frac{a}{4}(\mathbf{X}^*\mathbf{U} + \mathbf{U}^*\mathbf{X}) - \frac{1}{2}\mathbf{U}^*\mathbf{B}\mathbf{U} \tag{23}$$

Provided $\mathbf{B}^{-1}$ exists this may be re-arranged to give:

$$P = \frac{a^2}{8}\mathbf{X}^*\mathbf{B}^{-1}\mathbf{X} - \frac{1}{2}\left(\mathbf{U} - \frac{a}{2}\mathbf{B}^{-1}\mathbf{X}\right)^* \mathbf{B}\left(\mathbf{U} - \frac{a}{2}\mathbf{B}^{-1}\mathbf{X}\right). \tag{24}$$

Noting that $\mathbf{B}$ is positive definite, it is clear that without a motion constraint, the maximum power absorbed , P_o, is given by the first term in (24) when:

$$\mathbf{U} = \mathbf{U}_o \equiv \frac{a}{2}\mathbf{B}^{-1}\mathbf{X} \tag{25}$$

Then from the definition of the control matrix we obtain the optimal complex control:

$$\mathbf{C} = \mathbf{Z}^* \tag{26}$$

If $\mathbf{U}_o^*\boldsymbol{\Gamma}^{-2}\mathbf{U}_o \leq 1$ then $\mathbf{U} = \mathbf{U}_o$ gives the maximum power. If $\mathbf{U}_o^*\boldsymbol{\Gamma}^{-2}\mathbf{U}_o > 1$, then the power should be maximised subject to $\mathbf{U}^*\boldsymbol{\Gamma}^{-2}\mathbf{U} = 1$. This is achieved by introducing a Lagrange multiplier, μ. Following the approach of Evans [2] the optimal velocity is given by:

$$\mathbf{U} = \frac{a}{2}(\mathbf{B} + \mu\boldsymbol{\Gamma}^{-2})^{-1}\mathbf{X} \tag{27}$$

where μ is determined from the scalar equation,

$$\mathbf{X}^*\boldsymbol{\Gamma}(\boldsymbol{\Gamma}\mathbf{B}\boldsymbol{\Gamma} + \mu\mathbf{I})^{-2}\boldsymbol{\Gamma}\mathbf{X} = \frac{4}{a^2} \tag{28}$$

Substitution back into equation (1) gives the optimal complex control matrix:

$$\mathbf{C} = \mathbf{Z}^* + 2\mu\boldsymbol{\Gamma}^{-2} \tag{29}$$

Hence in order to satisfy the motion constraint, the damping effect of the control force must be increased.

3.4 Released Degrees of Freedom

In the previous formulation [1] it was assumed that power could be absorbed through all the prescribed degrees of freedom. In the present study the formulation has been generalised to permit non-absorbing (ie, released) degrees of freedom. The device is uncontrolled in these degrees of freedom and responds as if it were freely floating (apart from the effects of any coupling with the controlled degrees of freedom). Power is absorbed only through the controlled degrees of freedom.

In the previous study it was shown that in head-on seas a duck moving in two degrees of freedom could absorb almost as much power as the three degree of freedom case. This suggests that a cost-effective device will absorb power in an optimal number of degrees of freedom. However, fixing the device in any direction will result in large forces in severe wave conditions. We therefore investigate uncontrolled degrees of freedom and their effect on the performance of a device.

The formulation for optimal power absorption with a motion constraint is given in appendix A. The global motion constraint applies only to the controlled degrees of freedom. Large motions in the un-controlled degrees of freedom may therefore invalidate the linearity assumption.

For power absorption with optimal control over all the degrees of freedom, the device is tuned into a resonant motion, ie the applied mass and spring cancels with the real mass and spring of the system. Consequently the resulting motion and efficiency are independent of the restoring force and mass distribution of the device. For devices with un-controlled degrees of freedom, resonance is not induced in the released modes, and hence optimal motions and efficiencies are dependent on the restoring force and mass distribution.

First the equations of motion (1) are re-ordered so that the first m equations correspond to controlled degrees of freedom, and the remaining $m - n$ degrees of freedom are uncontrolled.

The equations of motion then become:

$$\begin{bmatrix} \mathbf{F}_c \\ 0 \end{bmatrix} = \begin{bmatrix} \mathbf{Z}_{cc} & \mathbf{Z}_{cf} \\ \mathbf{Z}_{fc} & \mathbf{Z}_{ff} \end{bmatrix} \begin{bmatrix} \mathbf{U}_c \\ \mathbf{U}_f \end{bmatrix} - a \begin{bmatrix} \mathbf{X}_c \\ \mathbf{X}_f \end{bmatrix} \tag{30}$$

Where c and f denote the controlled and uncontrolled partitions of vectors and matrices in the obvious manner.

The uncontrolled rows of (30) gives:

$$\mathbf{U}_f = \mathbf{Z}_{ff}^{-1}(a\mathbf{X}_f - \mathbf{Z}_{fc}\mathbf{U}_c) \tag{31}$$

which is then substituted into the controlled rows of (30) to give:

$$\mathbf{F}_c = \mathbf{Z}_{cc}^m \mathbf{U}_c - a\mathbf{X}_c^m \tag{32}$$

where the modified impedance is defined as $\mathbf{Z}_{cc}^m = \mathbf{Z}_{cc} - \mathbf{Z}_{cf}\mathbf{Z}_{ff}^{-1}\mathbf{Z}_{fc}$ and the modified excitation is defined as $\mathbf{X}_c^m = \mathbf{X}_c - \mathbf{Z}_{cf}\mathbf{Z}_{ff}^{-1}\mathbf{X}_f$

Equation (32) is now in the same form as equation (1). The optimal velocities, $\mathbf{U}_c$ may therefore be obtained using similar methods to the case of all degrees of freedom being controlled.

It is helpful to define a concise notation to refer to the power absorption configuration. For head waves incident on bodies with transverse symmetry at most three degrees of freedom are relevant: two orthogonal translations (eg heave and surge) and pitch. A precise power absorption configuration can be concisely denoted with five characters. The power absorbing degrees of freedom are specified with single letters, then an underscore, followed by the free degrees of freedom. For example:

- sh_p_ for controlled heave and surge with pitch released

- h_sp absorption in heave only, surge and pitch fixed
- h_p_s absorption in heave, with pitch uncontrolled and surge fixed

4 Numerical Solution

Power absorption calculations require accurate knowledge of the hydrodynamic coefficients. These are evaluated using a 3-D linear wave diffraction program, DPWAVE.

The latest version of DPWAVE was installed on a Sun SPARCcenter 2000. In this version the geometry is generated by a separate program. The discretised data may then be checked and modified before proceeding with the linear hydrodynamic calculations.

The new version of DPWAVE also contains routines for evaluating second-order hydrodynamic quantities such as steady and slowly varying drift forces. These low-frequency effects are relevant to devices with degrees of freedom with little or no restoring. Second-order yaw moments may have the beneficial effect of orientating a device to face the prominent wave direction. Second-order theory may eventually be used to predict non-linear power absorption. However, for the time being there is still much to be gained from linear theory alone.

The new installation has been checked by comparison with wet model tests, analytical results and by reproducing wave power calculations performed during the previous research programme.

4.1 Description of Method

The solution is based on the Green's function for a pulsating point wave source. The Green's function may be thought of as the most fundamental solution of the water wave problem. It satisfies all the necessary mathematical conditions in the absence of any bodies.

If there is a body in the fluid there is an extra mathematical condition that must be satisfied on the body surface. This states that the normal velocity of the fluid must match the normal velocity of the body, i.e. no fluid must flow through the body.

In the source distribution method wave sources are distributed over the surface of the body. The density of this distribution is evaluated by imposing the mathematical condition on the body surface. By the principal of superposition all the other conditions are automatically satisfied and the fluid motion is known.

The fluid force on the body is then found by direct integration over the body of the Bernoulli pressure.

- The excitation force is obtained by considering the scattering problem, i.e. that of a fixed body in the presence of waves.
- the added mass and damping matrices are found by considering the radiation problem for each degree of freedom, i.e. that of a moving body in otherwise still water.

4.2 Geometry Discretisation

The first step in the numerical evaluation of the hydrodynamic coefficients is to describe the equilibrium wetted surface of the device in terms of rectangular and triangular facets. Adjacent facets should be roughly the same size and ideally should be roughly square or equilateral. Smaller facets should be used at corners in order to resolve the spatial variation of the flow. The program also requires the orientation of the outward normal of each facet.

During the previous research contract subroutines were written to generate solo-duck type geometries and facet discretisations. In the current study we wish to examine a variety of geometries. It is not feasible to come up with a totally automated algorithm for producing discretisations. A viewing method has therefore been developed using UNIRAS subroutines to assist the generation of discretisations.

Three options exist for viewing the facet model: a wire-frame view; illuminated shading view and a normal shading view. The model may be viewed from any angle and magnification. Examples are shown in figures 1, 2 and 3 for the 720 facet model of the duck considered in the previous study. (The program exploits planes of symmetry to speed up the calculation and so only half of the wetted surface is defined)

The illuminated shading gives an overall perspective of the geometry. In the normal shading option, the inside surface of the facet is shaded in a different tone to the outside. This gives a visual check that the outward normal of each facet has been correctly defined.

Some gaps are seen in the 720 facet model used in the previous study [1], see figure 4. The largest of these have been closed up for the present calculations of the hydrodynamic coefficients, see figures 5 and 6. It has been shown that these gaps had very little effect on the results.

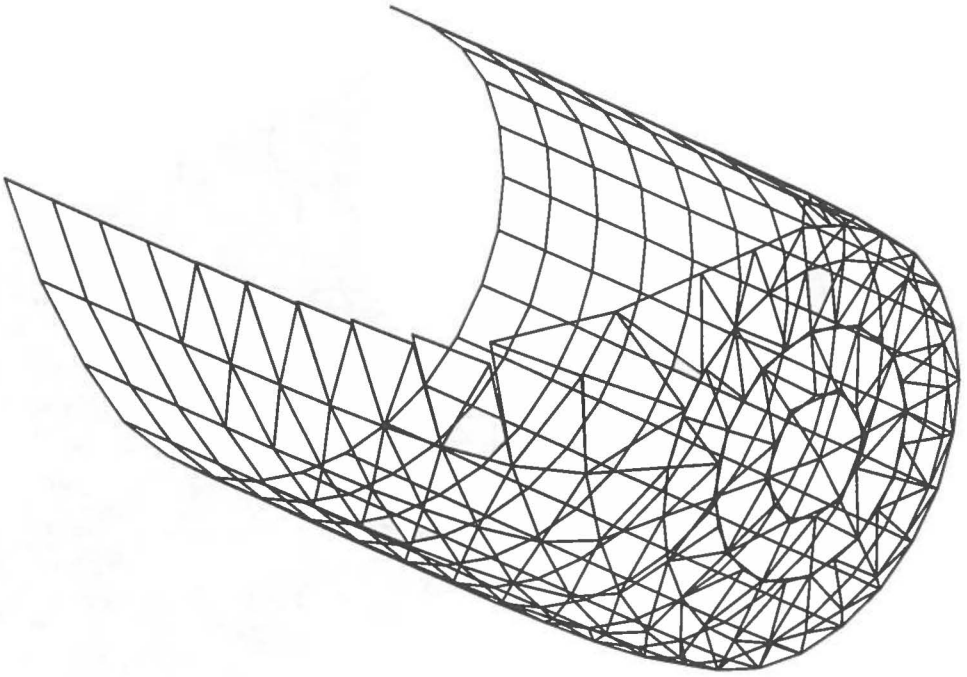

Figure 1: Wire-frame view of 720 facet solo duck discretisation

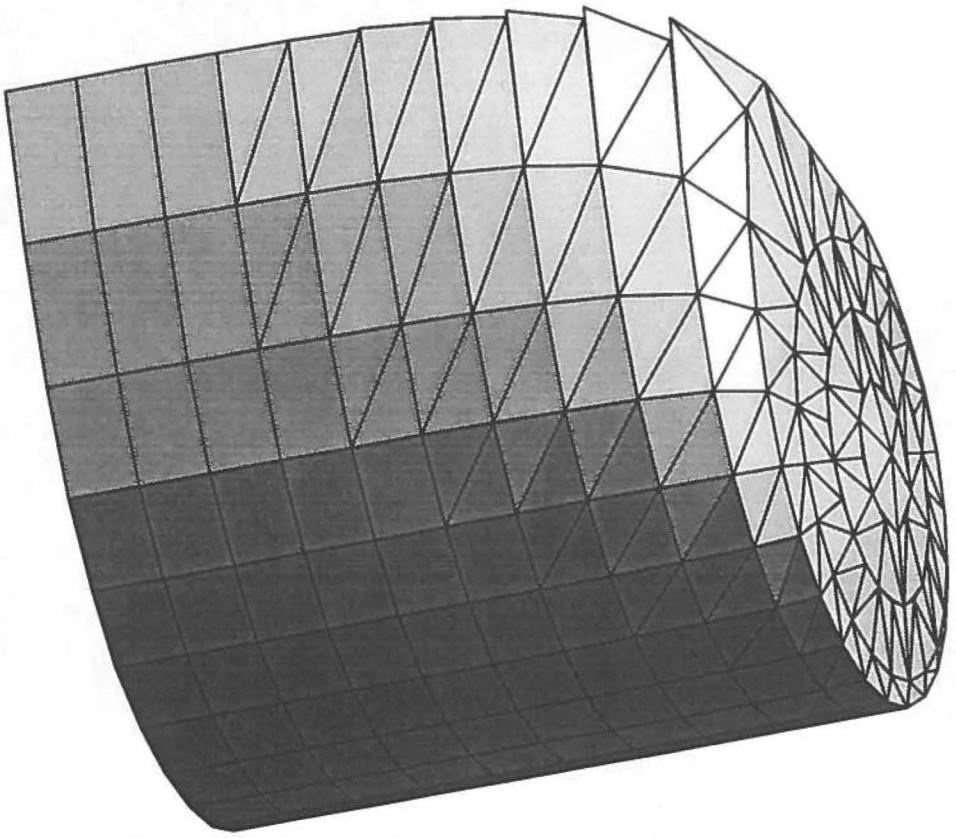

Figure 2: Illuminated view of 720 facet solo duck discretisation

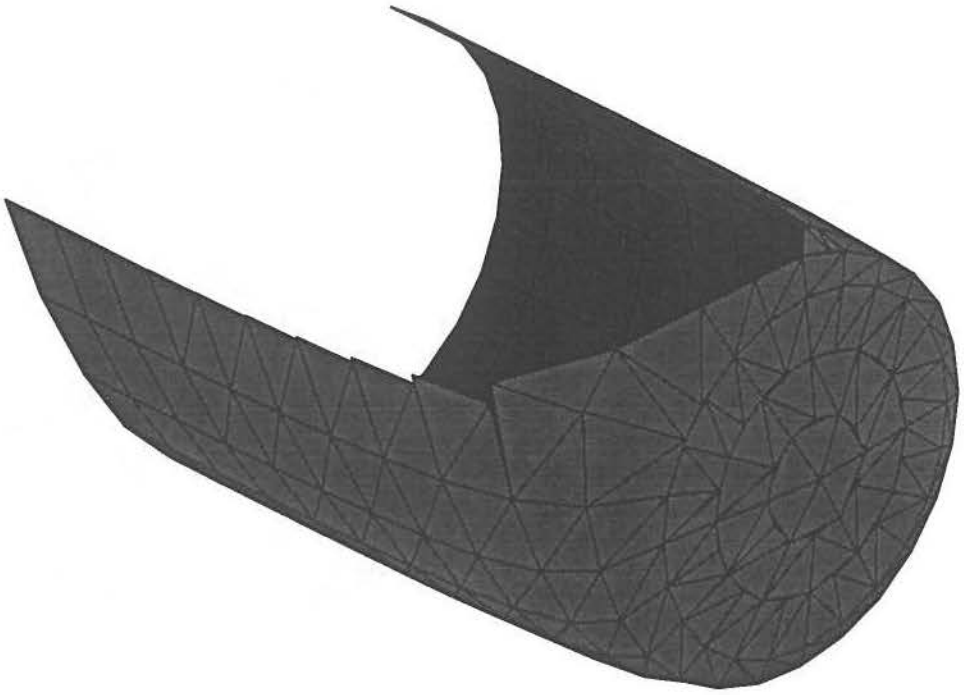

Figure 3: Normal-shading view of 720 facet solo duck discretisation

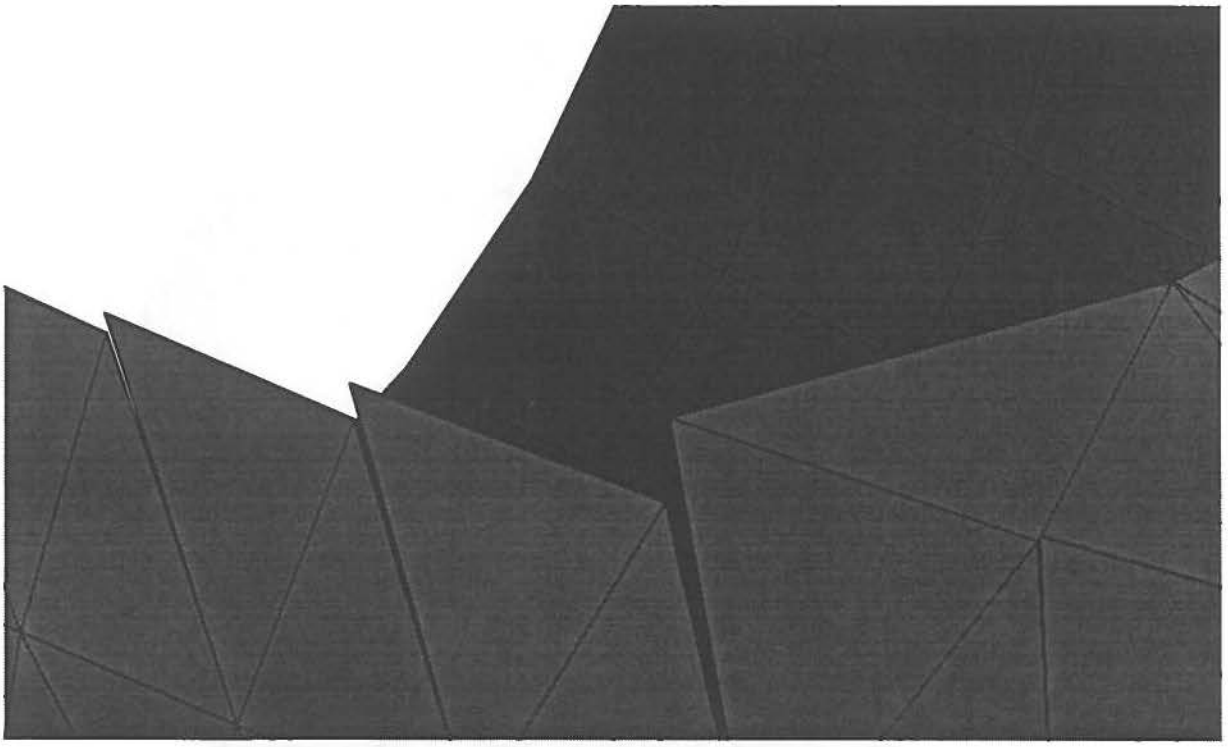

Figure 4: Close-up of 720 facet solo duck discretisation

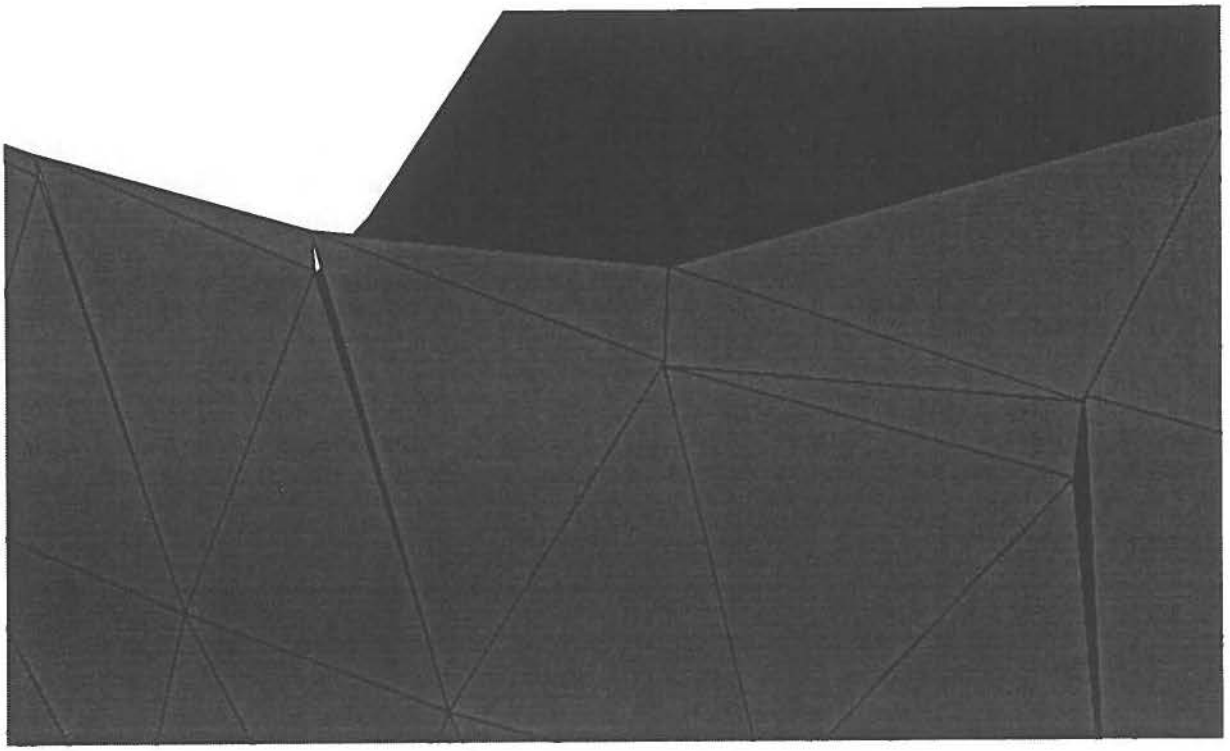

Figure 5: Close-up of modified 720 facet solo duck discretisation

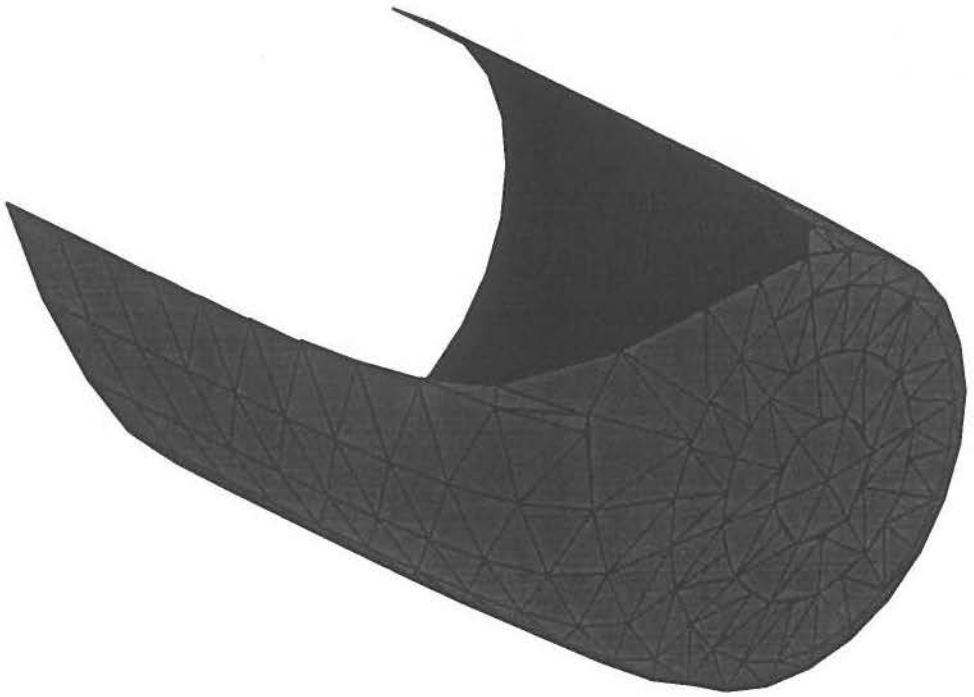

Figure 6: Modified 720 facet solo duck discretisation

5 Translational Devices

Over the last twenty years many designs of wave power devices have been proposed. Apart from fundamental theoretical studies, research has tended to be device orientated: eg performing wave tank experiments to investigate varying a limited set of parameters to optimise a particular design.

The numerical methods employed here, and in the previous solo duck study, enable many investigations in a small fraction of the time it would take to perform tank tests. It is now feasible to undertake a generic study to identify important general principles of wave power absorption without the limitations of having a specific device in mind.

The design parameters considered in this study are: the power absorption configuration, device geometry, volume displacement, mass, mass distribution, and excursion constraints. The performance of the device is quantified in terms of: the control forces required; the relative capture width; power absorbed, imaginary powers required, and the hypotenuse power ratio.

A systematic exhaustive parametric study would produce many volumes of graphs which would be difficult to analyse. We therefore choose combinations of parameters to explore regions of the parametric-space which seem to be of interest as the results emerge.

Purely translational devices are considered since their performance is independent of the mass distribution and choice of the reference point (ie the point at which the control forces are applied).

The study is concerned with symmetric bodies in head on waves, hence at most three degrees of freedom are considered: two orthogonal translations (eg heave and surge) and pitch.

Results are presented for surface-piercing ellipsoids with the same underwater volume as a 10 m radius hemisphere. Results for other size bodies may be inferred using Froude scaling. Results are plotted against wave period, from 5 seconds to 20 seconds in a water depth of 50 metres for wave amplitudes of 0.35m, 0.50m 0.71m 1.00m and 1.41m:

5.1 Half-Buoyant Hemisphere

The case of a metre radius hemisphere absorbing power with the optimal complex control was considered in the previous study [1]. It was shown that relative capture widths of up to two could be obtained for a heave or surge motion with an amplitude constraint of 0.25m. Heave attained the maximum efficiency at longer periods than surge. With both heave and surge absorbing power under the optimal complex control, relative capture widths of up to three were obtained with broader band widths than the single degree of freedom cases.

Here we first consider a 10 metre radius hemisphere absorbing power with the optimal real or complex control of heave and/or surge motion(s). The weight of the hemisphere is chosen to be half the buoyancy force.

5.1.1 Controlled in Heave

Results for the heave only power absorption configuration, h_sp, with the optimal complex control are shown in figure 7.

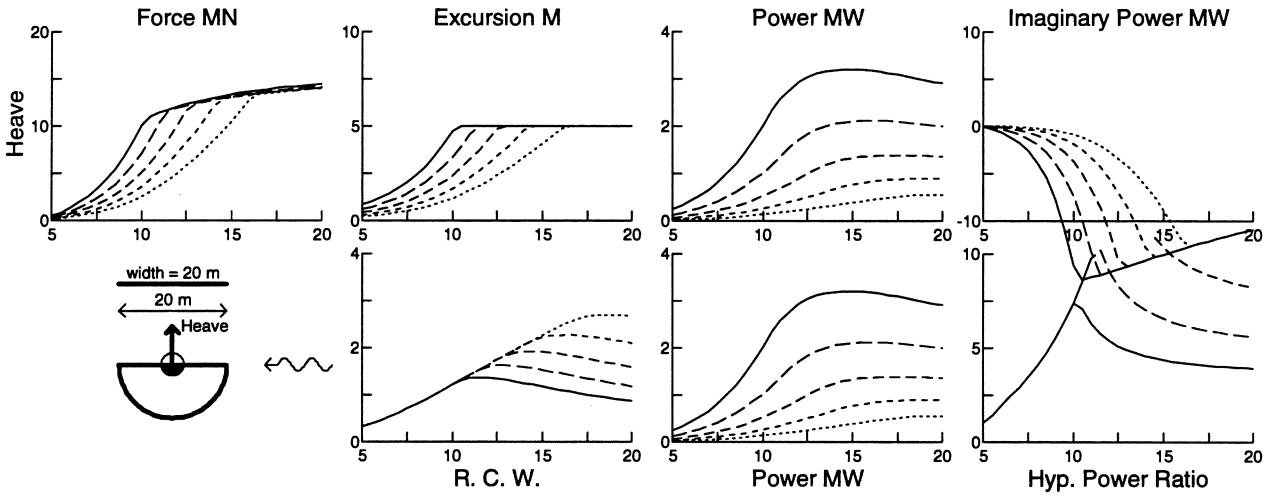

Figure 7: Complex control in heave (h_sp) for a 10m radius hemisphere .

For a wave amplitude of 1.41 metres, and periods below 10 seconds, the optimal complex control is achieved without reaching the 5 m excursion constraint. For 0.35 m wave amplitude the constraint is reached for all wave periods over 16 seconds. For the cases in which optimal complex control is achieved within the constraint the relative capture width attains the heaving axi-symmetric point absorber value of $\lambda/2\pi$. When the constraint is imposed the relative capture width falls away from the point absorber limit. The maximum power absorbed is about 3.2 MW for a 1.41 metre, 15 seconds wave. Power absorption levels remain high for longer waves but reduce rapidly for wave periods below 10 seconds.

As was noted in the previous study, relative capture widths are significantly greater than

one at most wave periods. However, it is seen in the present study that the imaginary powers are relatively large, giving hypotenuse power ratios of over 5 for capture width ratios over 1. This implies that a large amount of reactive power is being put into, and taken out of, the device motion over a cycle. Small inefficiencies in the power exchange mechanisms will be vastly amplified, resulting in a large (or total) loss in the average power absorbed over a cycle.

The HPR is one at the heave natural period of about 5 seconds. In this region (up to about 6 seconds) the optimal complex control is achieved with a relatively small amount of reactive loading. However the relative capture width only rises to about 0.5 at 6 seconds, and the absorbed power levels are relatively small.

The optimal real control requires no reactive loading and is achieved by applying the optimal damping, as given by equation (13). Results for the optimal real control are shown in figure 8.

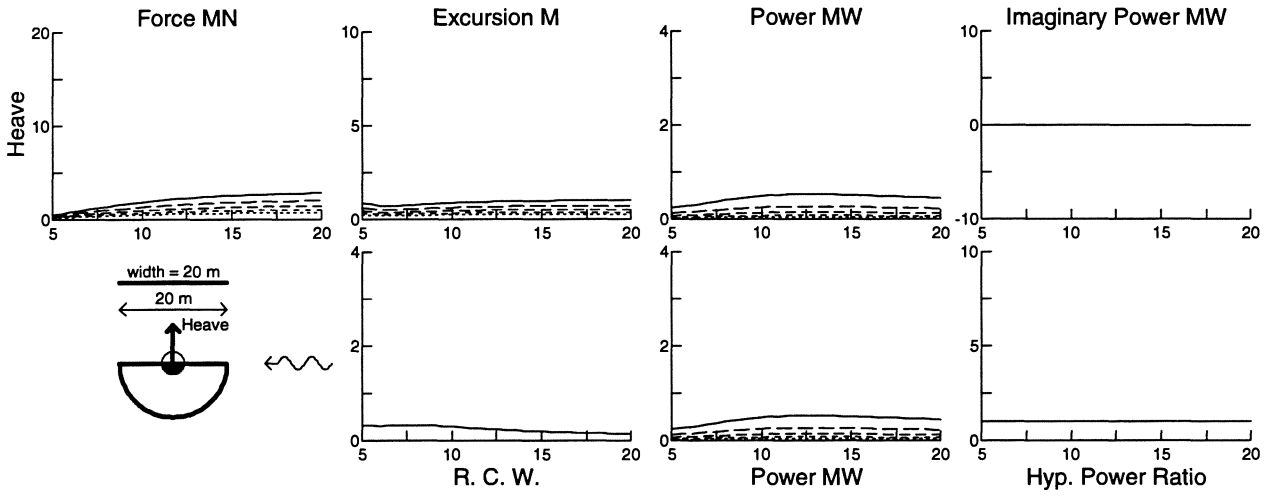

Figure 8: Real control in heave (h_sp) for a 10m radius hemisphere .

It is seen that the heave excursion does not reach the amplitude constraint, and so the heave velocity is given by equation (15). In the long wave limit the heave impedance is dominated by the restoring terms and is therefore purely imaginary and given by $\rho g A_w$, where A_w is the water plane area. The excitation force in the long wave limit is given by the product of the instantaneous wave elevation with $\rho g A_w$. It is therefore clear from equation (15), that in the long wave limit the heave excursion amplitude is $a/\sqrt{2}$ and leads the wave elevation by a phase of $\pi/4$. This is verified by figure (8). For real control, the imaginary power is zero and the HPR is 1. The power absorbed is much less than with optimal complex control. The RCW is independent of the wave amplitude because the excursion constraint is not reached. The RCW reaches a maximum of about 0.3 between 5 and 10 seconds and falls to about half this value at 20 seconds. The maximum power absorbed is 0.5 MW at about 13 seconds.

In summary, a half-buoyant heaving hemisphere of 20m diameter is a poor absorber because its natural period is well below the significant wave periods. The optimal complex control absorbs a lot of power but requires unrealistically large HPRs, whereas the optimal real control results in small excursions producing only small amounts of power.

Comparing the two control strategies at 6 seconds gives an indication of how an acceptable degree of reactive loading can increase power absorption. The optimal complex control gave RCW of 0.5 for an HPR of 2, whereas the optimal real control gave a RCW of 0.3 . Hence near resonance an acceptable degree of reactive loading has increased the absorbed power by approximately 70 percent.

5.1.2 Controlled in Surge

Results for the surge only power absorption configuration, s_hp, with the optimal complex control is shown in figure 9.

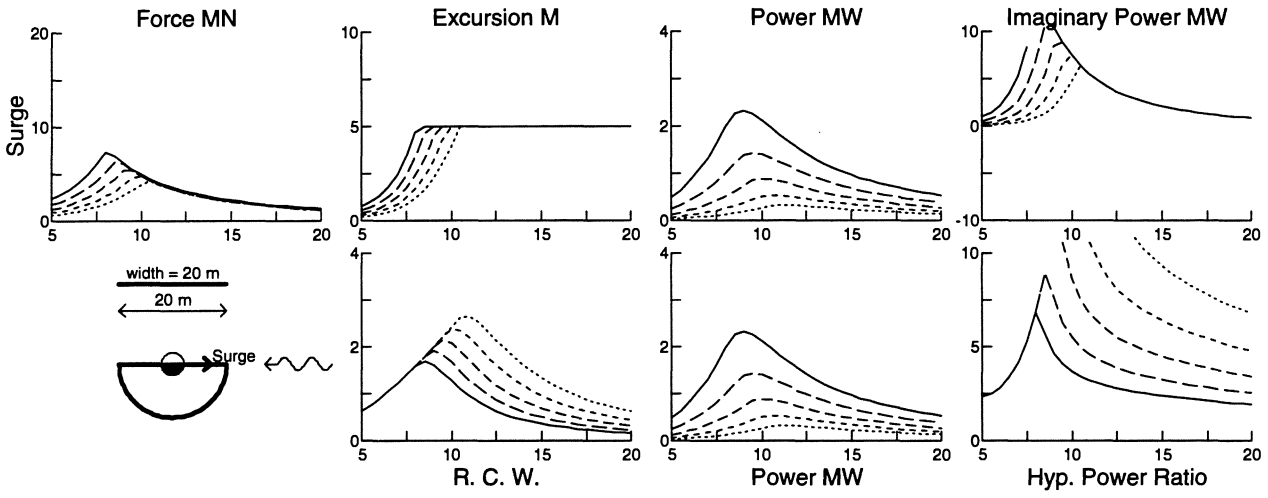

Figure 9: Complex control in surge (s_hp) for a 10m radius hemisphere .

The excursion constraint is first reached at lower wave periods than in heave: 8 seconds for 1.41 m ; 10.5 seconds for 0.35 m. This is because the surge motion has smaller damping. For the cases in which optimal complex control is achieved within the constraint, the capture width ratio attains the surging axi-symmetric point absorber value of λ/π. Again, the relative capture width falls away from the point absorber limit when the constraint is imposed. The maximum power absorbed is about 2.4 MW for a 1.41 metre, 8 second wave. Power absorption levels remain above 1 MW for wave periods between 6 and 15 seconds. However, HPRs are over 2.5 for all wave periods, hence complex control is unlikely to be practical for this case.

Results for the optimal real control are shown in figure 10. The surge excursion does not reach the amplitude constraint, and so the surge velocity is given by equation (15). The power absorbed is much less than with optimal complex control. The RCW reaches a maximum of about 0.5 at about 6 seconds and falls to less than half this value for periods less than 10 seconds. In 20 second waves the RCW is less than 0.1. The maximum power absorbed is 0.5 MW at about 7.5 seconds.

The surging hemisphere is a poor absorber because it does not have a natural period. As with the heave case, the optimal complex control absorbs a lot of power but requires

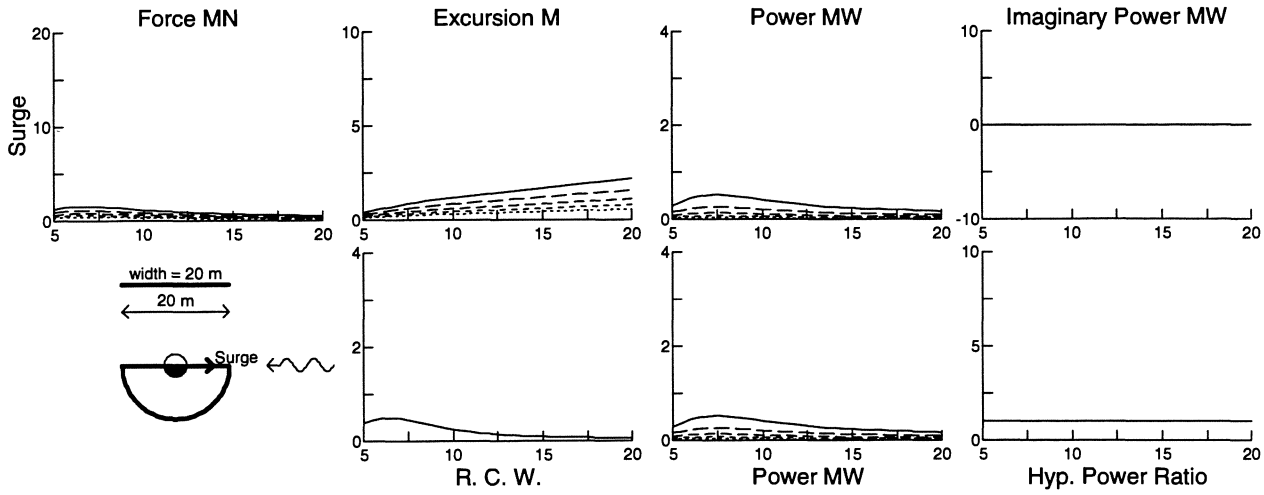

Figure 10: Real control in surge (s_hp) for a 10m radius hemisphere .

unrealistically large HPRs, whereas the optimal real control results in small excursions producing small amounts of power.

5.1.3 Released Degrees of Freedom

For a hemisphere, heave and surge degrees of freedom are uncoupled. Surge and heave do not have natural periods within the wave periods of interest, so excursions in the uncontrolled degrees of freedom are small and the linear theory remains valid. Consequently power absorption in heave is unaffected by releasing the surge degree of freedom. Similarly surge power absorption is unaffected by releasing heave.

5.1.4 Controlled in Heave and Surge

Results for optimal complex control for heave and surge power absorption configuration are shown in figure 11. The optimal control selects the best combination of heave and surge to produce the maximum power absorption within the global constraint.

The excursion constraint is first reached at 8 seconds for 1.41 m waves and 10.5 seconds for 0.35 m waves. For the cases in which optimal complex control is achieved within the constraint, the relative capture width attains the surging and heaving axi-symmetric point absorber value of $3\lambda/2\pi$. Again, the relative capture width falls away from the point absorber limit when the constraint is imposed. Surge is better than heave at absorbing power for 8 to 10 second periods and hence the optimal control requires more surge motion than heave. In longer wave periods heave is better than surge. For periods greater than 15 seconds almost all of the available excursion is taken up by heave, and the power absorbed is the same as for the case of surge being fixed, h_sp. The maximum power absorbed is about 3.5 MW for a 1.41 metre, 9 second wave. Power absorption levels remain above 3 MW for a wide range of periods: between 8 and 18 seconds.

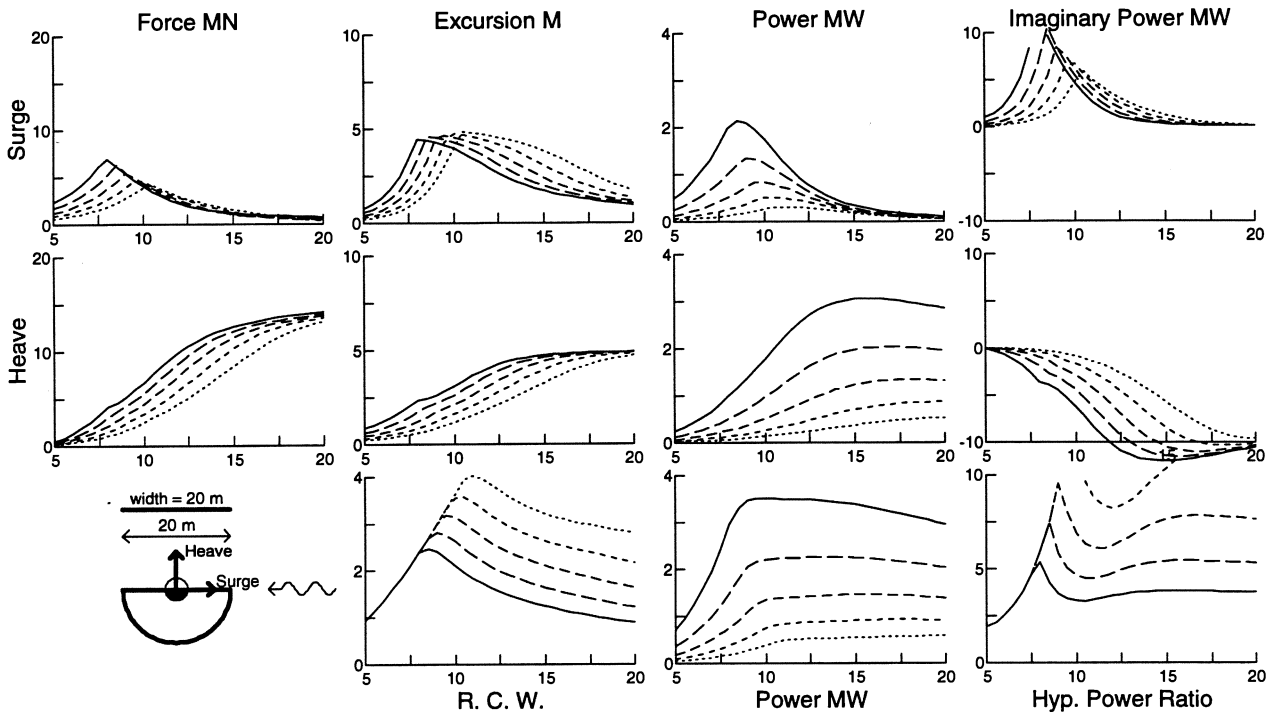

Figure 11: Complex control in surge and heave (s_hp) for a 10m radius hemisphere .

As in the single degree of freedom cases, the HPRs are large, and power losses in the power exchange mechanisms would result in a loss of all or most of the power absorbed.

The optimal real control for multi-degree of freedom absorption is beyond the scope of this study.

5.2 Reducing the Excursion Constraint

The cases considered above have shown that the optimal complex control can produce large RCW, but with the disadvantage of large HPR. This is because the excursions are amplified so as to absorb the maximum power. Away from resonance large reactive powers are required to produce such amplified motions. Such a control strategy is not practical because of unavoidable losses in any power exchange mechanism.

Optimal complex control with a reduced excursion constraint reduces the amplification of the body motions resulting in smaller HPRs. Here we halve the excursion constraint to 2.5 metres.

5.2.1 Controlled in Heave

Halving the constraint on the heave excursion gives the results in figure 12. With a reduced excursion constraint the constraint is reached at shorter wave periods. For a

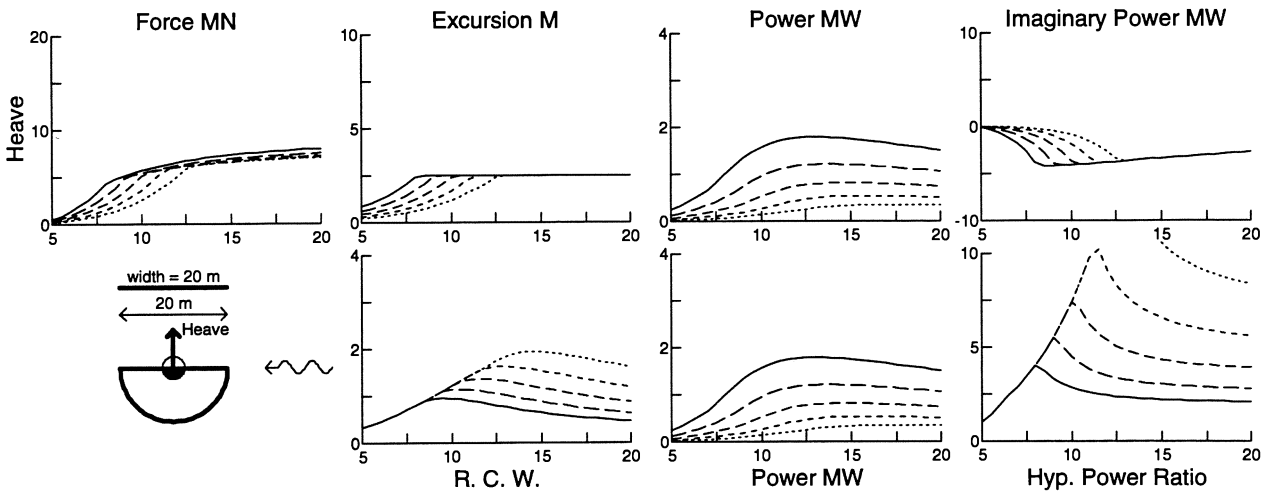

Figure 12: Complex control with a reduced excursion constraint in heave (h_sp) for a 10m radius hemisphere

wave amplitude of 1.41 m the constraint is reached at 8 seconds and the RCW and HPR fall away from their point absorber limits.

For an 11 seconds wave a RCW of about 1 is achieved with an HPR of about 2.5. This compares with: a) a RCW of 2.4 with an HPR of about 6 for complex control with a 5 m constraint; and b) a RCW of 0.25 with real control. Hence selecting the optimal complex control with a suitable amplitude constraint provides a reactive control with an acceptable HPR. In this example almost four times more power is absorbed with an acceptable amount of reactive control.

5.2.2 Controlled in Surge

Similar trends are apparent for surge, see figure 13. At 9 seconds complex control with a 2.5m constraint attains a RCW of 1 with an HPR of about 2, where as a 5m constraint attains a RCW of 1.5 with an HPR of about 5. This compares with a RCW of about 0.4 for real control.

5.2.3 Controlled in Heave and Surge

For the two degree of freedom case, figure 14, the 2.5 m constraint gives a RCW of 1.7 with an HPR of 2, where as the 5.0 m constraint gives a RCW of 2.4 with an HPR of 5.

In conclusion, the optimal complex control may be selected with an appropriate amplitude constraint to give a control with an acceptable HPR that absorbs significantly more power than real control.

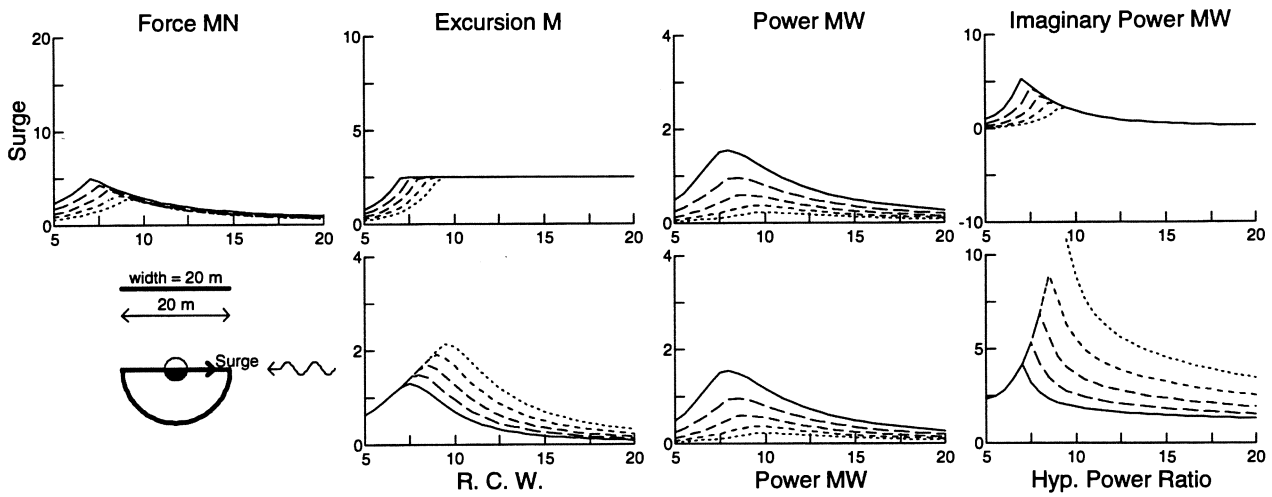

Figure 13: Complex control with a reduced excursion constraint in surge (s_hp) for a 10m radius hemisphere .

5.3 Variation of Mass

The optimal complex control provides a reactive force sufficient to negate the natural spring and inertia so as to induce resonance. Consequently changing the mass of the hemisphere will not affect the power absorption under the optimal complex control, but it will affect the reactive power required.

In the previous sections it was assumed that the hemisphere was half-buoyant. Here we consider a neutrally buoyant hemisphere of 2094 tonnes and a theoretically massless one.

5.3.1 Controlled in Heave

Results for the massless and neutrally buoyant hemispheres heaving under complex control are shown in figures 15 and 16.

The excursions, RCWs and real powers are unaffected by the mass. For the massless hemisphere the imaginary powers have increased. This is because the natural period has decreased to well below 5 seconds and so even more reactive power is required to induce resonance.

The natural period of the neutrally buoyant hemisphere has increased to just over 6 s. At resonance the imaginary power is zero and the HPR is 1. Above 6 seconds the HPR is less than the half-buoyant case because less reactive power is required to induce resonance. At 8 seconds complex control attains a RCW of 0.8 with an HPR of 2.5. This compares with an HPR of 4 for the semi-buoyant case, and 5.5 for the massless case.

In the long wave limit the results are not affected by changes in the mass since inertia terms are small and dominated by restoring terms.

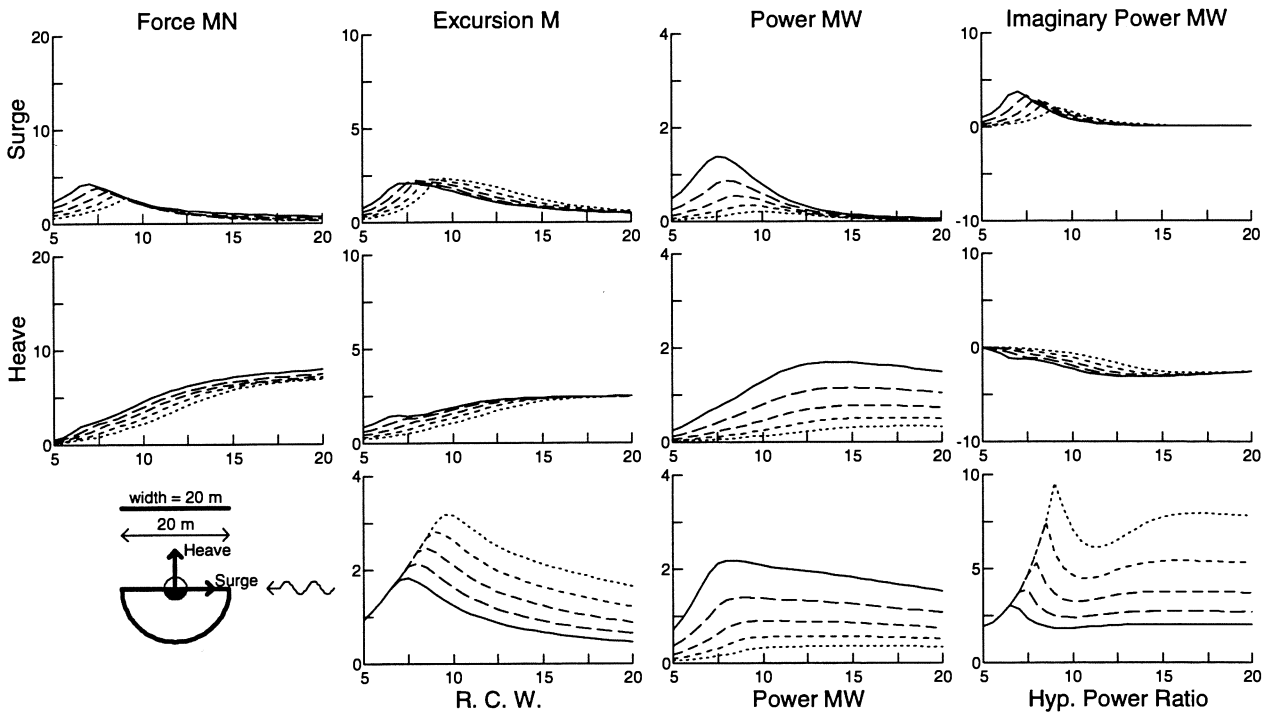

Figure 14: Complex control with a reduced excursion constraint in heave and surge (sh_p) for a 10m radius hemisphere .

Results for the massless and neutrally buoyant hemisphere under real control are given in figures 17 and 18.

The neutrally buoyant hemisphere attains higher RCW. At resonance the complex control is equivalent to the real control (since no reactive powers are required) and hence the same RCW is attained. At 8 seconds the neutrally buoyant hemisphere under real control attains a RCW of about 0.4. This compares with a RCW of about 0.3 for the half-buoyant case, and 0.25 for the massless case.

So choosing the mass of the device can bring resonance into the periods of interest. Then complex control can further extend the region of maximum power absorption.

5.3.2 Controlled in Surge

Figures 19 and 20 show the HPRs for the case of a massless hemisphere and a neutrally buoyant hemisphere surging under complex control.

The massless hemisphere gives lower HPR. This is because there is no restoring in surge and so the reactive power cancels out only inertia terms to induce resonance. At 6 seconds the point absorber RCW is attained with an HPR of 5.5 for the neutrally buoyant case, and 2.5 for the massless case.

In the long wave limit the inertia terms are still dominant (since the restoring force is

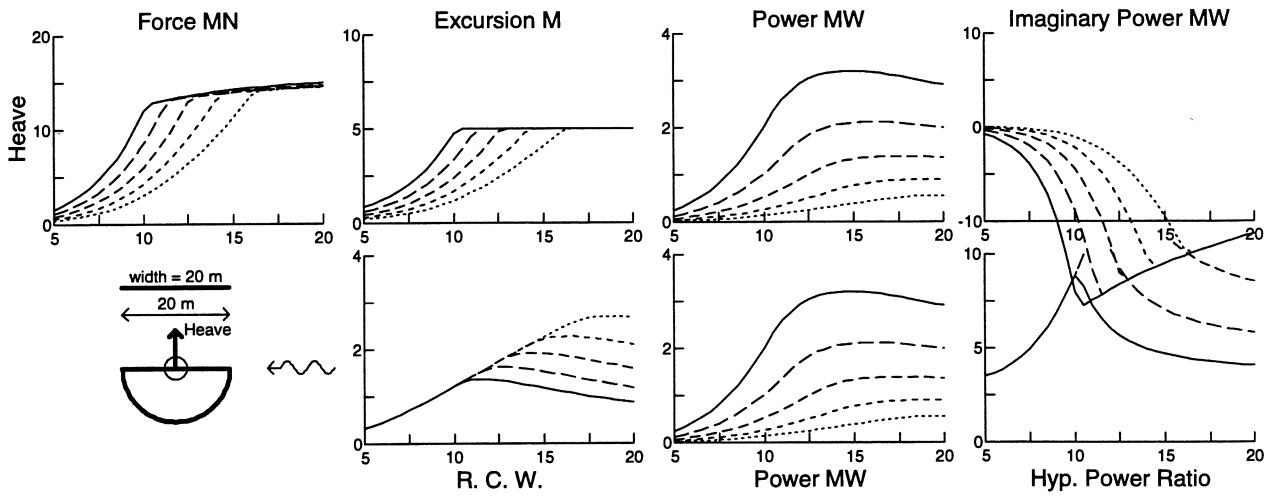

Figure 15: Complex control in heave (h_sp) for a massless hemisphere

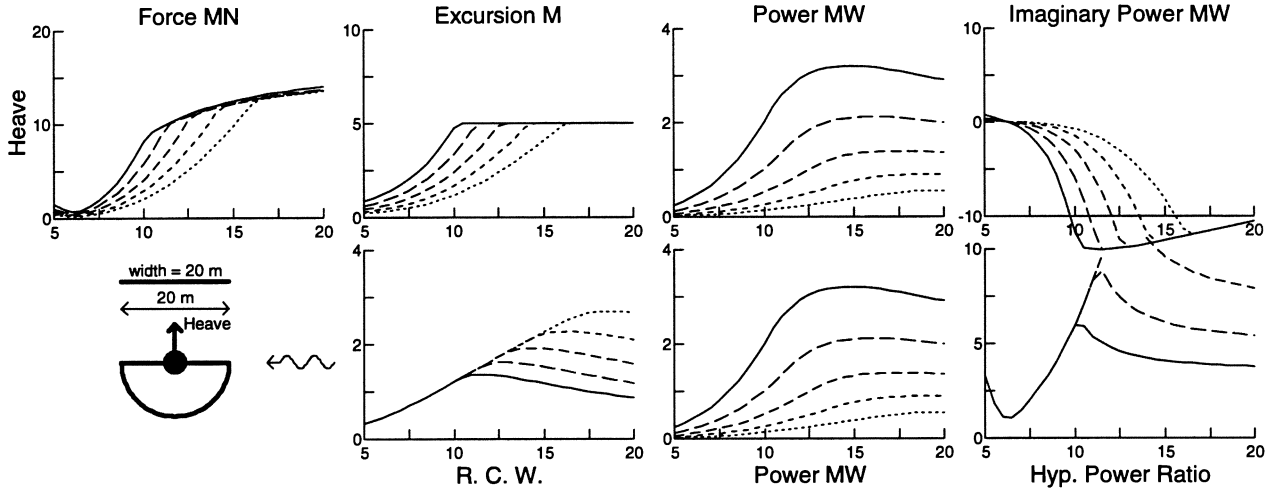

Figure 16: Complex control in heave (h_sp) for a neutrally buoyant hemisphere

zero) and hence the massless case still gives a lower HPR.

Results for real control are given in figures 21 and 22.

The massless hemisphere produces about twice as much power as the neutrally buoyant hemisphere. This is because the excursions are greater and therefore closer to the optimal excursions as given by complex control. At 5 seconds the massless hemisphere under real control attains almost as much power as with complex control, even though it is not close to resonance. This is because at short periods only small motions are required for optimal complex control.

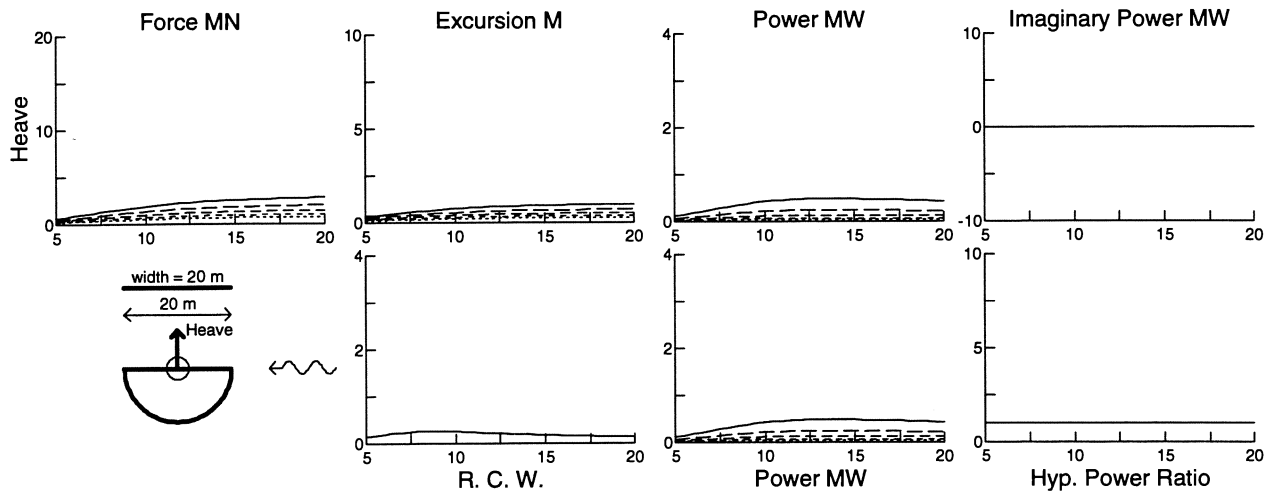

Figure 17: Real control in heave (h_sp) for a massless hemisphere

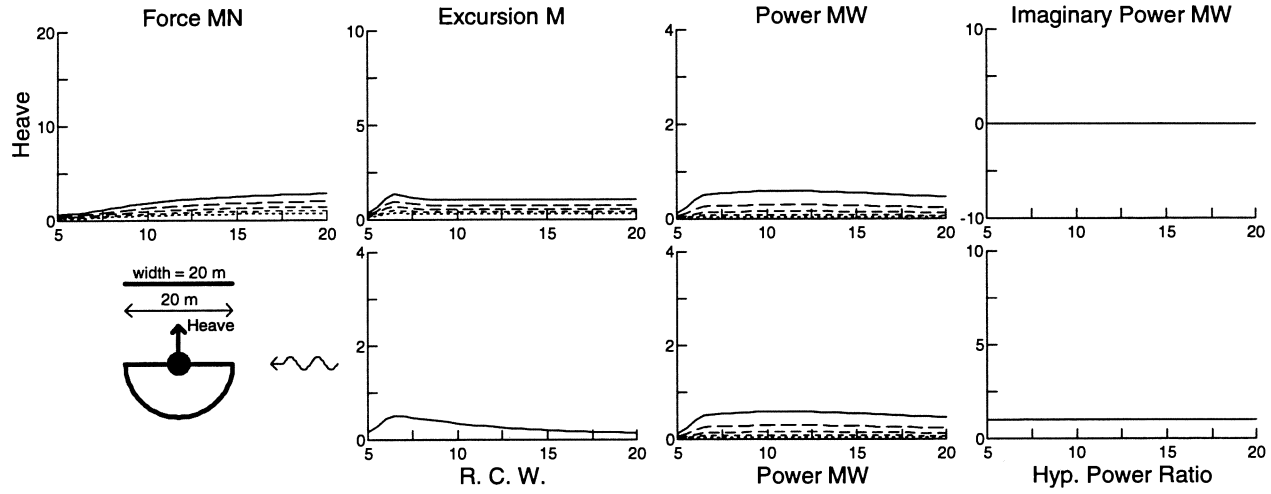

Figure 18: Real control in heave (h_sp) for a neutrally buoyant hemisphere

5.3.3 Controlled in Heave and Surge

Figures 23 and 24 show the HPRs for the case of a massless hemisphere and a neutrally buoyant hemisphere undergoing heave and surge motions with the optimal complex control.

Below 11 seconds the massless hemisphere attains the optimal power absorption with a lower HPR than the neutrally buoyant hemisphere. Above 11 seconds the trend is reversed. This is because at smaller periods surge is more important than heave in absorbing power, and (as shown above) a massless hemisphere in surge attains optimal absorption with lower HPR than the neutrally buoyant hemisphere. For longer periods heave is better at absorbing power, and so a neutrally buoyant hemisphere has lower HPR.

Ideally we require a hemisphere which has low inertia in surge, but is neutrally buoyant in heave. This could be achieved by suspending much of the mass the hemisphere at the end

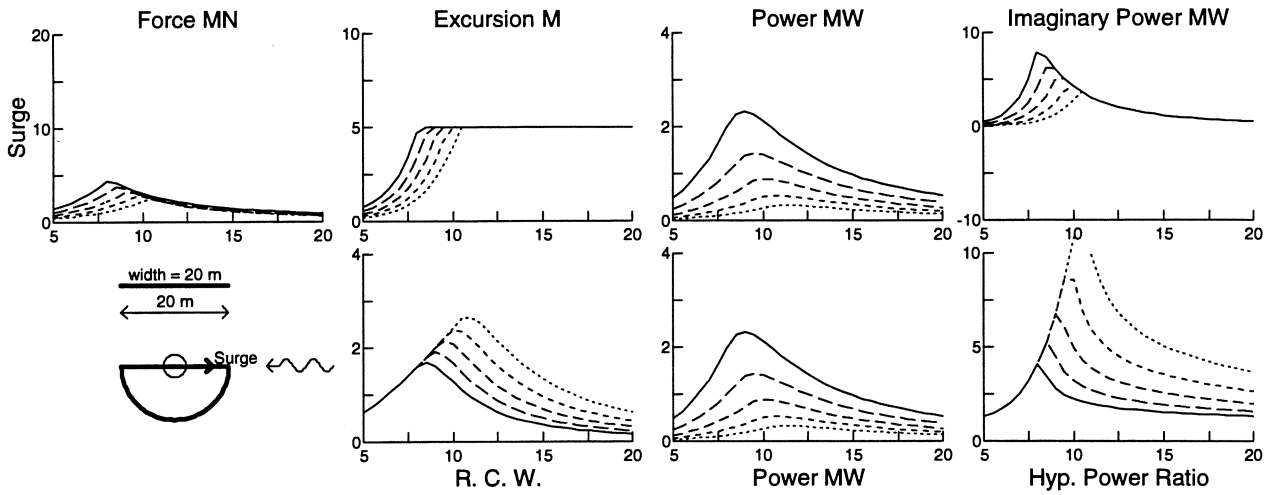

Figure 19: Complex control in surge (s_hp) for a massless hemisphere

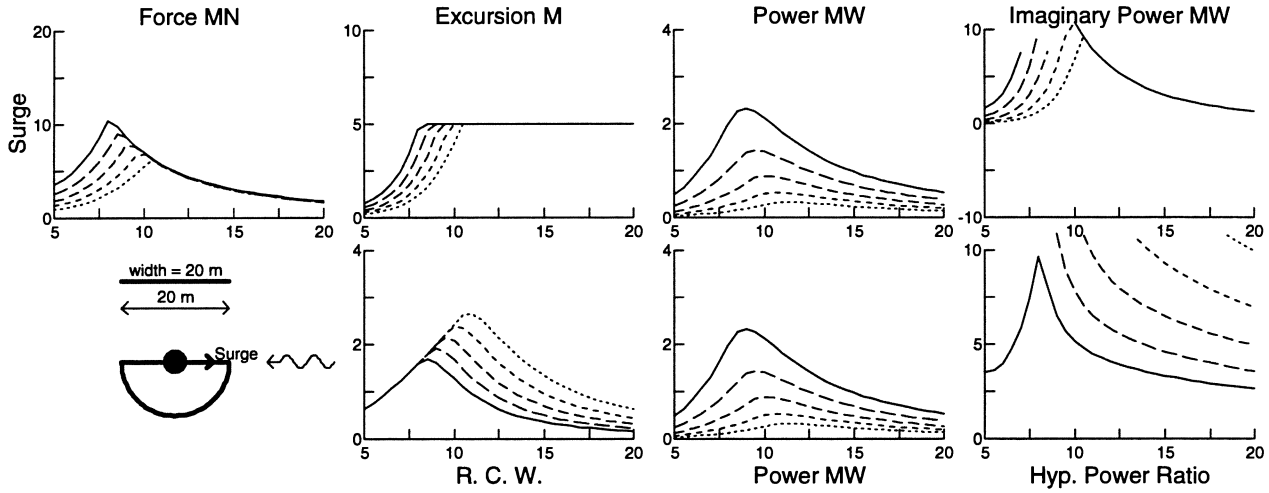

Figure 20: Complex control in surge (s_hp) for a neutrally buoyant hemisphere

of a long wire. For a heave motion the mass will accelerate, whereas for a surge motion the mass will remain fairly stationary. A similar effect will result if the mass is replaced with a flat plate designed to have the appropriate added mass in heave. Alternatively the surge motion could be replaced by a pitch motion about a concentrated centre of mass.

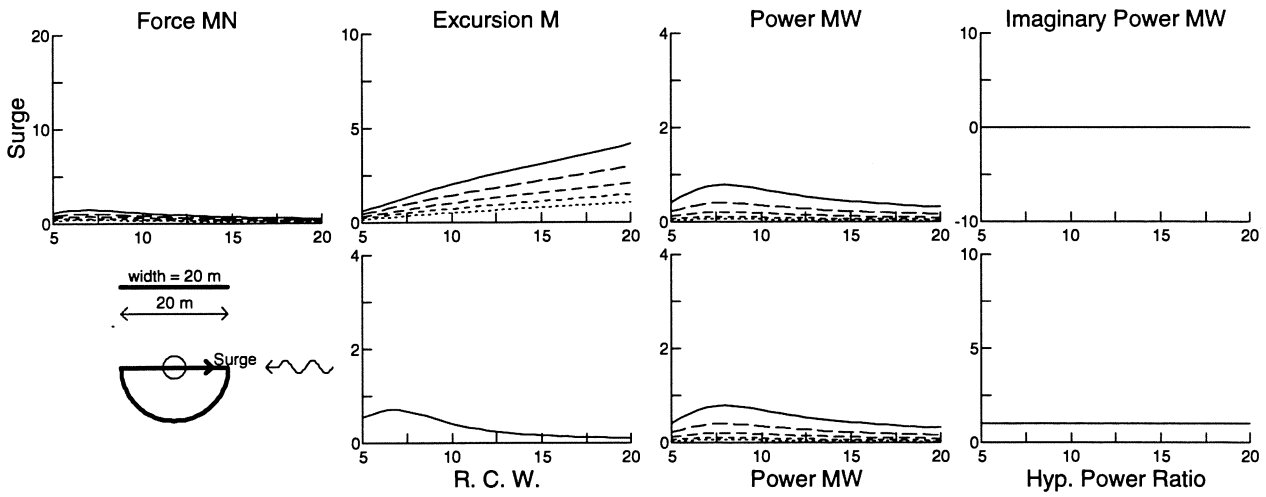

Figure 21: Real control in surge (s_hp) for a massless hemisphere

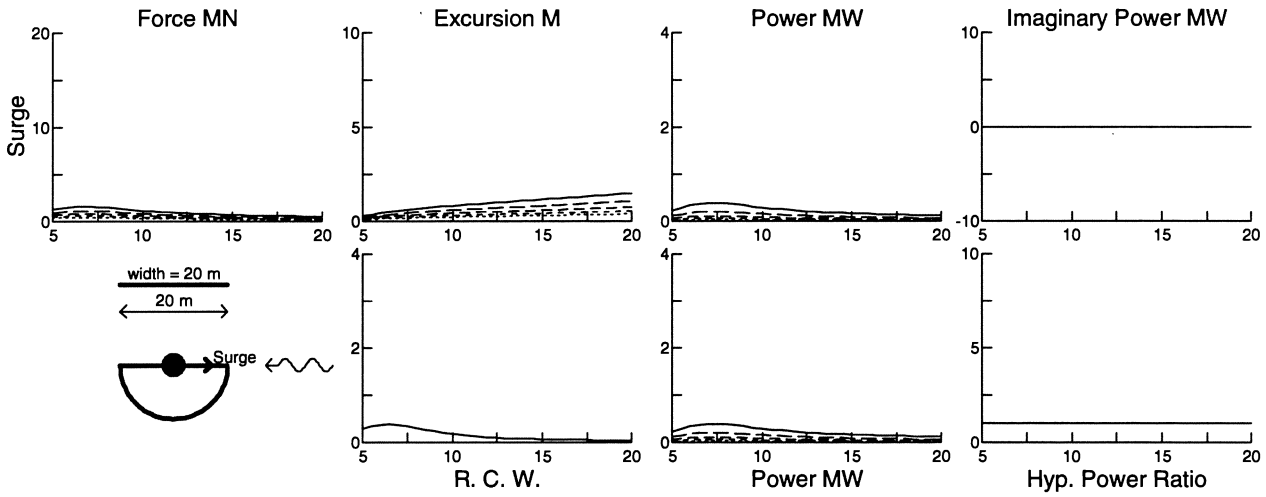

Figure 22: Real control in surge (s_hp) for a neutrally buoyant hemisphere

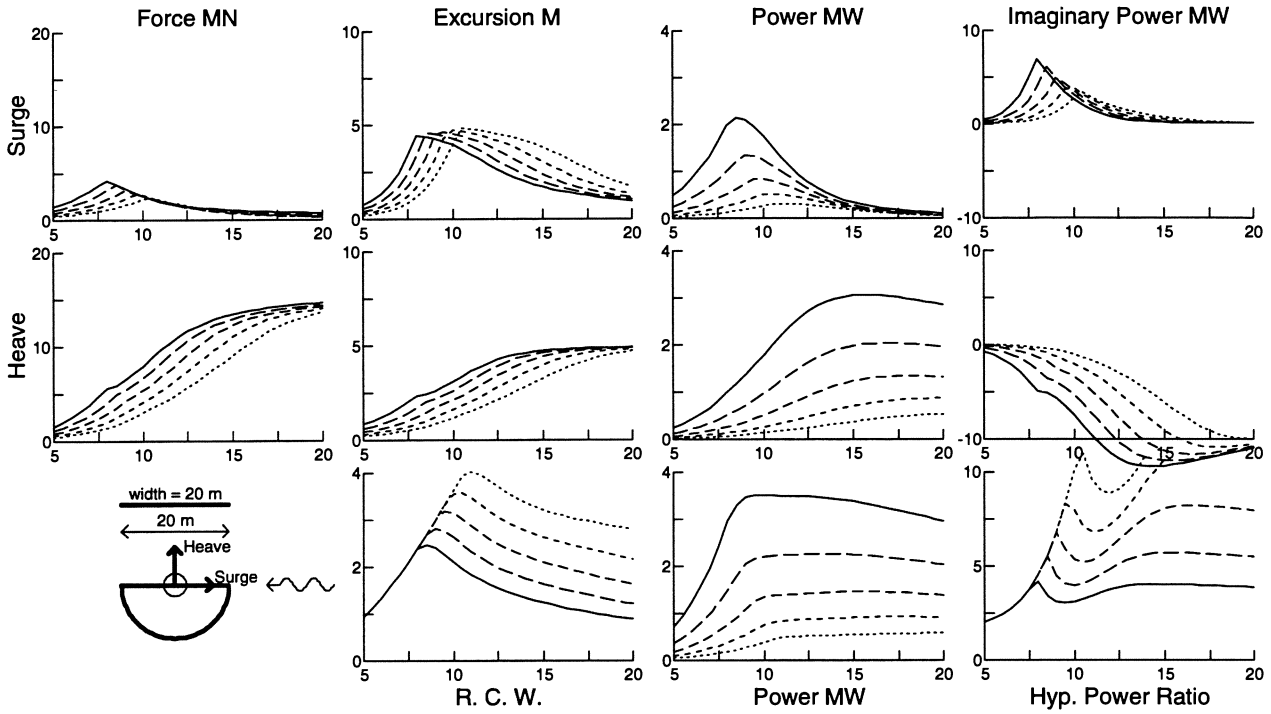

Figure 23: Complex control in surge and heave (sh_p) for a massless hemisphere

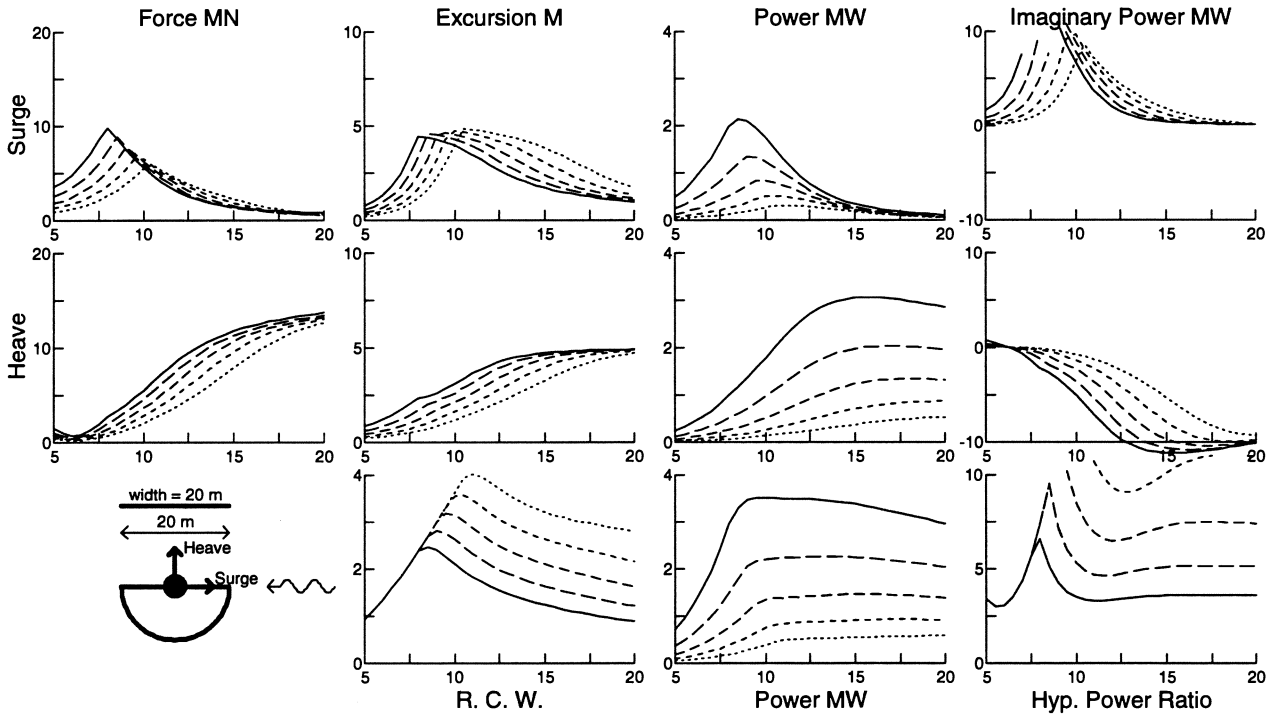

Figure 24: Complex control in surge and heave (sh_p) for a neutrally buoyant hemisphere

5.4 Inclined Degrees of Freedom

So far we have considered absorbing power through the heave or surge axis. Here we consider absorption in an inclined direction. The heave and surge axes are rotated to give the fore and aft axes respectively. A rotation of 30 degrees gives an aft axis 30 degrees to the horizontal, and a fore axis 30 degrees to the vertical. Here rotations of 30, 45 and 60 degrees are considered.

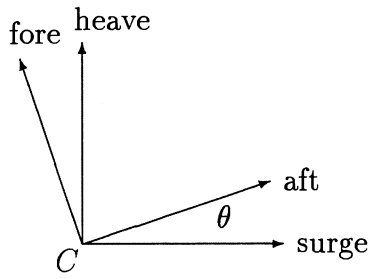

Figure 25: Definition of fore and aft degrees of freedom

Quantities are expressed with respect to the fore and aft system by simple transformations. A vector in the fore and aft system, $\mathbf{U}'$, is obtained from the vector in the surge and heave system,$\mathbf{U}$ by:

$$\mathbf{U}' = \mathbf{R}^T\mathbf{U} \tag{33}$$

where $\mathbf{R}$ is the transformation matrix defined by:

$$\mathbf{R} = \begin{bmatrix} cos\theta & -sin\theta & 0 \\ sin\theta & cos\theta & 0 \\ 0 & 0 & 1 \end{bmatrix}$$

and T denotes the transpose. Matrices transform according to the rule:

$$\mathbf{Z}' = \mathbf{R}^T\mathbf{Z}\mathbf{R} \tag{34}$$

Once all quantities have been obtained in the inclined system the power absorption calculations proceed as before.

5.4.1 One Controlled Degree of Freedom

The performance of the semi-buoyant hemisphere is investigated as the axis of absorption ranges from: surge; 30° aft; 45° aft; 60° aft; heave; 30° fore; 45° fore; 60° fore and negative surge (a negative surge axis is equivalent to a positive surge axis).

Results for absorption in a single degree of freedom under the optimal complex control are shown in figures 26 to 34

Degree of freedom	Natural period
heave	5 s
30^o fore, 60^o aft	6 s
45^o fore, 45^o aft	8 s
60^o fore, 30^o aft	11 s
surge	infinite

Table 1: Natural periods for half-buoyant 10 metre hemisphere

The results for surge and heave shown in section 5.1 are duplicated here in figures 26, 30 and 34. The heave natural period is just below 5 seconds, whereas surge has an infinite natural period since the restoring is zero.

The natural period for the fore and aft directions increases as the angle to the vertical increases, as is shown in table 1.

Results for the 30^o fore and 60^o aft cases (figures 31 and 29) do not differ greatly from the heave case. Large HPRs are required above 8 s. For 1.41 m wave amplitude at 11 seconds period all three cases give very similar RCW. For periods below 11 seconds the 60^o aft case has lower RCW than the heave case, whereas the 30^o fore case has higher RCW. At 5 seconds the RCW for the 60^o aft case drops to almost zero, whereas the 30^o fore case attains a RCW of 1 — double the heave case.

These trends are explained by considering the fore and aft degrees of freedom as specific combinations of heave and surge, ie: 60^oaft $= \frac{\sqrt{3}}{2}$heave $+ \frac{1}{2}$surge; 30^ofore $= \frac{\sqrt{3}}{2}$heave $- \frac{1}{2}$surge. So surge and heave components are in phase for 60^o aft, and in anti-phase for the 30^o fore case. Since heave has a symmetric wave pattern and surge has an asymmetric wave pattern the surge component will increase or decrease the power absorption — depending on the relative phases. At 5 seconds the RCW of 1 for the fore case is almost as large as the two degree of freedom case shown in figure 11. This is because the optimal two degree of freedom motion happens to be close to a fore motion, ie heave and surge in anti-phase. For periods above 11 seconds the heave case has higher RCW than the fore and aft cases. This is because the surge components are small in long waves and the power absorption is dominated by the heave component.

The 45^o fore and aft cases have 8 second natural periods, and the 60^o fore and 30^o aft cases have 11 second natural periods. These natural periods are at the lower and upper bounds of the most important wave periods for the west coast of Scotland. For reasons described above, the fore cases perform better than the aft cases at periods less than 11 seconds. At 5 seconds the fore case gives RCW almost as large as the 2 degree of freedom case shown in figure 11

At all periods the fore case attains higher RCW with lower HPR than the surge case. The fore cases also perform better than heave for periods less than 11 s.

Results with real control are shown in figures 35 to 43. The 30^o fore and 60^o aft cases

reach the 5 m excursion constraint near the 11 seconds natural period. The other cases do not reach the constraint because they have lower natural periods at which the damping is greater. As with complex control, the fore cases perform better than the aft cases at shorter periods. At resonance the real control attains same RCW as with complex control. The 60^o aft case is of particular interest since large RCW are absorbed with real control. The value of complex control away from resonance is readily apparent by comparing figures 33 and 42. At 8.5 seconds complex control produces 80 percent more power with a HPR of 2.

5.4.2 One Controlled and One Released Degrees of Freedom

It may be undesirable to fix a device, since large wave forces will have to be resisted in storm conditions. Here we investigate the effects of permitting non-absorbing degrees of freedom. The theory is described in section 3.4. The control strategies and power absorption calculations are similar to the case of one absorbing degree of freedom with the others fixed. The impedance matrix and excitation force vector are modified to account for the released degree of freedom. The excursion constraint is applied only to the controlled degree of freedom. For a hemisphere, heave and surge are uncoupled. Thus power absorption in one is not affected by freeing the other. This is not the case for fore and aft degrees of freedom.

Results for absorption in one degree of freedom under the optimal complex control with the other perpendicular degree of freedom free are shown in figures 44 to 51.

For the heave and surge cases it is seen that the motions in the free degrees of freedom remain small and are well within the linear regime.

It is seen that the imaginary powers are zero at two periods for each case. These correspond to two natural periods, one at the heave natural period and one at the natural period of the uncontrolled degree of freedom. Whilst two natural periods may be expected, it is unclear why they should be so close to the single degree of freedom natural periods. An analytical investigation to explain this proved too complex and it is not clear if these trends will generalise to all cases.

In the previous study [1] it was hypothesised that releasing a degree of freedom would reduce power absorption. However, for wave periods between 5 seconds and about 12 seconds power absorption in the aft cases is larger when the device is free to move in the perpendicular fore direction. For the 30^o aft case, figures 27 and 45, it is seen that at 7.5 seconds about 40 percent more power is absorbed with the same HPR by releasing the 30^o fore degree of freedom.

Wave excitation and the control force induce large motions in the released degrees of freedom. At long periods the controlled degree of freedom always reaches its constraint. Consequently for cases in which the free degree of freedom is either 30^o fore or 60^o aft very large motions are induced since the free degree of freedom will adjust so that the float rides the waves. This also implies that the net volume displaced by the device is reduced

and explains why releasing a degree of freedom reduces power absorption for long wave periods.

Results with real control are shown in figures 52 to 59. For the 60° aft case (figure 55) and the 30° fore case (figure 55) large motions are induced in the released degree of freedom at the natural period (about 11 seconds). There is sufficient coupling with the controlled degree of freedom to absorb large amounts power from the released degree of freedom. It should be noted that in these cases the large excursions may give rise to significant hydrodynamic non-linearities, which would invalidate the results.

5.4.3 Two Controlled Degrees of Freedom

Results for absorption in two degrees of freedom under the optimal complex control are shown in figures 60 to 63

The power absorption is the same for all orientations of the fore and aft degrees of freedom. However the power through the fore and aft axes does depend on the orientation. For the heave and surge case shown in figure 60 positive time-averaged power is absorbed through heave and surge at all frequencies. However, for the fore and aft cases large amounts of negative time-averaged power occur in the aft degrees of freedom. This implies that time-averaged power is required to be put into the aft motions, which is then absorbed by the fore motion.

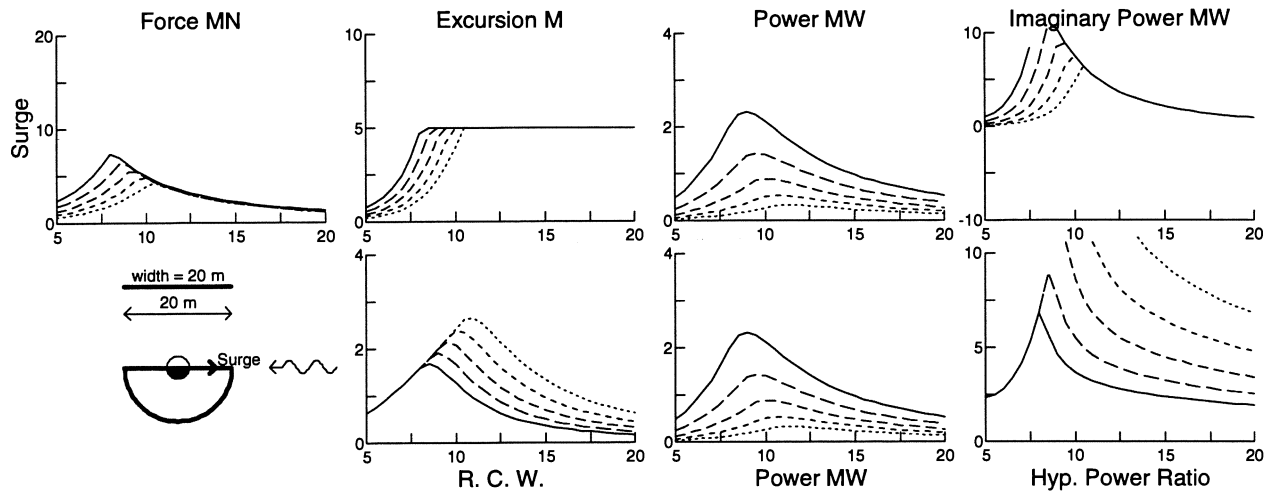

Figure 26: Complex control in surge (s_hp) for a 10m radius hemisphere .

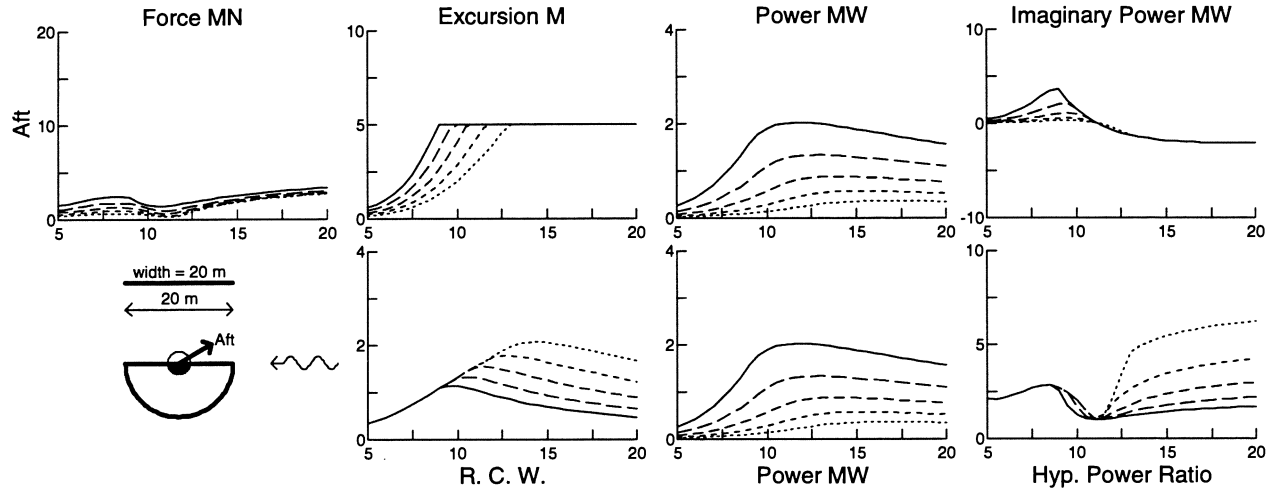

Figure 27: Complex control for 30 degrees aft for a 10m radius hemisphere .

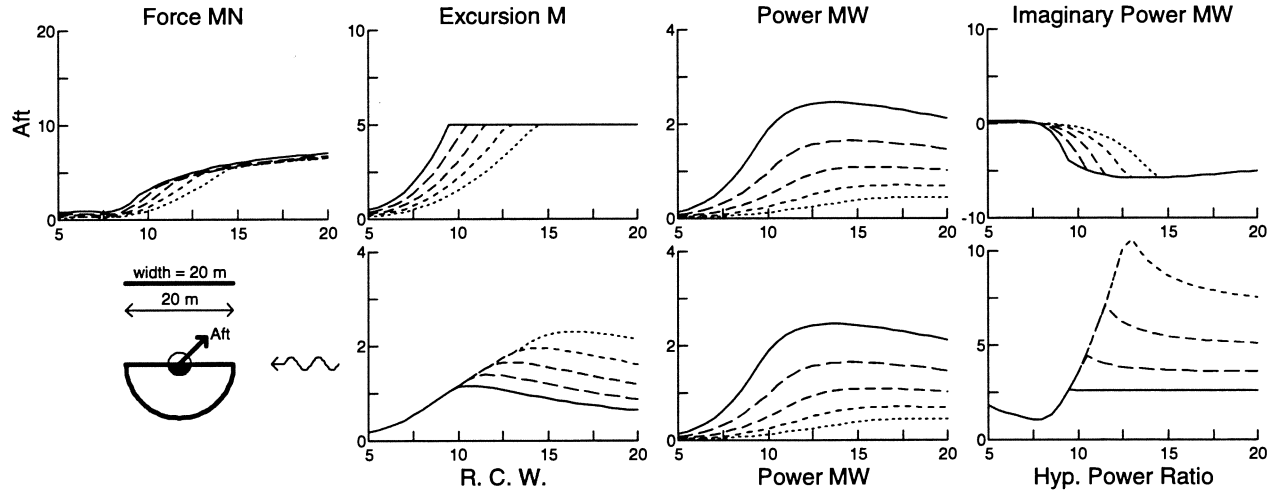

Figure 28: Complex control for 45 degrees aft for a 10m radius hemisphere .

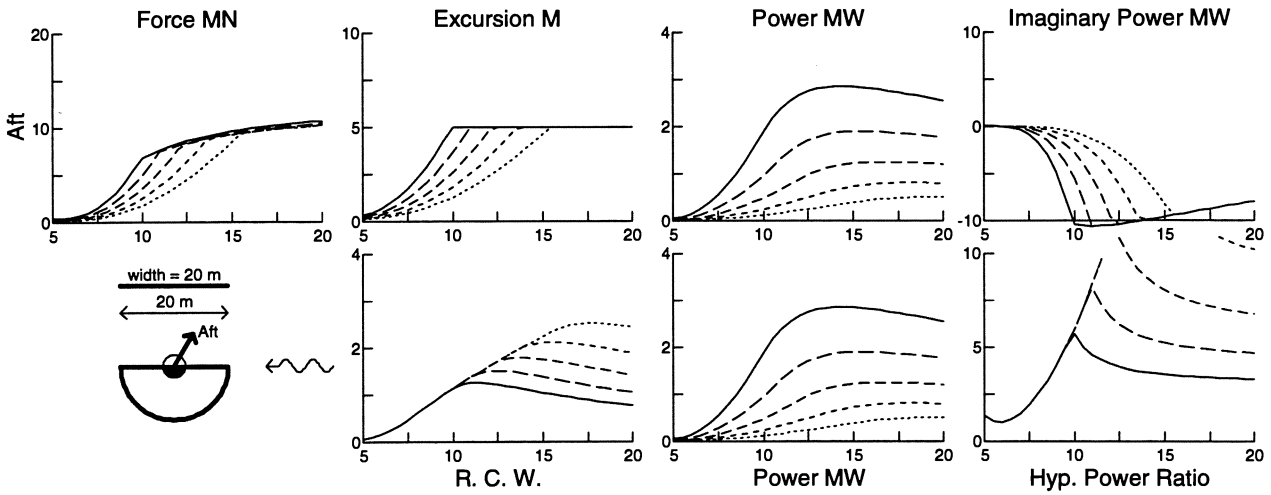

Figure 29: Complex control for 60 degrees aft for a 10m radius hemisphere .

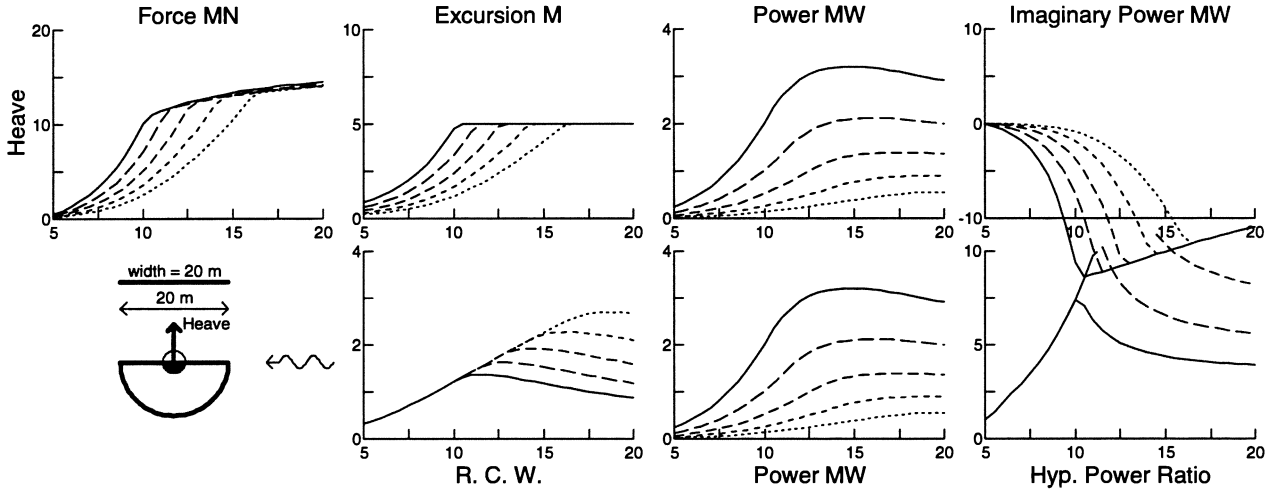

Figure 30: Complex control in heave (h_sp) for a 10m radius hemisphere .

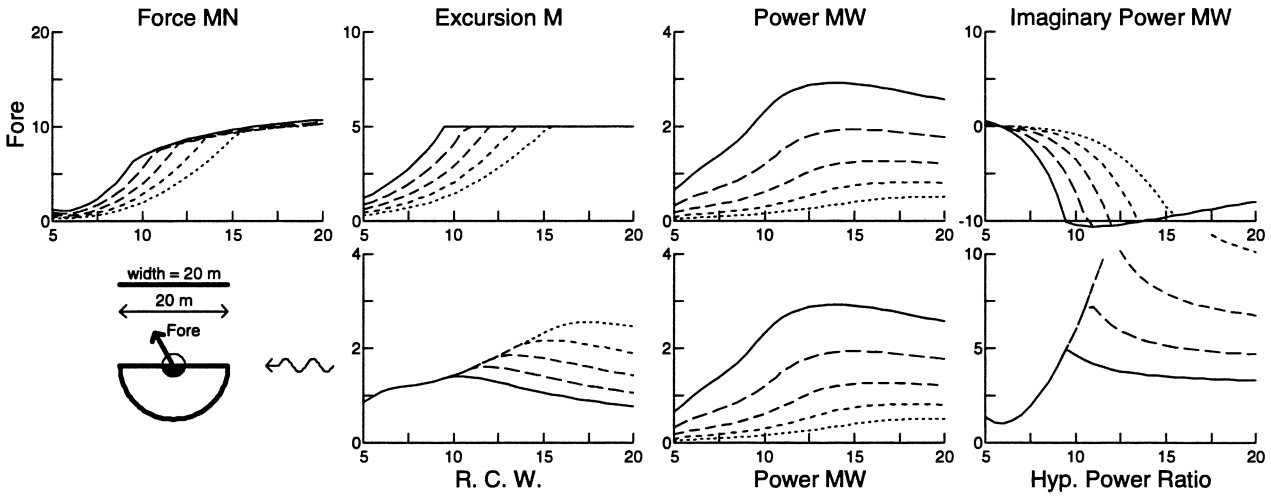

Figure 31: Complex control for 30 degrees fore for a 10m radius hemisphere .

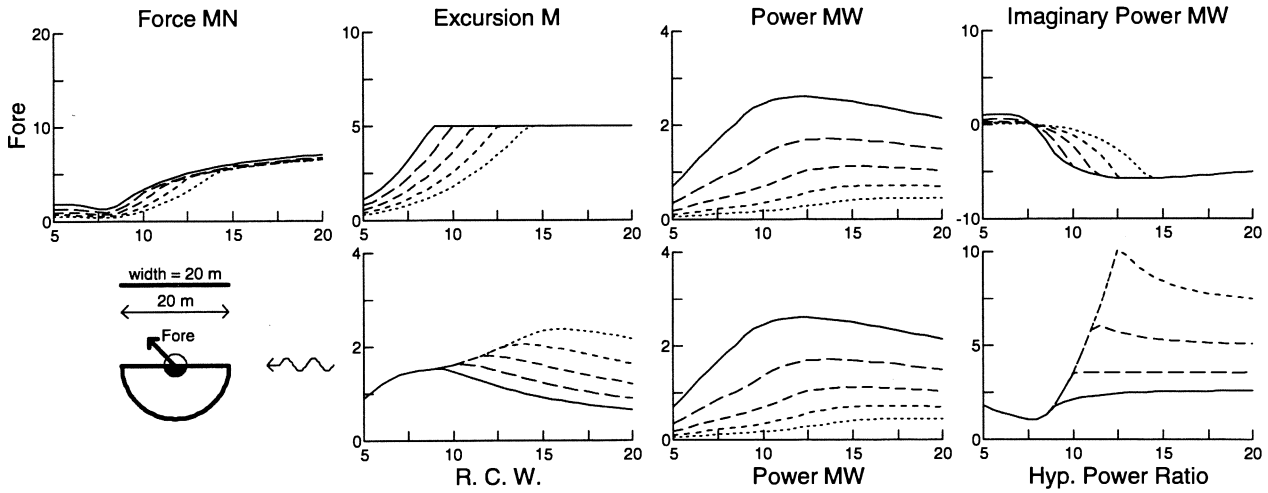

Figure 32: Complex control for 45 degrees fore for a 10m radius hemisphere .

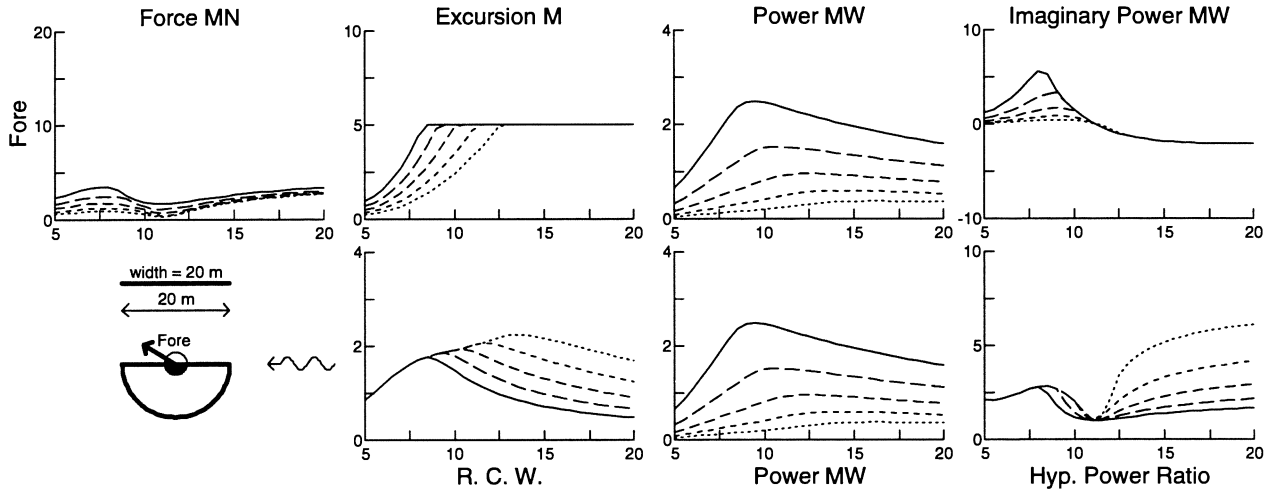

Figure 33: Complex control for 60 degrees fore for a 10m radius hemisphere .

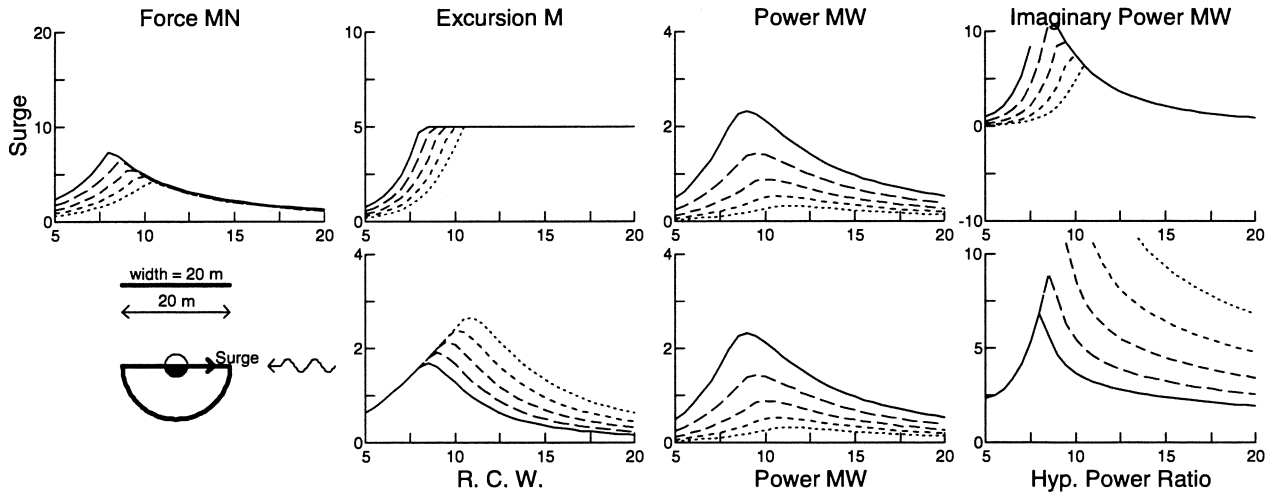

Figure 34: Complex control in surge (s_hp) for a 10m radius hemisphere .

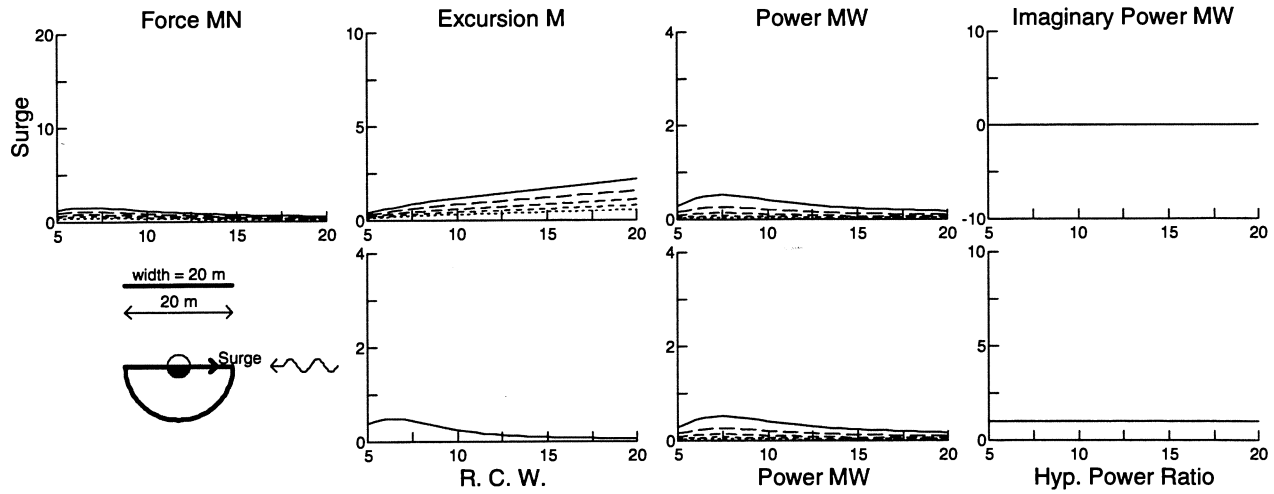

Figure 35: Real control in surge (s_hp) for a 10m radius hemisphere .

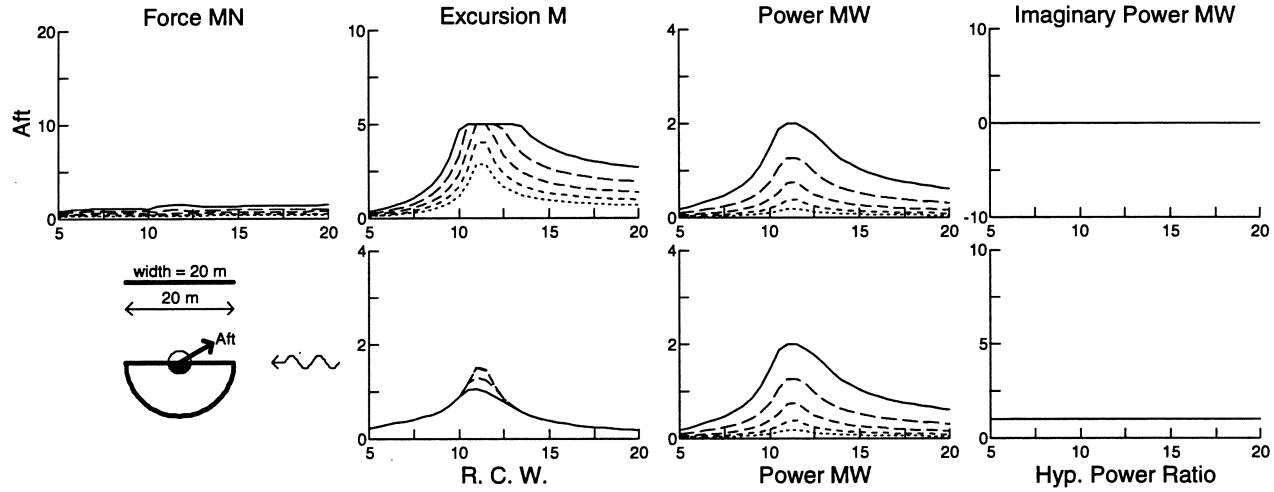

Figure 36: Real control for 30 degrees aft for a 10m radius hemisphere .

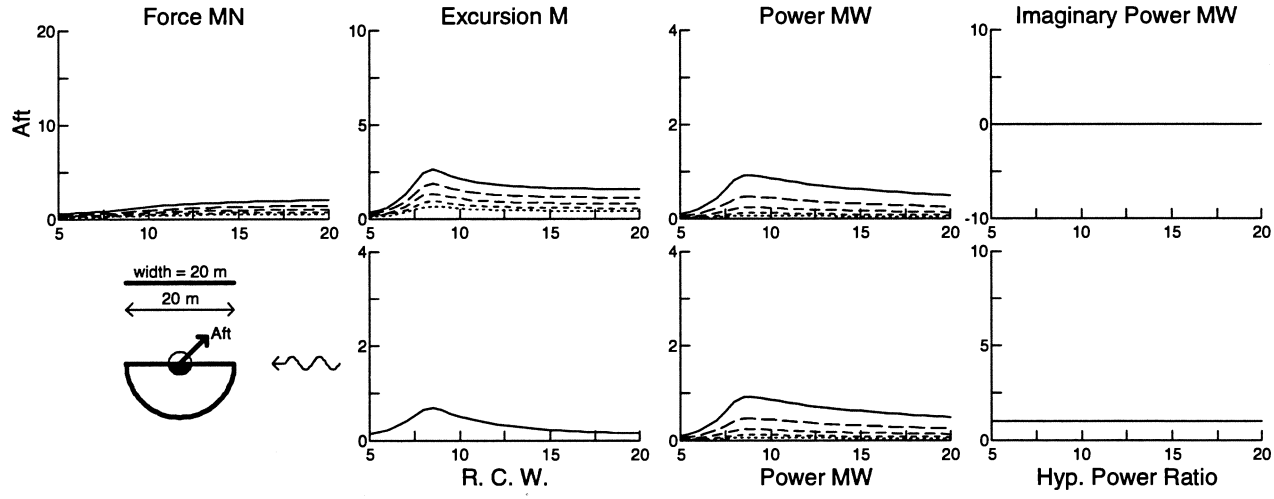

Figure 37: Real control for 45 degrees aft for a 10m radius hemisphere .

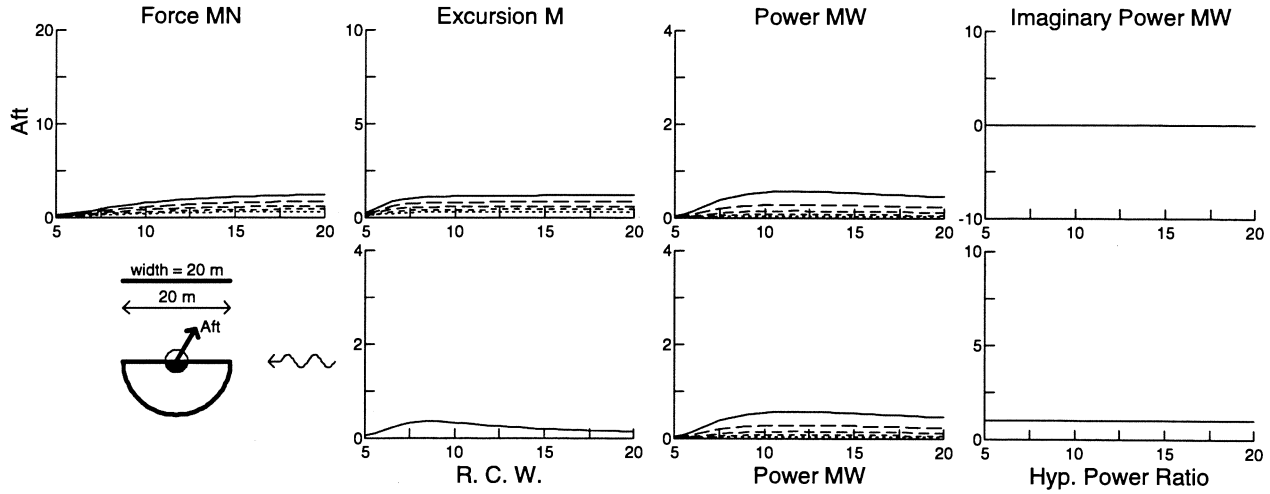

Figure 38: Real control for 60 degrees aft for a 10m radius hemisphere .

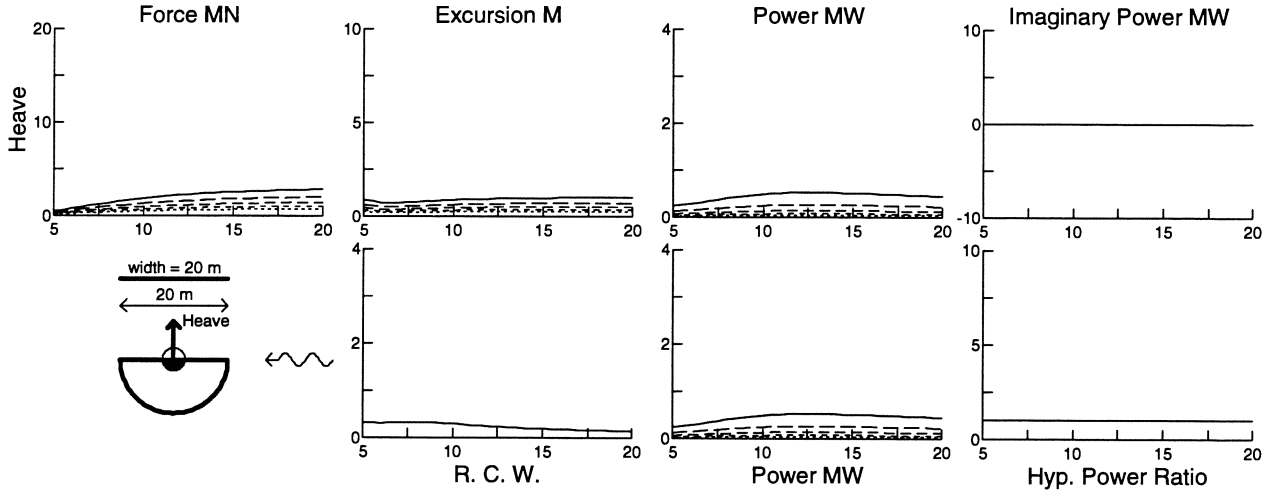

Figure 39: Real control in heave (h_sp) for a 10m radius hemisphere .

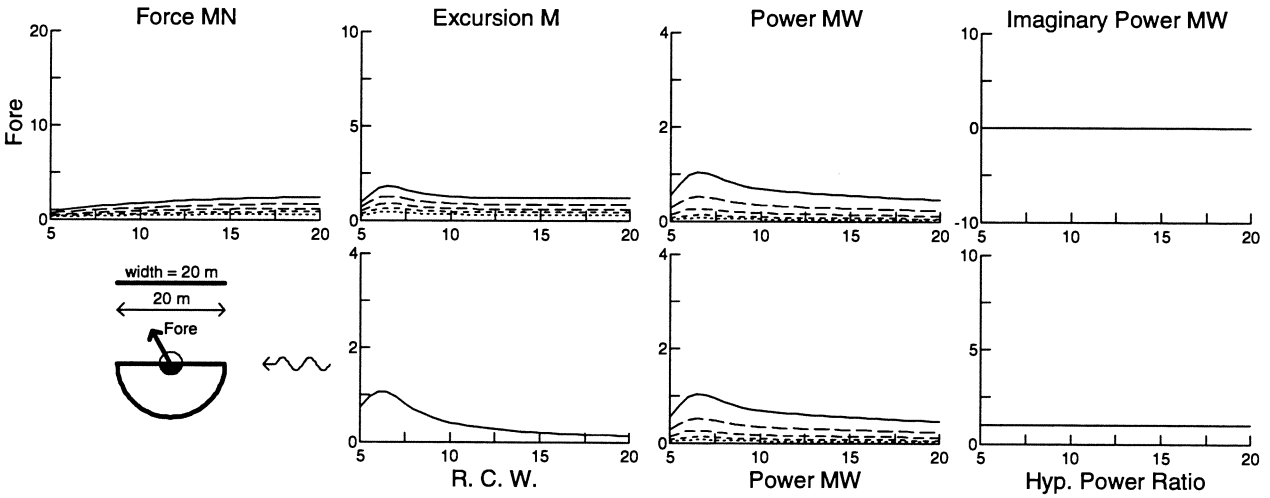

Figure 40: Real control for 30 degrees fore for a 10m radius hemisphere .

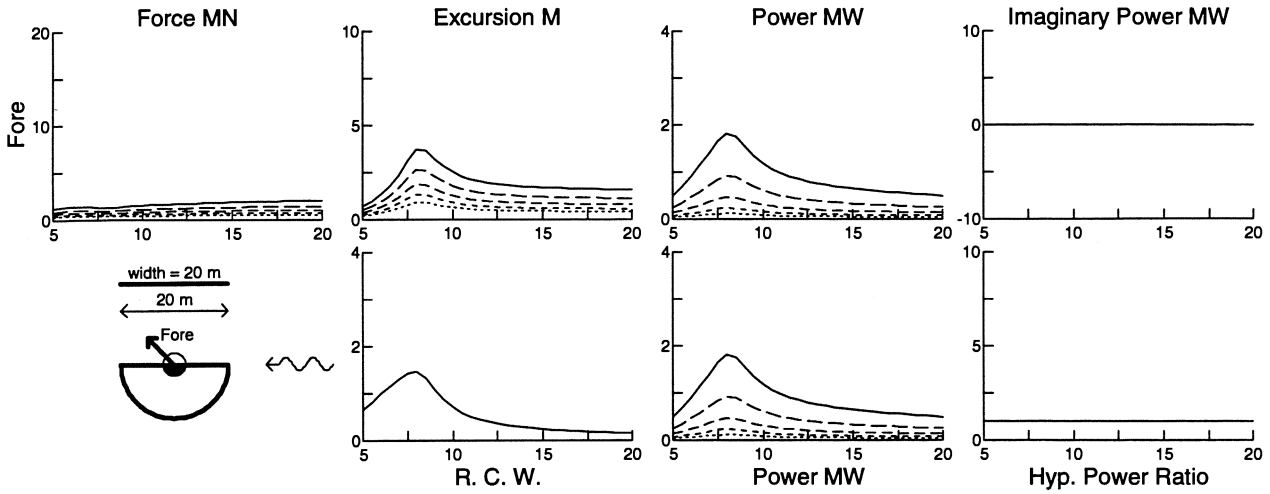

Figure 41: Real control for 45 degrees fore for a 10m radius hemisphere .

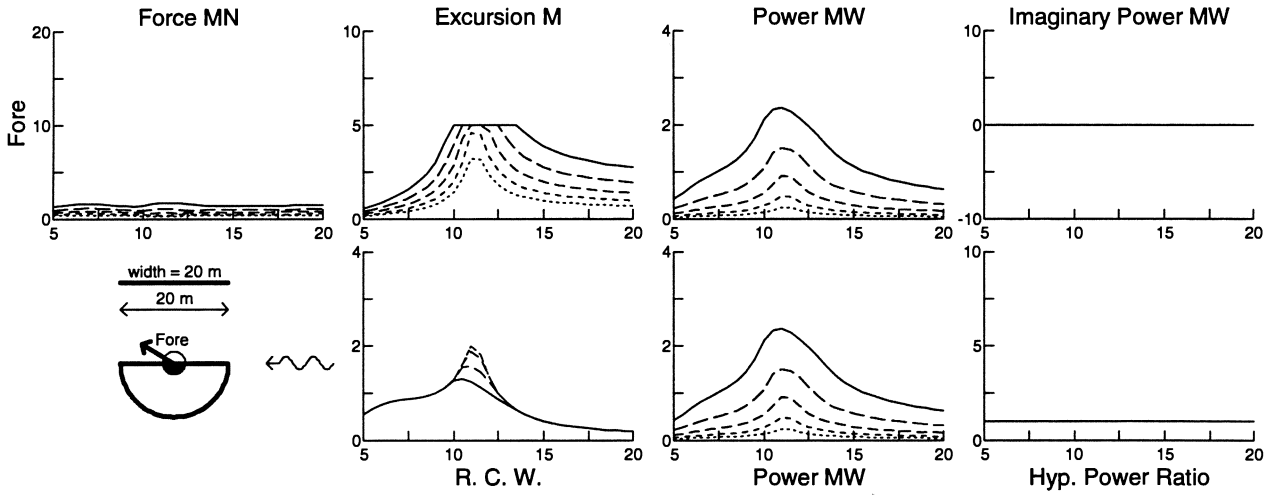

Figure 42: Real control for 60 degrees fore for a 10m radius hemisphere .

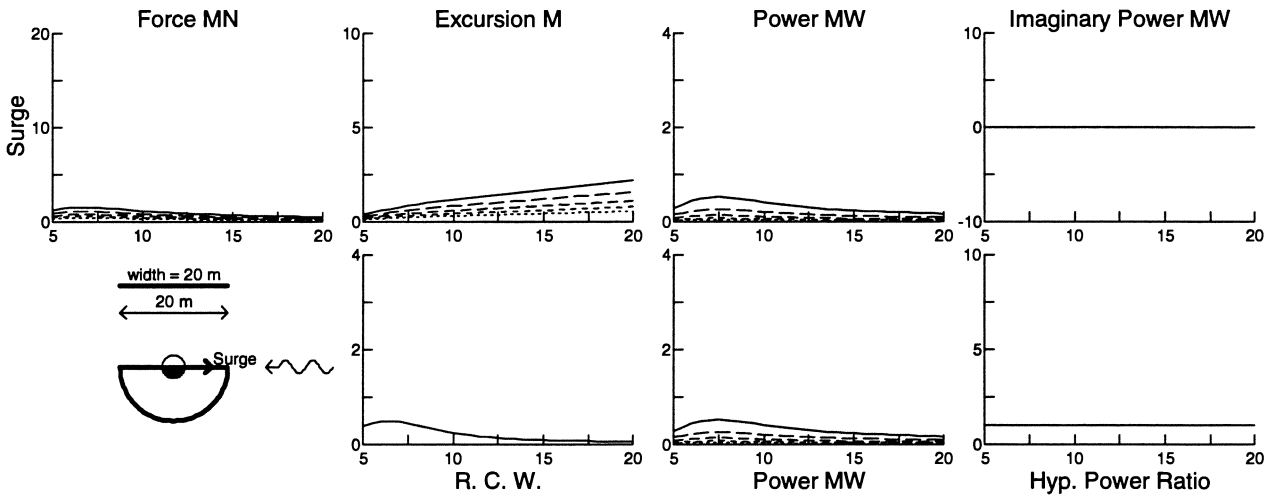

Figure 43: Real control in surge (s_hp) for a 10m radius hemisphere .

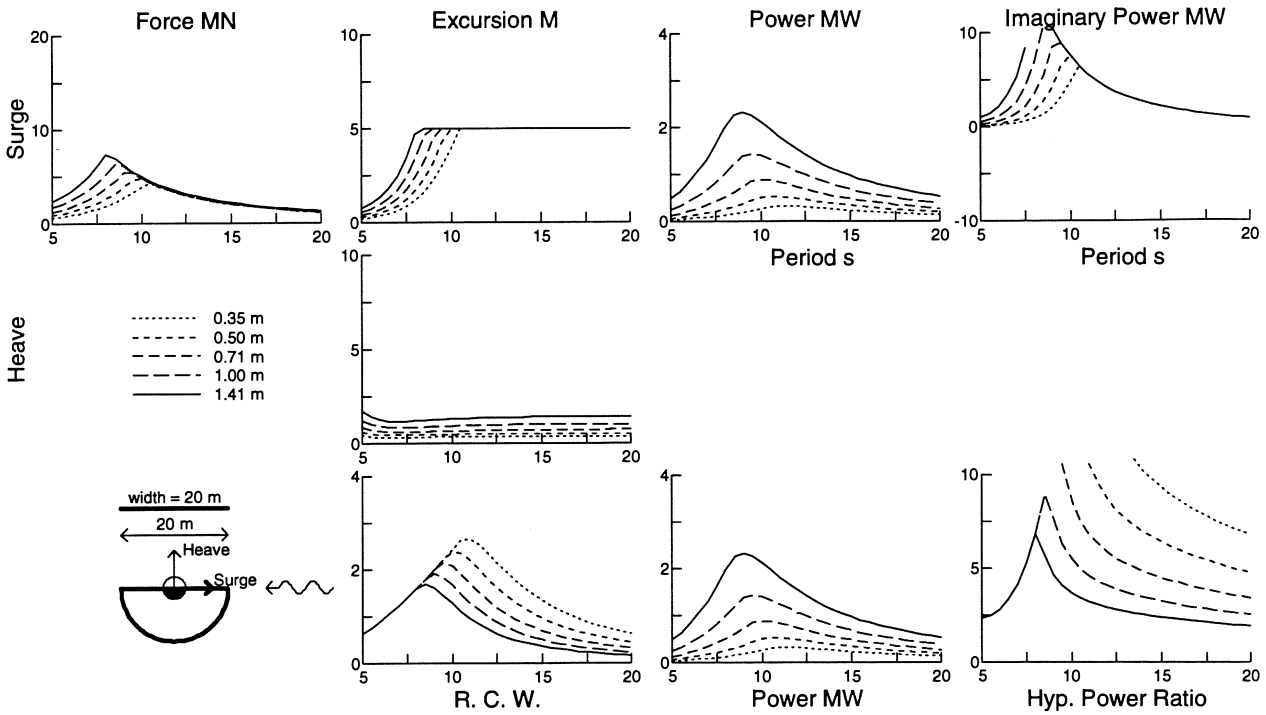

Figure 44: Complex control in surge (s_h_p) for a 10m radius hemisphere .

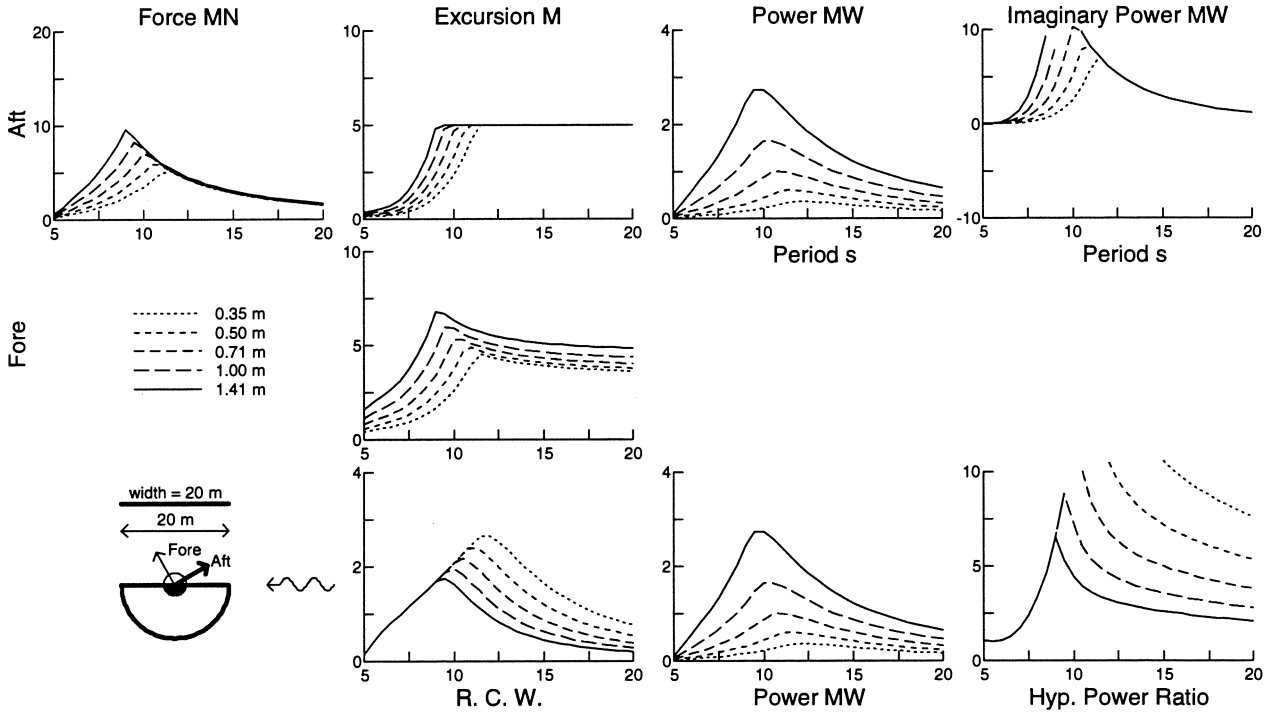

Figure 45: Complex control for 30 degrees aft for a 10m radius hemisphere .

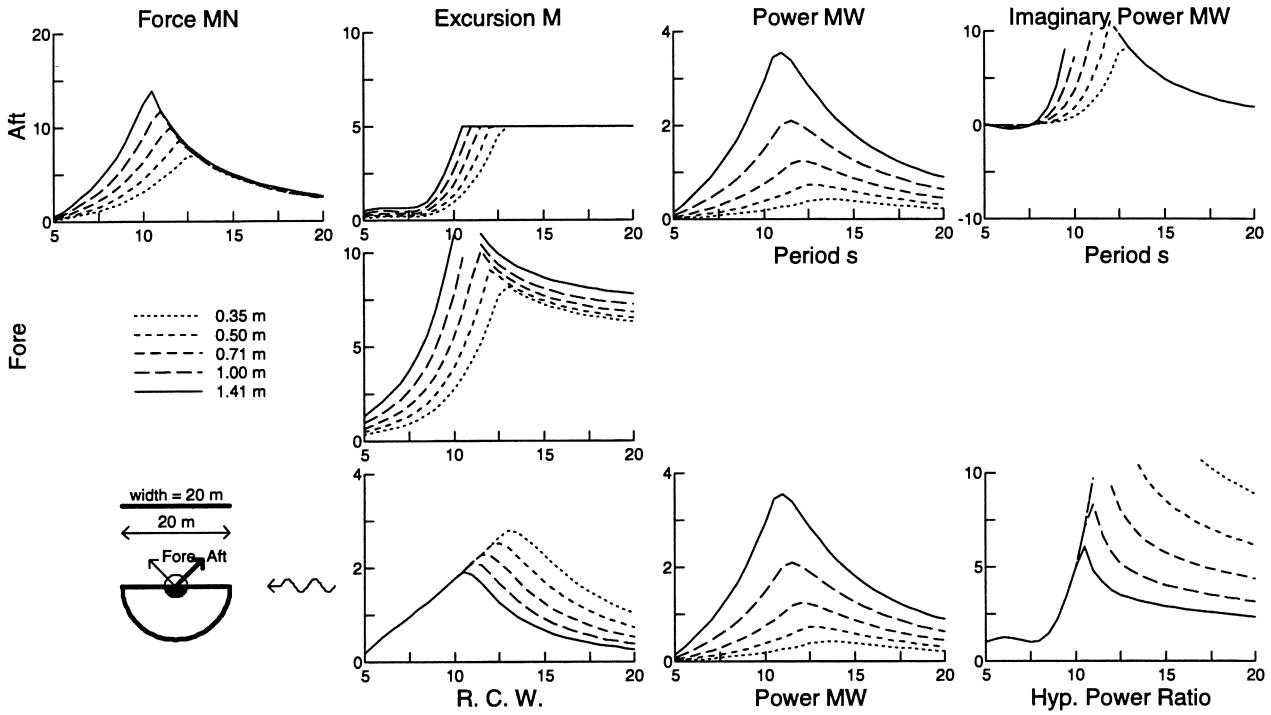

Figure 46: Complex control for 45 degrees aft for a 10m radius hemisphere .

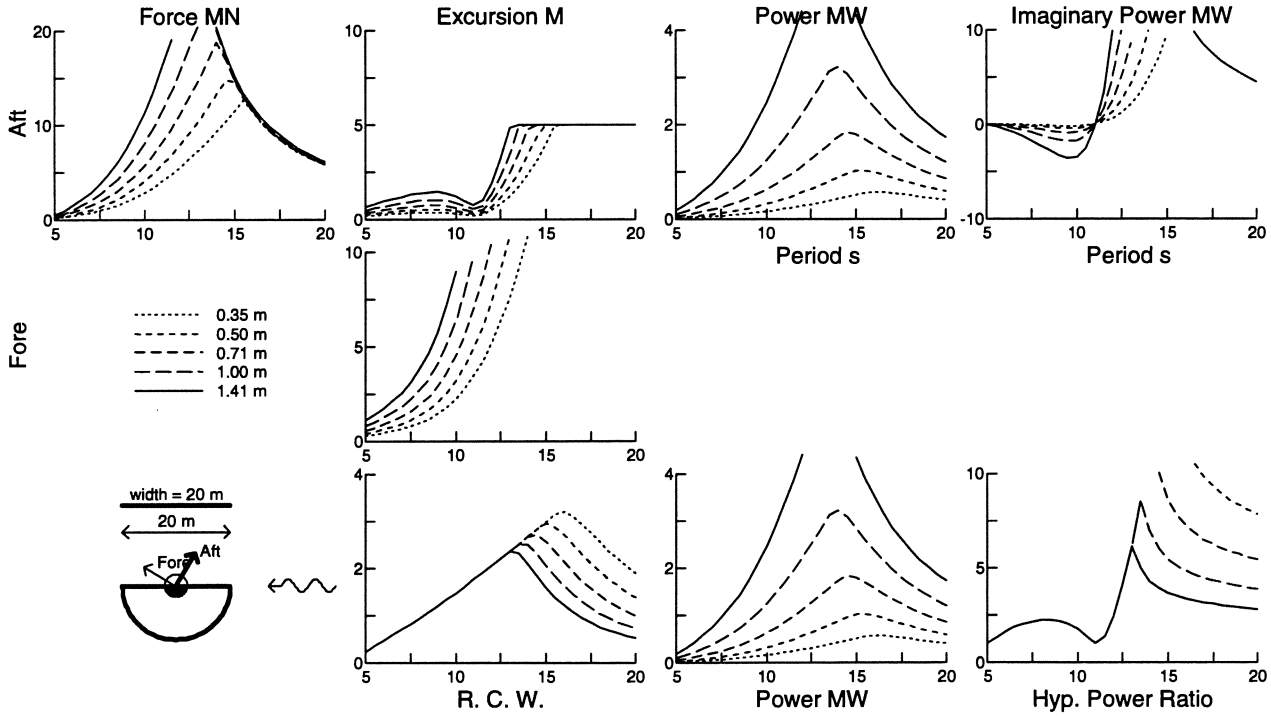

Figure 47: Complex control for 60 degrees aft for a 10m radius hemisphere .

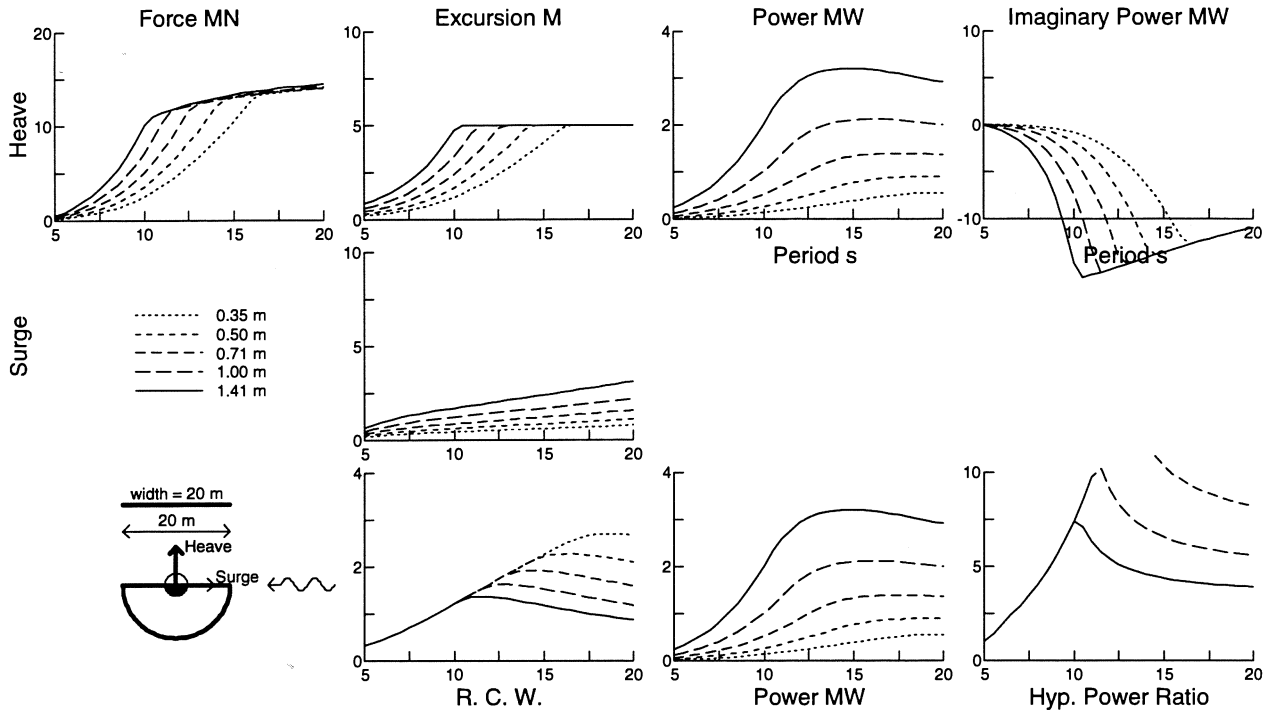

Figure 48: Complex control in heave (h_s_p) for a 10m radius hemisphere .

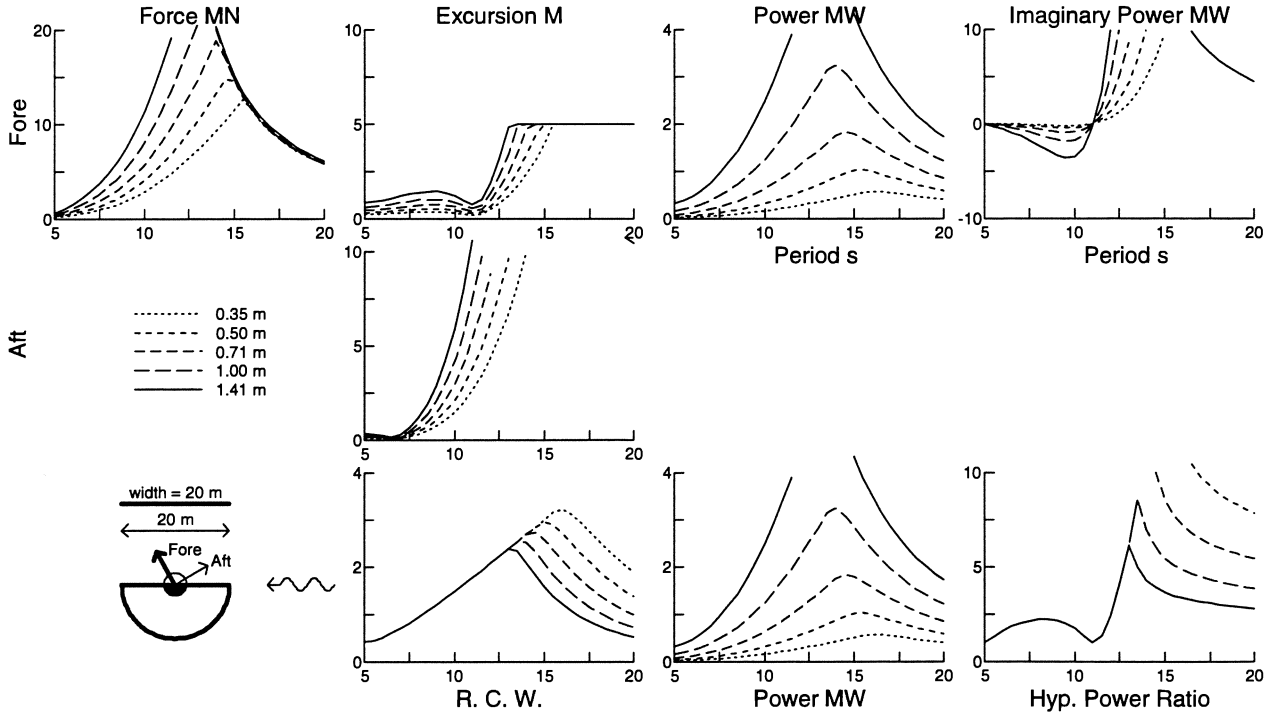

Figure 49: Complex control for 30 degrees fore for a 10m radius hemisphere .

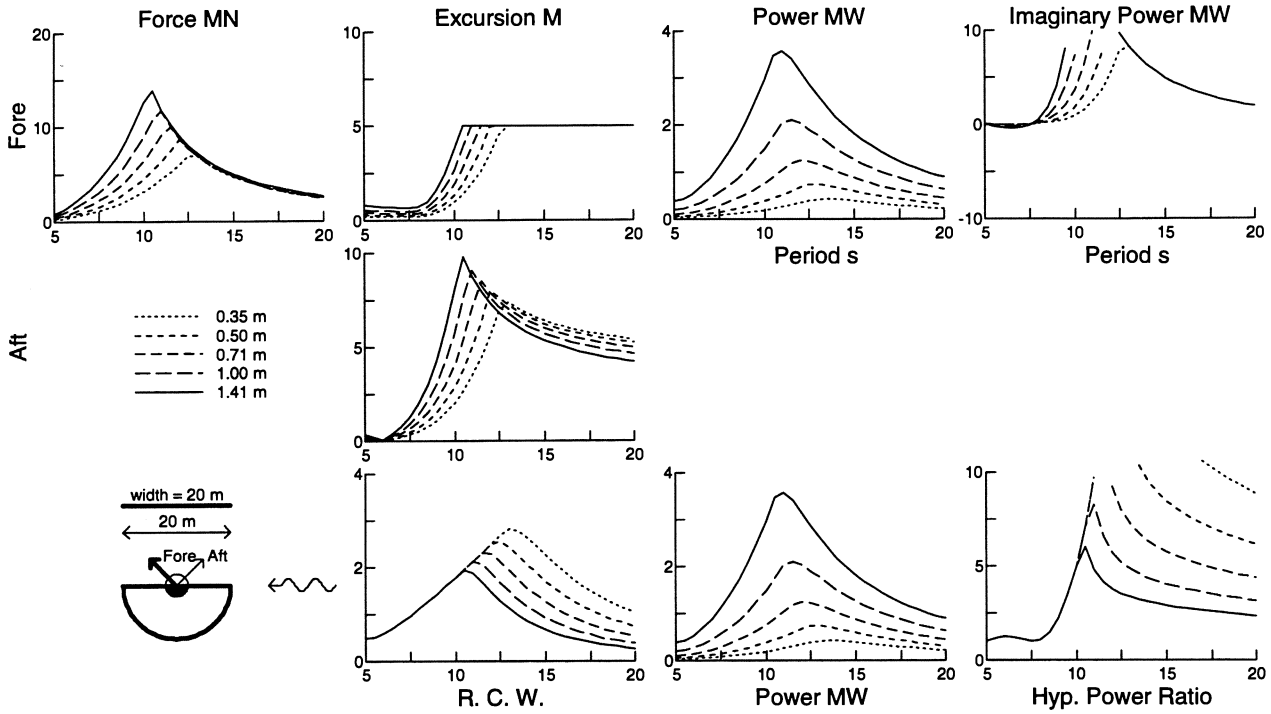

Figure 50: Complex control for 45 degrees fore for a 10m radius hemisphere .

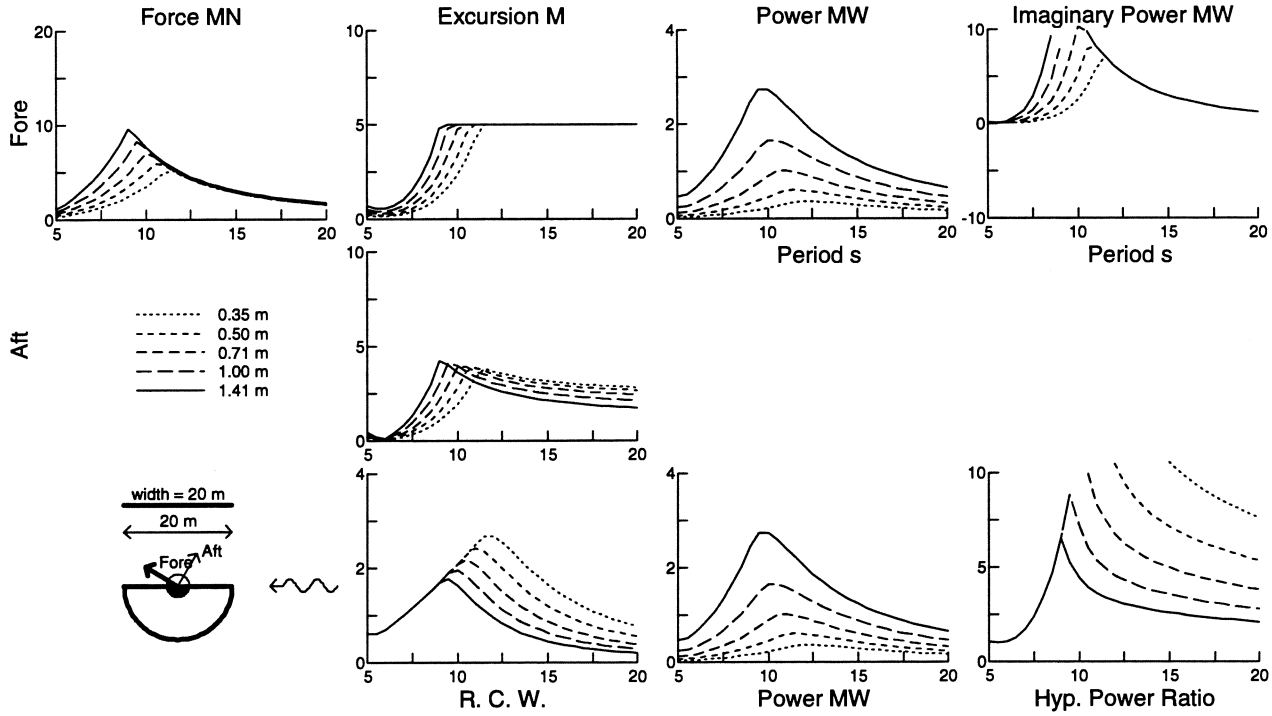

Figure 51: Complex control for 60 degrees fore for a 10m radius hemisphere .

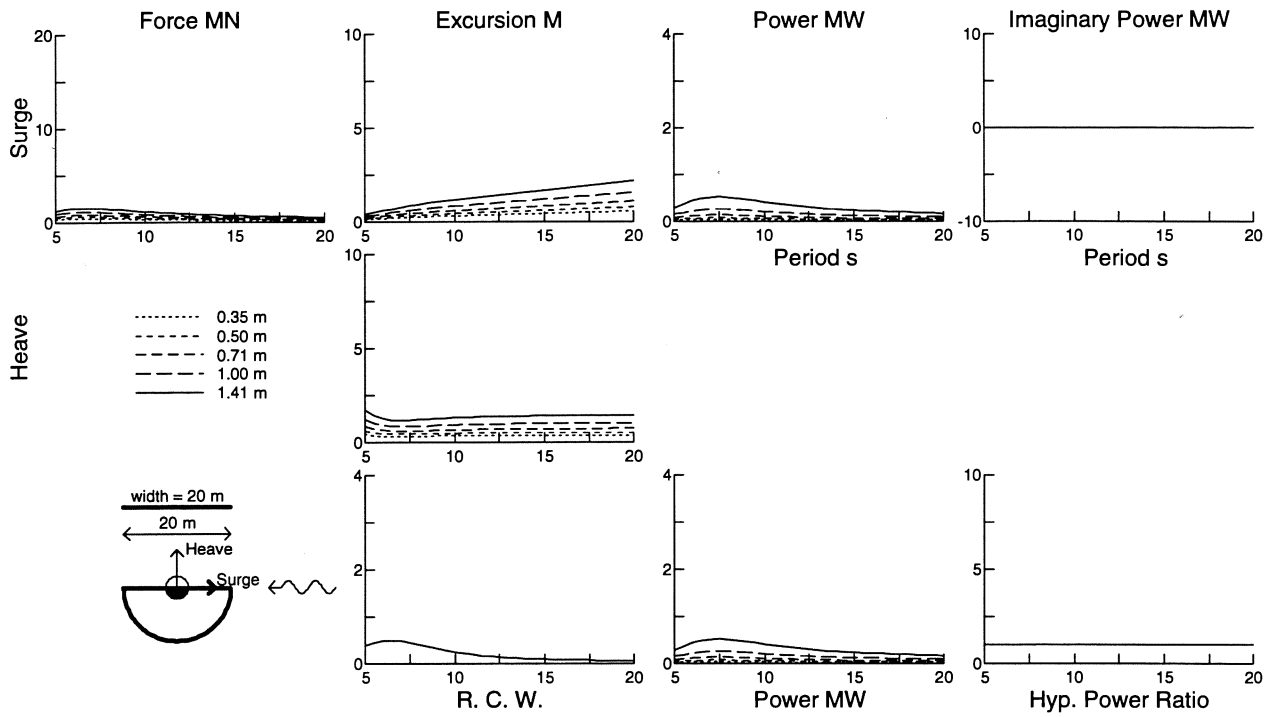

Figure 52: Real control in surge (s_h_p) for a 10m radius hemisphere .

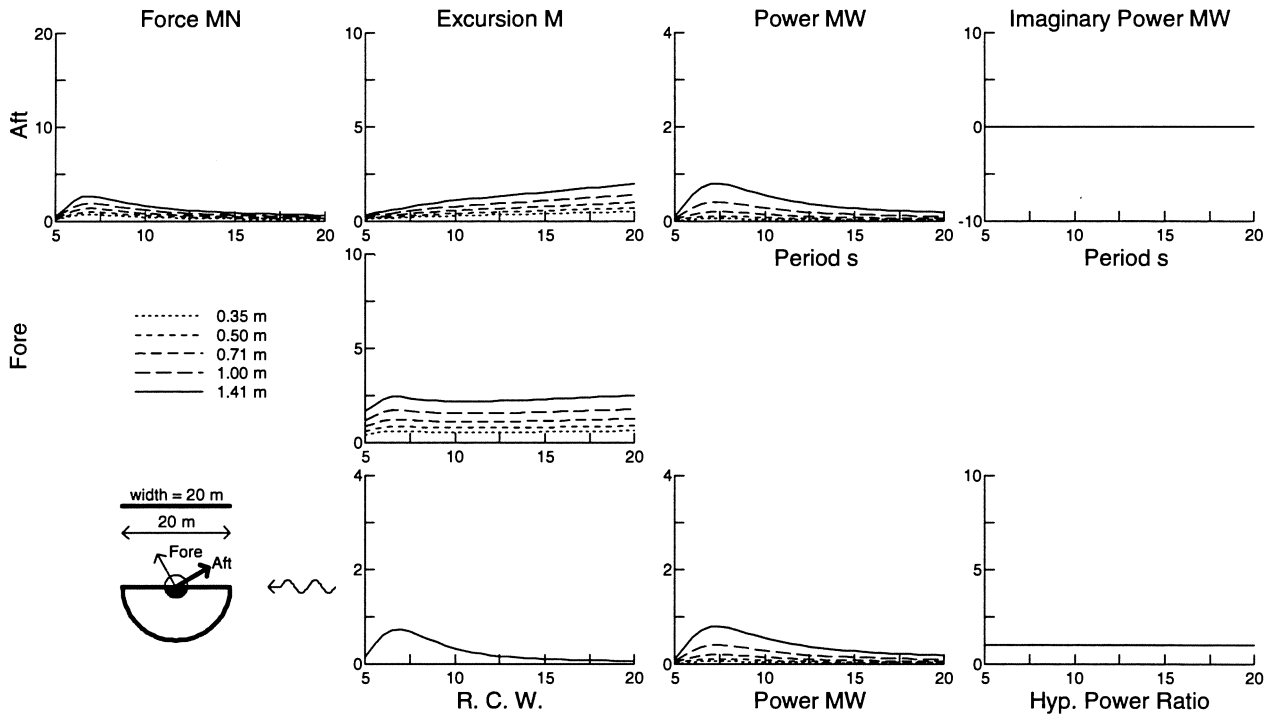

Figure 53: Real control for 30 degrees aft for a 10m radius hemisphere .

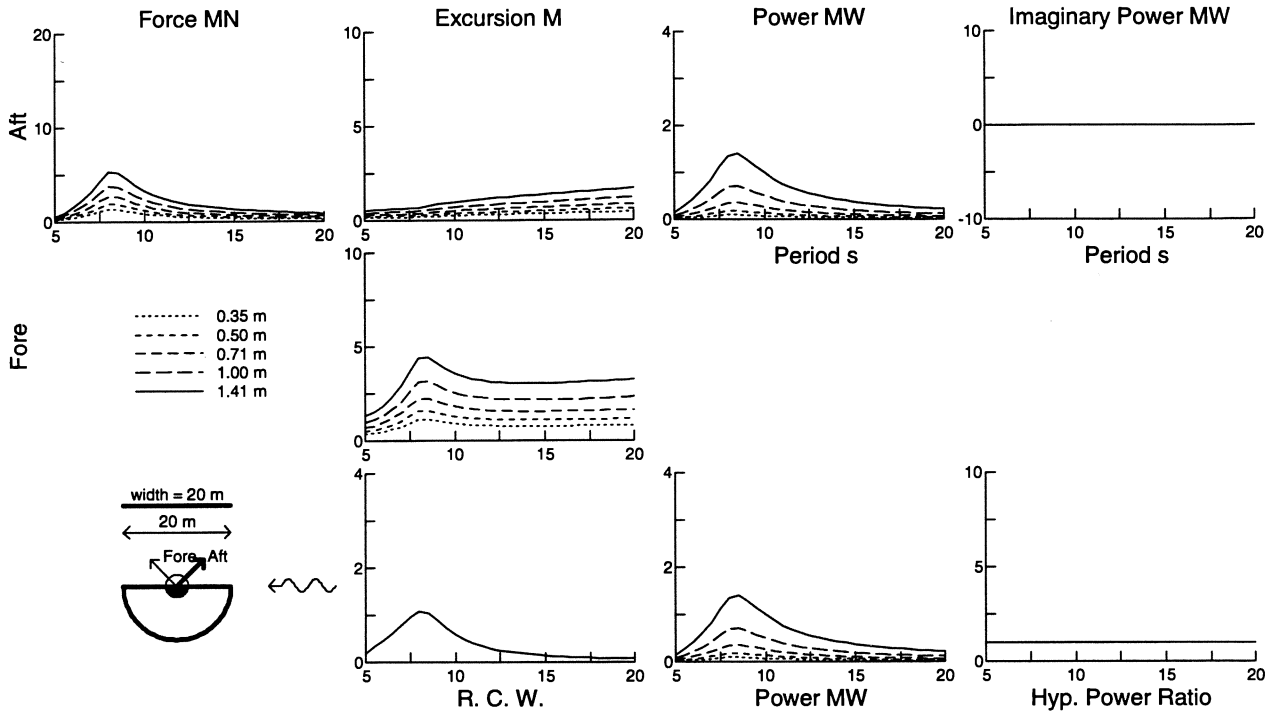

Figure 54: Real control for 45 degrees aft for a 10m radius hemisphere .

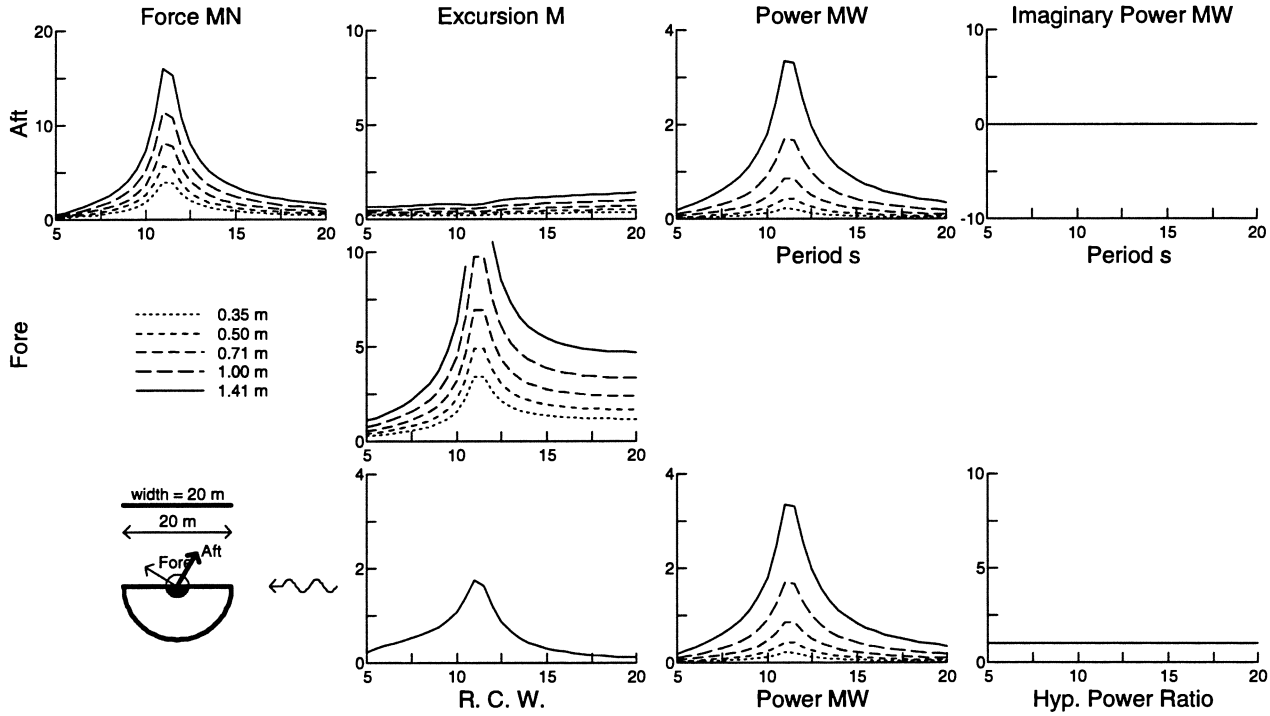

Figure 55: Real control for 60 degrees aft for a 10m radius hemisphere .

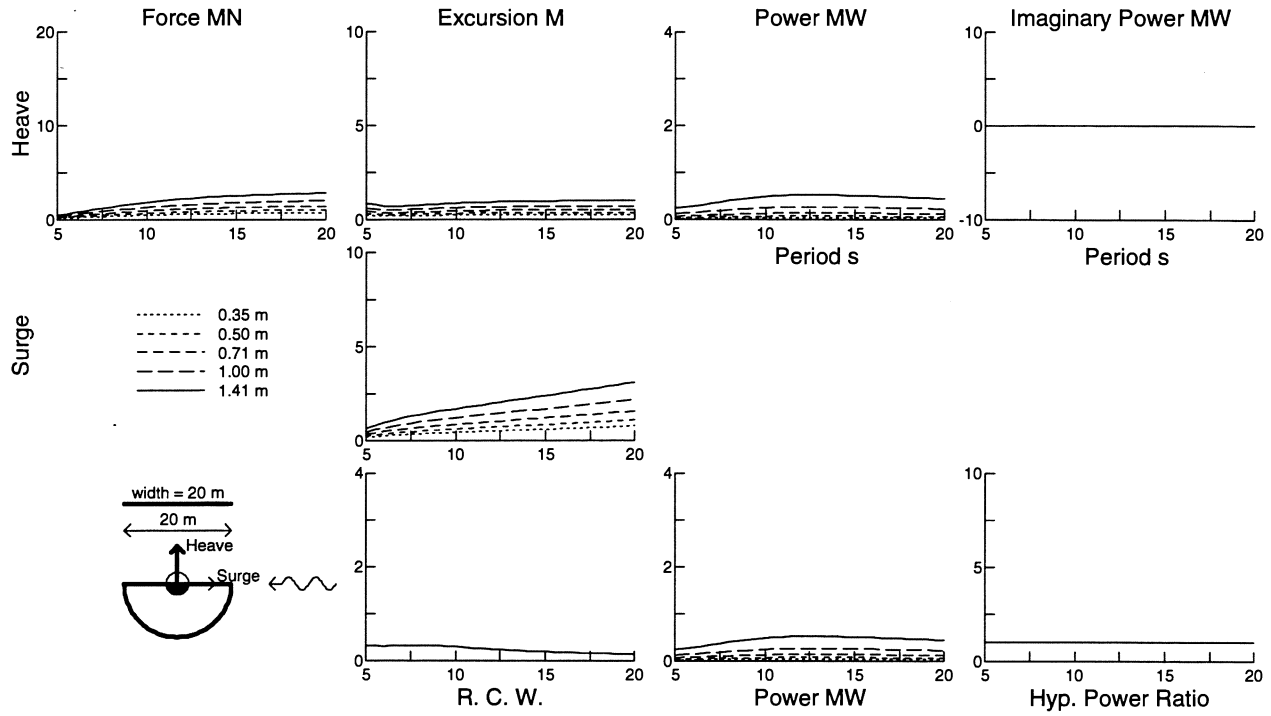

Figure 56: Real control in heave (h_s_p) for a 10m radius hemisphere .

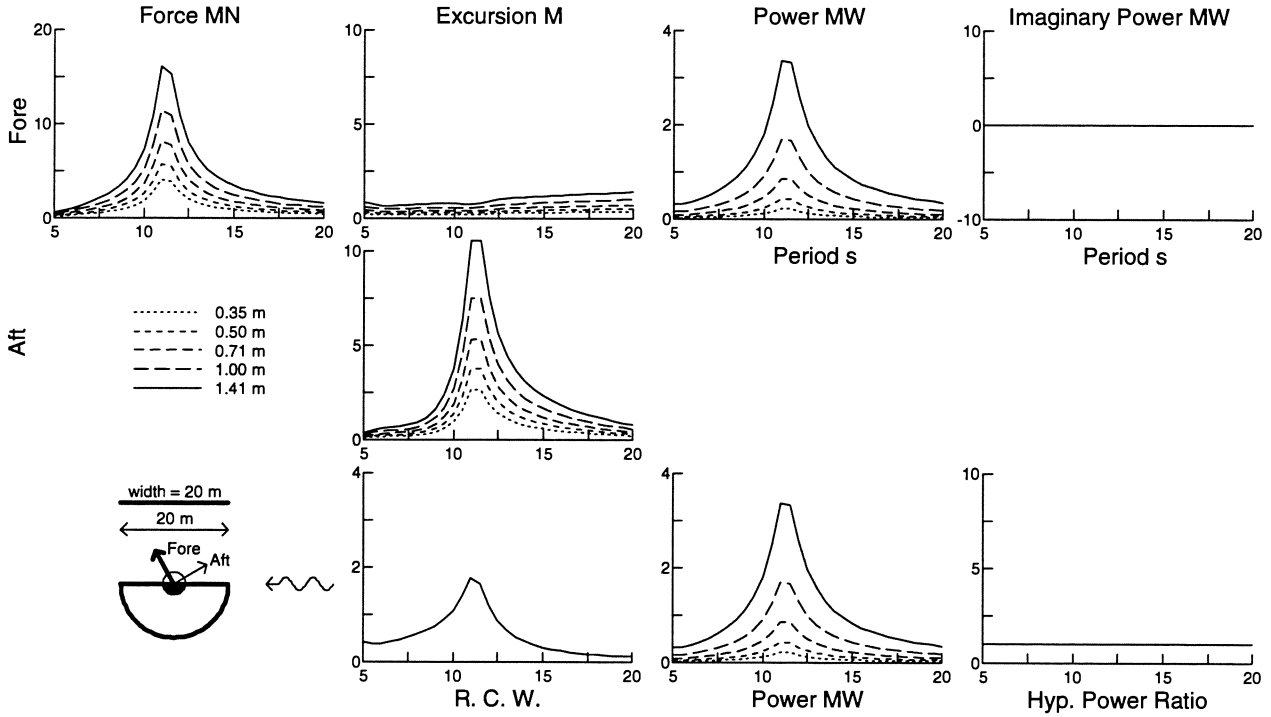

Figure 57: Real control for 30 degrees fore for a 10m radius hemisphere .

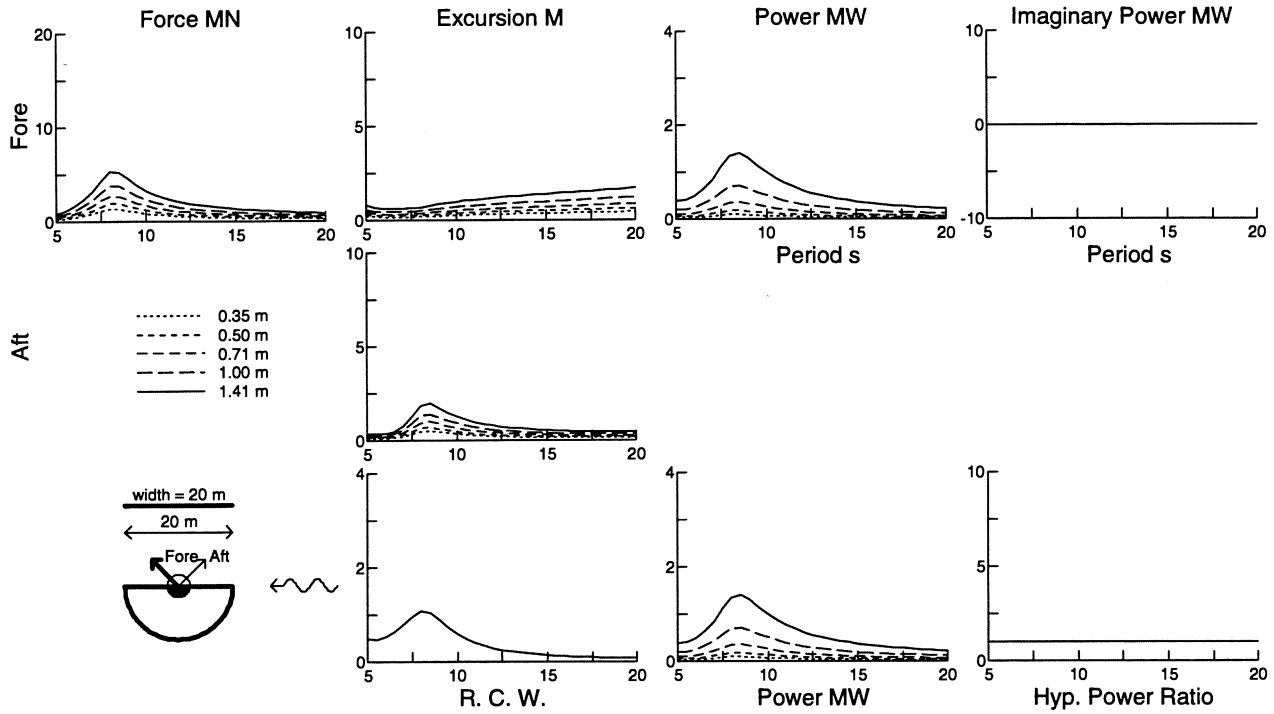

Figure 58: Real control for 45 degrees fore for a 10m radius hemisphere .

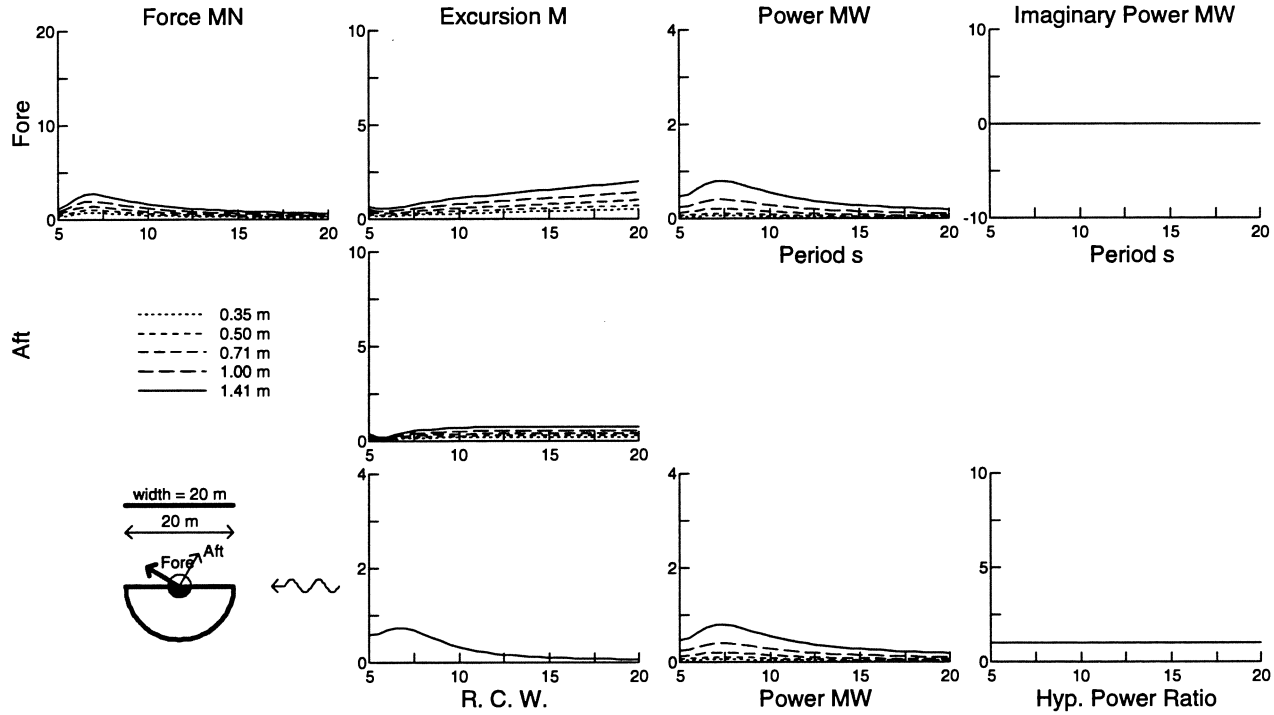

Figure 59: Real control for 60 degrees fore for a 10m radius hemisphere .

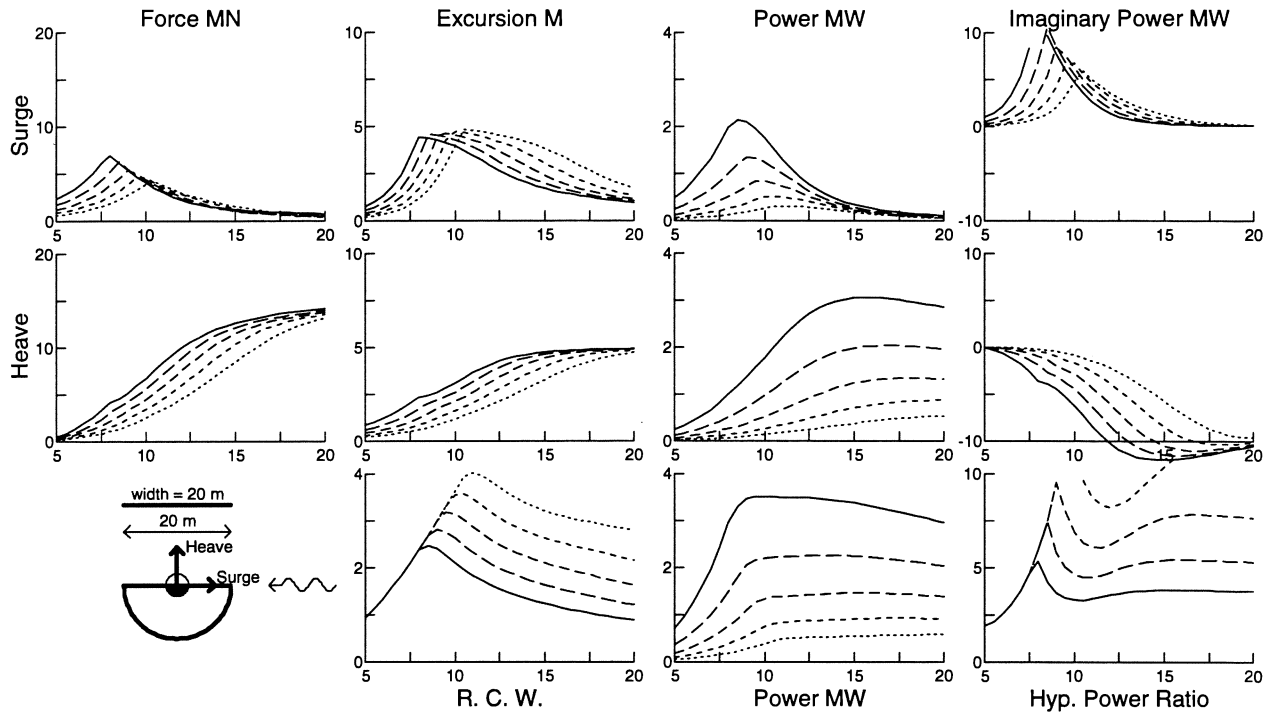

Figure 60: Complex control in surge and heave (sh_p) for a 10m radius hemisphere .

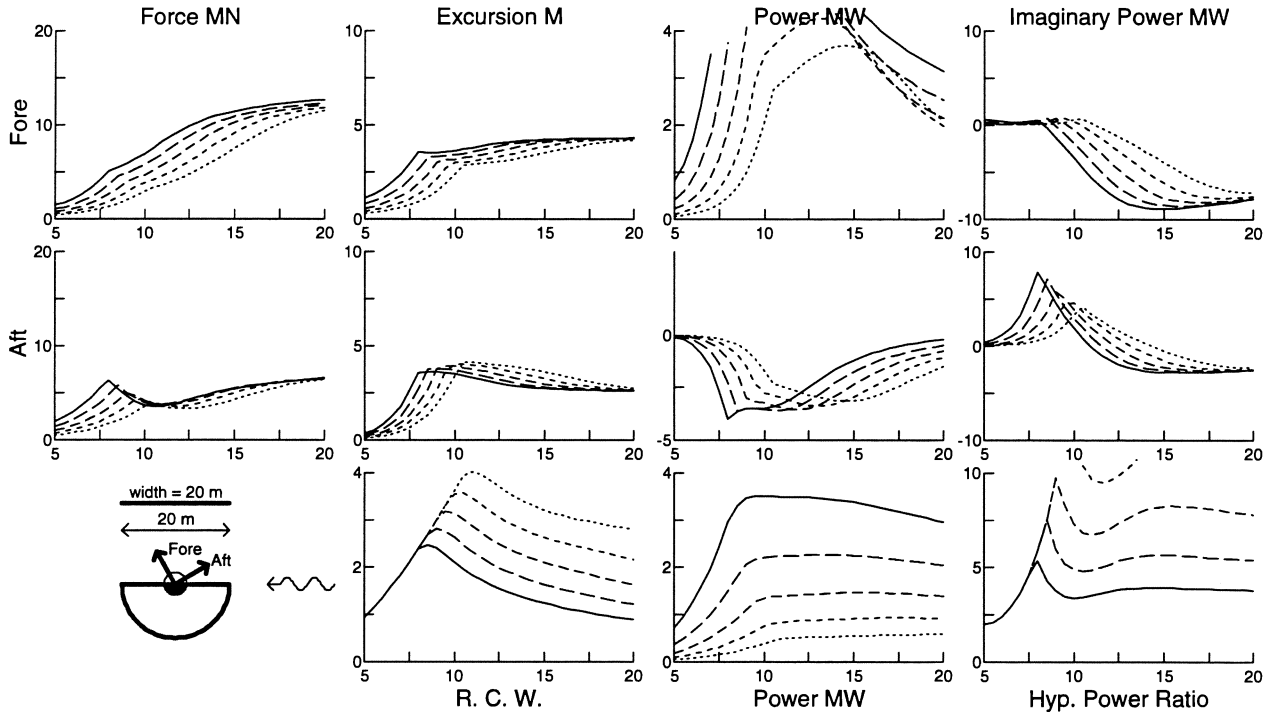

Figure 61: Complex control for 30 deg fore & aft for a 10m radius hemisphere .

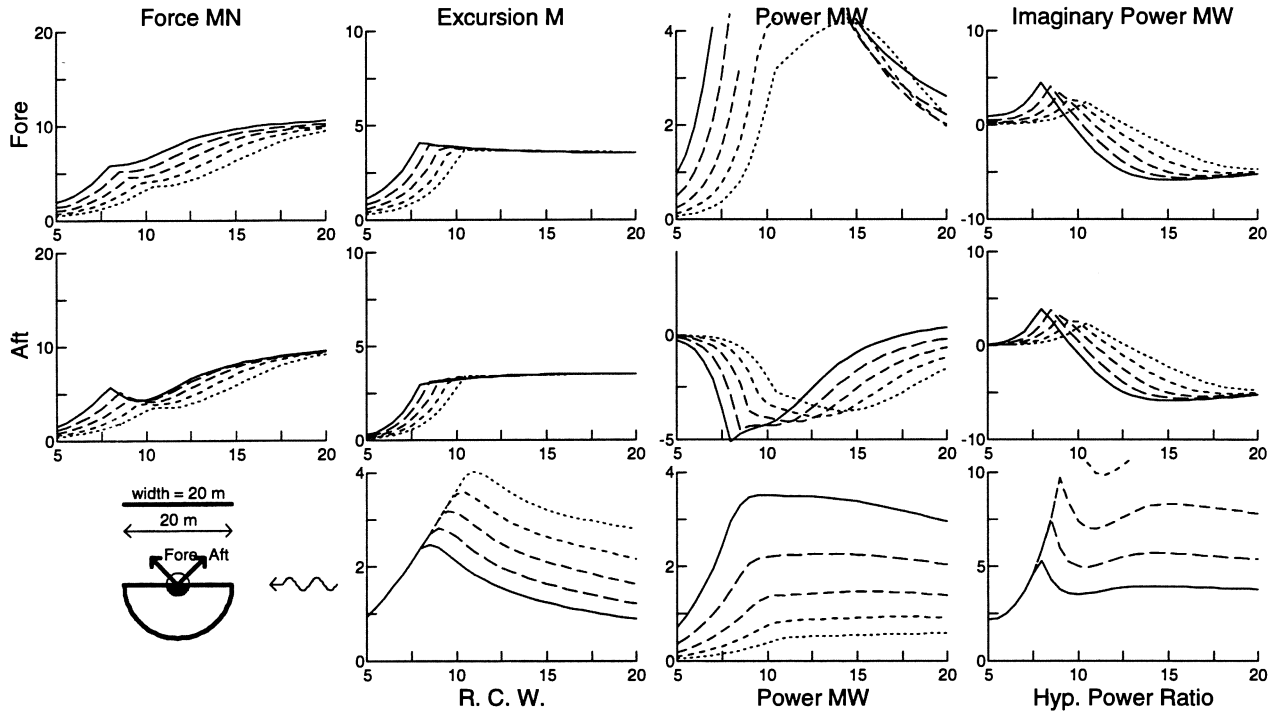

Figure 62: Complex control for 45 deg fore & aft for a 10m radius hemisphere .

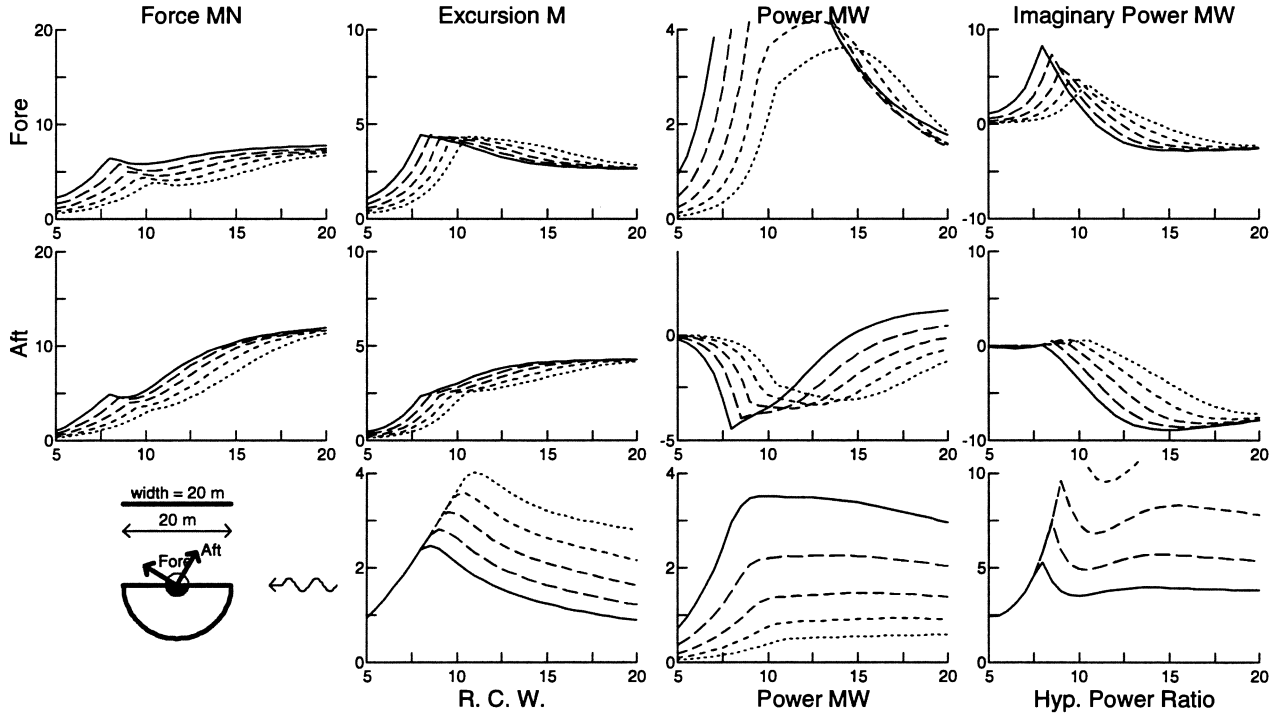

Figure 63: Complex control for 60 deg fore & aft for a 10m radius hemisphere .

5.5 Variation of Geometry

The effect of variations in geometry is investigated by considering simple volume-conserving transformations of the 20 metre diameter hemisphere. These are specified by: x-stretch, y-stretch, z-stretch and xz-shear. The xz-shear is a translation in the x-direction proportional to a z-offset from the water-plane, z=0. The notation used to describe the resulting ellipsoids is an e, followed by the x-stretch, y-stretch, z-stretch and xz-shear in numbers separated by underscores. For example:

- e10_10_10_0, the 10m radius hemisphere considered in the previous sections
- e10_14_07_0, the half-ellipsoid 28 meters wide, 20 meters 'thick' with a draft of 7 meters
- e10_14_07_1, the duck-like geometry shown in figure 64

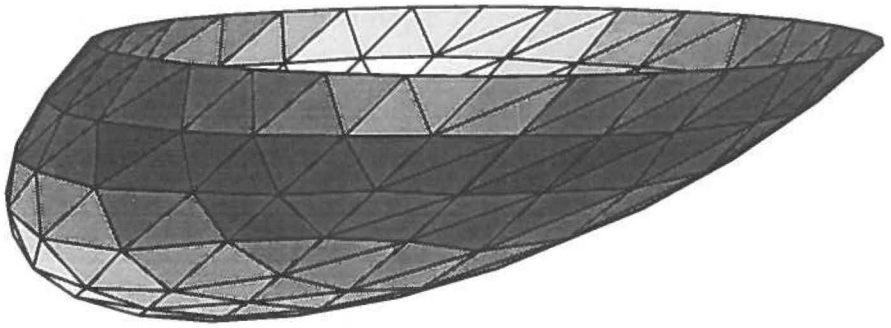

Figure 64: View of the discretisation a duck-like ellipsoid e10_14_07_1

5.5.1 Stretched Hemispheres

The hemisphere is transformed such that one dimension remains unchanged, one dimension is stretched by a factor of $\sqrt{2}$, and the remaining dimension is compressed by a factor of $\sqrt{2}$.

Results are presented for the single degree of freedom case with the optimal complex control.

In figure 65 the results for the hemisphere (figures 26 to 33) are summarised.

Figures 66 and 67 show the results for the ellipsoids obtained by keeping the thickness (ie. the dimension in the head-on wave direction) constant and stretching and compressing the remaining dimensions. The 28m wide, 7m draft ellipsoid, e10_14_07_0, has a larger water-plane area than the original hemisphere. Consequently more power is absorbed in the long wave limit for all cases except surge. Conversely the 14m wide, 14m draft ellipsoid, e10_07_14_0, performs worse in the long period limit. In particular, it is noted that the 60° fore case, e10_14_07_0, absorbs more power with lower HPR than the e10_10_10_0 case. For surge the transformations have only a small effect on the results.

Results for transformations with the width invariant are shown in figures 68 and 69. In the long wave limit the e14_10_07_0 case produces larger powers due to the larger water-plane area (excluding the surge case). For shorter periods (and at all periods for surge), the e07_10_14_0 case produces more power.

With the draft invariant, the water plane area is also unchanged and it is seen that (figures 70 and 71) in all cases (except surge) the long period power absorbed is unaffected by the transformation. At lower periods the wider hemisphere attains the largest power absorption.

Out of the six transformations in the 8 different degrees of freedom considered, the highest powers are attained by the e07_14_10_0 ellipsoid in the 60° fore degree of freedom.

5.5.2 Sheared Hemisphere

Results for the positive and negative sheared hemispheres (e10_10_10_1 and e10_10_10_-1) are shown in figures 72 and 73. It is seen that the shear does not affect the results for periods above about 12 seconds.

At low periods the positive shear gives reduced power absorption in surge and aft degrees of freedom, but increased power for heave and fore degrees of freedom.

The negative shear does not affect power absorption in surge and heave, gives more power for aft cases and less power for fore cases.

5.5.3 Stretched and Sheared Hemisphere

Combining the best stretched case with the best sheared case gives the e07_14_10_1 ellipsoid, figure 74. It is seen that this case performs better than both the best stretched case and the best sheared case.

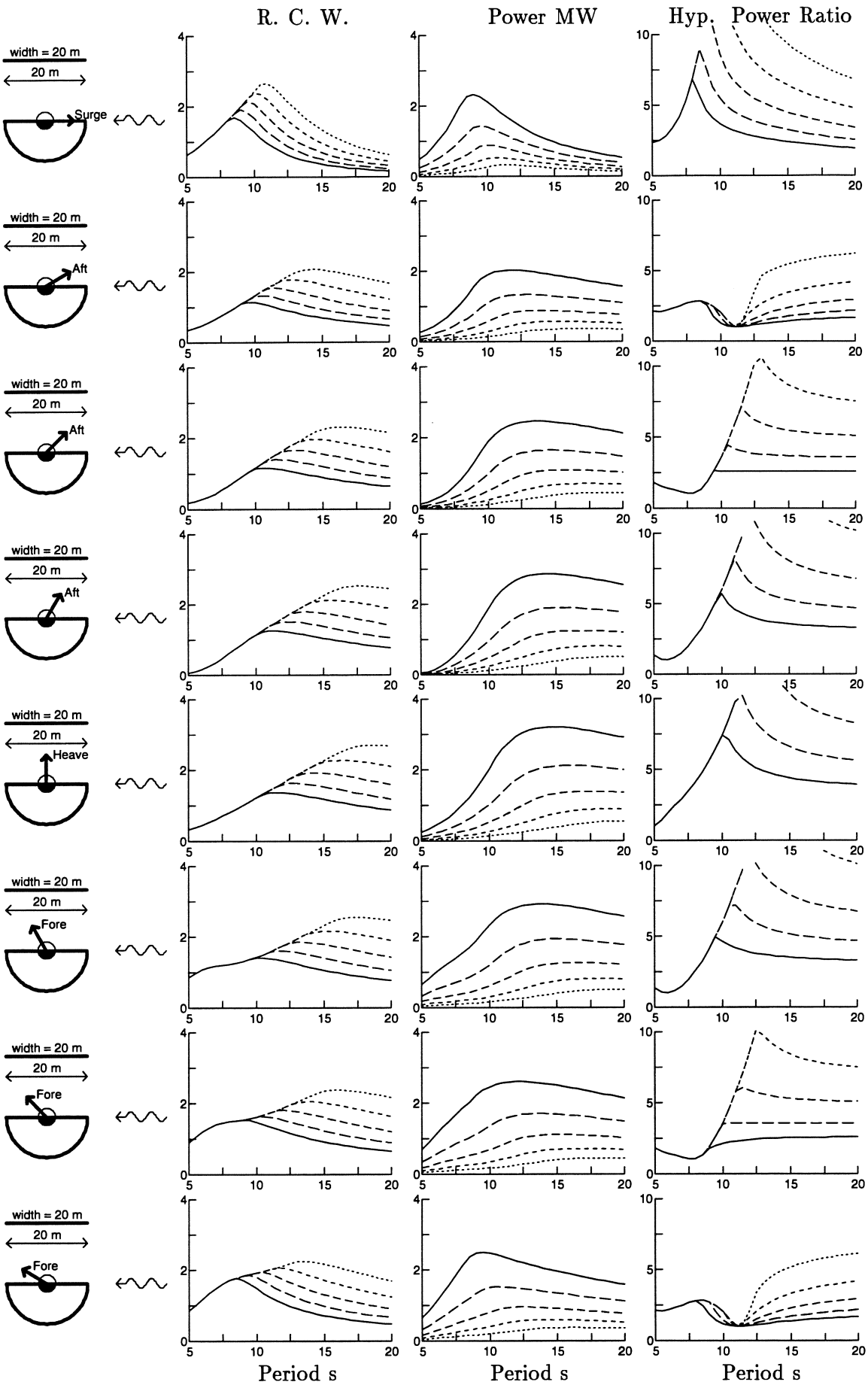

Figure 65: Complex control for 10m radius hemisphere, e10_10_10_0, in a single degree of freedom

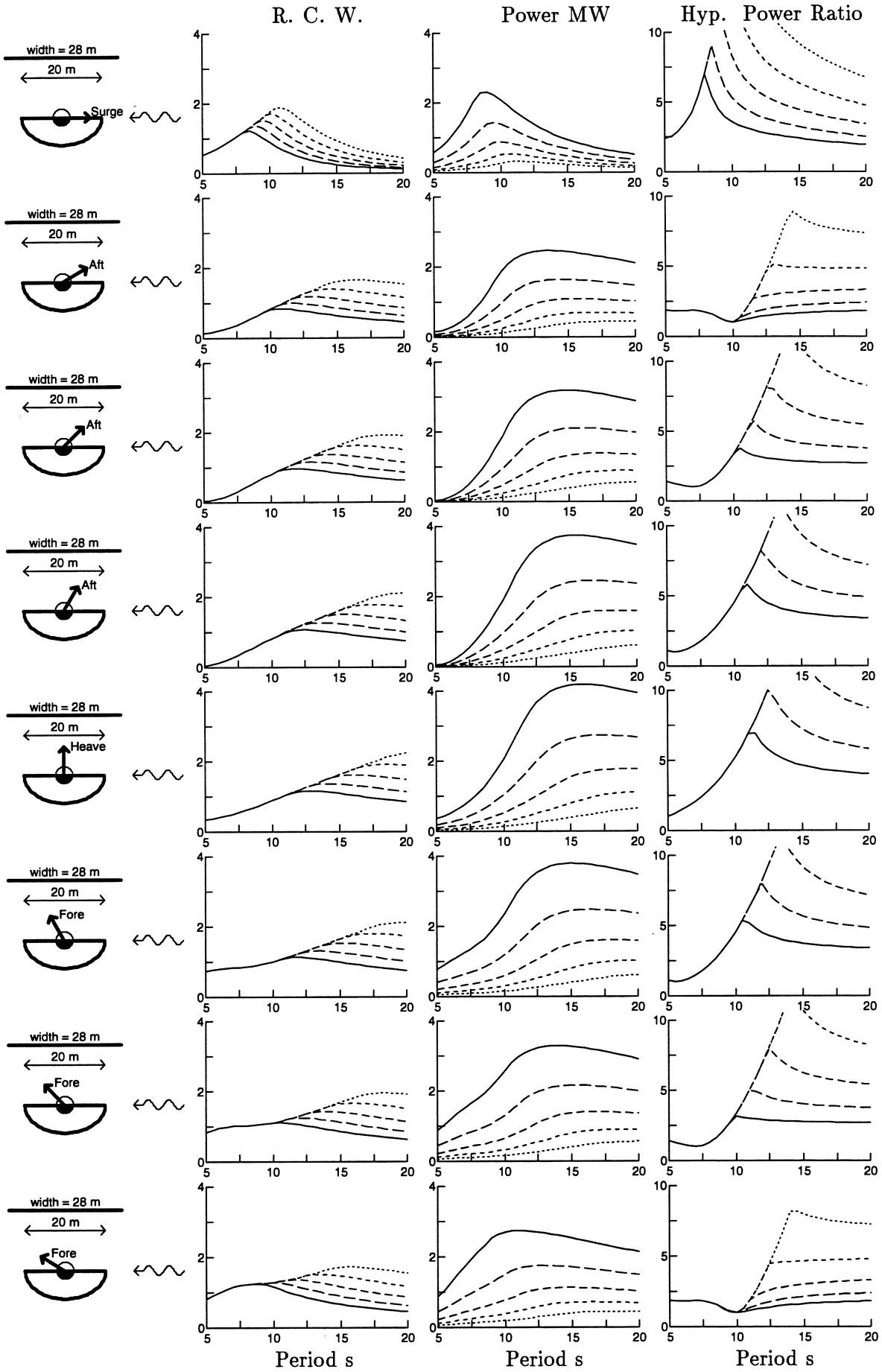

Figure 66: Complex control for a stretched 10m radius hemisphere, e10_14_07_0, in a single degree of freedom

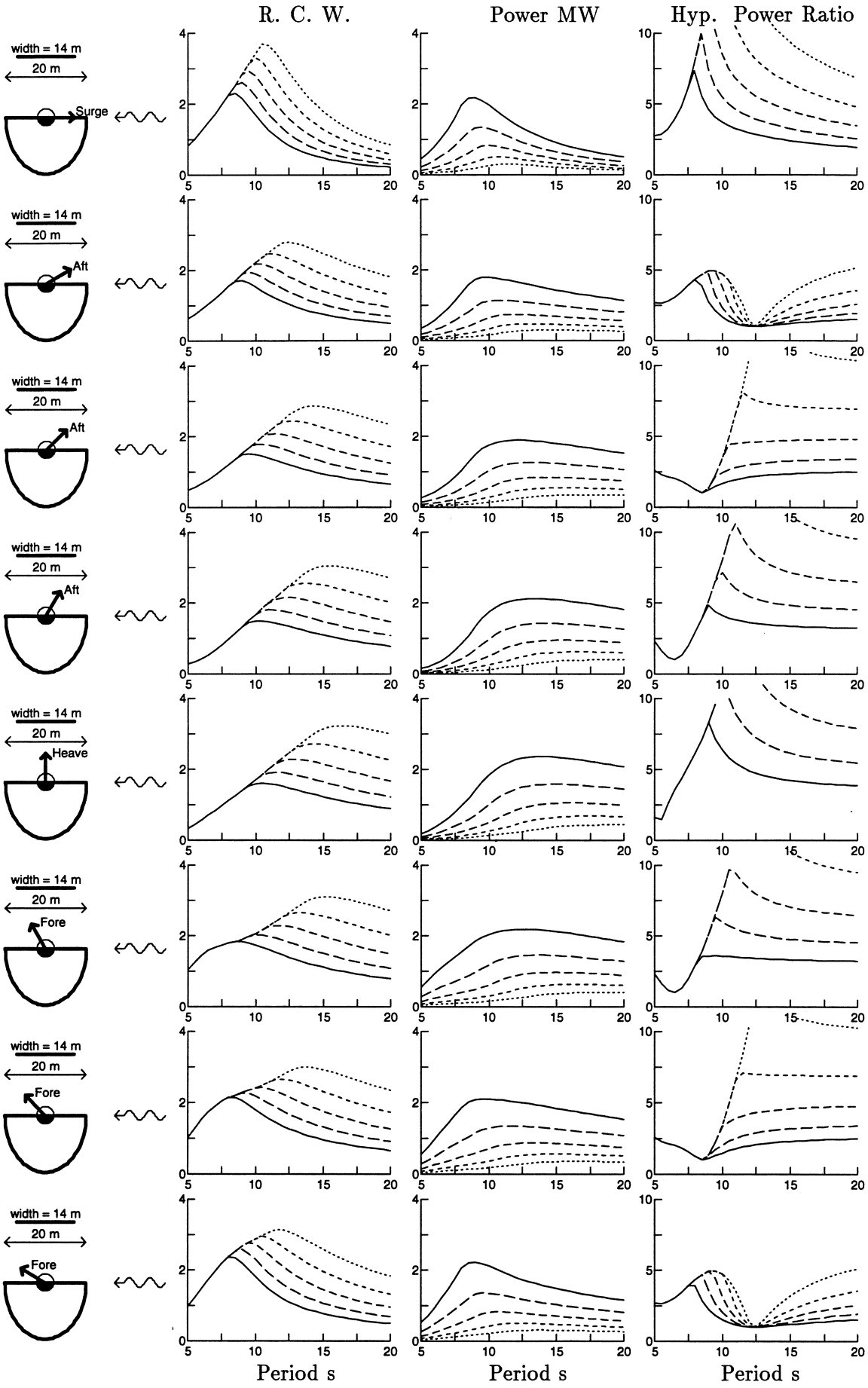

Figure 67: Complex control for a stretched 10m radius hemisphere, e10_07_14_0, in a single degree of freedom

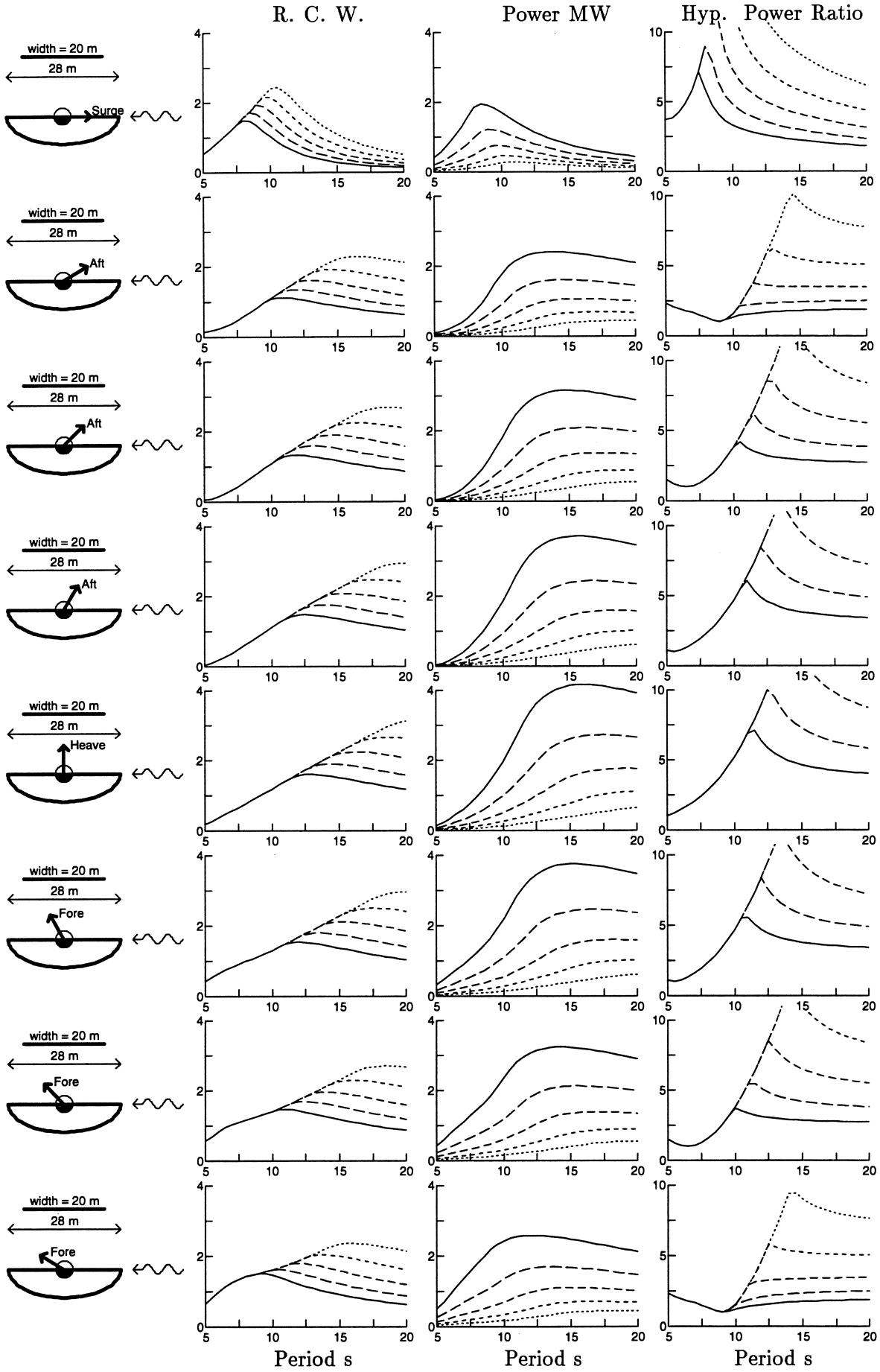

Figure 68: Complex control for a stretched 10m radius hemisphere, e14_10_07_0, in a single degree of freedom

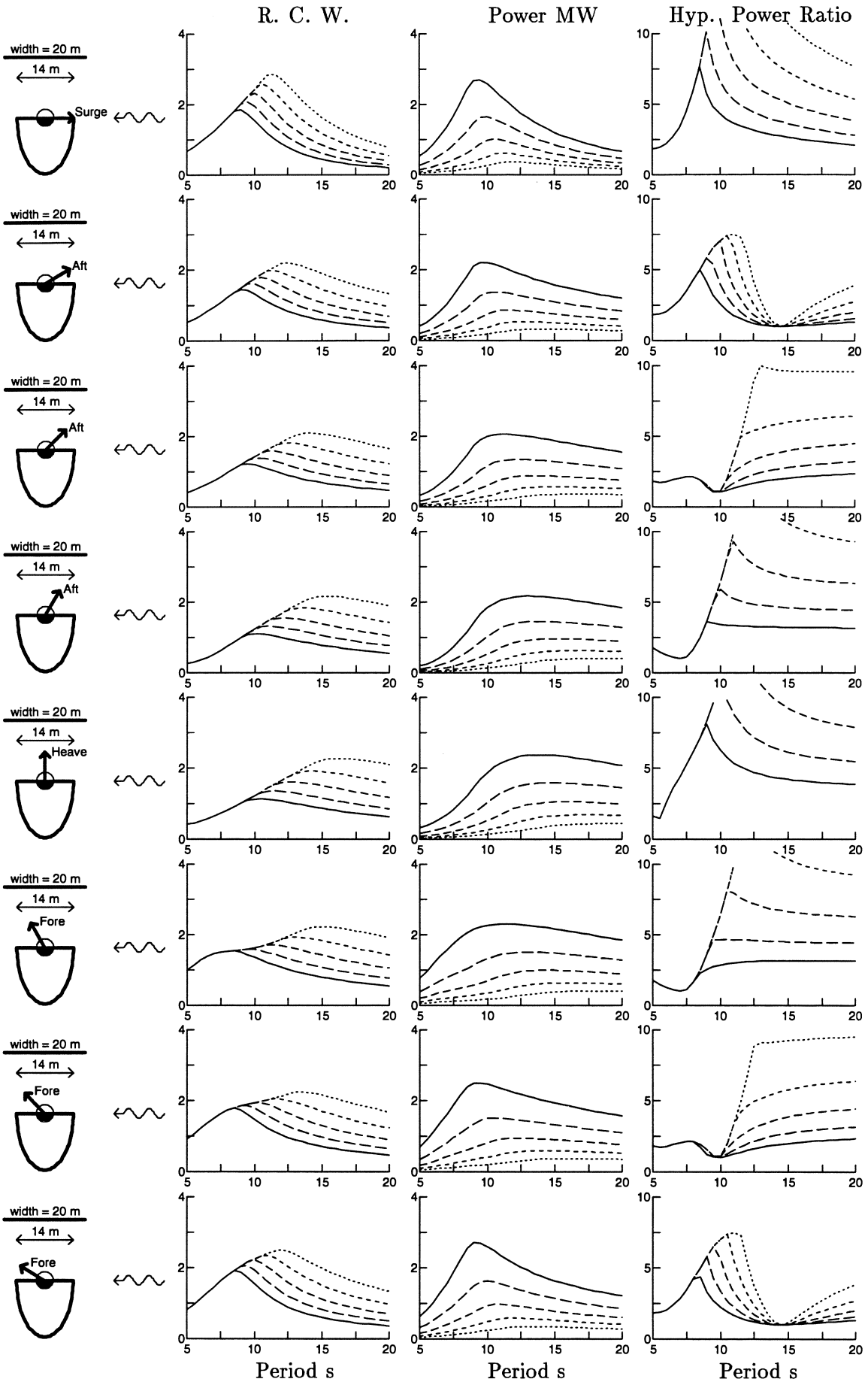

Figure 69: Complex control for a stretched 10m radius hemisphere, e07_10_14_0, in a single degree of freedom

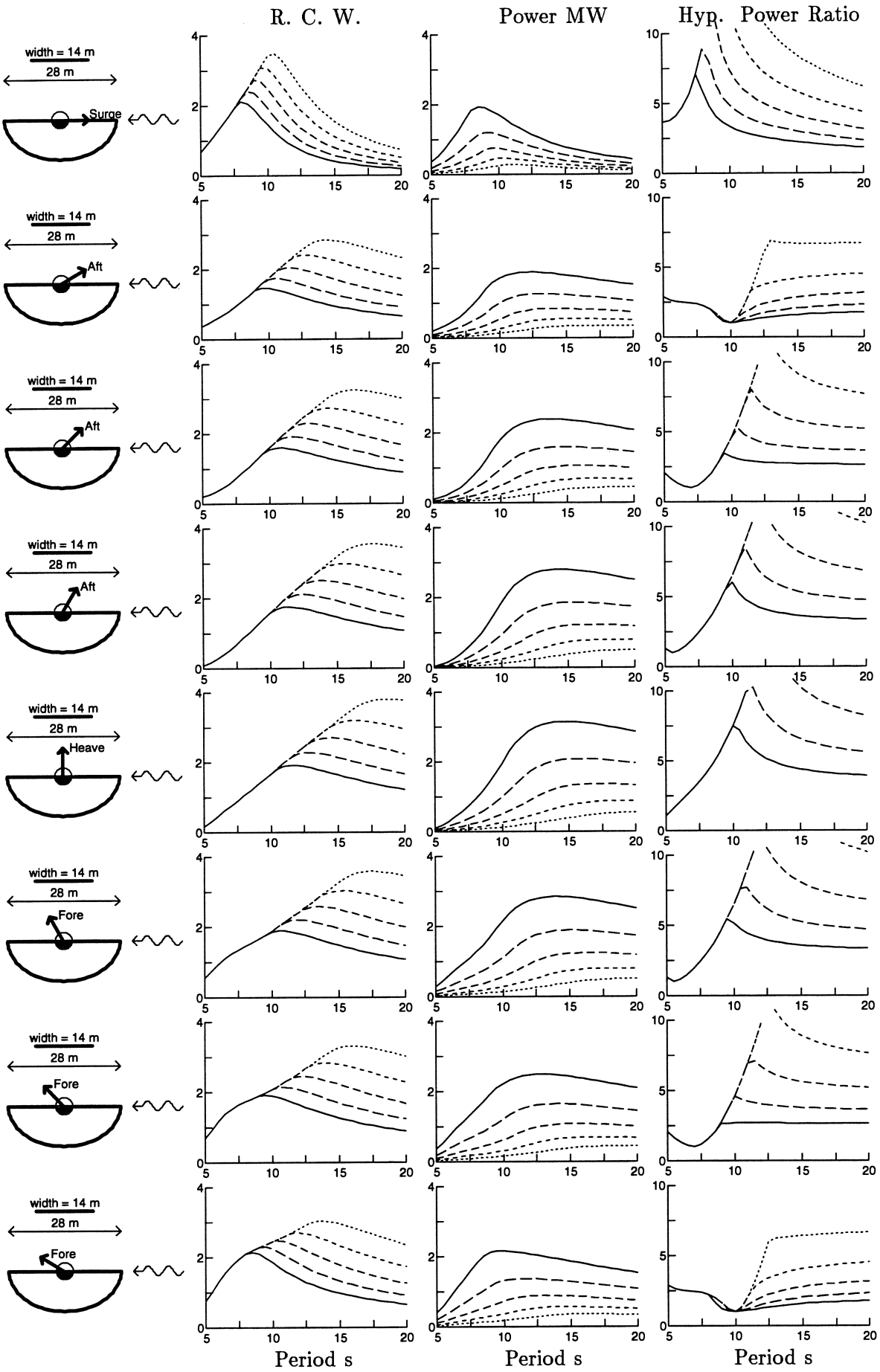

Figure 70: Complex control for a stretched 10m radius hemisphere, e14_07_10_0, in a single degree of freedom

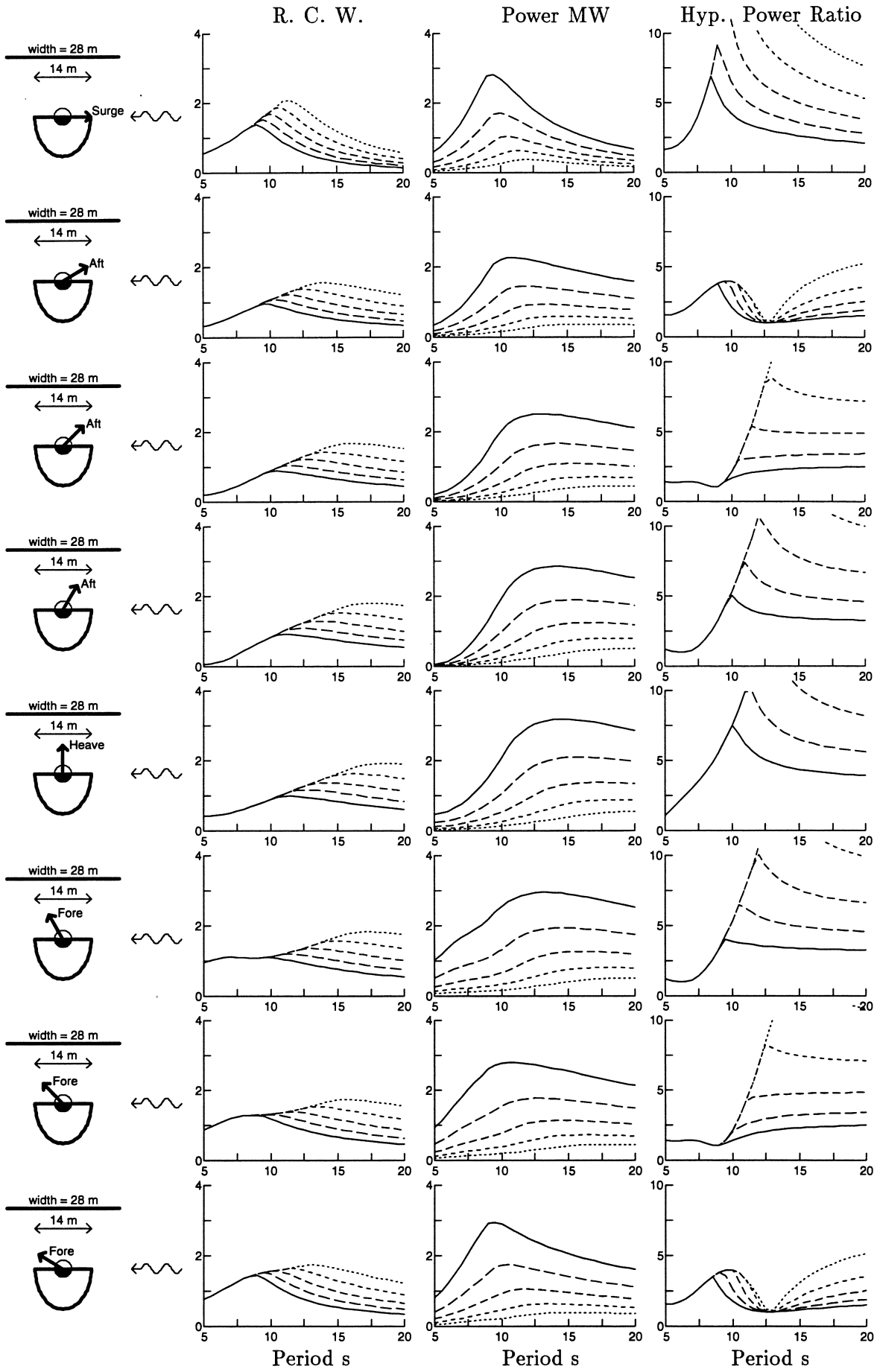

Figure 71: Complex control for a stretched 10m radius hemisphere, e07_14_10_0, in a single degree of freedom

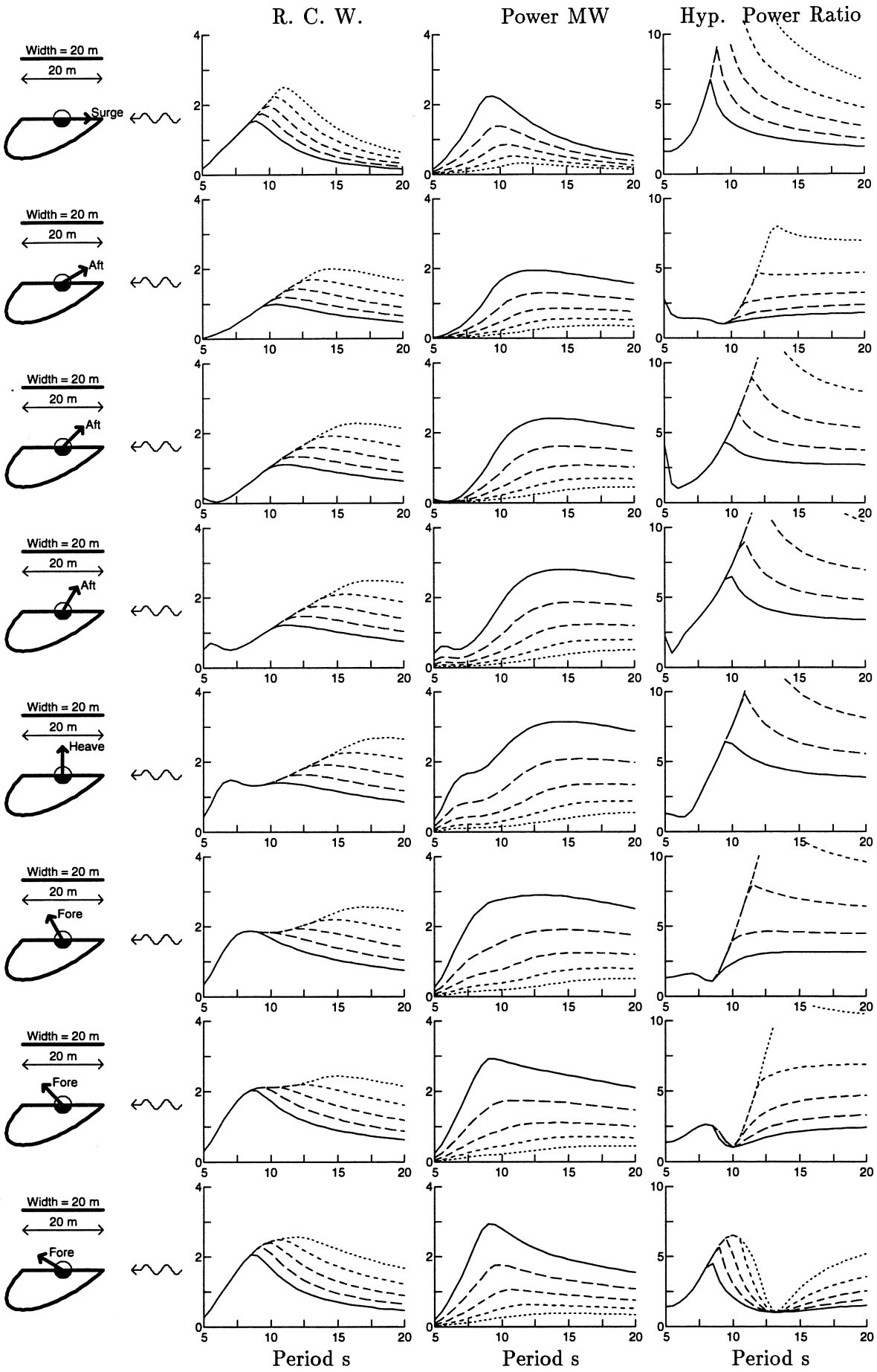

Figure 72: Complex control for a sheared 10m radius hemisphere, e10_10_10_1, in a single degree of freedom

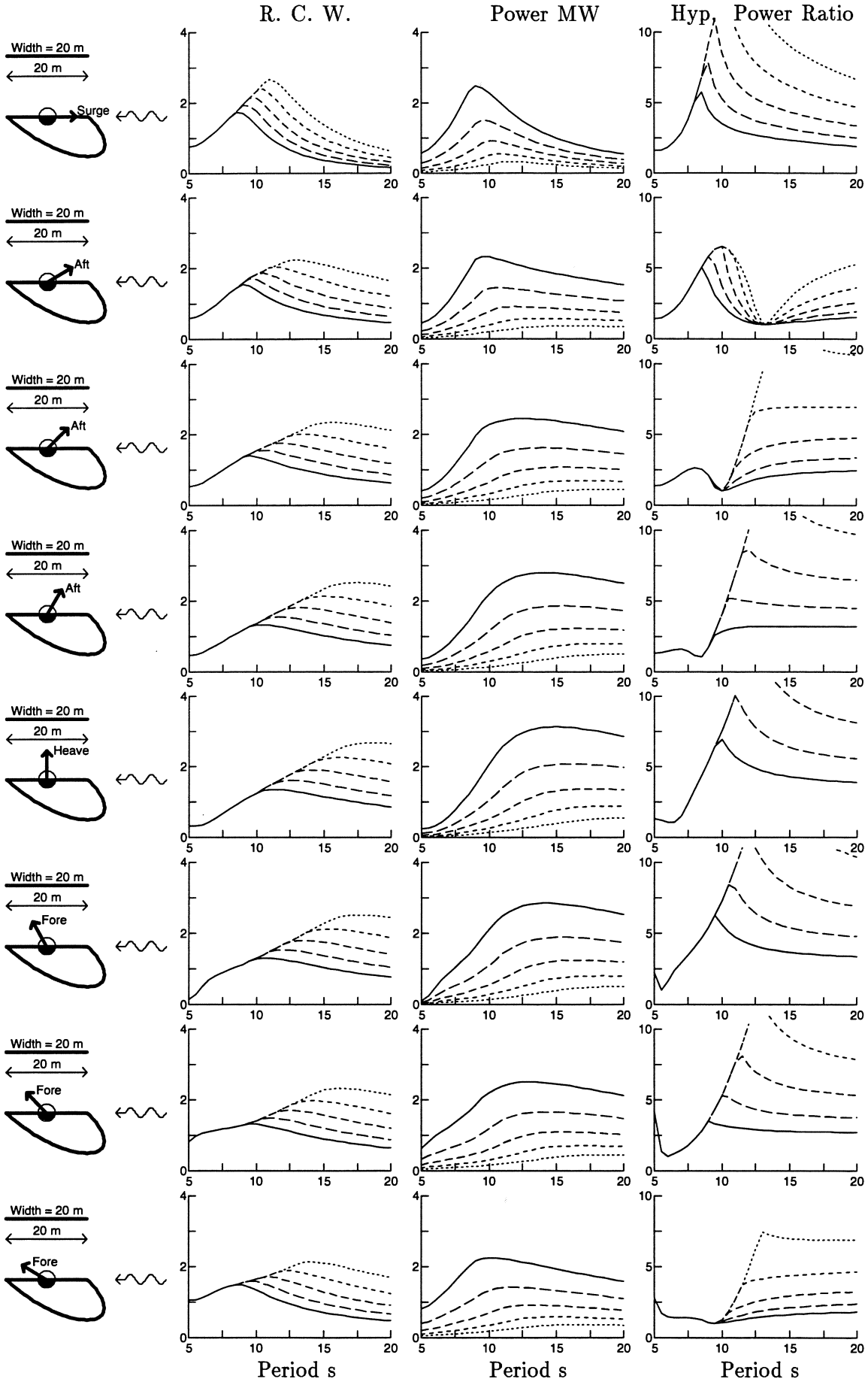

Figure 73: Complex control for a sheared 10m radius hemisphere, e10_10_10_-1, in a single degree of freedom

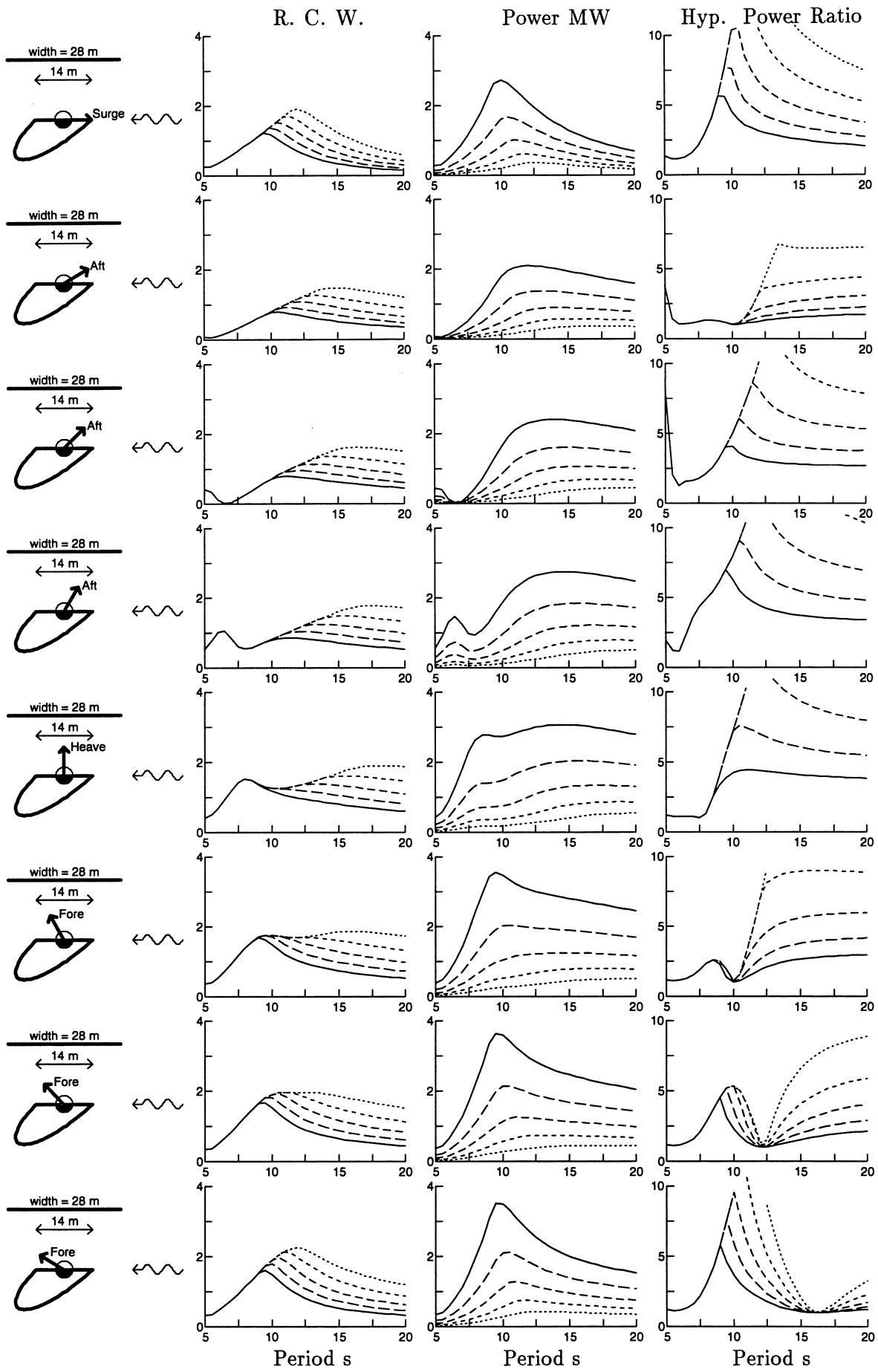

Figure 74: Complex control for a sheared 10m radius hemisphere, e07_14_10_1, in a single degree of freedom

6 The Solo Duck

Here we present results for the 10 m diameter, 29 m wide solo duck considered in [1]. The weight is chosen to be 4percent of the static buoyancy force in order to bias the tension legs. The global constraint on the excursions of the controlled degrees of freedom are as before: 2.5 metres for the translational motions and 0.5 radians for pitch. Hydrodynamic coefficients are evaluated using the 720 facet discretisation shown in figure 6. Predictions of excursions, relative capture widths and powers are plotted against wave period, from 5 seconds to 20 seconds in a water depth of 60 metres for wave amplitudes of 0.35m, 0.50m 0.71m 1.00m and 1.41m.

6.1 Surge Heave and Pitch System

We first consider all possible power absorption configurations based on the surge, heave and pitch system. Each degree of freedom may be either: i) held fixed; ii) uncontrolled (ie free or released) or iii) controlled (ie power absorbing with an amplitude constraint). This gives 19 different power absorption configurations to be investigated.

6.1.1 One Controlled Degree of Freedom

Results for a single absorbing degree of freedom are shown in figures 75 to 77. Surge heave and pitch each attain RCW of about 1.3 for the 1.41m wave amplitude. Surge power absorption peaks at about 9.5 seconds. whereas heave and pitch peak at about 8 seconds.

Surge requires only small imaginary powers at about 6 seconds. This is not strictly a resonance since surge does not have a restoring force. The low HPR at 6 seconds is due to a very small added mass, combined with a relatively large damping.

The heave natural period is at about 7 seconds and for a wave amplitude of 1.41 m the HPR remains below 2.5 for all wave periods considered.

The pitch natural period is at about 5.5 seconds and the HPR remains below about 3 for all wave periods.

6.1.2 One Controlled and One Released Degrees of Freedom

Results for one degree of freedom released are shown in figures 78 to 83. Releasing heave or pitch increases power absorption in surge. For power absorption in heave or pitch, releasing a degree of freedom reduces power absorption.

The peak in the power absorption curve for the h_sp case (figure 76) is not present in the

h_s_p case. In section 5 this was shown to be due to the asymmetry of the duck section. A similar trend is seen for the p_s_h case.

The p_h_s and h_p_s cases have dramatic reductions in power absorption by releasing a degree of freedom. This is explained by the free degree of freedom adjusting to the *path of least resistance.* Both pitch and heave motions result in a net volume being displaced. The free degree of freedom allows the duck to ride the waves and consequently the overall net volume displaced is small. A similar effect was noted in section 5, figure 51.

6.1.3 One Controlled and Two Released Degrees of Freedom

For surge (figure 84) releasing two degrees of freedom, s_hp_, gives more power than the s__hp case, but only about the same as the s_h_p and s_p_h cases. The large heave motions in the s_h_p case are reduced by releasing both heave and pitch.

The p_sh_ and h_sp_ have even poorer performance than the p_h_s and h_p_s cases.

6.1.4 Two Controlled Degrees of Freedom

As was noted in section 5, the amplitude constraint is applied to only the controlled degrees of freedom. It is therefore possible that more power can be obtained with an x_y_z configuration than an xy__z configuration. However, for the duck in surge, heave, pitch system this does not occur and the two degree of freedom case is always better than power absorption in less degrees of freedom.

6.1.5 Two Controlled and one Released Degrees of Freedom

With power absorption in 2 degrees of freedom releasing the third always results in a loss of power absorbed. This loss is fairly small for sh_p_ and sp_h_, but quite large for hp_s_.

6.1.6 Three Controlled Degrees of Freedom

Power absorption in all three degrees of freedom provides at least as much power as any other configuration. In the region of 7 seconds the shp__ case produces the same amount of power as each of the two degree of freedom cases, sh__p, sp__h and hp__s. This is due to the singularity in the damping matrix, as discussed in [1].

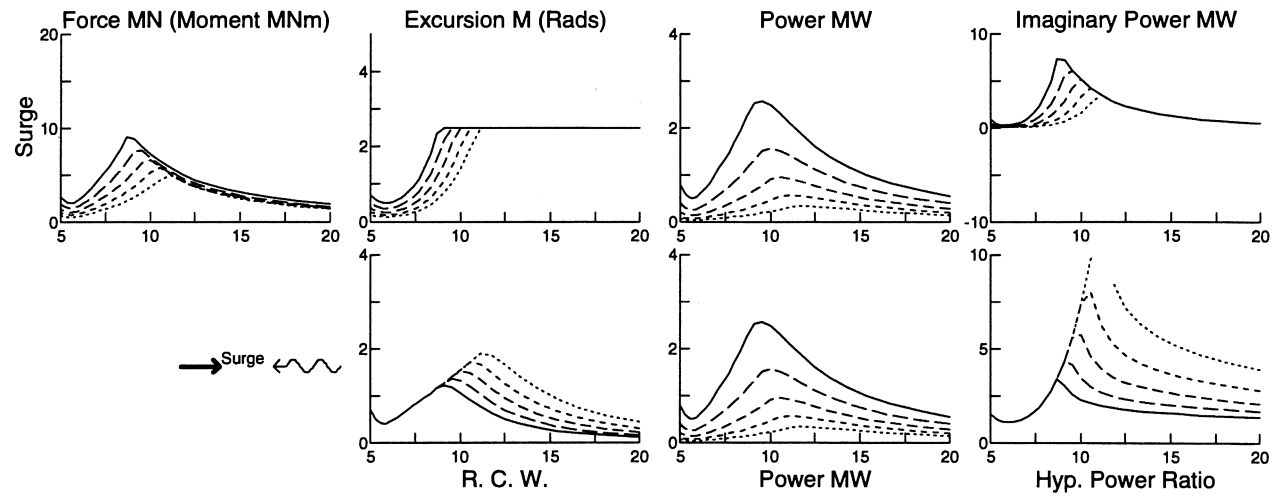

Figure 75: s__hp configuration solo duck with complex control

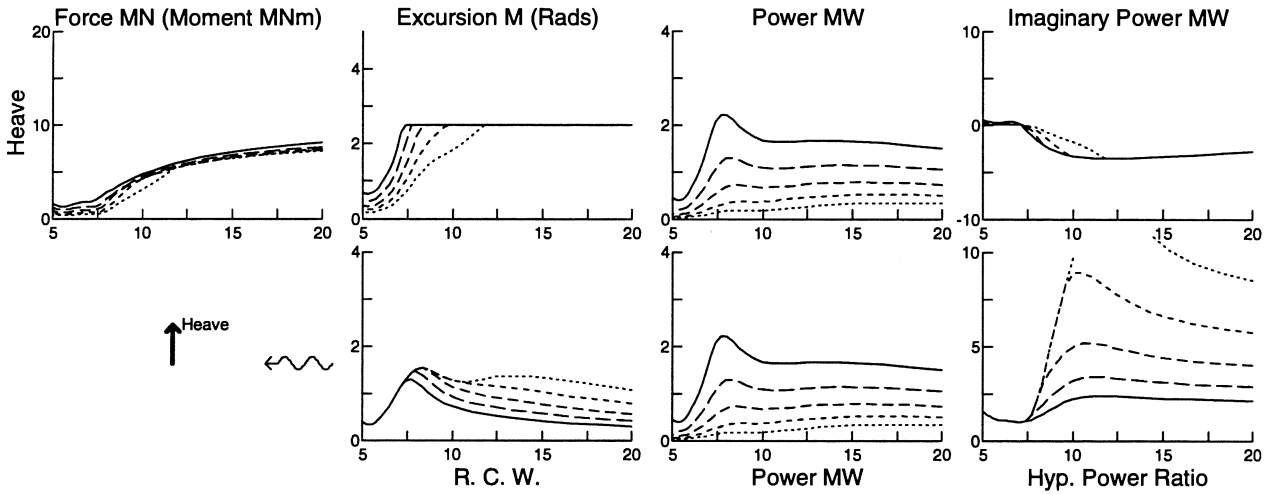

Figure 76: h__sp configuration solo duck with complex control

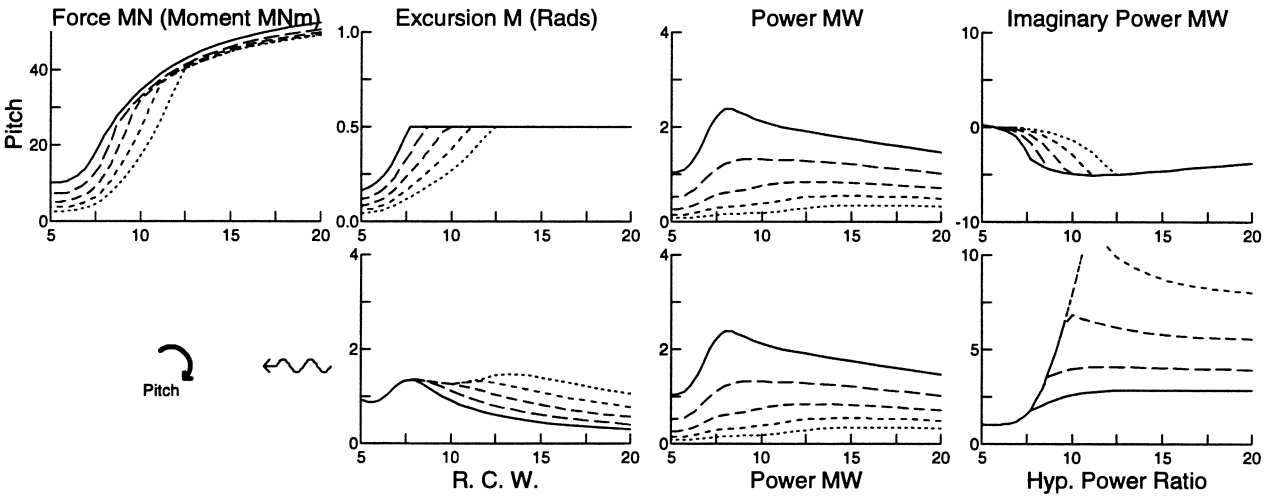

Figure 77: p__sh configuration solo duck with complex control

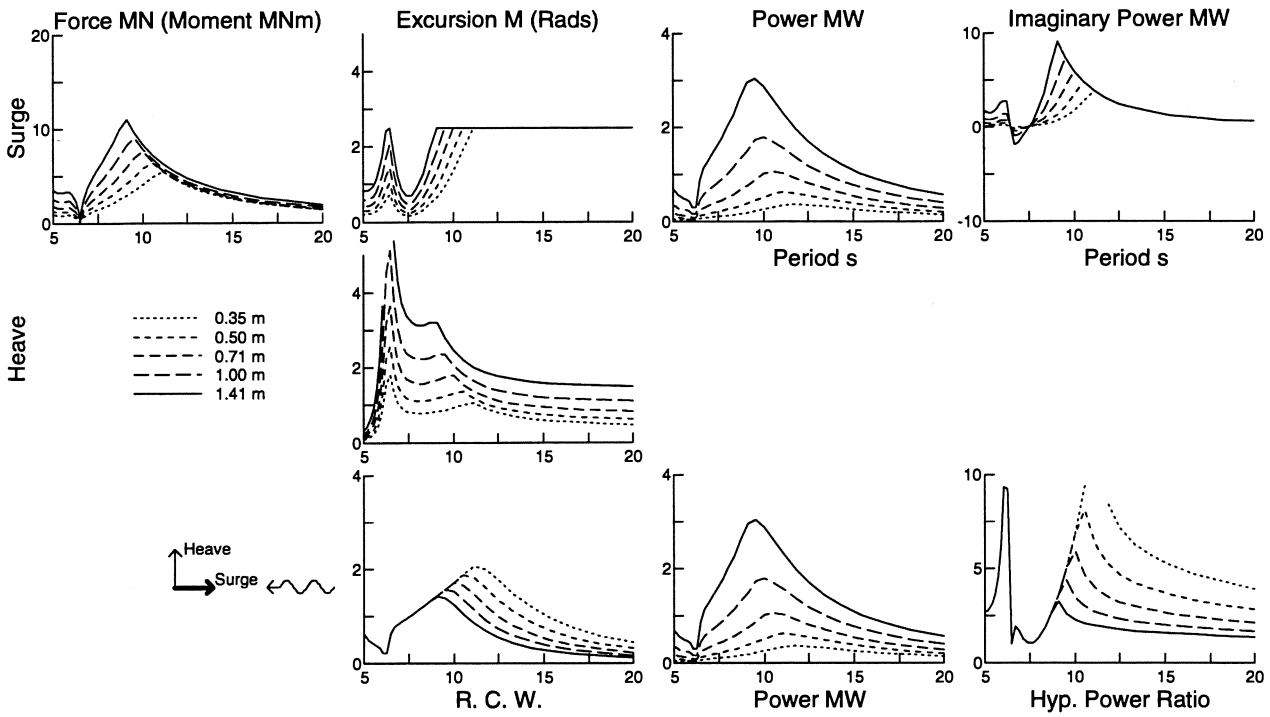

Figure 78: s_h_p configuration solo duck with complex control

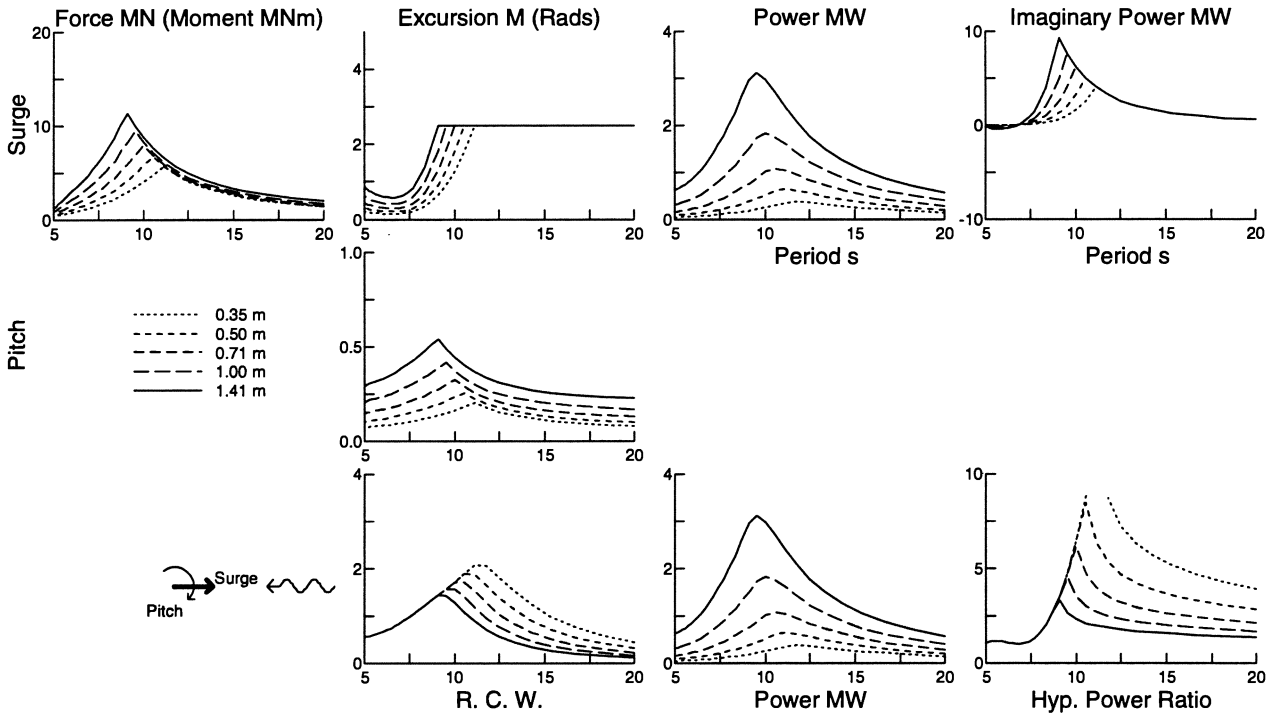

Figure 79: s_p_h configuration solo duck with complex control

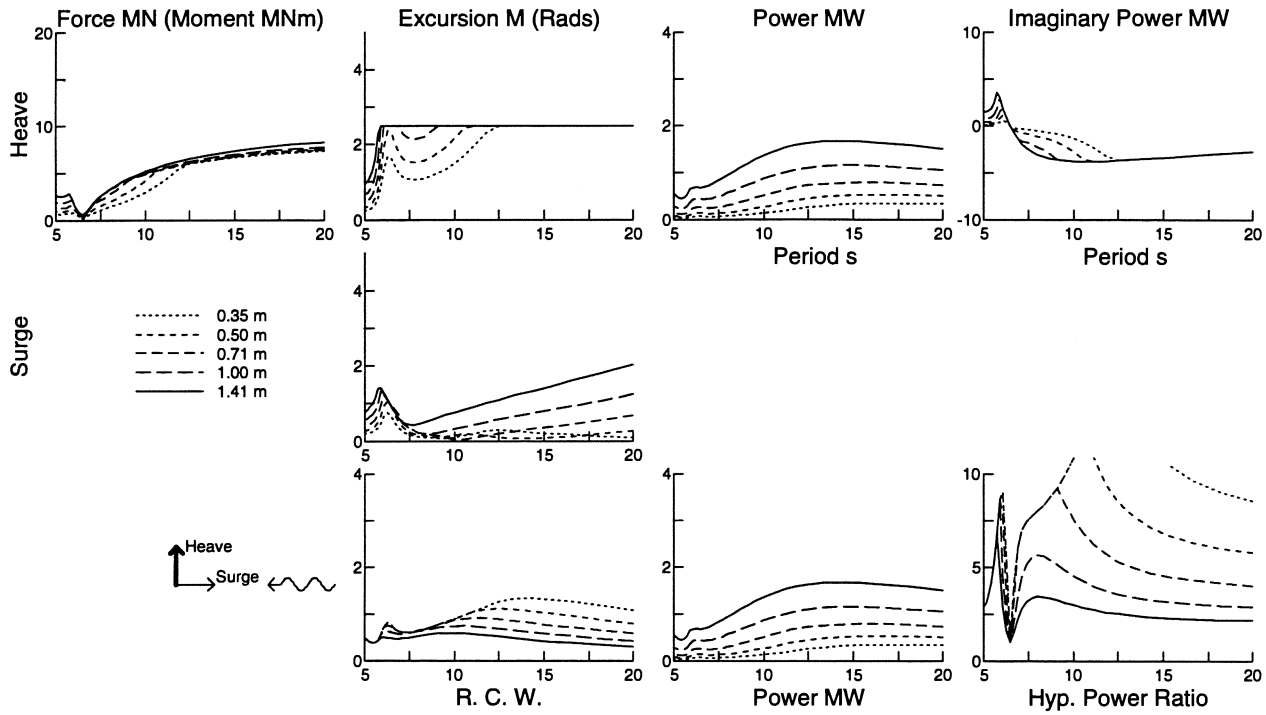

Figure 80: h_s_p configuration solo duck with complex control

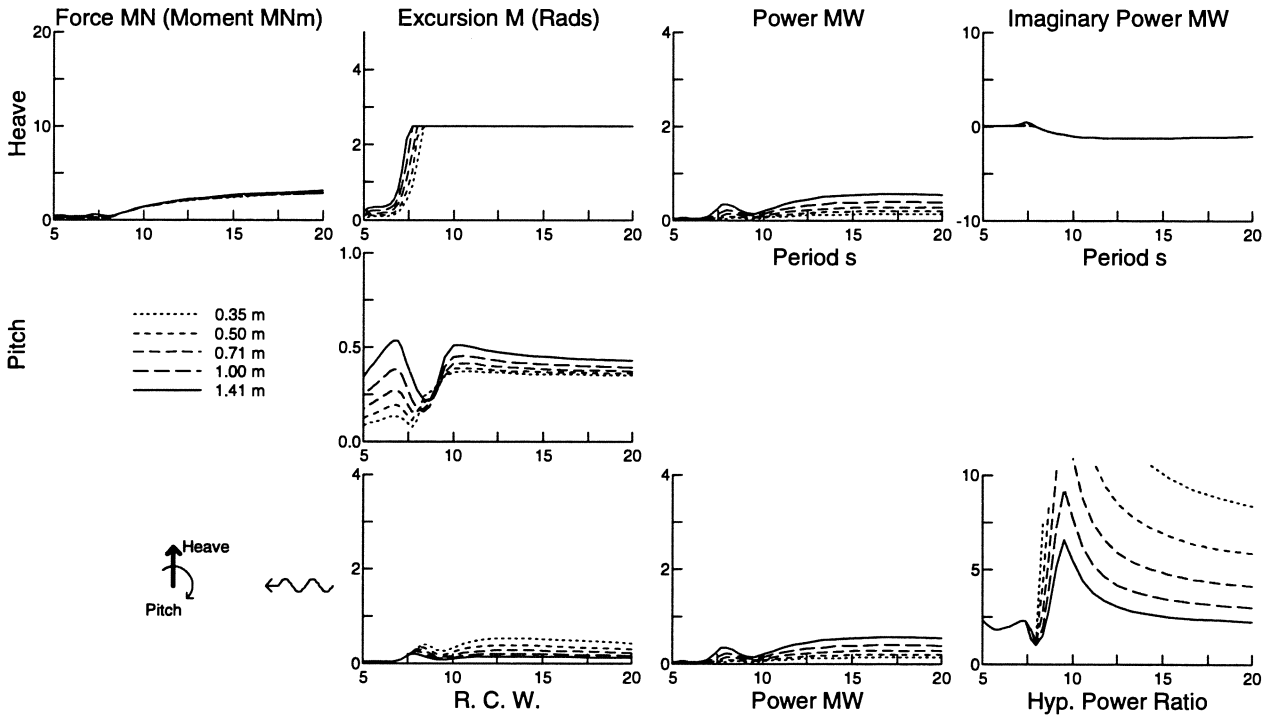

Figure 81: h_p_s configuration solo duck with complex control

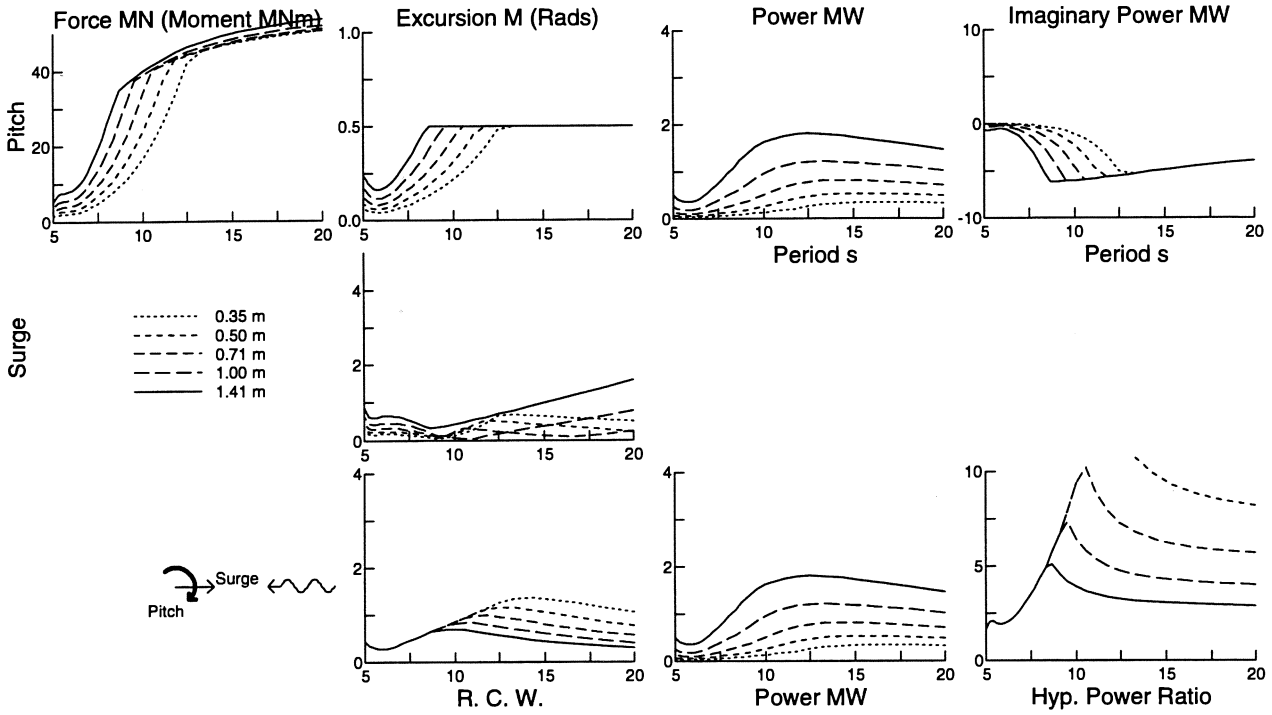

Figure 82: p_s_h configuration solo duck with complex control

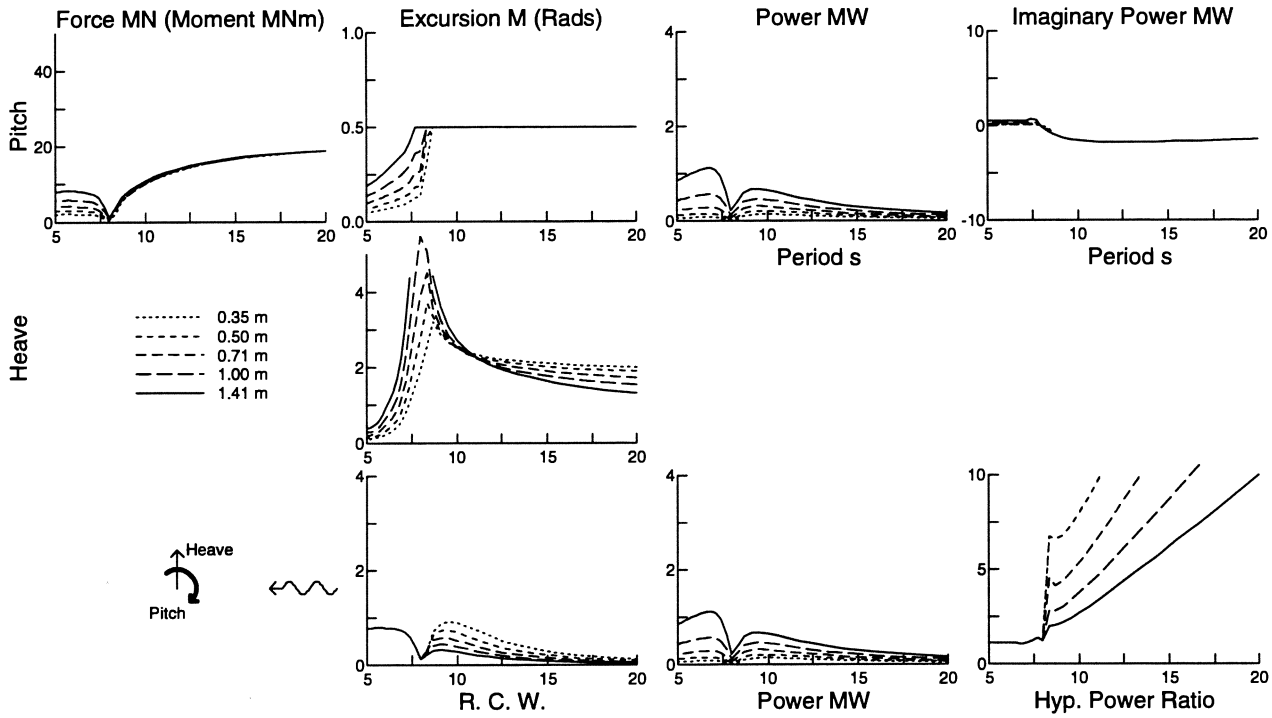

Figure 83: p_h_s configuration solo duck with complex control

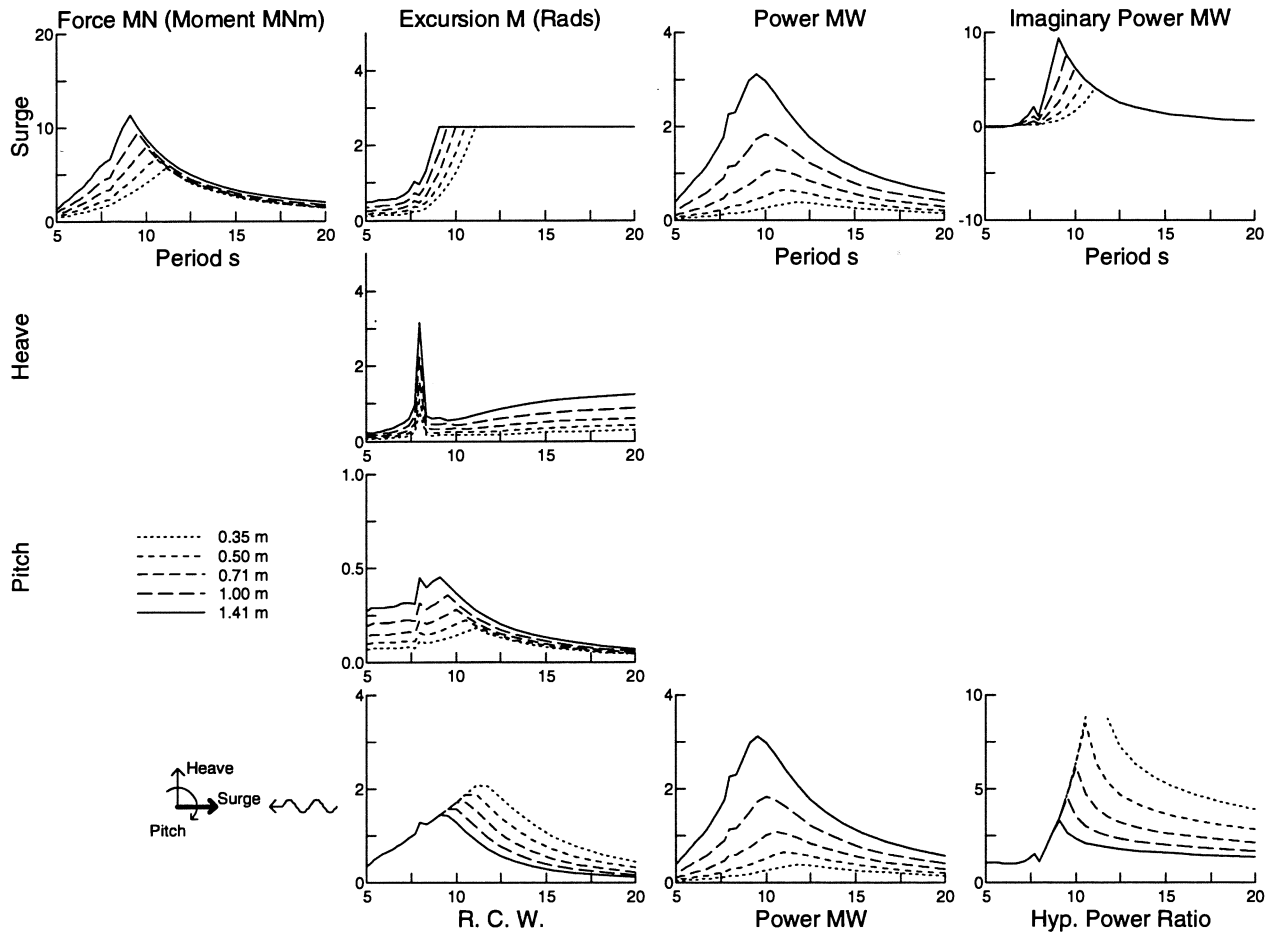

Figure 84: s_hp_ configuration solo duck with complex control

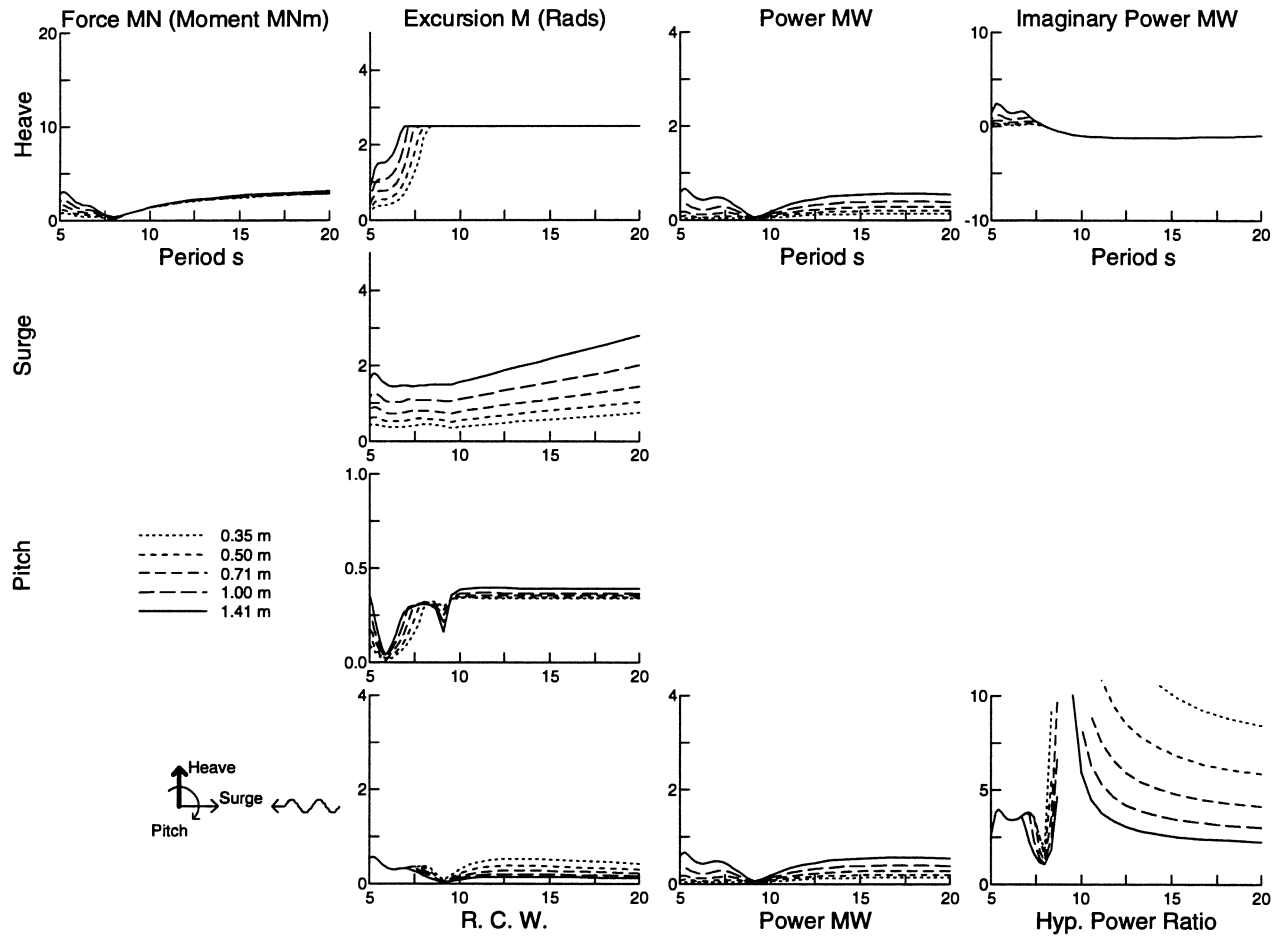

Figure 85: h_sp_ configuration solo duck with complex control

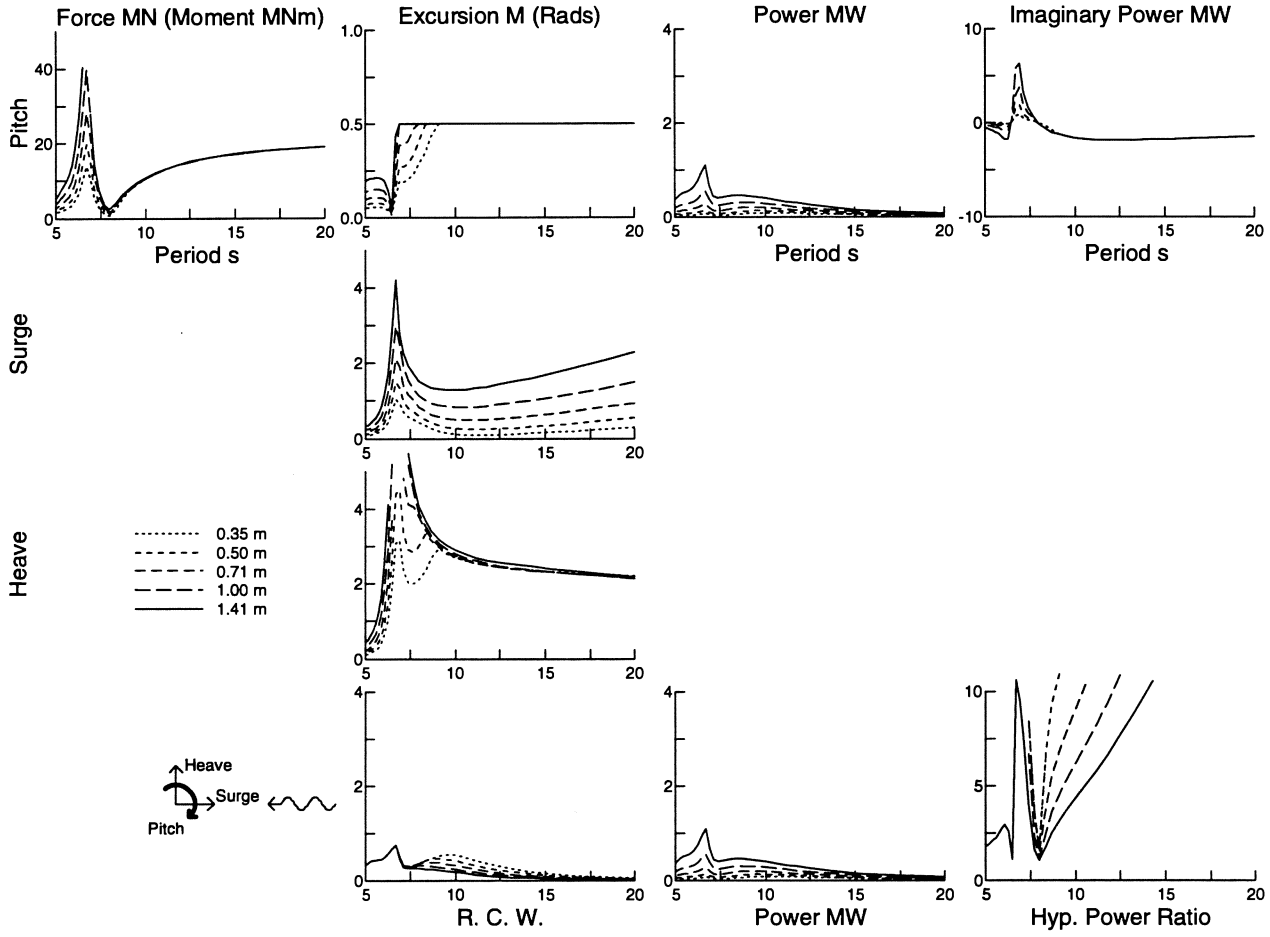

Figure 86: p_sh_ configuration solo duck with complex control

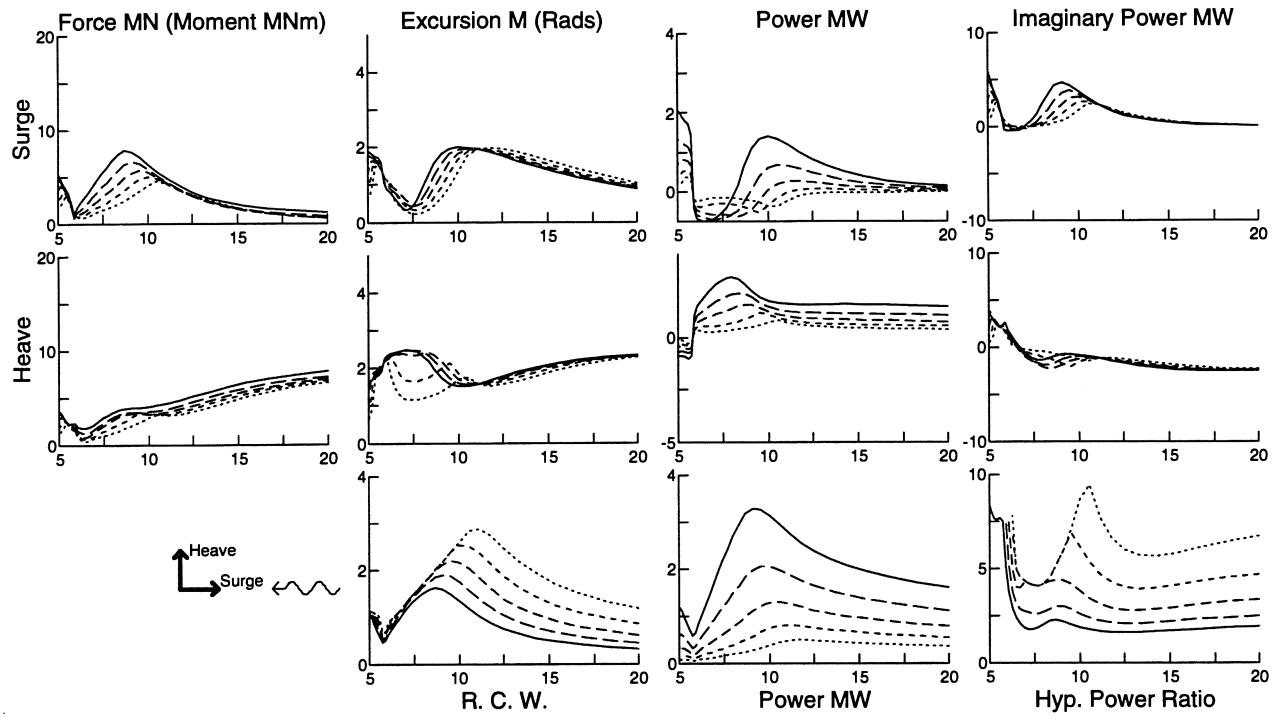

Figure 87: sh_p configuration solo duck with complex control

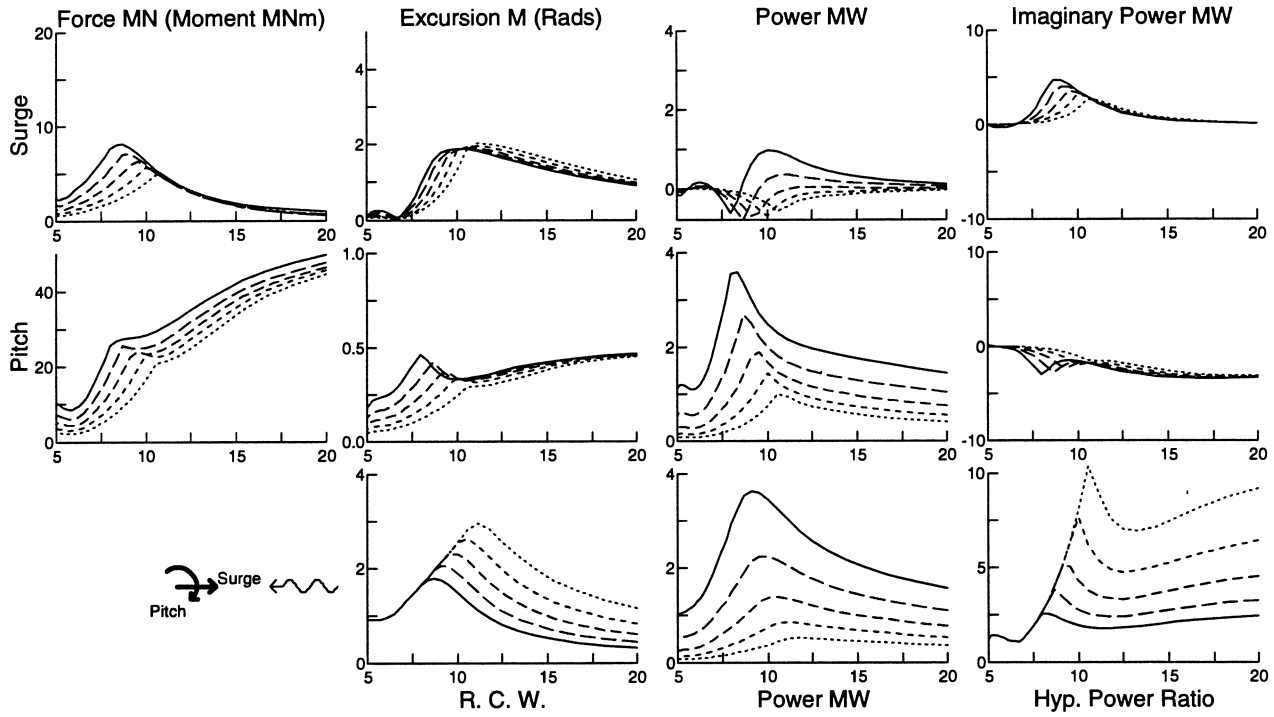

Figure 88: sp_h configuration solo duck with complex control

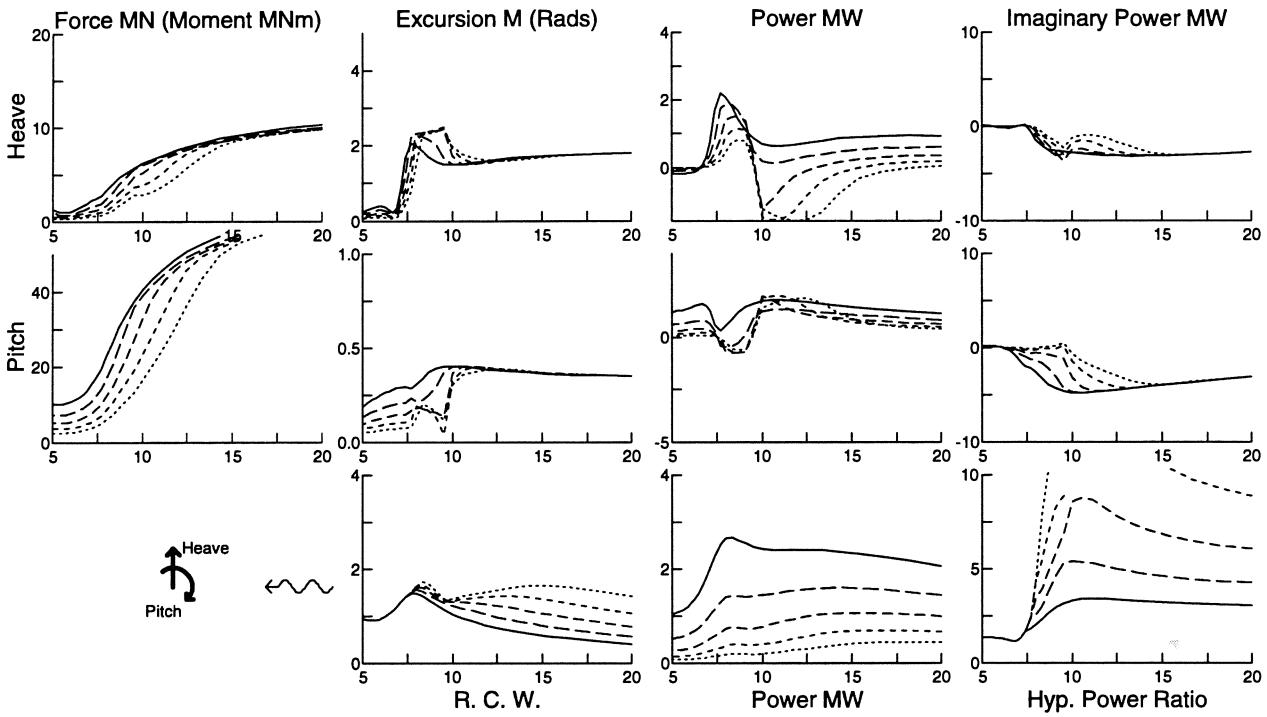

Figure 89: hp_s configuration solo duck with complex control

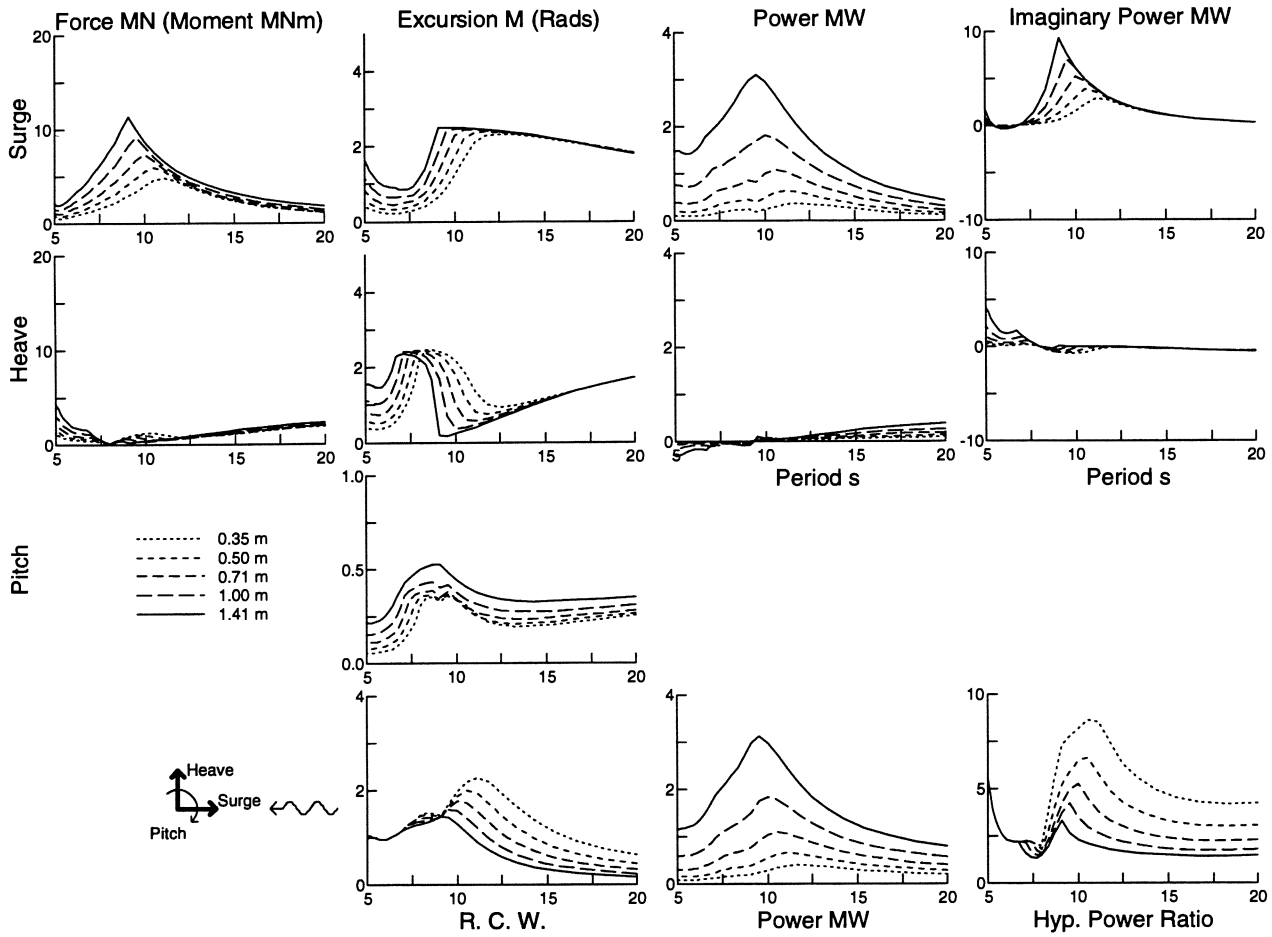

Figure 90: sh_p_ configuration solo duck with complex control

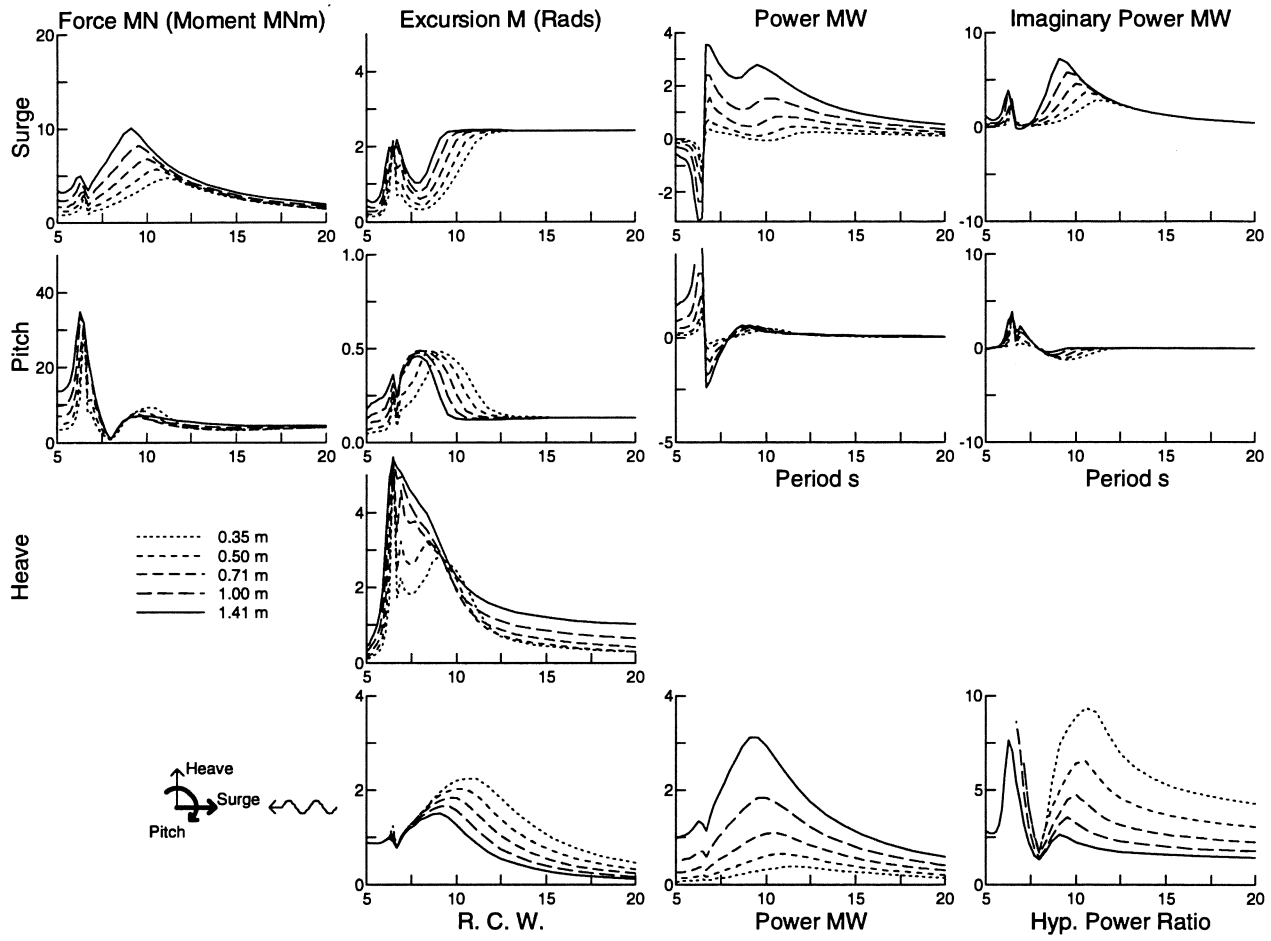

Figure 91: sp_h_ configuration solo duck with complex control

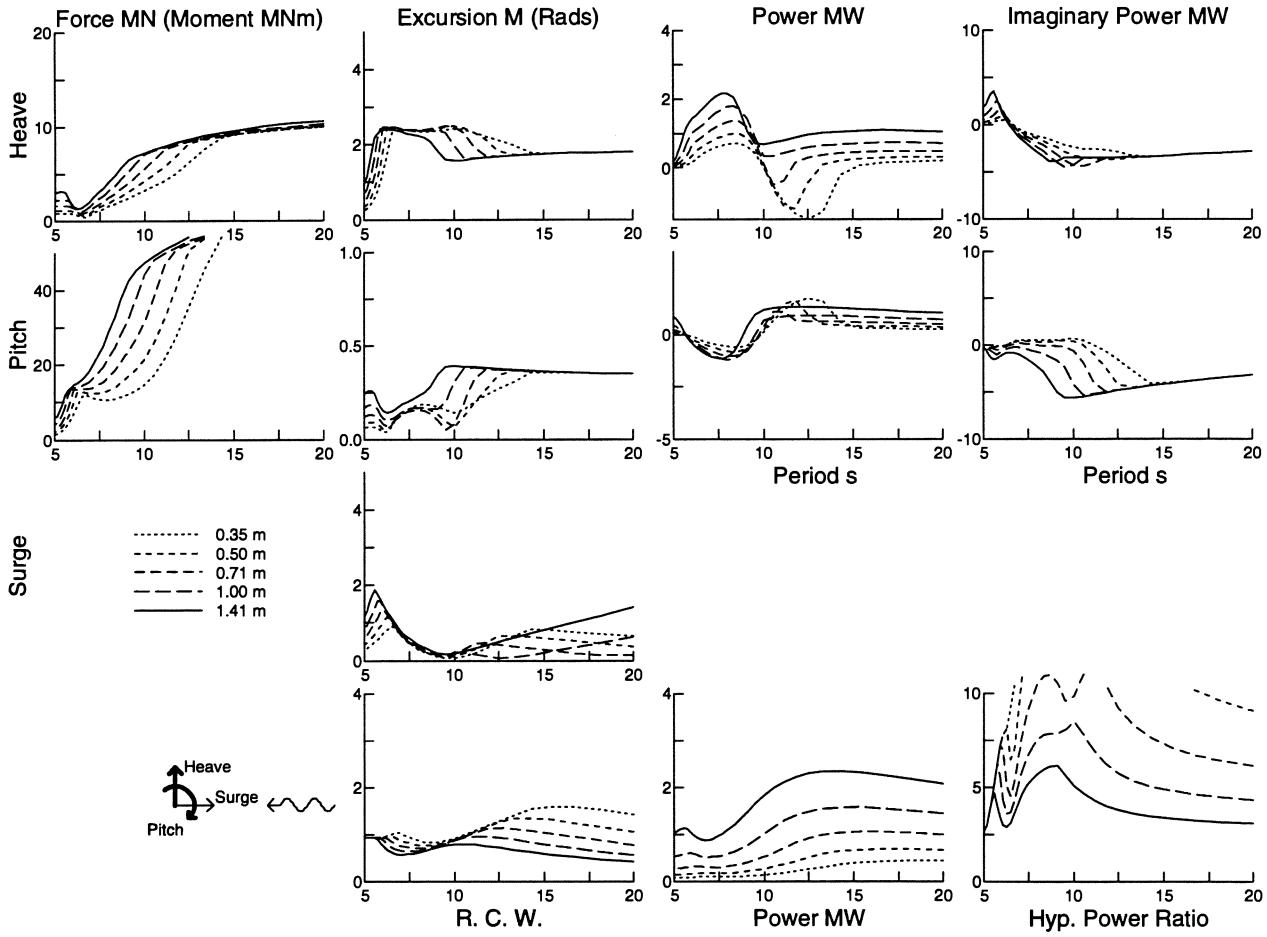

Figure 92: hp_s_ configuration solo duck with complex control

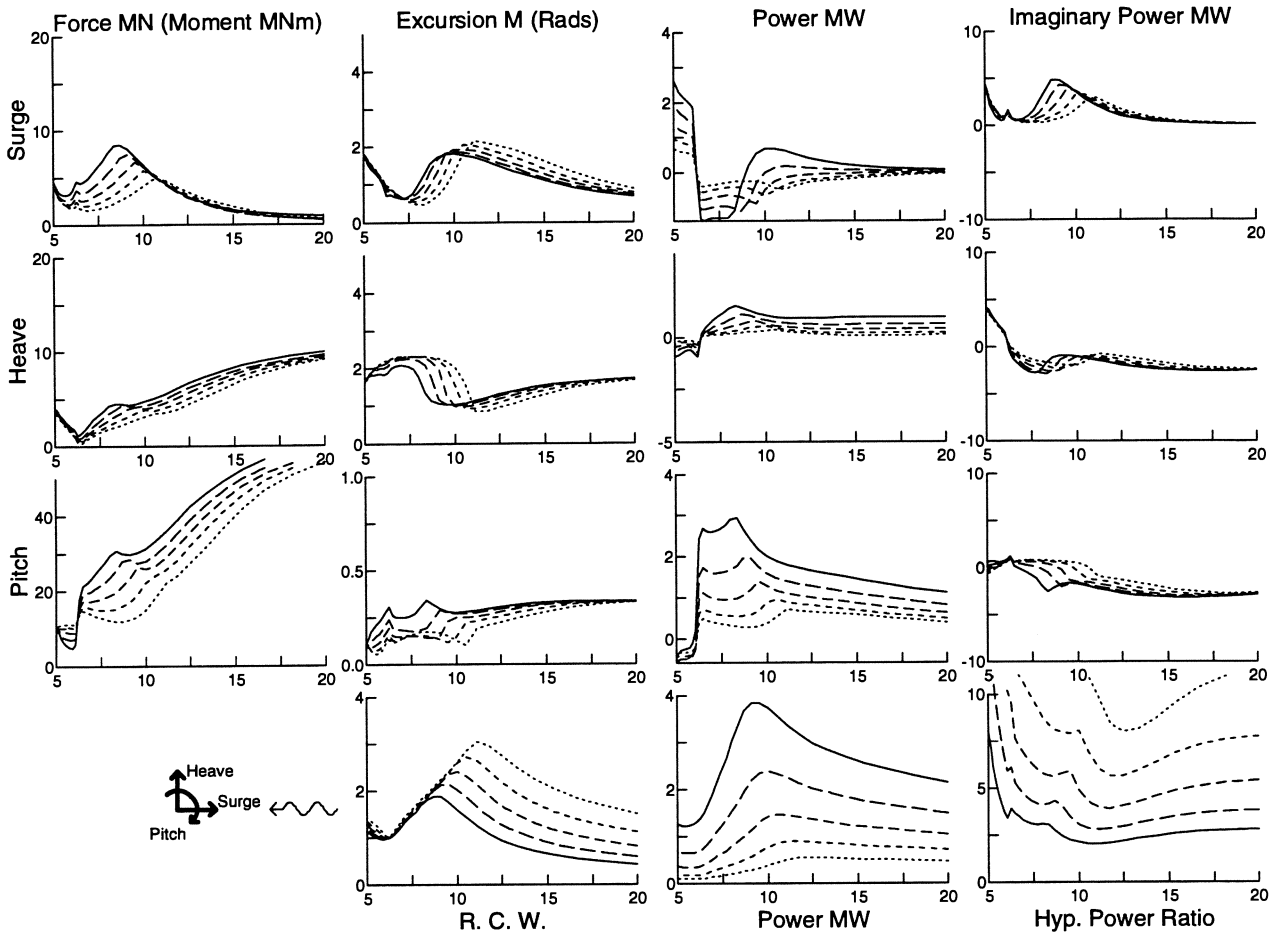

Figure 93: shp__ configuration solo duck with complex control

6.2 Inclined degrees of freedom

The fore and aft inclined degrees of freedom are defined in section 5.4 on the Translational Devices. Here the angle of rotation from the surge-heave-pitch system to the fore-aft-pitch system is 45°.

6.2.1 One Controlled Degree of Freedom

45° fore (figure 94) is the best single degree of freedom case. It outperforms s__hp and a__fp (figures 75 and 95) at all frequencies and outperforms h__sp and p__sh (figures 76 and 77) between about 8 and 14 seconds.

6.2.2 One Controlled and One Released Degree of Freedom

Releasing a fore or aft degree of freedom (figures 97, 99, 101 and 102) results in large motions in the released degree of freedom. Surprisingly the released motions increase the power absorbed. However these predictions may be invalidated by non-linearities. It is noted that these results are in contrast to h_p_s and p_h_s cases for which large motions did not occur and power absorption was reduced.

Pitch has moderately large motions when released (figures 98 and 100, which may be expected to be within the linear regime. Releasing pitch results in only small power losses in the f_p_a, but larger losses in the a_p_f case.

6.2.3 One Controlled and Two Released Degrees of Freedom

For f_ap_ and a_fp_ (figures 103 and 104) large motions occur in the free degrees of freedom and large powers are predicted at around 15 seconds. However below 12 seconds power absorption levels are small.

For the p_fa_ case (figure 105) large motions occur at short periods associated with the heave natural period. Power absorption levels are considerably less since the duck is free to ride the waves, rather than reacting against them.

6.2.4 Two Controlled Degrees of Freedom

All two degree of freedom cases (figures 106, 107 and 108), perform well , the best being the fp__a case.

6.2.5 Two Controlled and One Released Degrees of Freedom

Releasing fore or aft (figures 110 and 111) reduces power absorption except where large motions are induced in the free degrees of freedom.

Releasing pitch (figure 109) reduces power slightly at all frequencies.

6.2.6 Three Controlled Degrees of Freedom

As would be expected the fap__ case (figure 112) produces the same power as the shp__ case (figure 93). Around 7 seconds fap__ case produces the same amount of power as the fp__a and ap__f (figures 107 and 108) cases. This is due to the singular nature of the three degree of freedom damping matrix.

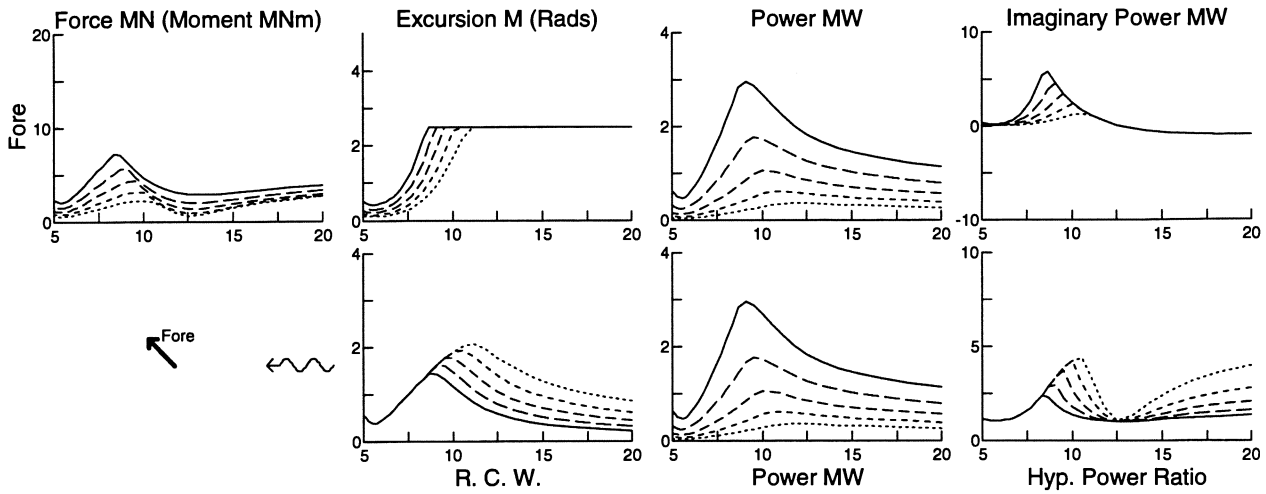

Figure 94: f_ap configuration solo duck with complex control

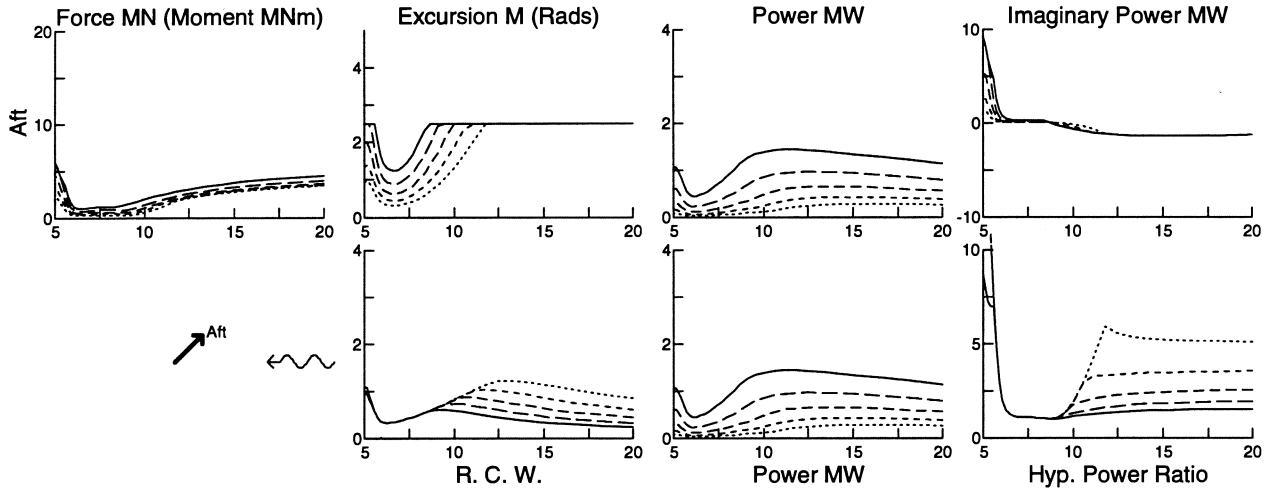

Figure 95: a_fp configuration solo duck with complex control

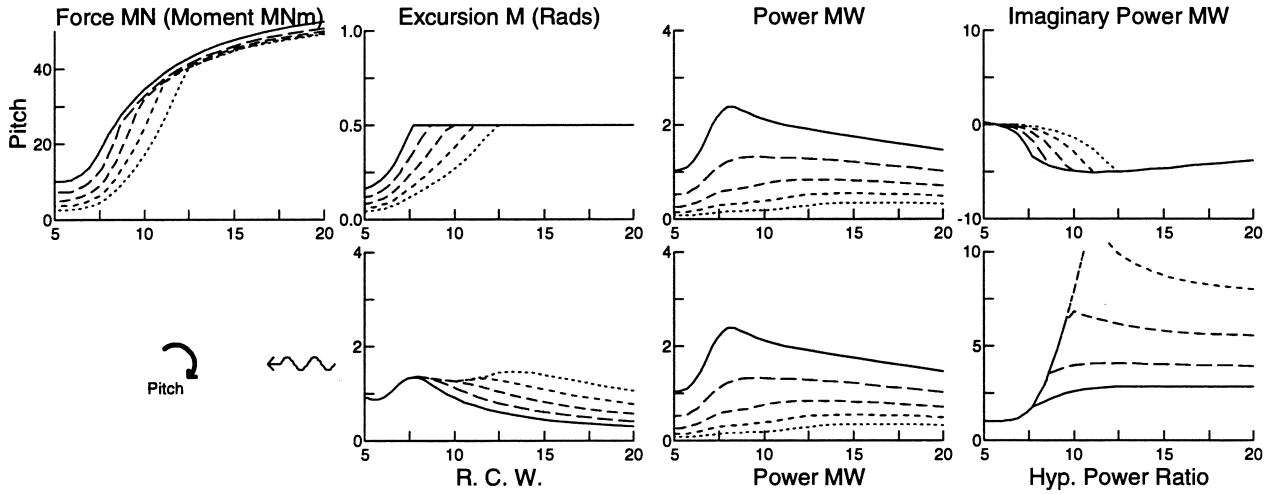

Figure 96: p_fa configuration solo duck with complex control

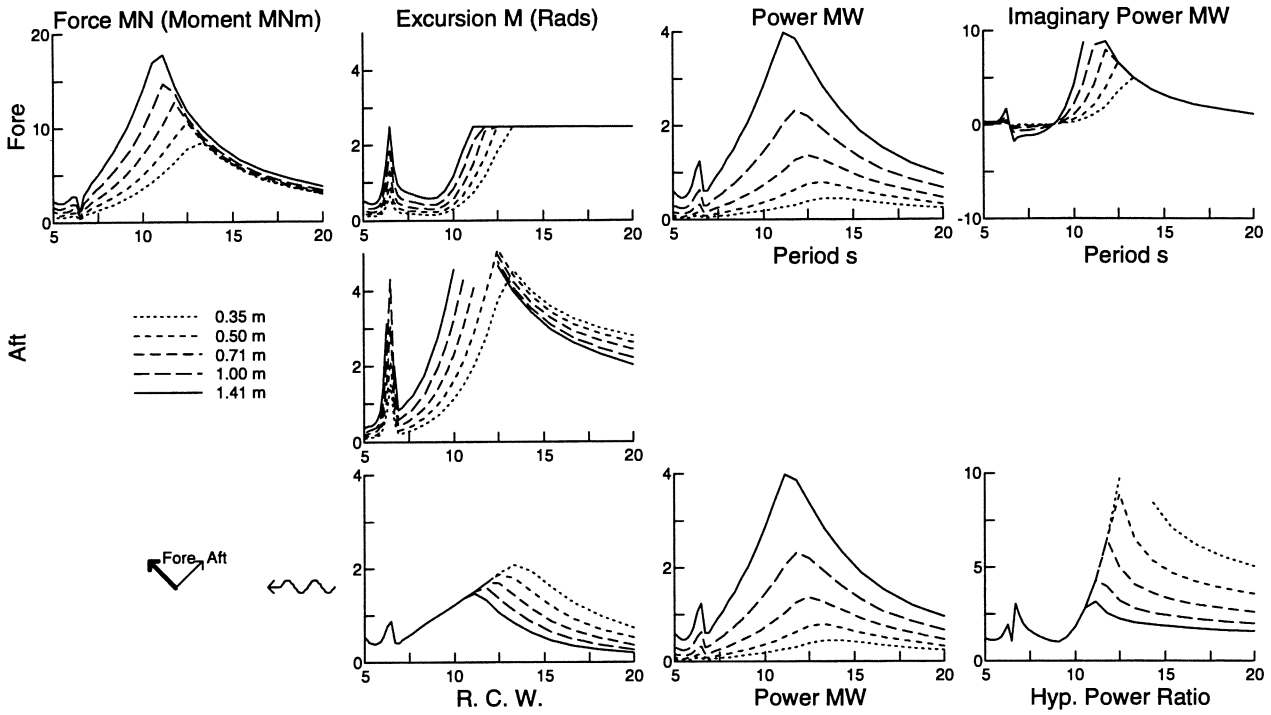

Figure 97: f_a_p configuration solo duck with complex control

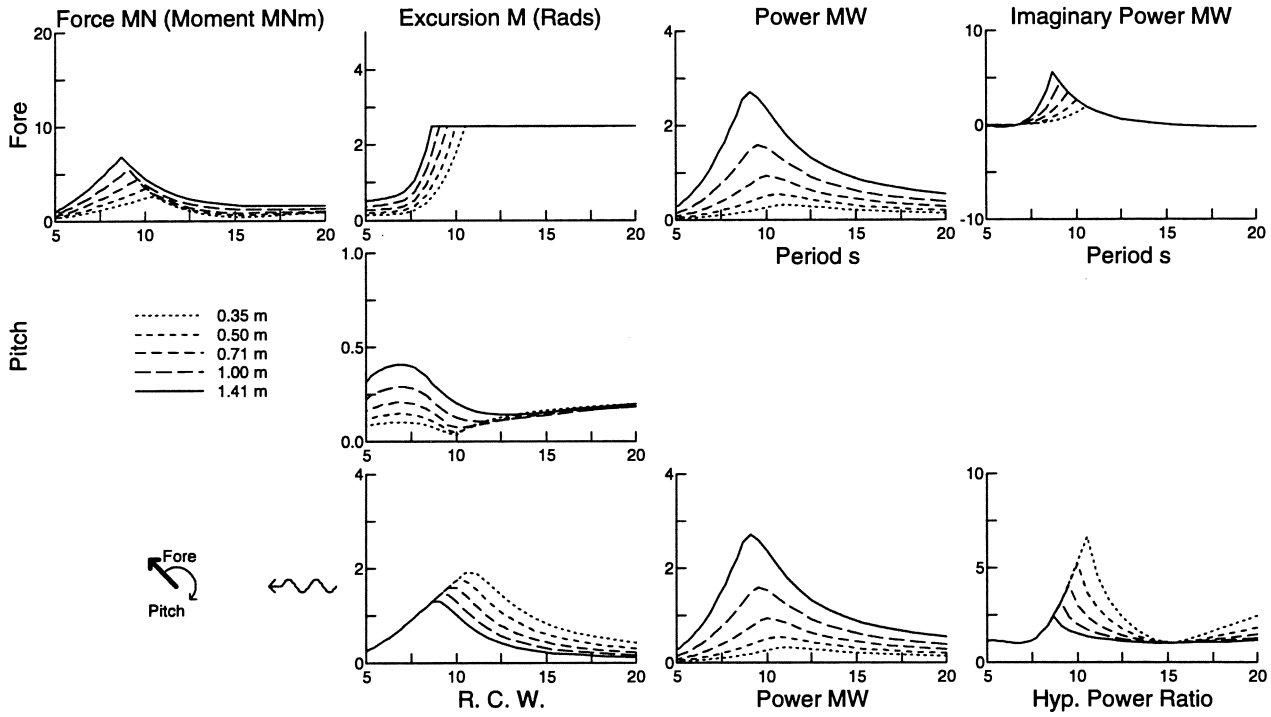

Figure 98: f_p_a configuration solo duck with complex control

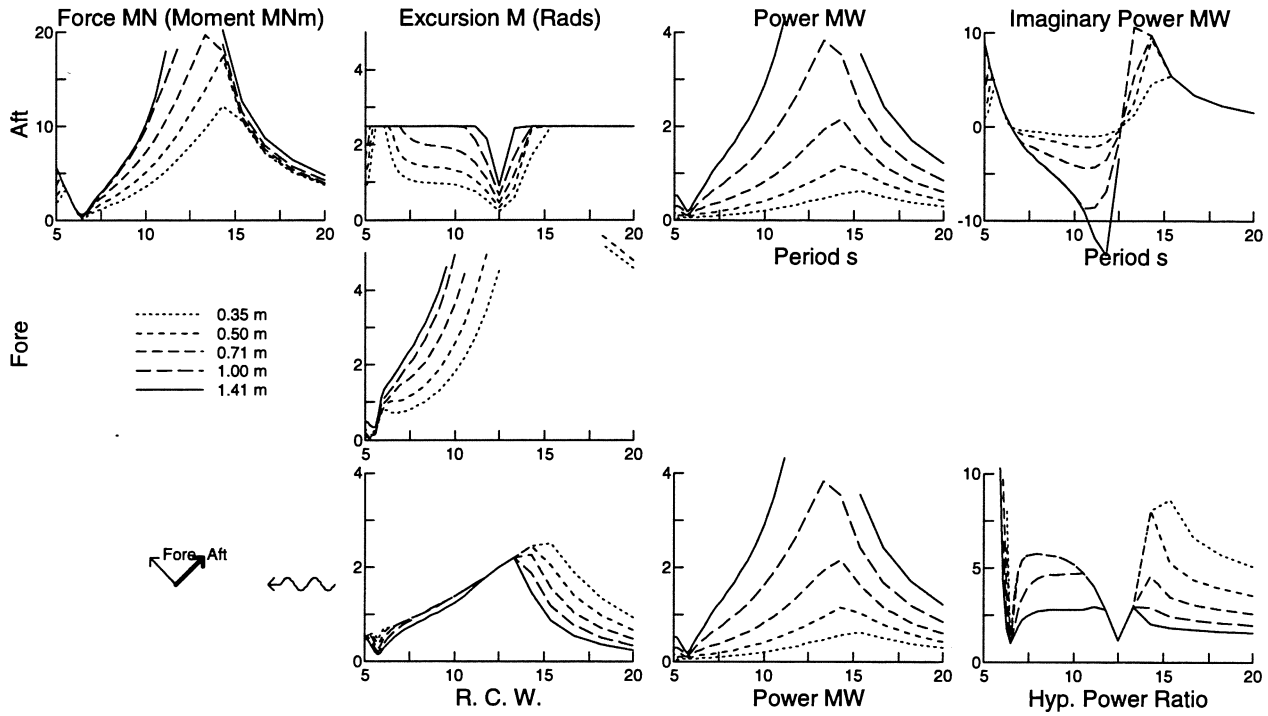

Figure 99: a_f_p configuration solo duck with complex control

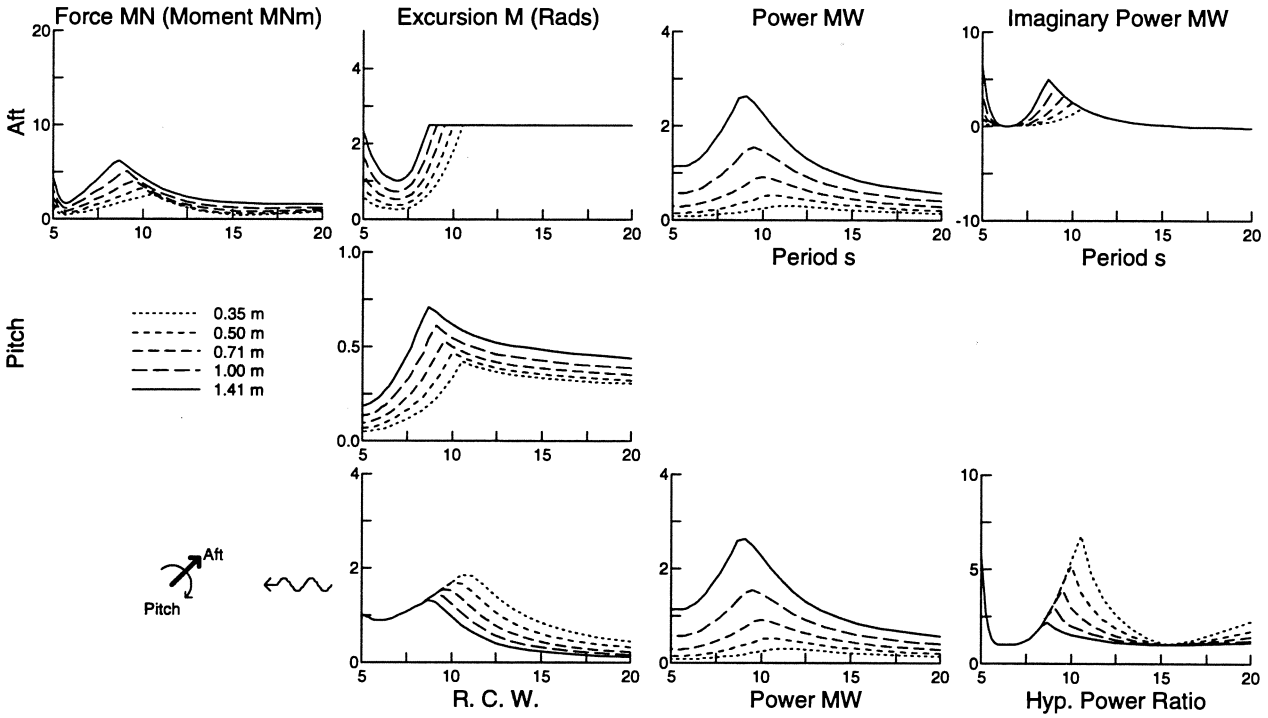

Figure 100: a_p_f configuration solo duck with complex control

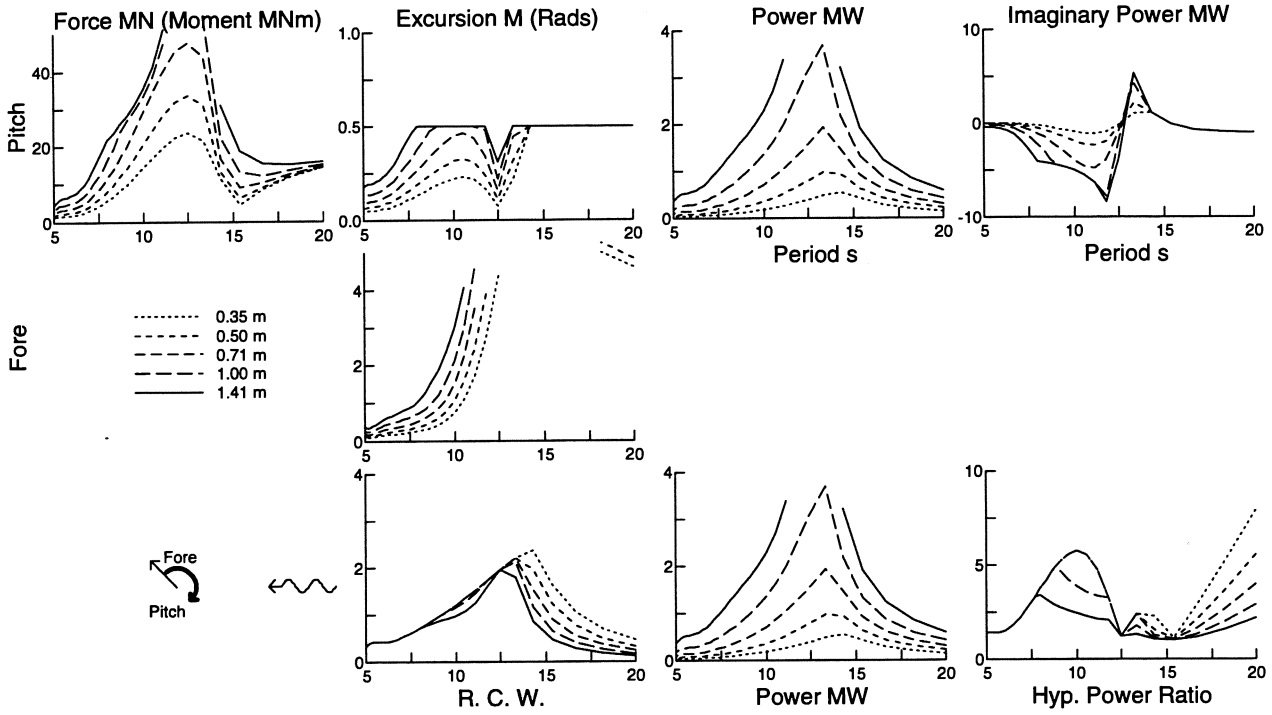

Figure 101: p_f_a configuration solo duck with complex control

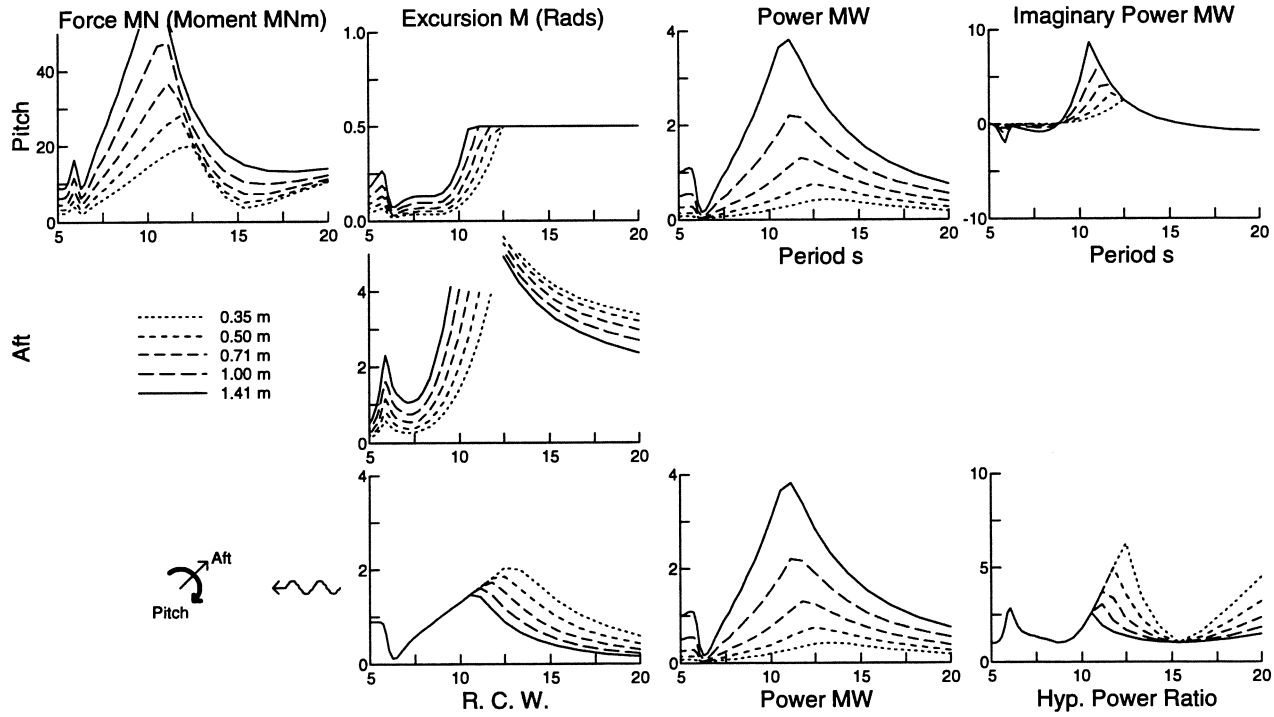

Figure 102: p_a_f configuration solo duck with complex control

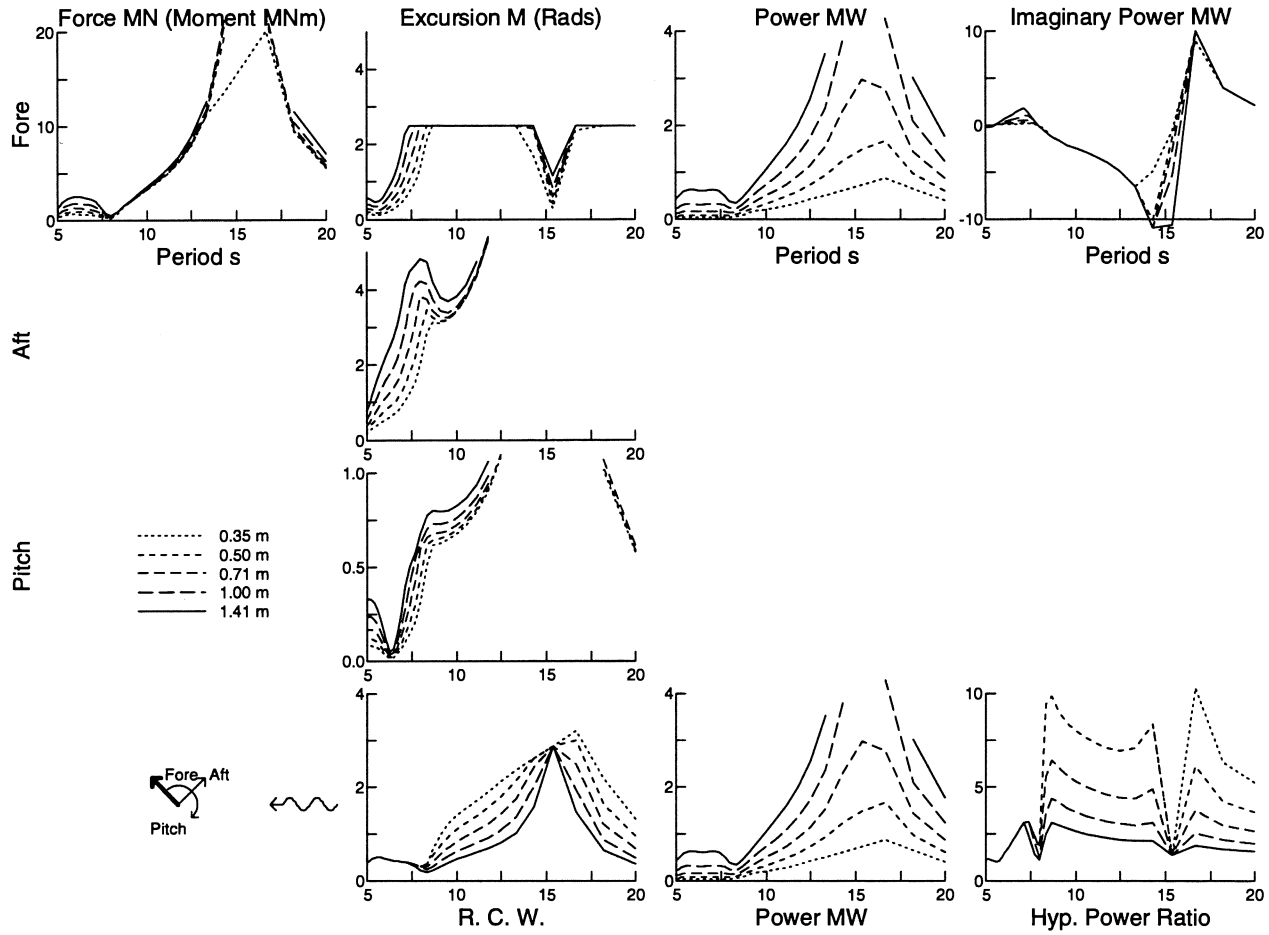

Figure 103: f_ap_ configuration solo duck with complex control

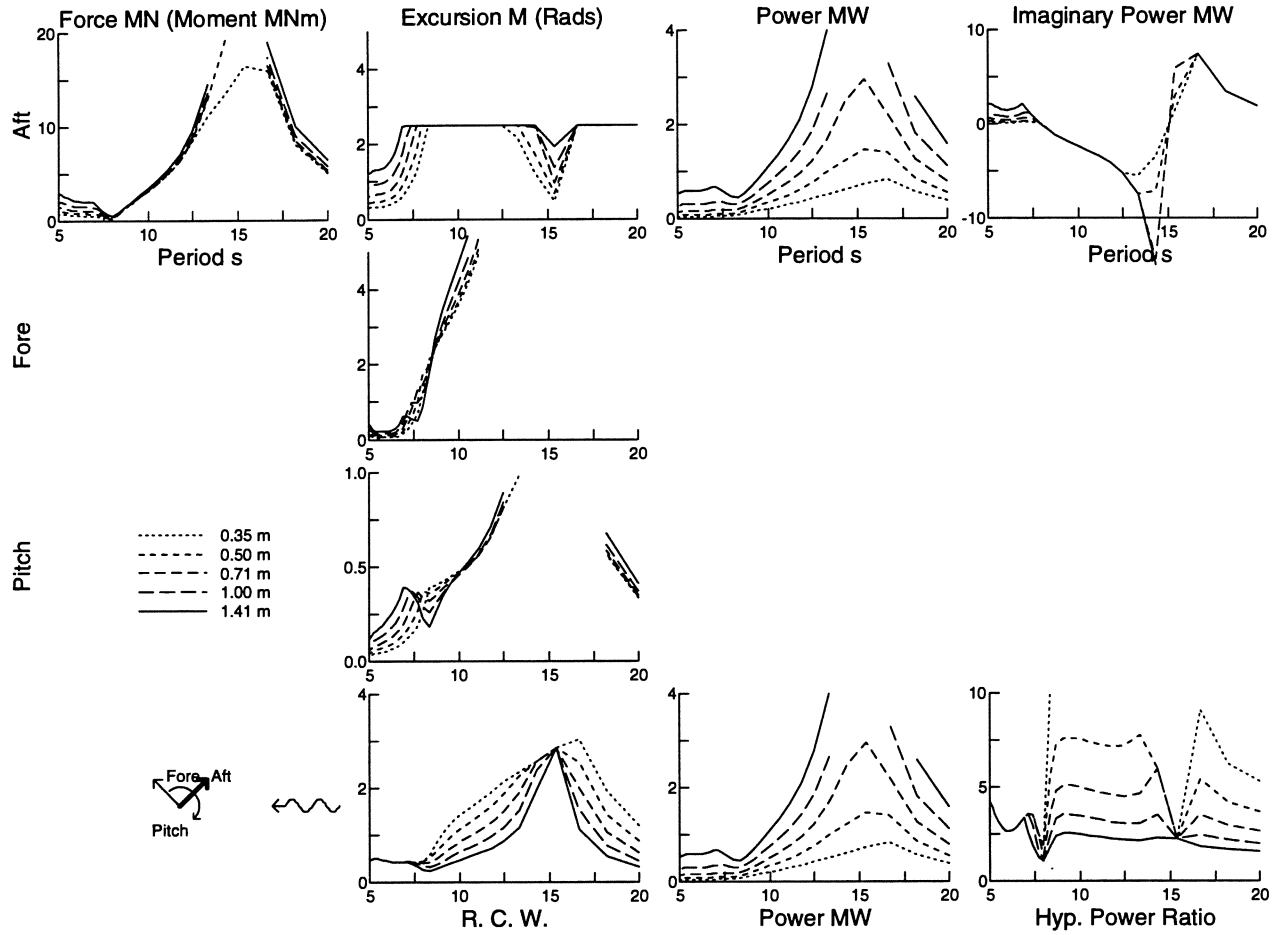

Figure 104: a_fp_ configuration solo duck with complex control

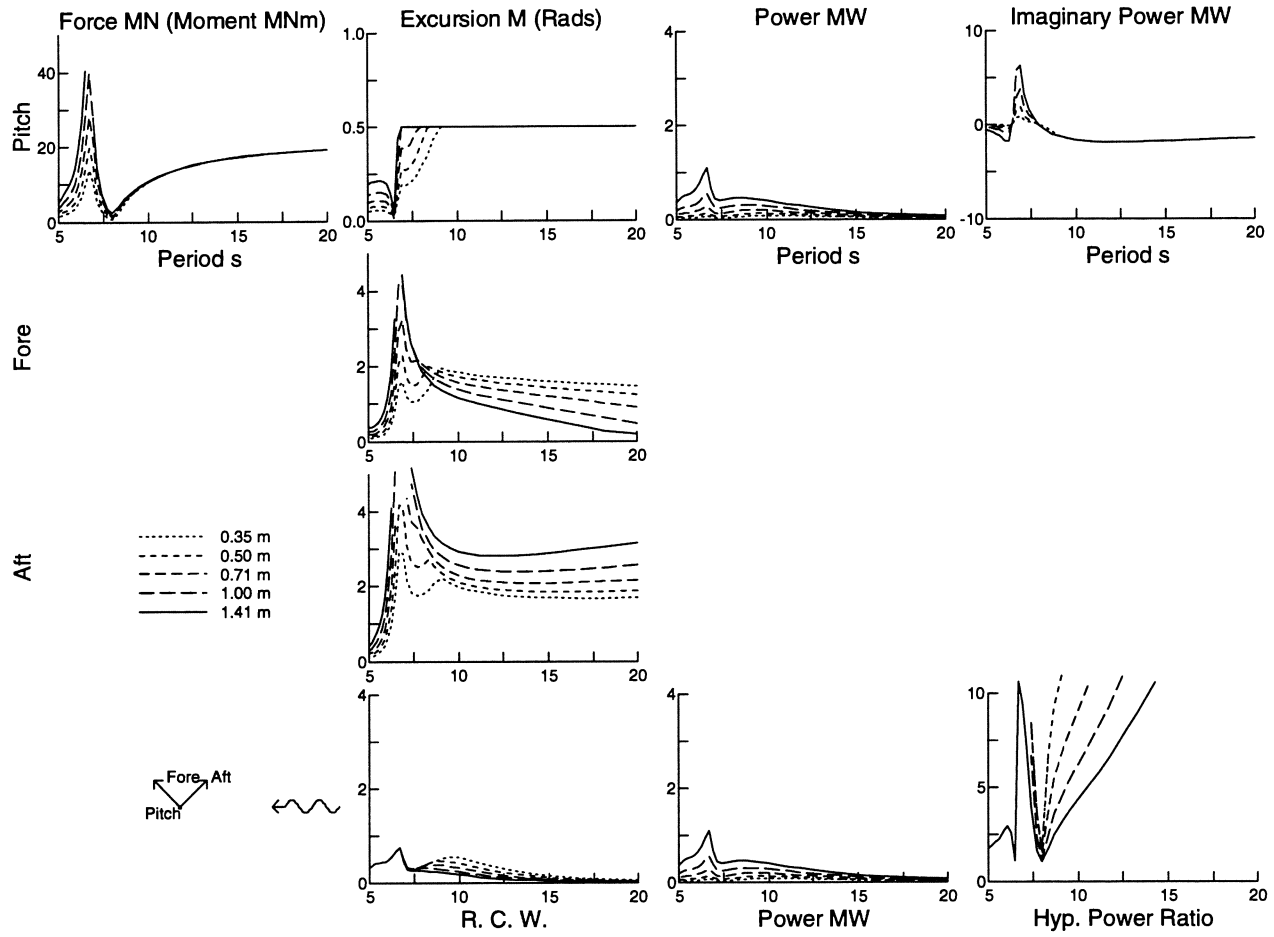

Figure 105: p_fa_ configuration solo duck with complex control

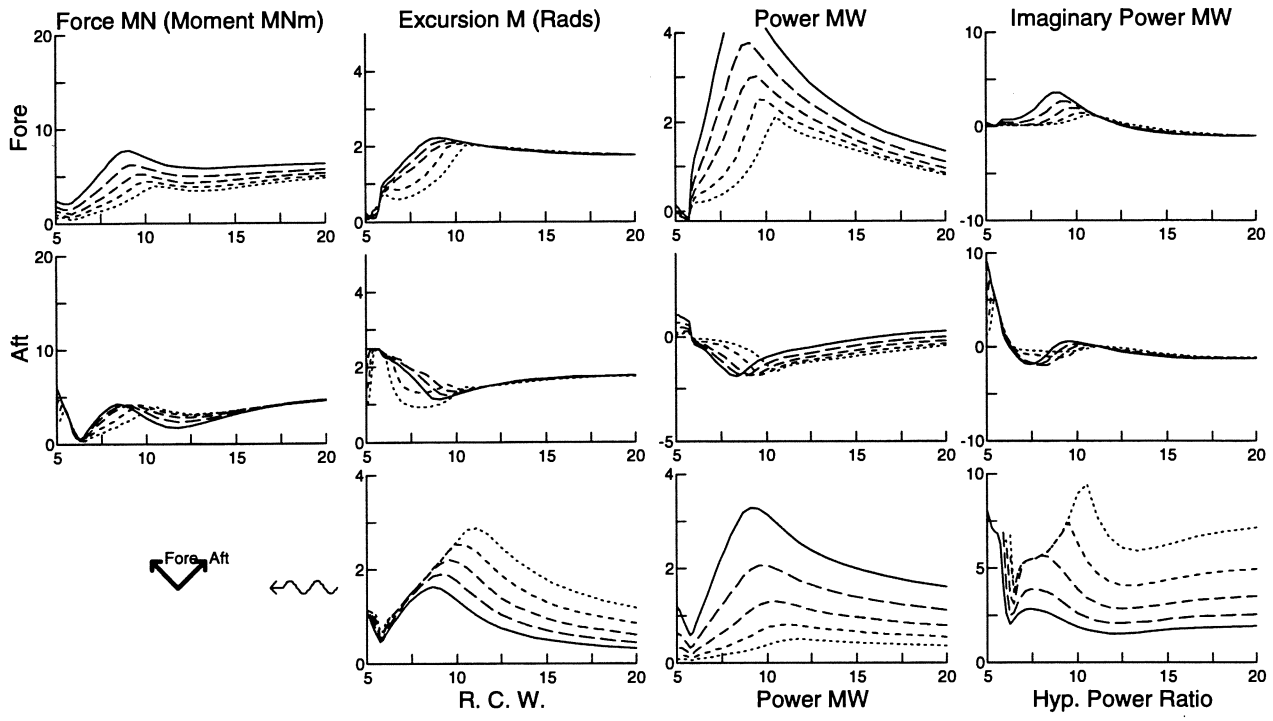

Figure 106: fa__p configuration solo duck with complex control

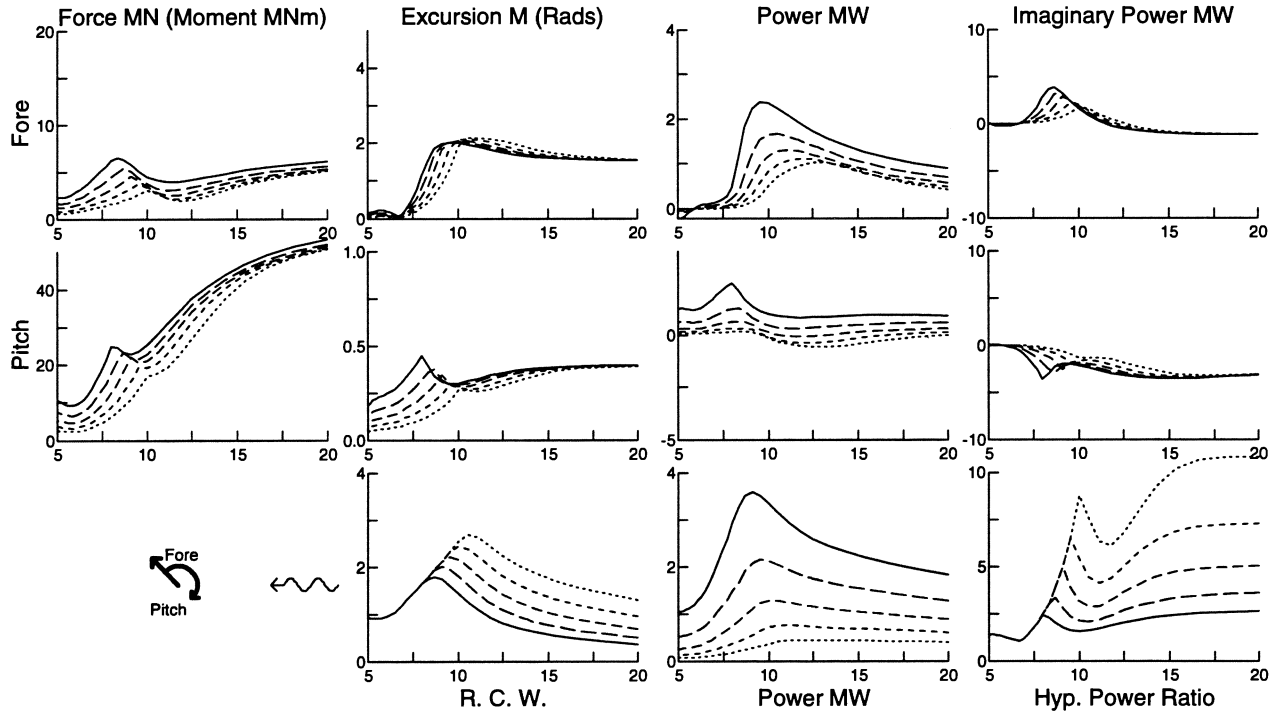

Figure 107: fp__a configuration solo duck with complex control

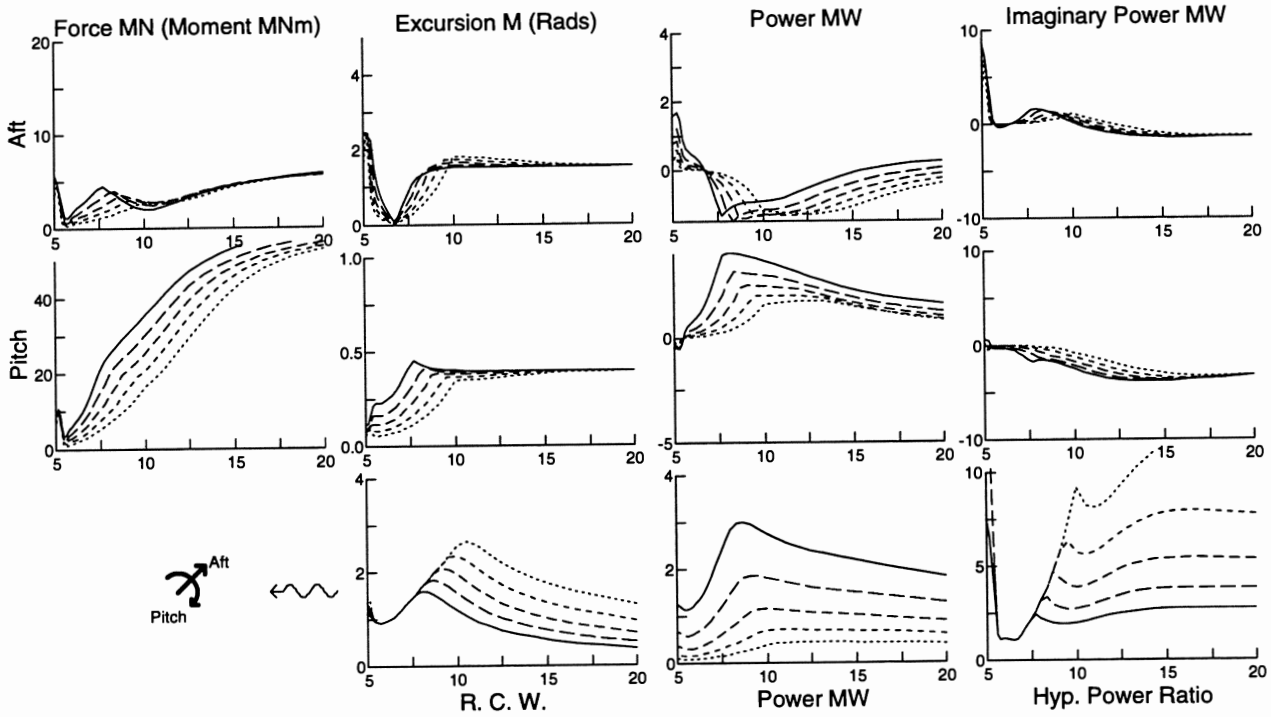

Figure 108: ap_f configuration solo duck with complex control

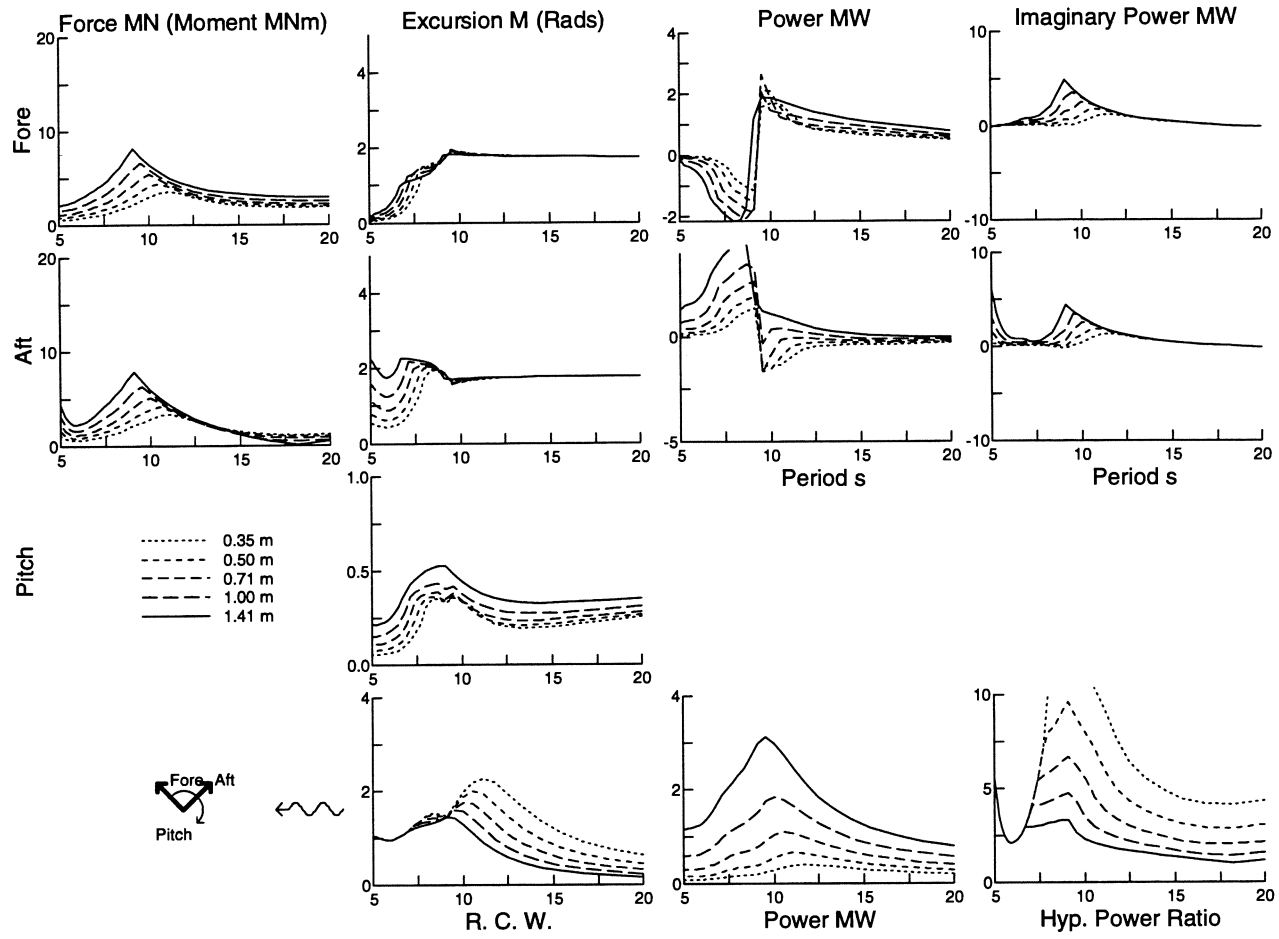

Figure 109: fa_p_ configuration solo duck with complex control

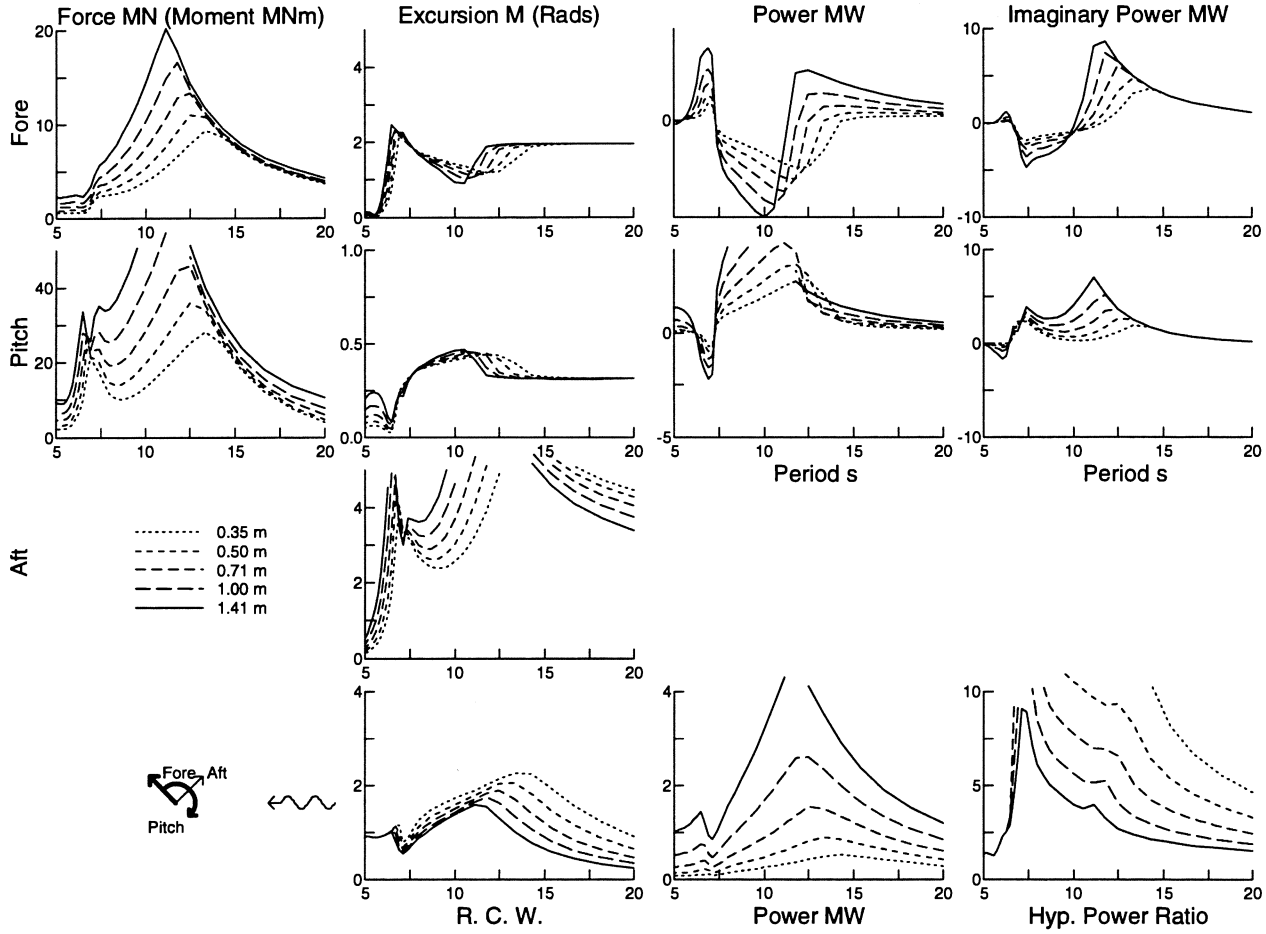

Figure 110: fp_a_ configuration solo duck with complex control

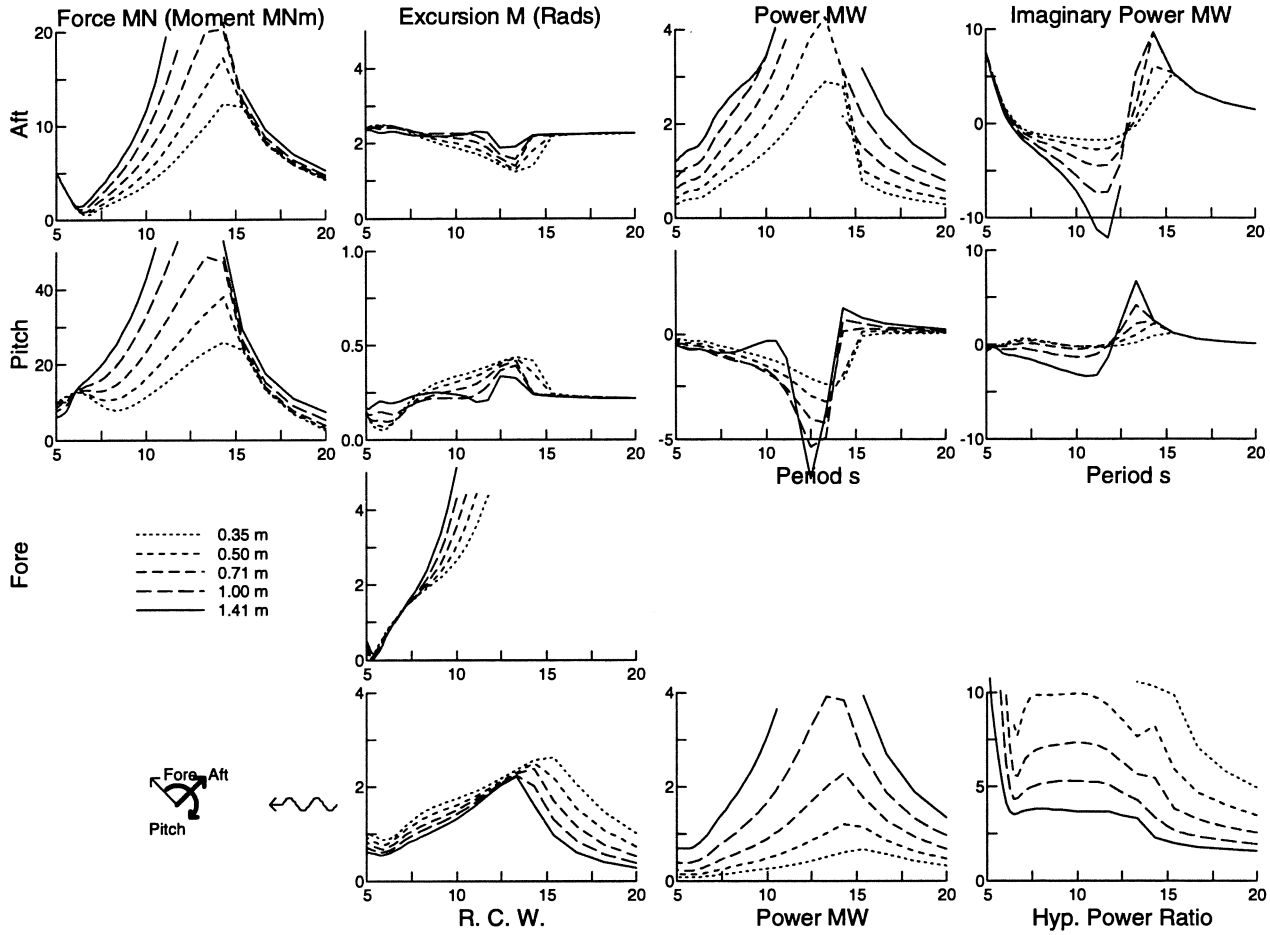

Figure 111: ap_f_ configuration solo duck with complex control

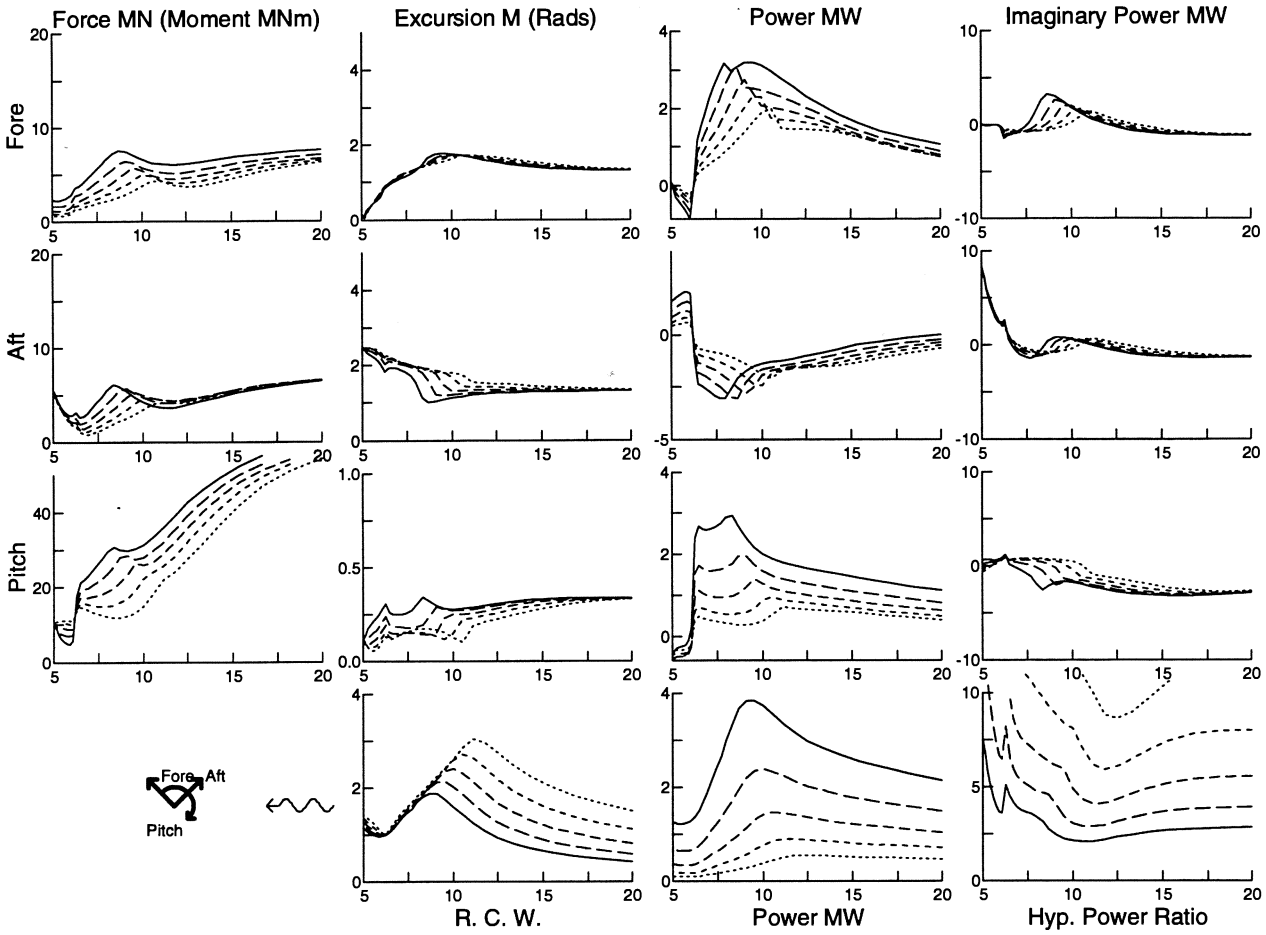

Figure 112: fap__ configuration solo duck with complex control

7 Solo Ducks of Three Widths

The solo duck considered in the previous project [1] had a sharp 90° edge at its rear for the dynammeter in model tests. Such edges induce vortex shedding which will result in energy losses. In practice a rounded duck will be desirable. In this section we consider the rounded ducks used by Woodhead [10] in the study on "Snatch Loads on Solo Ducks".

Three widths of duck are considered 19m, 29m and 49m. The discretisations used to evaluate the hydrodynamic coefficients are shown in figures 113, 114 and 115.

The mass of each duck is 40% of is buoyancy in order to bias the tension legs, and the centre of gravity is at an elevation of 16° from the axis of the duck, at a distance which is determined by the equilibrium conditions.

Results are presented for the optimal complex control in surge, heave and pitch (figures 116 to 118).

A wider duck gives at least as much power as a shorter duck. It is interesting to note that there are regions in which ducks of different widths give almost the same power, for example

- 19m and 29m wide ducks, around 7 seconds, for 1.41m wave amplitude
- 19m and 29m wide ducks, around 8 seconds for 1.00m wave amplitude
- all three ducks, around 8.5 seconds for 0.71m wave amplitude

It is thought that this is due to the singularities in the damping matrices at around 8s. Consider the following reasoning:

1. In section 6, in the region of the singularity, the three degree of freedom case produced no more power than the two degree of freedom cases.
2. In section 6, in the region of the singularity, the two degree of freedom cases were absorbing without reaching the amplitude constraint.
3. Optimal absorption without reaching the amplitude constraint is the same as without an amplitude constraint.
4. From point absorber theory it is known that without an amplitude constraint the maximum power absorbed is independent of the *size* of the body.
5. Consequently the width of the body is not important near the singularities.

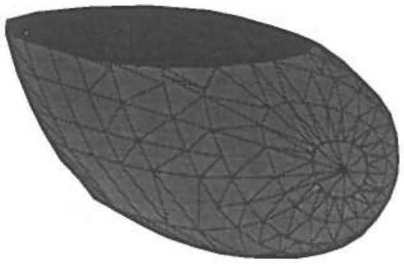

Figure 113: Rounded solo duck discretisation, width = 19m

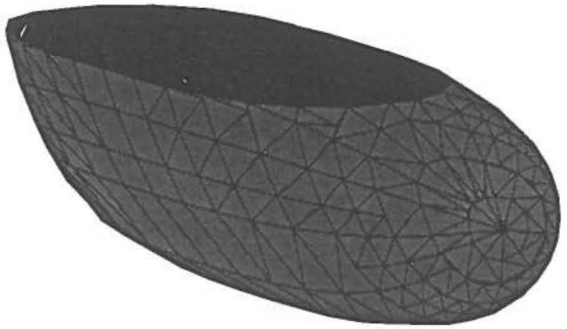

Figure 114: Rounded solo duck discretisation, width = 29m

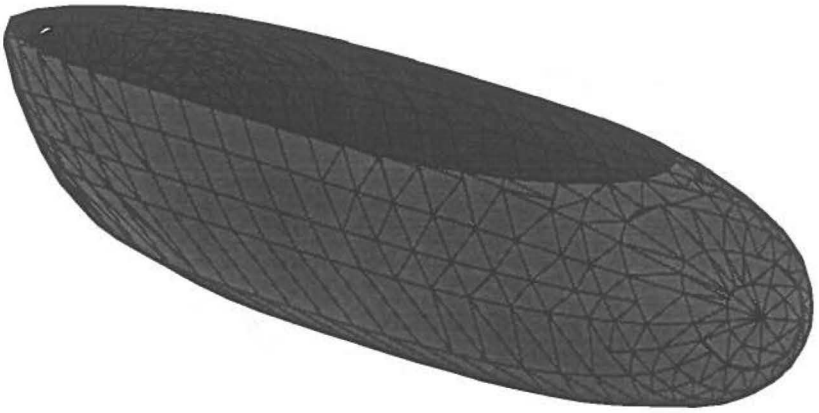

Figure 115: Rounded solo duck discretisation, width = 49m

width	period of max. power	max.power	max.power/width	H.P.R
19m	8.5s	2.6 Mw	0.137 Mw/m	2.4
29m	9.3s	3.7 Mw	0.128 Mw/m	2.2
49m	10.4s	5.6 Mw	0.114 Mw/m	2.2

Table 2: Maximum power absorption for each solo duck

The wave period at which maximum power is absorbed, increases with the width of the duck, see table 2.

The volume of each duck is proportional to its width. Hence the 19m wide duck attains the highest power absorption per unit volume.

The relative capture width in long waves is the same for all three widths. As the period decreases the relative capture width increases, reaches a maximum and then decreases. This maximum occurs at longer periods for the wider ducks.

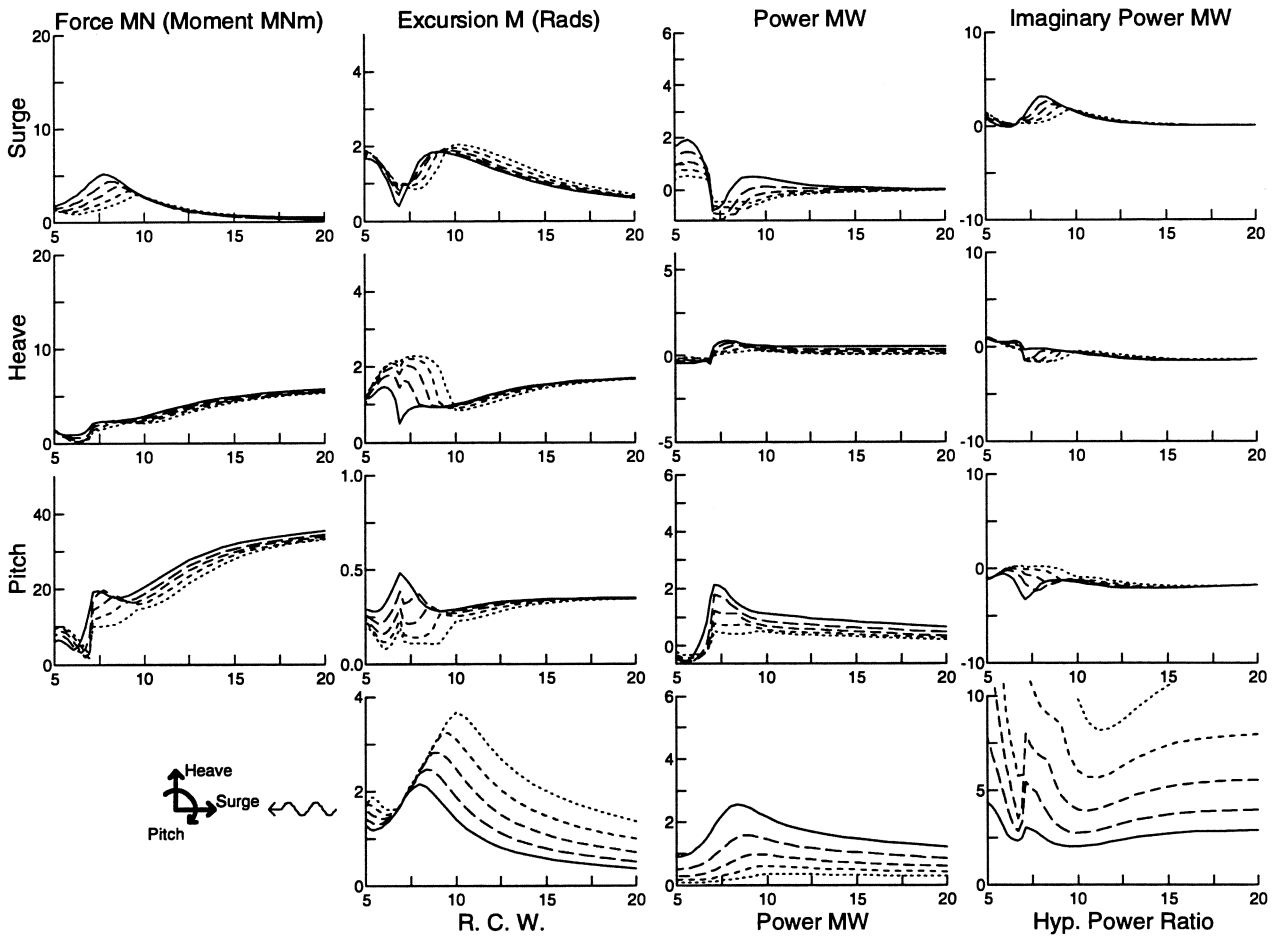

Figure 116: shp__ configuration for 19m wide rounded solo duck with complex control

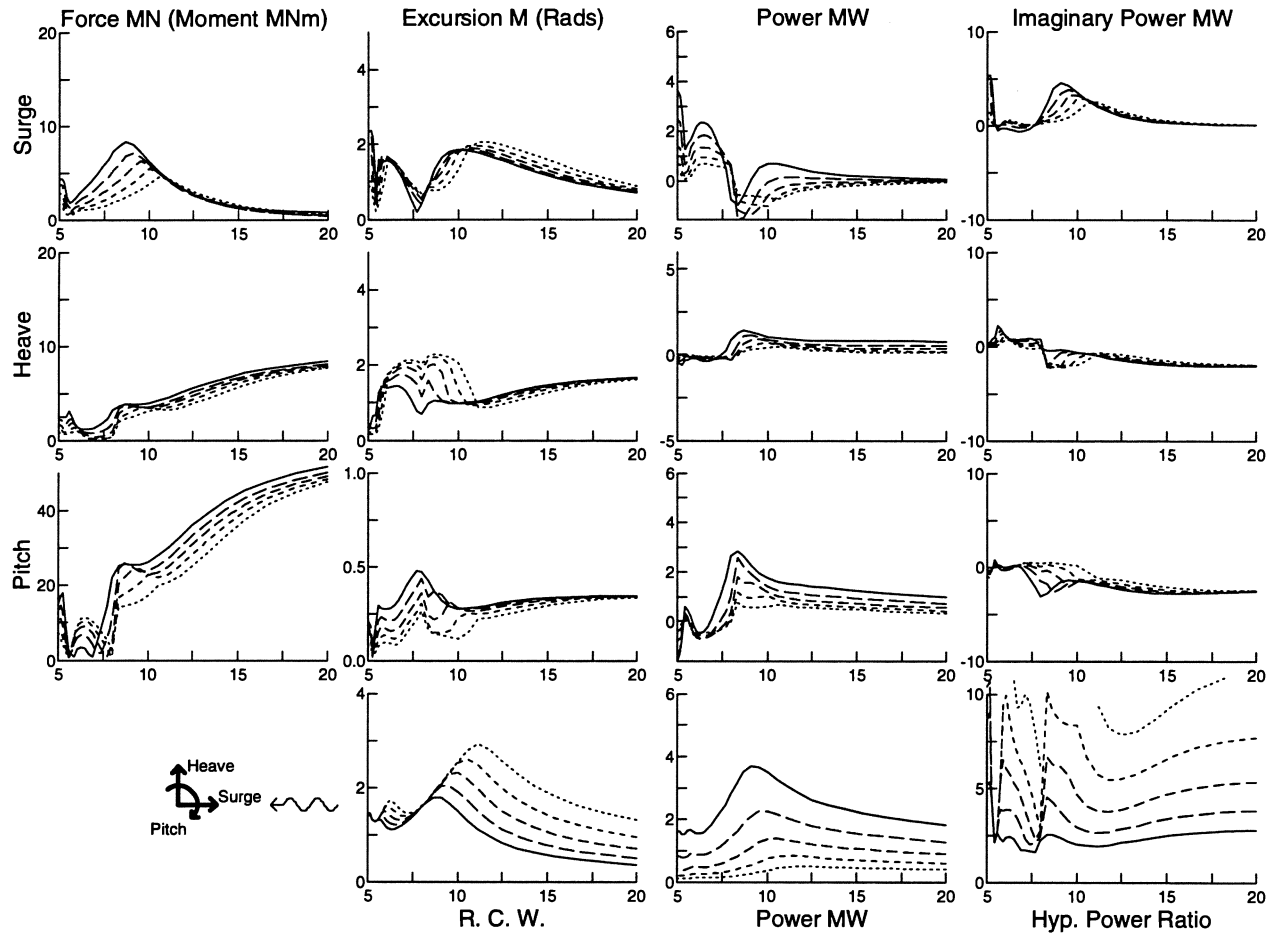

Figure 117: shp__ configuration for 29m wide rounded solo duck with complex control

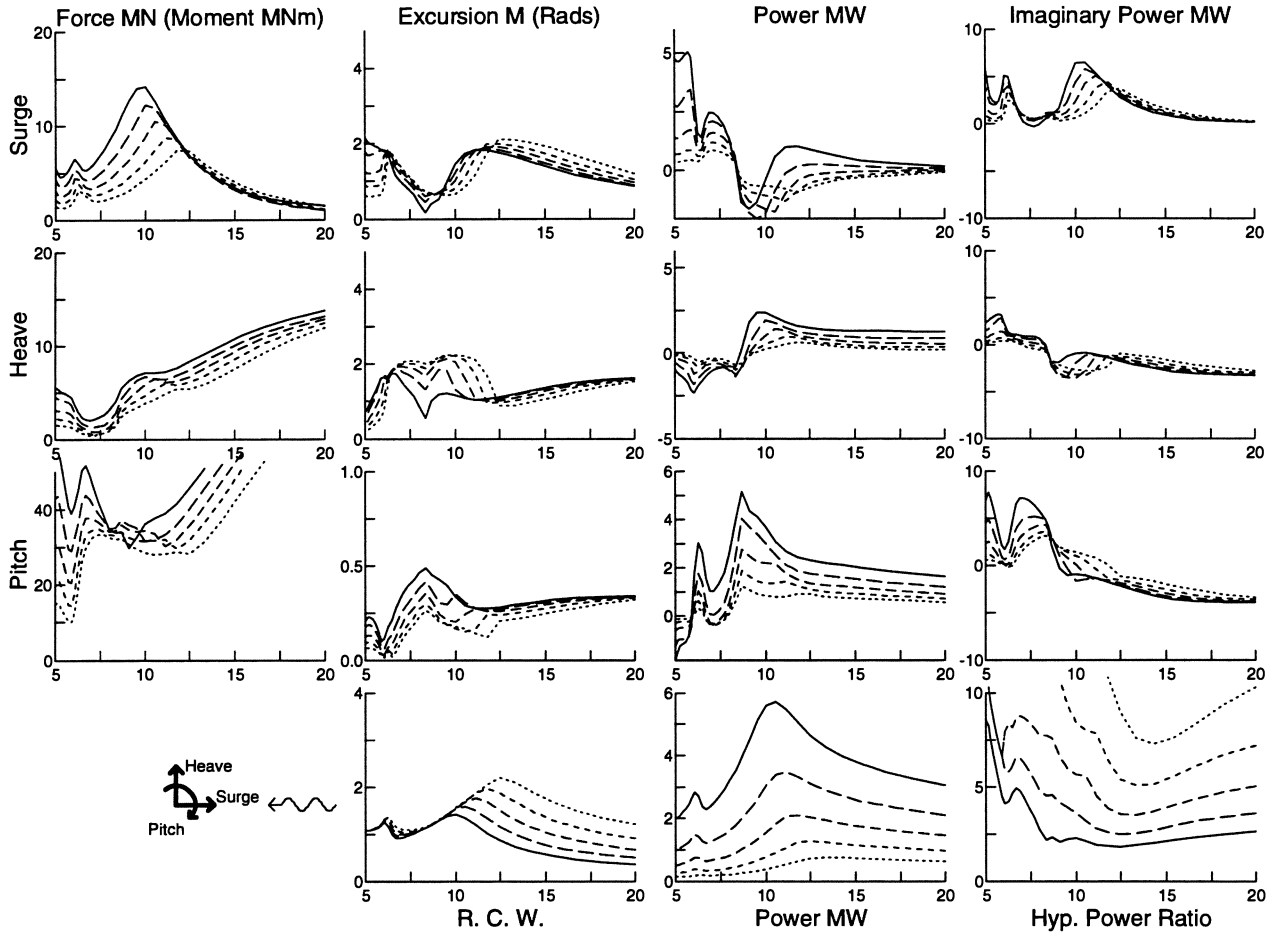

Figure 118: shp__ configuration for 49m wide rounded solo duck with complex control

8 Contribution to JOULE

In this section the contribution to the European Community JOULE programme is described.

The JOULE start-up meeting in Gothenberg in April 1994 was the first formal meeting between all participants in the programme to discuss details of the research. The meeting brought together device teams, hydrodynamic theoreticians and hydraulic designers, for co-operative research on offshore wave energy converters.

It was decided that I would make the following contributions:

1. Continue with studies on translational devices.
2. Provide hydrodynamic coefficients for time-domain studies by device teams: i)to give exact linear time-domain hydrodynamics for small and moderate wave amplitudes; ii) to give approximate non-linear time-domain hydrodynamics for large wave amplitudes.
3. Provide linear frequency-domain results with optimal complex control and optimal real control for comparison with time-domain solutions by device teams.

8.1 Hydrodynamic Coefficients

Graphs are given for the added mass matrix, damping matrix and excitation force vector for the two floats discussed.

The flat float has a diameter of $6m$, a height of $1.5m$ and is half submerged, giving a volume displacement of $21.2m^2$

The tall float has a diameter of $3.3m$, a height of $5m$ and is also half submerged giving a volume displacement of $21.4m^2$.

Hydrodynamic coefficients are evaluated using the 3-D source distribution method. Discretisations for the two floats are shown in figures 119 and 120. It is expected that the results are accurate to within a few percent.

The reference point C^m (see figure 131) is located at the centre of the base of the float.

The complex excitation force, f, is defined by:

$$F(t) = Re[fe^{-i\omega t}] \tag{35}$$

and is with respect to a wave elevation ζ:

$$\zeta(t) = sin[kx - \omega t] \tag{36}$$

Hence, for heave in the long wave limit $f = -\frac{i}{4}\rho g \pi D^2$

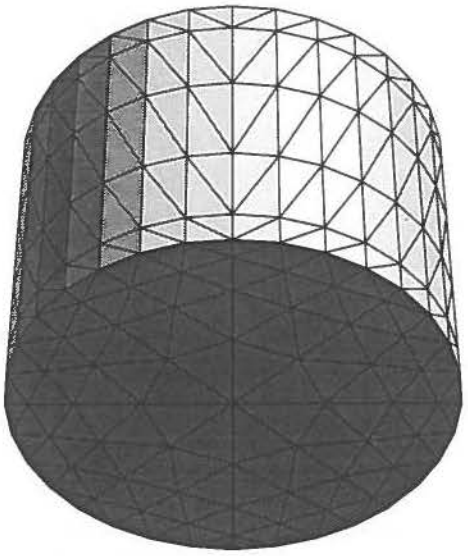

Figure 119: Discretisation for tall float

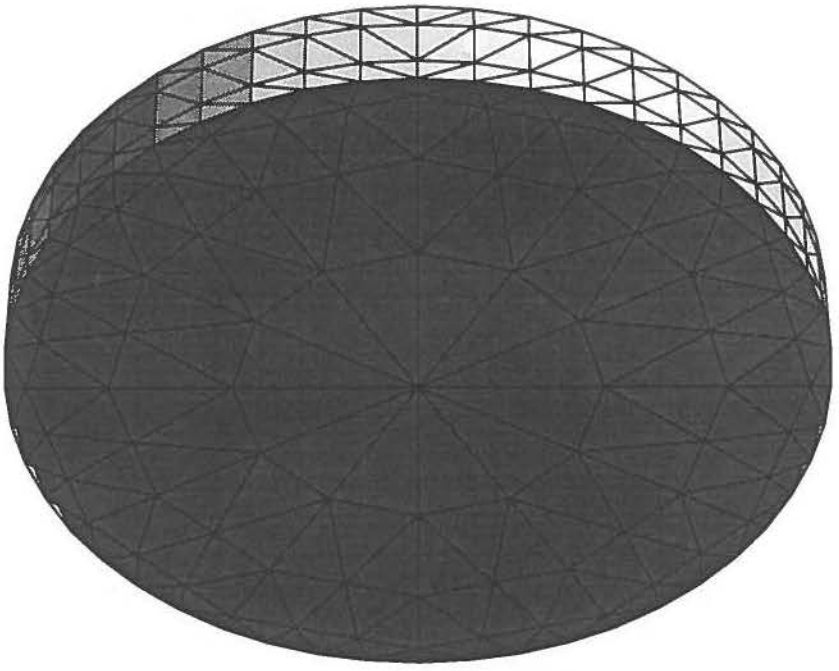

Figure 120: Discretisation for flat float

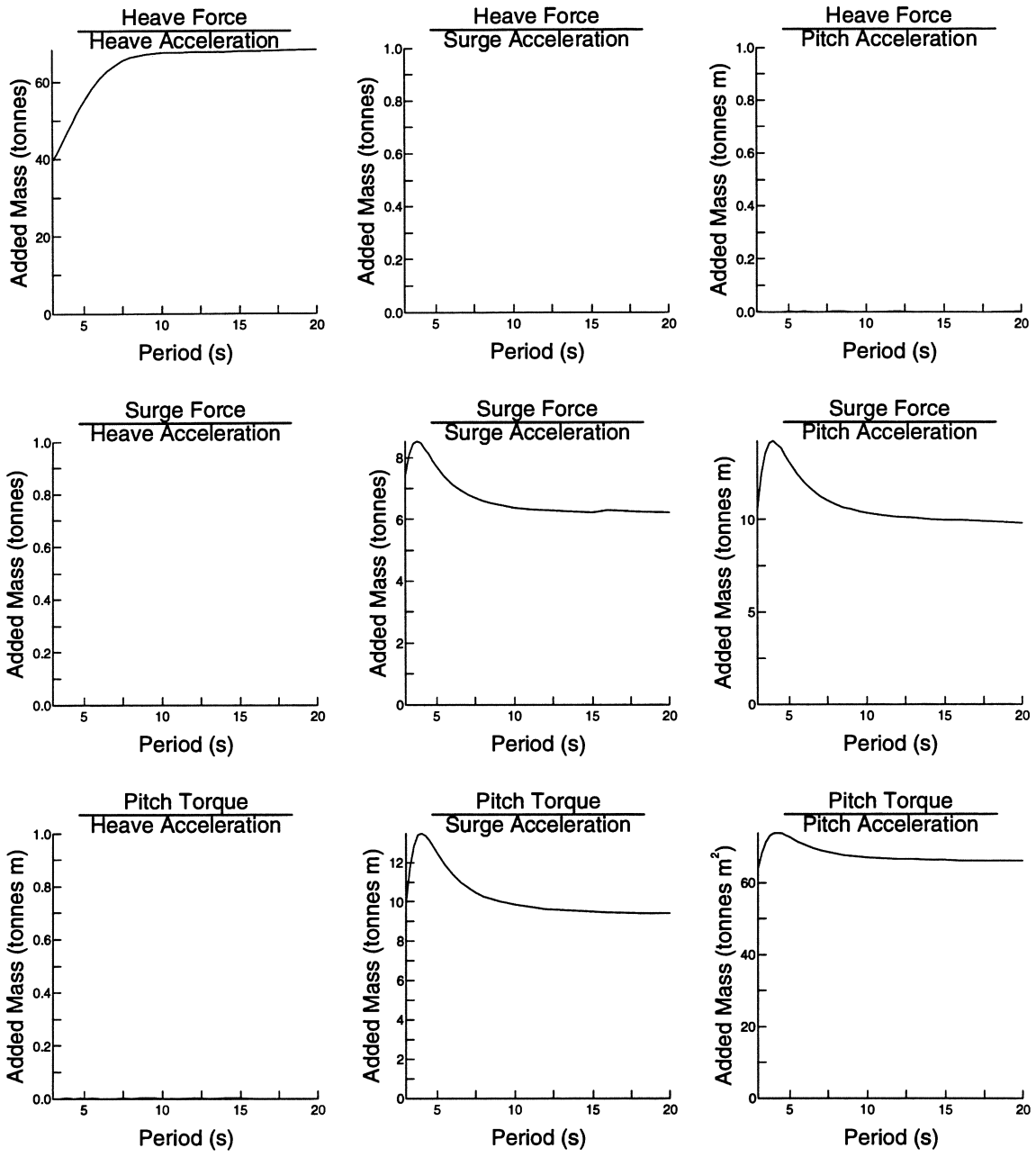

Figure 121: Added Mass matrix for flat float

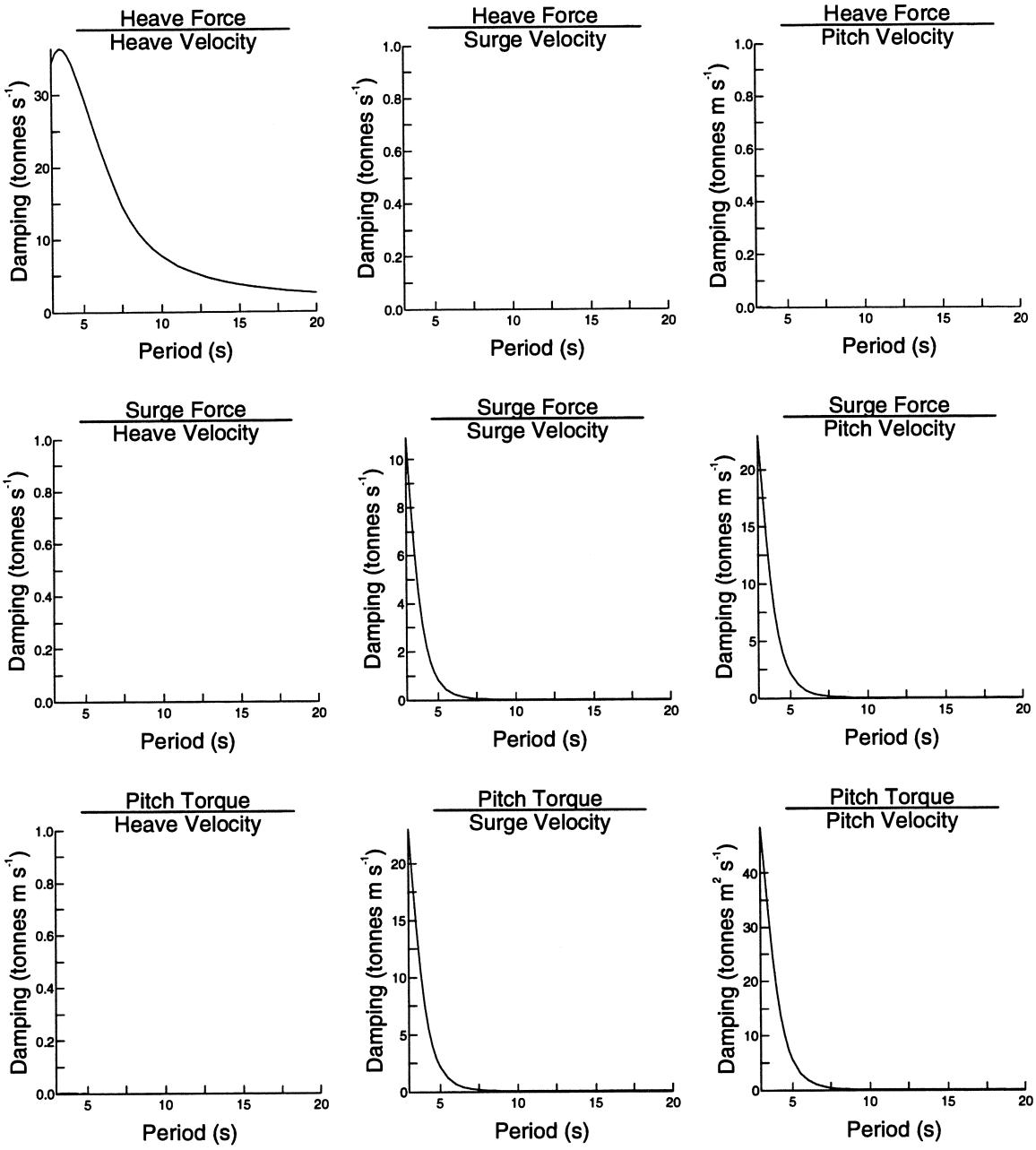

Figure 122: Damping matrix for flat float

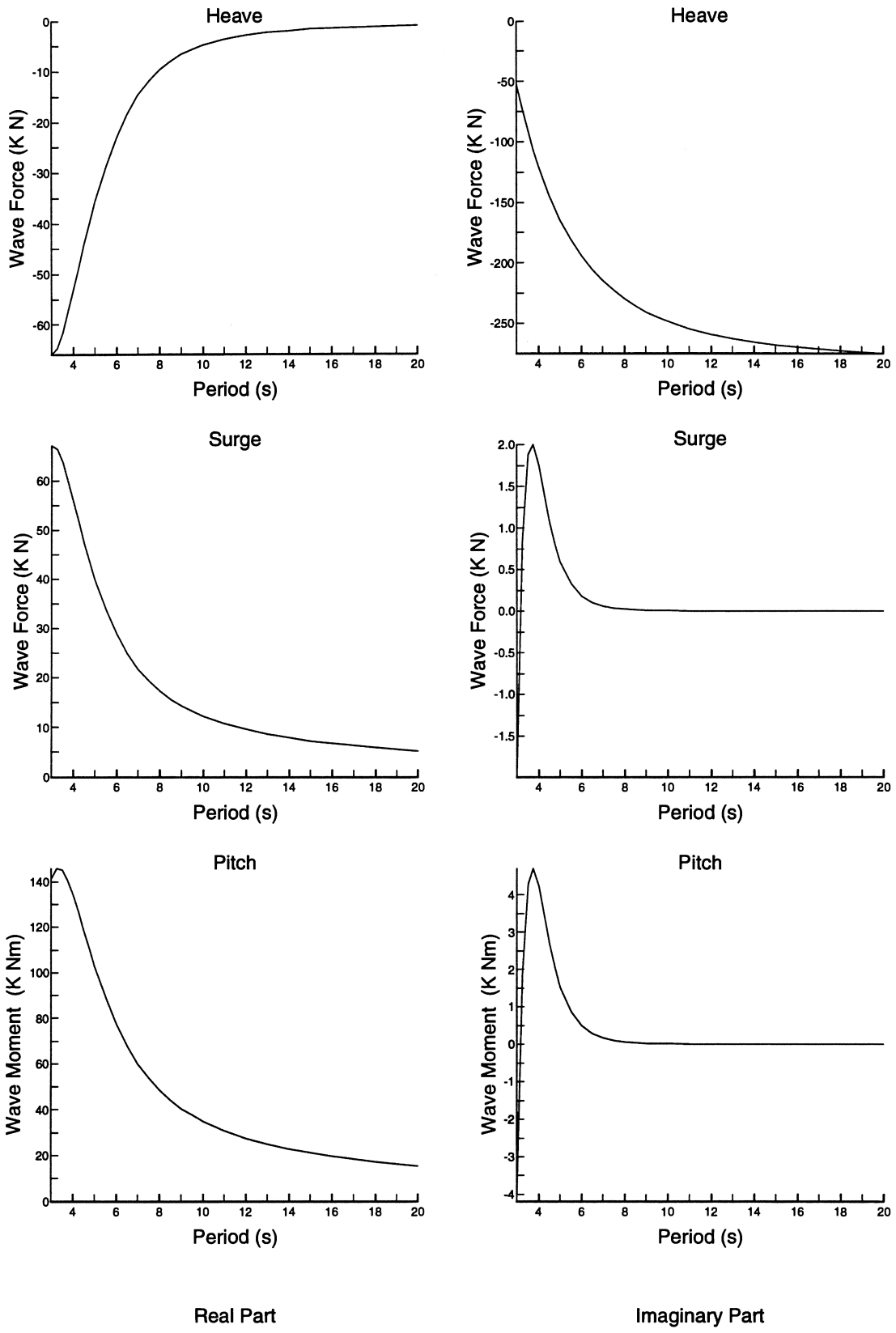

Figure 123: Wave excitation for flat float

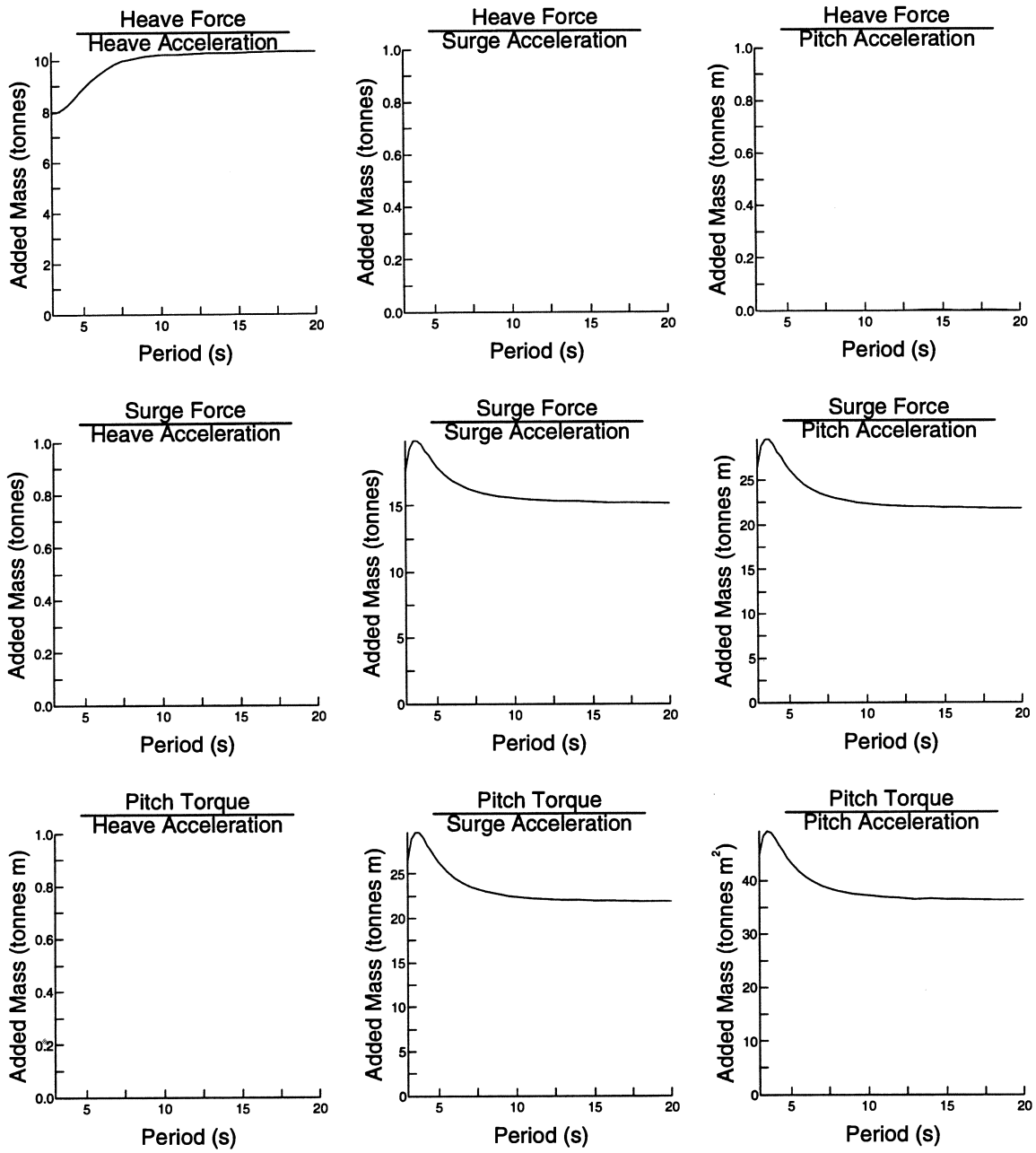

Figure 124: Added Mass matrix for tall float

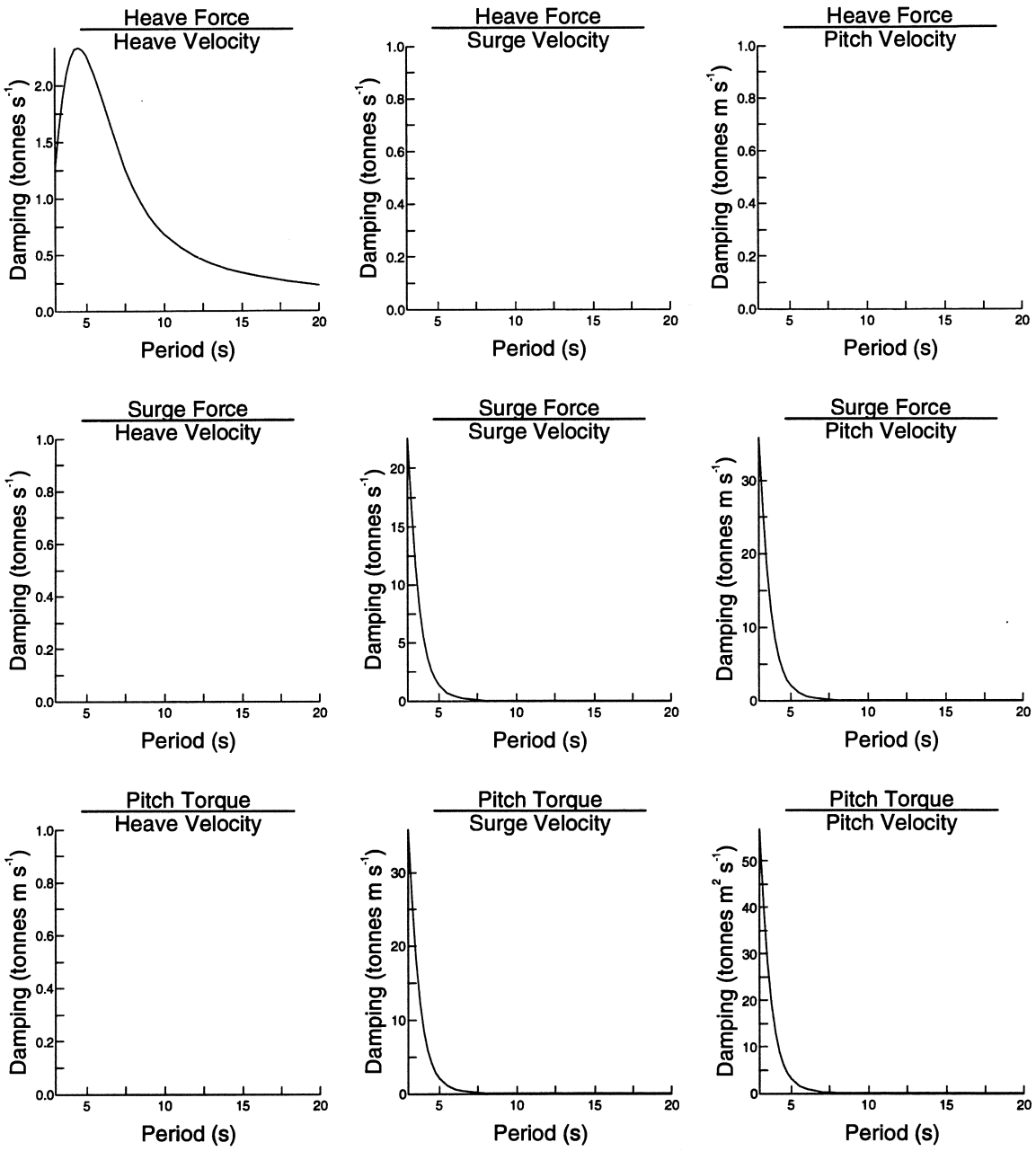

Figure 125: Damping matrix for tall float

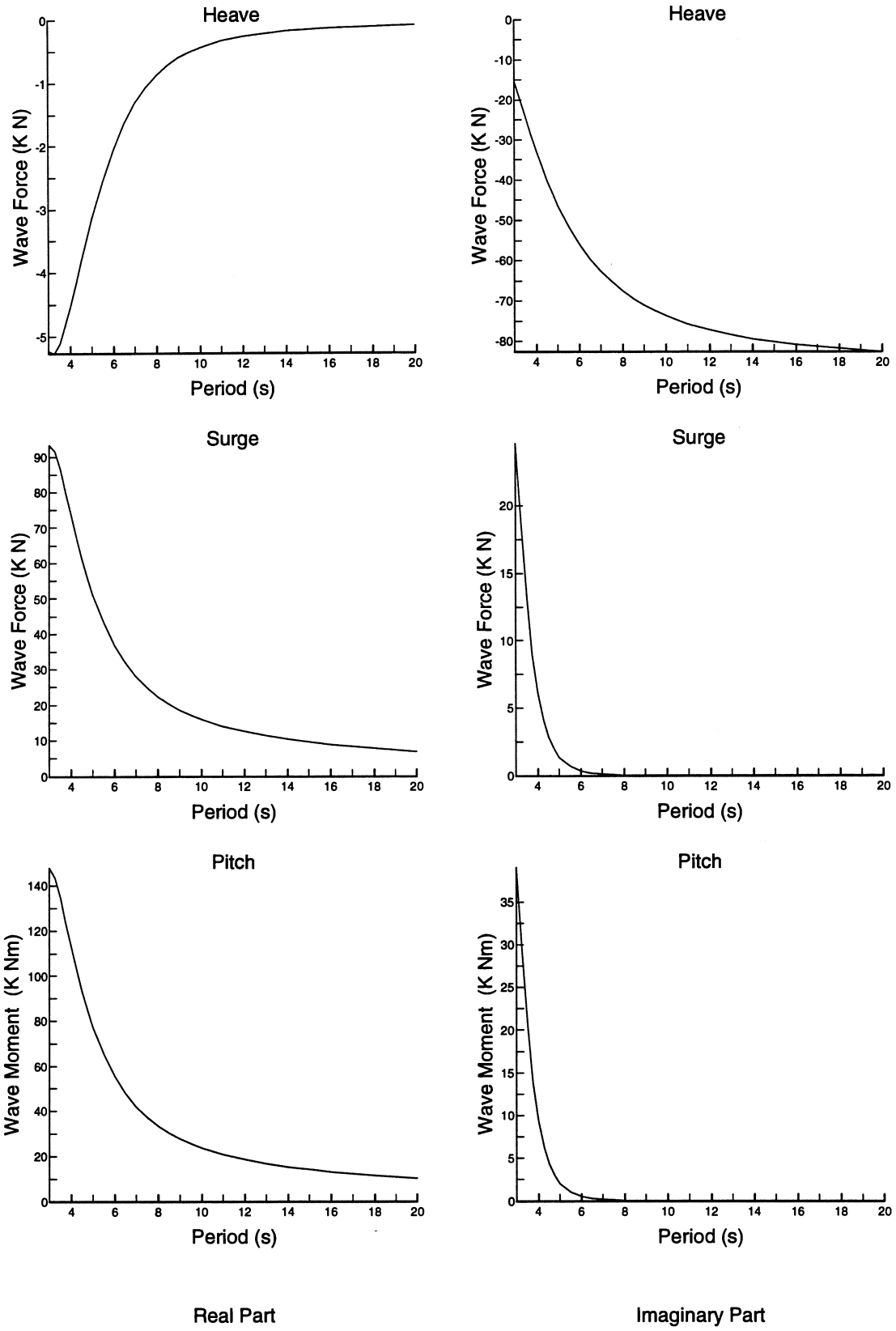

Figure 126: Wave excitation for tall float

8.2 Some Power Absorption Calculations

Two control strategies are considered for power absorption in heave: i) the optimal complex control, ii) the optimal real control. These are described in section 3. In both cases an amplitude constraint is imposed on the heave excursion. The floats are free to move in sway and pitch, however these motions are uncoupled with heave and therefore do not affect the power calculations.

These results assume that the float reacts against an infinite mass (ie is attached to the sea bed) and are therefore not valid for slack moored devices, except *perhaps* for very short wave periods. The results should be valid for tight moored devices at wave amplitudes for which linearity and engineering limitations are not exceeded.

Graphs are given for: the amplitude of the heave control force; the excursion amplitudes for heave, surge and pitch; the power absorbed; the imaginary power; the relative capture width and the hypotenuse power ratio.

The heave control force and the excursion amplitudes for surge and pitch are dependent on the mass distribution of the floats. The weight of the floats are one fifth of the buoyancy force, with the centre of mass at the centre of the floats and pitch moment of inertia of $2886 kgm^2$

The amplitude constraint is chosen to be half the height of the floats.

Results are presented for five incident wave amplitudes ranging from 0.35 m to 1.41 m.

8.3 Optimal Complex Control

Here the constraint is imposed in terms of an absolute amplitude, rather than in terms of a constraint on the ratio of the heave amplitude with the wave amplitude, as presented in Evans [2].

For a small enough wave amplitude, optimal power absorption is obtained without motions reaching the constraint. In such cases the control coefficient is the complex conjugate of the impedance, see equation 21. As the wave amplitude is increased the constraint is eventually reached. For larger wave amplitudes the optimal control is obtained by adding extra damping in order to limit the motions to the imposed constraint.

A large hypotenuse power ratio implies that, over a cycle, large amounts of power are being put into and taken out of the motion of the float, compared with the relatively small time-averaged power absorbed. Losses in the power exchange mechanisms will be amplified and the predicted power absorption will be unattainable. It is thought that hypotenuse power ratios greater than about three are impractical for efficient power absorption, although this figure will greatly depend on the efficiency of the power exchange mechanisms.

Results for the flat and tall buoy in heave are shown in figures 127 and 129.

The tall float has a surge/pitch resonance at about 4.5 seconds resulting in large predicted excursions. In practice these would be reduced due to non-linear effects and viscous damping.

For both floats the constraint is reached at most frequencies. Both have the same power absorptions, although the tall float undergoes larger displacements and has much larger HPRs (except at the heave resonance where it is unity).

8.4 Optimal Real Control

A real control coefficient corresponds to applying damping only. For a small enough wave amplitude the optimal control coefficient is the modulus of the impedance, see equation 13. The imaginary powers are therefore zero and the hypotenuse power ratios are one.

Results for the flat and tall buoy in heave are shown in figures 128 and 130.

As expected, at the heave natural periods the power absorbed with real control is the same as with complex control. Away from resonance the power absorbed using real control is greatly reduced from that of complex control. For the flat float case, at a wave amplitude of 0.5 m real control produces less than half the power from complex control at a hypotenuse power ratio of 2. The same is true for the tall float at 1.41 m wave height.

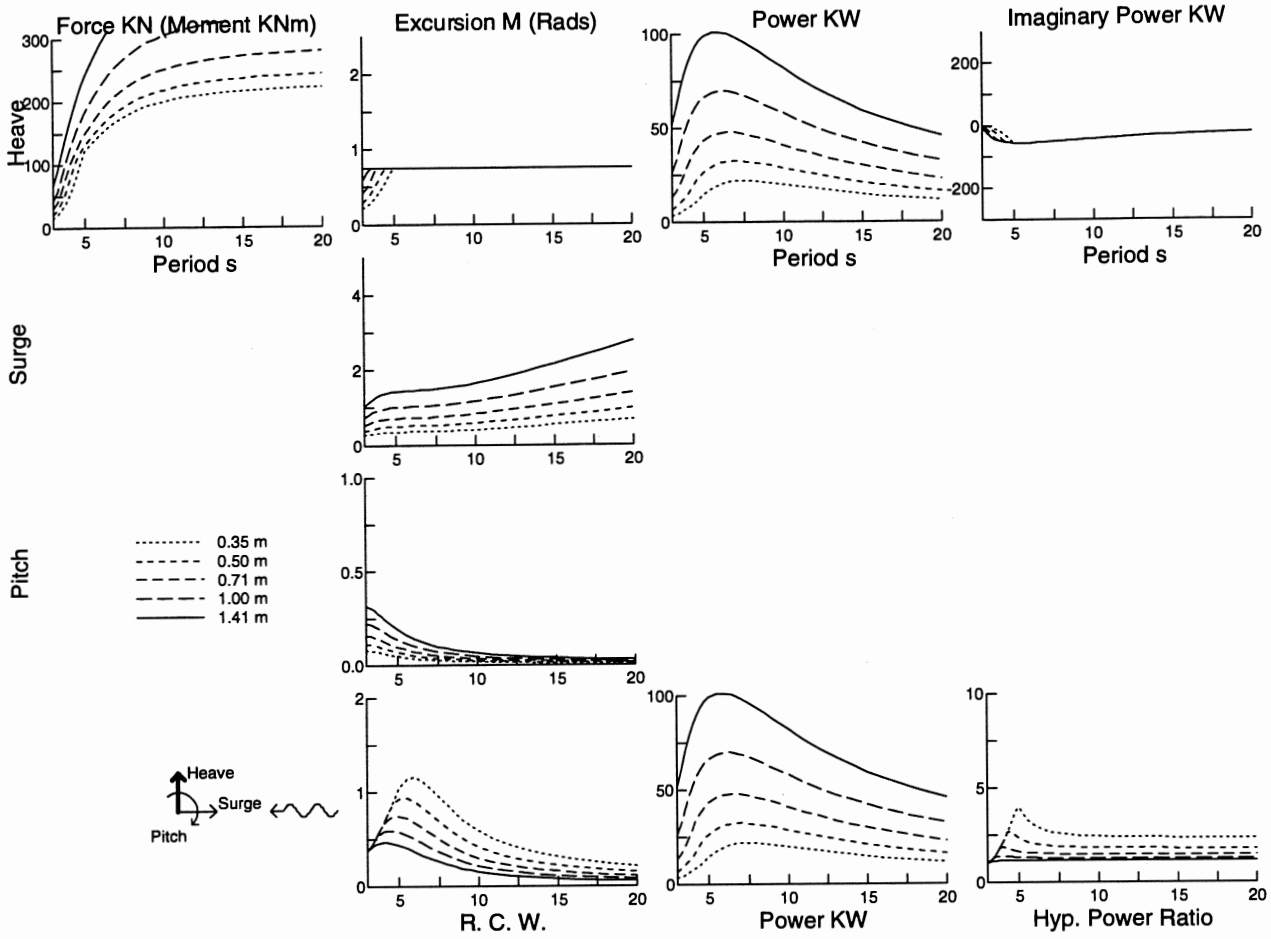

Figure 127: Power absorption for flat float with optimal complex control in heave

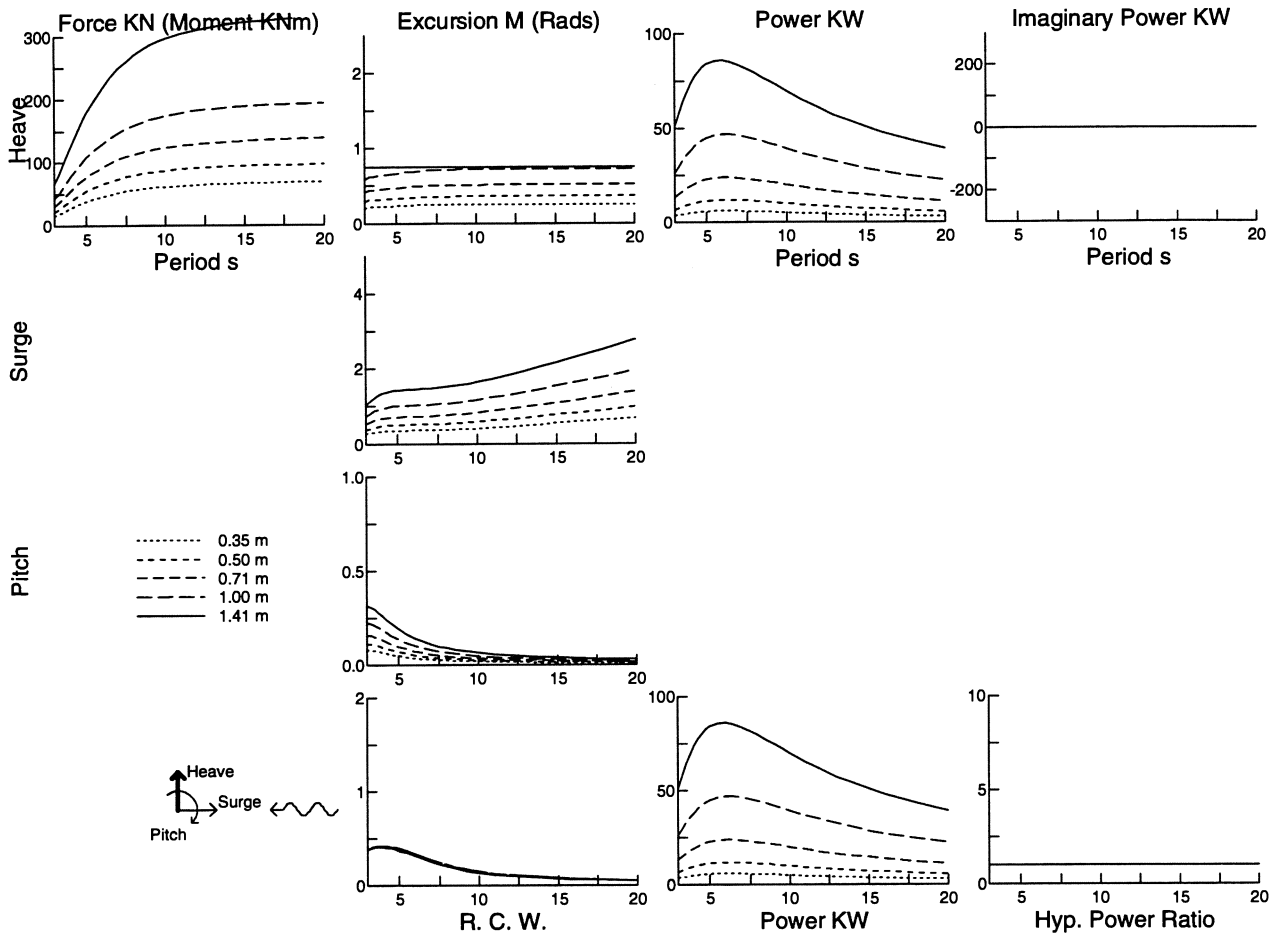

Figure 128: Power absorption for flat float with optimal real control in heave

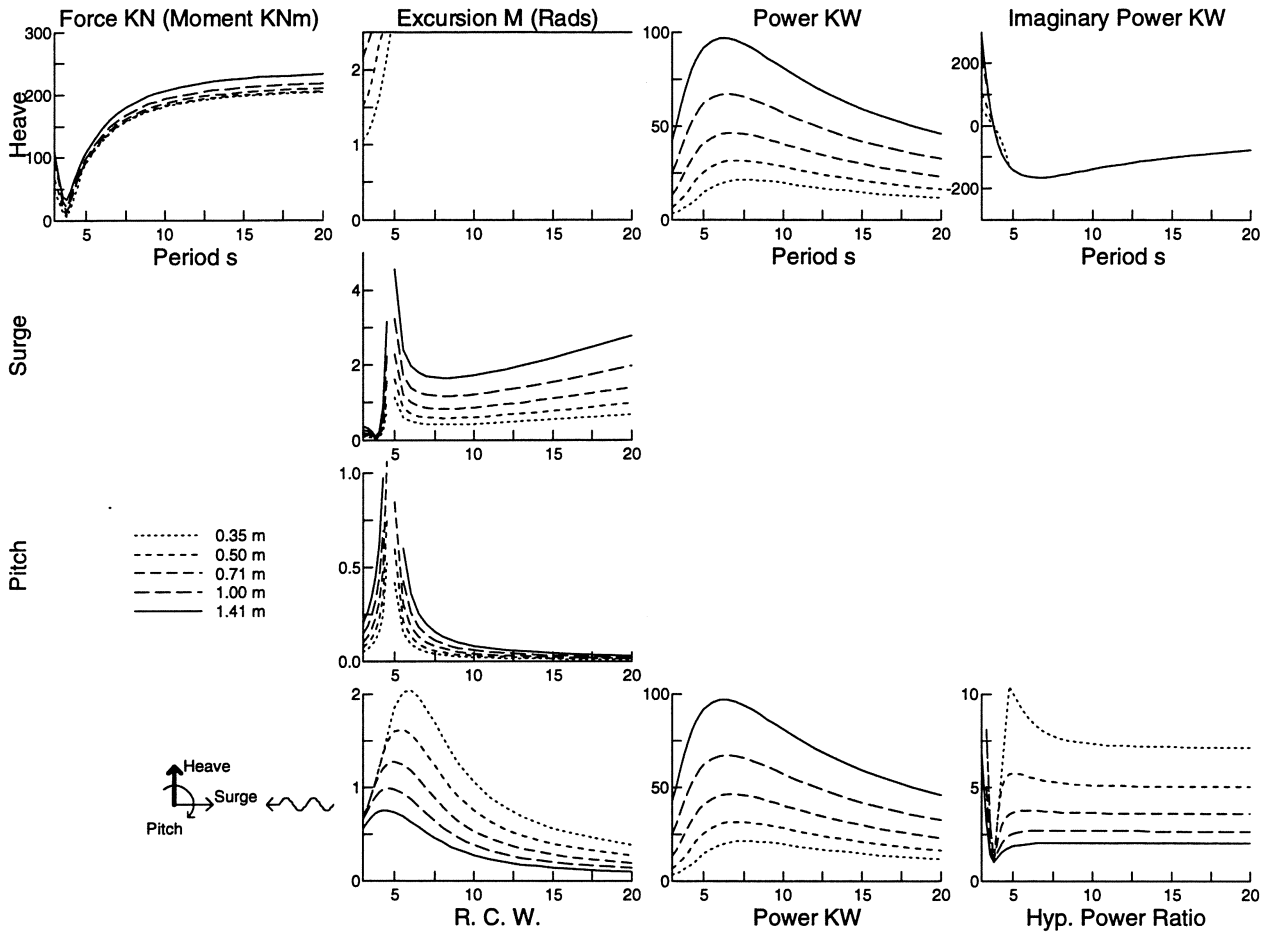

Figure 129: Power absorption for tall float with optimal complex control in heave

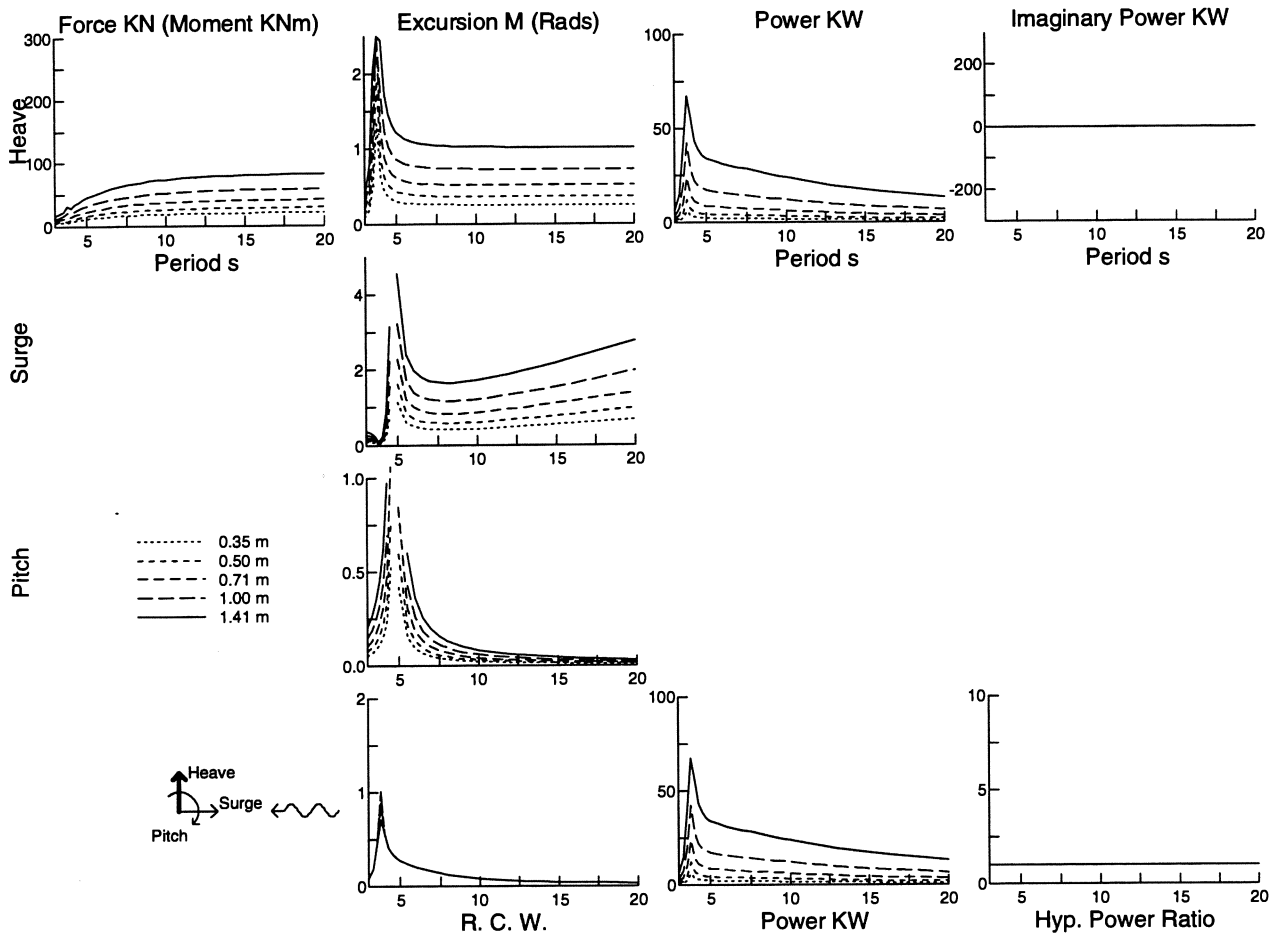

Figure 130: Power absorption for tall float with optimal real control in heave

References

[1] Pizer, D.J. 'Numerical Prediction of the Performance of a Solo Duck', Department of Mechanical Engineering, University of Edinburgh, July 1992. (Full text included as appendix B)

[2] Evans, D. V. 'Maximum wave-power absorption under motion constraints', Applied Ocean Research, 1981 **3** No. 4, 200.

[3] Pizer, D.J. 'Maximum wave-power absorption of point absorbers under motion constraints', Applied Ocean Research, V 15, 1993, pp22-34

[4] Evans, D. V. 'A theory for wave-power absorption by oscillating bodies', J. Fluid Mech., 1976, **77**, 1

[5] Mei, C. C. 'Power extraction from water waves', J. Ship. Res., 1976, **20**, 63

[6] Newman, J. N. 'The interaction of stationary vessels with regular waves', Proc. 11th Symp. Naval Hydrodynamics, London, 1976, p 491.

[7] Evans, D. V. and Linton, C. M. 'Hydrodynamics of wave-energy devices' Joule 1, Annex report B1, Device Fundamentals Hydrodynamics.

[8] Pizer, D.J. and Sayer P. 'A Second-Order Study of Low-Frequency Semi-submersible Motions', Proc 2nd International Offshore Engineering Conference, Singapore, 1993

[9] Pizer, D.J. 'The Influence of Second-Order Wave effects on the Roll and Pitch Motions of Semisubmersibles' PhD Thesis, University of Strathclyde, 1994.

[10] Woodhead, P.L. 'Solo Duck Mooring Forces', Department of Mechanical Engineering, University of Edinburgh 1993.

A Linear Wave Theory

The equations of motion for a floating body are presented in the following four subsections. Details of the formulation may be found [8] and [9].

A.1 Description of the Motions

The formulation is generalised in that displacements are defined with respect to an arbitrarily specified reference point C, rather than the centre of gravity or a point in the equilibrium of the free-surface. Moments are evaluated with respect to the instantaneous position of the reference point — rather than its equilibrium position.

The six degrees of freedom of the rigid body motion are defined by ξ_i, $i = 1 \ldots 6$, where $\boldsymbol{\xi} = (\xi_1, \xi_2, \xi_3) = \underline{C^m C}$ represents the translational displacements of surge, sway and heave, and $\boldsymbol{\alpha} = (\xi_4, \xi_5, \xi_6)$ represents the rotational displacements of roll, pitch and yaw which transform the $\mathbf{i}, \mathbf{j}, \mathbf{k}$, vectors onto the $\mathbf{i}', \mathbf{j}', \mathbf{k}'$, vectors. For a given motion of the body $\boldsymbol{\xi}$ will depend on the choice of C, whereas $\boldsymbol{\alpha}$ is independent of C. See figure 131.

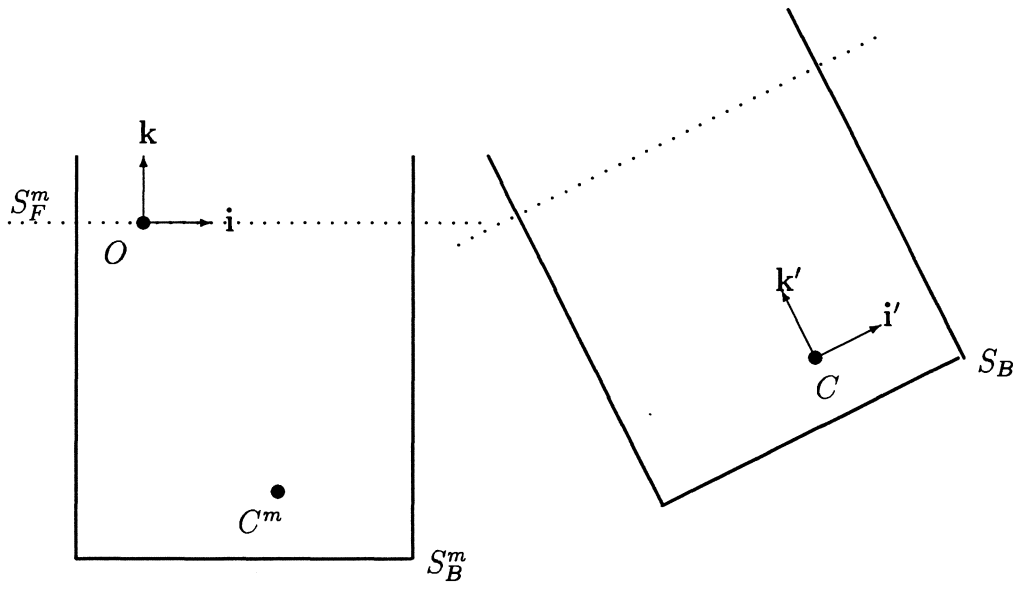

Figure 131: Definition of $\boldsymbol{\xi}$ and $\boldsymbol{\alpha}$

A.2 Equations of Motion

The equations of motion are derived from Newton's laws of motion and the properties of rigid body motion. Neglecting non-linear terms gives:

$$\mathbf{F}^{(0)} + \mathbf{F}_G^{(0)} + \mathbf{F}_C^{(0)} = \mathbf{0} \tag{37}$$

$$\mathbf{F}^{(1)} + \mathbf{F}_G^{(1)} + \mathbf{F}_C^{(1)} = m\ddot{\boldsymbol{\xi}}^{(1)} + m\ddot{\boldsymbol{\alpha}}^{(1)} \times \mathbf{x}'_G \tag{38}$$

$$\mathbf{M}^{(0)} + \mathbf{M}_G^{(0)} + \mathbf{M}_C^{(0)} = \mathbf{0} \tag{39}$$

$$\mathbf{M}^{(1)} + \mathbf{M}_G^{(1)} + \mathbf{M}_C^{(1)} = m\mathbf{x}'_G \times \ddot{\boldsymbol{\xi}}^{(1)} + I_c\dot{\boldsymbol{\omega}}^{(1)} \tag{40}$$

Where $\mathbf{F}$ and $\mathbf{M}$ are the force and moment due to the water, $\mathbf{F}_G$ and $\mathbf{M}_G$ are due to gravity, and $\mathbf{F}_C$ and $\mathbf{M}_C$ are the control force and moment. m is the mass of the device, I_c is its inertia tensor with respect to the reference point, C, the superfix $^{(0)}$ denotes zeroth order (equilibrium) quantities, and $^{(1)}$ denotes linear dynamic quantities.

In cases where the buoyancy force, $\mathbf{F}^{(0)}$, and moment, $\mathbf{M}^{(0)}$, are not balanced by the zeroth order gravity force, $\mathbf{F}_G^{(0)}$, and moment, $\mathbf{M}_G^{(0)}$, there must be other external forces, $\mathbf{F}_C^{(0)}$ and moments, $\mathbf{M}_C^{(0)}$ in order to satisfy the equilibrium condition.

A.3 Forces and Moments Due to Gravity

The gravity forces and moments are derived in [8]. Neglecting non-linear terms gives:

$$\mathbf{F}_G^{(0)} = -mg\mathbf{k} \tag{41}$$

$$\mathbf{F}_G^{(1)} = 0 \tag{42}$$

$$\mathbf{M}_G^{(0)} = -mg\mathbf{x}'_G \times \mathbf{k} \tag{43}$$

$$\mathbf{M}_G^{(1)} = -mg(\boldsymbol{\alpha}^{(1)} \times \mathbf{x}'_G) \times \mathbf{k} \tag{44}$$

$$\tag{45}$$

where $\mathbf{x}'_G$ is the centre of gravity.

A.4 Forces and Moments Due to the fluid

The hydrostatic ($\mathbf{F}^{(0)}$ and $\mathbf{M}^{(0)}$) and hydrodynamic ($\mathbf{F}^{(1)}$ and $\mathbf{M}^{(1)}$) forces and moments are given by:

$$\mathbf{F}^{(0)} = \rho g V \mathbf{k} \tag{46}$$

$$\mathbf{M}^{(0)} = \rho g V \begin{bmatrix} +y'_b \\ -x'_b \\ 0 \end{bmatrix} \tag{47}$$

$$\mathbf{F}^{(1)} = -\rho \int_{S_B^m} \mathbf{n}' \Phi_t^{(1)} \, dS - \rho g A[\xi_3^{(1)} + \xi_4^{(1)} y_f' - \xi_5^{(1)} x_f']\mathbf{k} \tag{48}$$

$$\begin{aligned} \mathbf{M}^{(1)} = & -\rho \int_{S_B^m} \mathbf{x}' \times \mathbf{n}' \Phi_t^{(1)} \, dS \\ & -\rho g \begin{bmatrix} +Ay_f' \xi_3^{(1)} + (AL_{yy}' + Vz_B')\xi_4^{(1)} - AL_{xy}' \xi_5^{(1)} - Vx_B' \xi_6^{(1)} \\ -Ax_f' \xi_3^{(1)} - AL_{xy}' \xi_4^{(1)} + (AL_{xx}' + Vz_B')\xi_5^{(1)} - Vy_B' \xi_6^{(1)} \\ 0 \end{bmatrix} \end{aligned} \tag{49}$$

Where $\Phi^{(1)}$ is the linear velocity potential, A is the water-plane area, V is the volume displacement, x_B is the centre of buoyancy, L_{xy} ... are moments of the water-plane area and (x_f, y_f) is the centroid of the water-plane area. The surface integrals are performed over the equilibrium wetted surface of the body, S_B^m, and may be separated from the displacements to give added masses, dampings and wave excitation terms.

B Numerical Prediction of the Performance of a Solo Duck

The report describing the previous research contract has been included here for easy reference.

Numerical Prediction of the Performance of a Solo Duck

David Pizer

July 17, 1992

Summary

The motion of a solo-duck wave-energy absorber in 3-dimensional waves is investigated using a computer program based on linear water-wave diffraction theory. Numerical predictions of the hydrodynamic coefficients are compared with experimental results and known analytical results.

Due to singularities in the damping matrix, large displacements are required in order to achieve the maximum efficiencies — even at high frequencies. Some modification to complex conjugate control is required in order that the linear assumption is not invalidated.

The consideration of maximum power absorption under a motion constraint provides information for the design of a new controller which no longer exhibits singular behaviour.

Linear predictions of forces, angles, displacements, power and efficiencies are presented for a solo duck.

Contents

1 Introduction

The Solo duck differs from the spine based system in that it is a *point absorber* type of wave-energy device. Theoretically such devices may absorb more power than is incident in the width of sea they occupy. However, in practice this theoretical maximum may be unobtainable. The longer the wavelength and the smaller the body, the larger its displacement must be in order to attain the maximum efficiency. At some point the linear theory breaks down and the results are not valid. In this study the practicality of the point absorber effect is investigated by evaluating the maximum power absorption under a constraint on the amplitude of the displacements.

Since the start of the wave power project at Edinburgh in 1973 the behaviour of wave energy plants have mainly been investigated by small-scale model testing. Numerical methods have been restricted to the idealised two-dimensional case, which is of little use in investigating the properties of point absorber devices.

In this study a three-dimensional linear water-wave diffraction program is used to investigate the performance of a solo duck. The program models the interaction of a water wave with a rigid object under the assumption that the displacements are small enough to be linear. This assumption is known to be valid in other applications.

The numerical procedure begins with the generation of a multi-faceted approximation to the shape being studied — usually convex objects like ducks, the Bristol cylinder or ships. It can also handle objects like semi-submersibles but perhaps not 'concave' objects like oscillating water columns.

The program computes the fluid flow around the body produced by an approaching wave field of a specified frequency, approach angle and water depth. The forces and torques on the body are then evaluated directly from the hydrodynamic pressure at each facet. See section 4 for a brief description of the numerical method.

Numerical results are verified by comparison with published numerical computations for a sphere [1], and with experimental results obtained by Skyner [2] for a solo duck.

First use of the program produces exciting results in agreement with the point absorber theory, see section 3. For example, a relative capture width of 15 can be obtained for a 20 second wave period. However sober reappraisal shows that to achieve this the duck would have to jump clear of the water in a 1 millimetre wave.

Clearly some reasonable limits on the amplitudes of the motions must be imposed. The ones we have selected for this report are that the duck motion will be linear up to an amplitude of a quarter of a duck diameter, and a pitch rotation of half a radian. Model tests will be needed to confirm this choice.

With these constraints imposed further numerical analysis computes how the ideal control should be modified to yield optimal power absorption — still assuming linear hydrodynamic behaviour.

2 General conclusions

1. A three-dimensional linear wave-diffraction computer program can now be a productive design tool for the linear regime.

2. The method gives good agreement with well-known analytical results for simple geometries. For a 256 faceted sphere the results are within 3 %

3. The agreement with the experimental measurements of hydrodynamic coefficients presented by Skyner in 1987 is fairly good. Comparisons are given in section 5.

4. A duck model with 320 facets produces results which are within 3 % of a much larger number of facets. Computing for 30 frequencies and 19 wave angles for one model takes eight hours using a computer power of 15 MIPS. With overnight and weekend batch runs this is now an acceptable productivity.

5. The damping matrix was found to exhibit a variety of singularities. Some of these were unexpected and have important consequences. In particular, the displacements required in order to attain maximum power absorption become very large — even for a large body at high wave frequencies.

6. The optimistic hopes for point absorbers should be modified by the application of motion constraints. Even when these are imposed, the duck is able to absorb power from outside the width of sea it occupies. A 10 metre diameter, 29 metre wide, solo duck has a relative capture width of a little over 2 for the centre of the South Uist wave spectrum in power levels of about 20 KW/metre. Efficiencies for various wave amplitudes, wave directions and frequencies are given in section 7.

7. In head-on waves the difference in productivity between a duck using any two degrees of freedom is not much below (10 %) that of using all three degrees of freedom.

8. In oblique waves the efficiency of a pitch-fore-aft system decreases only slightly for long waves, but is halved for short waves. See figure 18.

9. It is not surprising to find that in head waves the results for 3 degrees of freedom are identical to those for the full 6 possible degrees. However for oblique waves there are interesting and surprising differences : With 6 degrees of freedom in short oblique waves the duck gives more output than in a the head sea. At 40 degrees at a wavelength of 7 duck diameters, the oblique output is almost double that of the head sea.

10. The increased efficiency of the six degrees of freedom system in short oblique waves suggests that the performance of the duck may be improved by modifying its geometry and/or by considering an array of solo ducks.

3 Power Absorption Theory in Three Dimensions

3.1 Linear Wave Diffraction Theory

Virtually all theoretical progress on the interaction of water waves with a floating body has been based on the assumption of an irrotational incompressible inviscid fluid which undergoes only small displacements from its static equilibrium state. This linear theory has proven highly successful in predicting the motions of ships and offshore structures, even in relatively severe environments.

3.1.1 The principal of superposition

A powerful property of all linear theories is that solutions of elementary problems may be superposed to give the solution of a complicated problem. Systematic comparison between theory and experiment throughout such a synthesis identifies regions of validity of the theory and provides great insight.

3.1.2 The frequency domain

It is assumed throughout this study that all time-dependence is harmonic with circular frequency ω. The time-dependence of a quantity $U(t)$ is then removed by the introduction of the complex variable U:

$$U(t) = Re\{Ue^{i\omega t}\}$$

3.2 Key Theoretical Results of 3-D Power Absorption

The theoretical fundamentals of wave power absorption appeared in 1976 with independent publications By Evans [3] , Mei [4] and Newman [5]. A review of the key results relevant to a point absorber device follows.

3.2.1 Hydrodynamic forces

Using the principal of superposition the hydrodynamic forces and torques, represented by the complex vector $\mathbf{F}_H$, may be decomposed into its fundamental components:

$$\mathbf{F}_H = \mathbf{X} - i\omega\mathbf{A}\mathbf{U} - \mathbf{B}\mathbf{U} \tag{1}$$

$\mathbf{X}$ is the excitation force and is the hydrodynamic force exerted on a body fixed in waves. The added mass $\mathbf{A}$ and damping $\mathbf{B}$ terms result from the motion of the body in otherwise

still water. **X**, **A** and **B** may be found either by experiments, such as those conducted by Skyner [2], or by numerical methods, as described in section 4.

Note, there exists an important identity relating the damping and the excitation force:

$$B_{ij} = \frac{1}{8\lambda P_w} \int_0^{2\pi} X_i^*(\theta) X_j(\theta)\, d\theta \tag{2}$$

where λ is the wave length, θ is the wave angle and P_w is the power of the incident wave per metre of wavefront.

3.2.2 Power absorption

The power imparted to the body by the fluid is given by the scalar product of the hydrodynamic force and the velocity. This is averaged over a wave period to give the time averaged power, P . The maximum power absorption is

$$P = \frac{1}{8}\mathbf{X}^*\mathbf{B}^{-1}\mathbf{X} \tag{3}$$

and is attained when the velocity of the body is given by

$$\mathbf{U} = \frac{1}{2}\mathbf{B}^{-1}\mathbf{X} \tag{4}$$

Here $*$ denotes the complex conjugate transpose, and $\mathbf{B}^{-1}$ is the inverse of the matrix **B**.

3.2.3 Efficiency

The capture width l of a device is defined as the length of wave front over which the device absorbs 100 % of the incident power.

$$l = \frac{P}{P_w} \tag{5}$$

The efficiency is expressed in terms of its relative capture width η. This is defined as the capture width divided by the device width, W:

$$\eta = \frac{l}{W} \tag{6}$$

Hence, relative capture widths greater than 1 mean that the device is absorbing more power than is in the width of sea it occupies.

3.2.4 Axi-symmetric bodies

For axi-symmetric bodies, symmetry gives the angular dependence of the excitation force and the integrals in (2) may be evaluated to give:

$$l = \frac{\lambda}{2\pi} q \tag{7}$$

where q is the q-factor which is dependent upon the mode(s) of motion . For heave $q = 1$, for surge (or pitch) $q = 2$, and for heave and surge (or pitch) $q = 3$.

This is perhaps a surprising result. It implies that the power absorbed is independent of the size of the body and is unlimited as the wavelength increases. There are, of course, limitations to this result. The the longer the wavelength and the smaller the body, the larger its displacement must be in order to attain the maximum efficiency. At some point the assumptions of linear theory must be invalidated. Nevertheless efficiencies greater than one are attainable, and may result in three-dimensional point absorber devices being more cost-effective than elongated bodies.

3.2.5 The small device limit

For general three dimensional bodies the angular dependence of the excitation force can only be found numerically and non integer q-factors will result. However in the limiting case of a small device in long waves the angular dependence of the excitation force is known. For heave $q \rightarrow 1$, for surge $q \rightarrow 2$, and for pitch $q \rightarrow 1$ if the pitching motion has a net volume displacement, otherwise $q \rightarrow 2$. These results are also limited by the assumptions of linear theory.

3.3 The Control Force

The correct external control force $\mathbf{F}_C$ must be applied to the device to make it move with the optimal velocity and extract the most power. $\mathbf{F}_C$ may be achieved by applying appropriate spring, inertia and damping to the system. These are expressed in terms of the complex control matrix $\mathbf{C}$,

$$\mathbf{F}_C = -\mathbf{C}\mathbf{U} \tag{8}$$

The real part of $\mathbf{C}$ is the applied damping, through which power is absorbed. The imaginary part of $\mathbf{C}$ represents spring or inertia.

On solving the equations of motion it may be shown that for maximum power absorption

$$\mathbf{C} = \mathbf{Z}^* \tag{9}$$

where $\mathbf{Z}$ is the impedance matrix of the body. Z_{ij} is the inertia and fluid force in the i^{th} mode due to a unit velocity in the j^{th} mode. This form of C is known as complex conjugate control.

4 Numerical Evaluation of the Hydrodynamic Forces

Numerical methods exist for modelling the interaction of water waves with a floating body for two or three dimensions in water of infinite or constant finite depth. They more or less fall into two categories:
a) specific geometries — in which geometric properties are used to simplify the problem analytically ;
b) general geometries — in which the geometry is specified by a finite number of data points.

Solutions for specific geometries appeared first, (2-D Ursell [6], 3-D Havelock [1]), and have served as useful checks on the accuracy of the general solutions.

4.1 Three-Dimensional Source-Distribution Method

For this report a 3-D, finite depth, general geometry solution is used, based on the source distribution method described by Garrison and Chow [7]. The computer code used in this study was developed by the author at the University of Strathclyde as part of a doctoral study on the motions of semi-submersibles.

4.1.1 Description of method

The solution is based on the Green's function for a pulsating point wave source. The Green's function may be thought of as the most fundamental solution of the water wave problem. It satisfies all the necessary mathematical conditions in the absence of any bodies.

If there is a body in the fluid there is an extra mathematical condition that must be satisfied on the body surface. This states that the normal velocity of the fluid must match the normal velocity of the body, i.e. no fluid must flow through the body.

In the source distribution method wave sources are distributed over the surface of the body. The density of this distribution is evaluated by imposing the mathematical condition on the body surface. By the principal of superposition all the other conditions are automatically satisfied and the fluid motion is known.

The fluid force on the body is then found by direct integration over the body of the Bernoulli pressure.

- **X** is obtained by considering the scattering problem, i.e. that of a fixed body in the presence of waves.
- **A** and **B** are found by considering the radiation problem for each of the degrees of freedom, i.e. that of a moving body in otherwise still water.

4.1.2 Numerical Implementation

The surface of the body is represented by a mesh of n rectangular and triangular facets. Under the approximation of a constant source density over each facet, the continuous source distribution is replaced by n discrete point sources at the centre of each facet. The mathematical condition on the body surface then reduces to an $n \times n$ matrix equation for the source strengths.

The number of facets and their distribution must be chosen to ensure convergence to the required accuracy. Near corners, or regions of high curvature, a finer mesh must be used to resolve the fluid flow adequately.

For bodies with one (or two) planes of symmetry only half (or a quarter) of the number of facets need be defined. Symmetry reduces the computation time considerably (by a factor of 64 for a body with two planes of symmetry).

For simple smooth geometries, such as a sphere, convergence to within a few percent may be expected with relatively few facets. Figure 1 shows convergence to the added mass and damping coefficients obtained by Havelock [1] for a heaving hemisphere. It is seen that the solution has converged to within a few percent for the 256 case.

The computational time increases with n^2 for up to 300 facets, beyond which an n^3 relationship emerges. Each frequency of the 256 facet case in figure 1 required 10 mins CPU time on a 15 MIP I486 processor. Computations may be conducted for multiple wave angles without significantly increasing the CPU time.

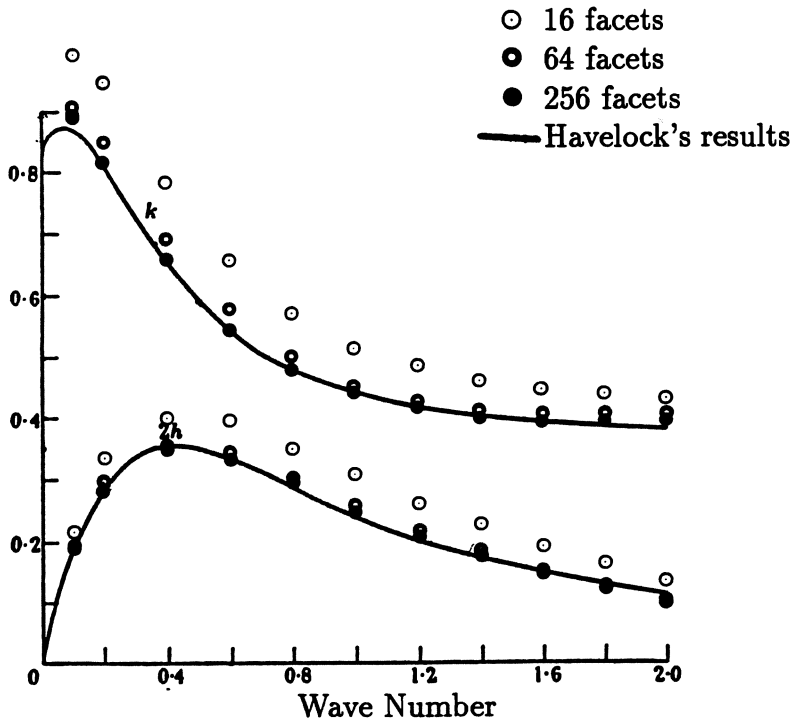

Figure 1: Convergence of numerical solution for the case of a hemisphere of unit radius. k and 2h are added mass and damping coefficients respectively.

5 Comparison with Experimental Study

A 3-D experimental study on the performance of a solo duck was compleated by Skyner [2] in 1987. In this section comparisons are made with his experimental results.

5.1 Outline of Skyner's Study

5.1.1 Description of experiments

Using a rig originally designed for 2-D narrow tank testing Skyner performed 3-D pitch-heave-surge experiments in the linear regime.

Experiments were performed to find the excitation force, $\mathbf{X}$, and the complex impedance matrix, $\mathbf{Z}$ which were then used to make power absorption predictions.

These predictions were then compared with results obtained from power absorption experiments with the ducks motion being governed by a synthesised linear controller, implemented on a digital computer.

5.1.2 Skyner's key findings

Some inconsistencies were apparent in the measured damping when different experimental methods were employed, especially at low frequencies.

In regular waves, relative capture widths of 1.6 were achievable when the wavelength was about 15 duck diameters.

For longer wavelengths the efficiency is reduced and does not attain the small device limit.

Using impedances obtained from force and velocity measurements, Skyner's synthesised efficiencies can be predicted within the limits of tank repeatability.

5.2 Numerical Evaluation of Hydrodynamic Forces

A geometry generating routine was written to produce the facet data required in the numerical solution. Only half the geometry is generated since the program exploits symmetry to speed up the calculation. To compute 7 frequencies requires 2 hours for a 320 facet representation and 10 hours for 720 facets.

A comparison of the results using these two representations indicates that the 320 facet solution has converged to within about a 3 % error.

5.3 Comparison With Experimental Forces and Impedances

5.3.1 Excitation forces

The excitation forces are the forces on a fixed duck in the presence of an incident wave.

Figures 2 and 3 shows Skyner's experimental results compared with the 320 facet numerical model. In general the agreement is excellent. The discrepances which occur are largest in the 90° case. This is thought to be due to the vertical flat mounting struts. These are transparent to 0° and 180° incident waves, but interact with oblique incident waves.

5.3.2 Impedance matrix

Each term in the impedance matrix gives the force in one mode due to a displacement in another mode in otherwise still water.

In figure 4 the numerical results are compared with Skyner's. In general the comparison is good but there are discrepances which again may be due to effect of the struts. Energy conservation studies by Nebel [9] using the same rig have recently shown that there are losses which are at present unaccounted for. These could be due to real phenomena associated with the fluid flow, or else there may be a problem with the rig.

Figure 5 shows the damping obtained by Skyner using two different experimental methods. It is seen that there is a discrepancy between the two methods at low frequencies. The numerical results agree with the damping obtained from measuring the radiated wave field, rather than with the direct method of measuring forces and velocities.

5.4 Numerical Evaluation of Efficiency

The computed forces and impedances were used to predict the maximum efficiency of the duck under the optimal complex conjugate control.

At first the solution was found to be erratic and produced nonsensical results. After searching for errors in the software it was discovered that the damping matrix (i.e. the real part of the impedance matrix) displayed a variety of singularities. These were unexpected and have important numerical and physical consequences.

The physical meaning of a singularity in the damping matrix is the existence of a combination of motions which has zero damping. Such a combination of motions, called a 'wave-free mode', results in no waves being radiated from the duck. Using the relation between damping and excitation force (2) this also implies a zero excitation force of the wave free mode.

Close to the singularity, the damping in the wave free mode will be small, as will the excitation force. Recalling the expression for power absorption in section 2:

$$P = \frac{1}{8}\mathbf{X}^*\mathbf{B}^{-1}\mathbf{X} \qquad \text{where} \qquad \mathbf{U} = \frac{1}{2}\mathbf{B}^{-1}\mathbf{X}$$

and using the relation (2), it may be shown that whilst $\mathbf{B}^{-1}$ becomes large in the singular mode, $\mathbf{X}$ becomes small in a manner that results in P remaining constant. However, the velocity $\mathbf{U}$ required for optimal absorption becomes large, and the assumptions of linearity are invalidated. This implies that near a singularity in the damping matrix the optimal power absorption is not achievable.

The numerical difficulties associated with the singular damping matrix were overcome by evaluating the damping using (2). This ensures that rounding inaccuracies in $\mathbf{X}$ and $\mathbf{B}$ are consistant with the damping relation and so are not amplified by the singularity when the power is evaluated.

5.5 Comparison with Experimental Efficiencies

Figure 6 shows comparison between Skyner's experimental efficiencies for the pitch-heave-surge system and the pitch-only system. In general the experimental efficiencies are smaller than the numerical predictions. This is to be expected because the singular nature of the damping matrix leads to an inaccurate synthesis of complex conjugate control. For the single deree of freedom case we would expect better agreement at frequencies above 1 Hz. The low experimental values are thought to be due to an unidentified loss of energy.

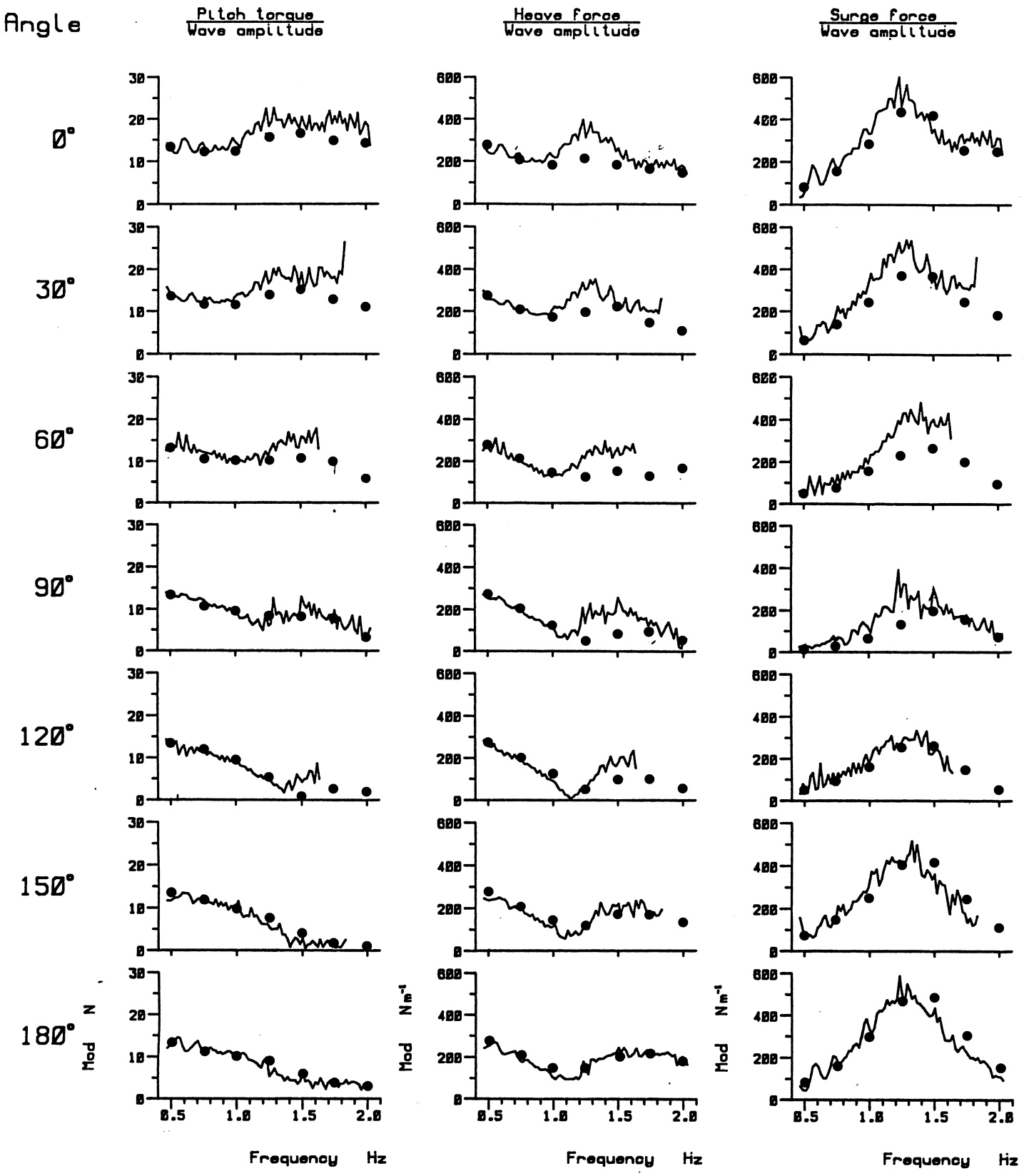

Figure 2: Excitation forces on the duck, amplitude. — experimental results, • numerical results

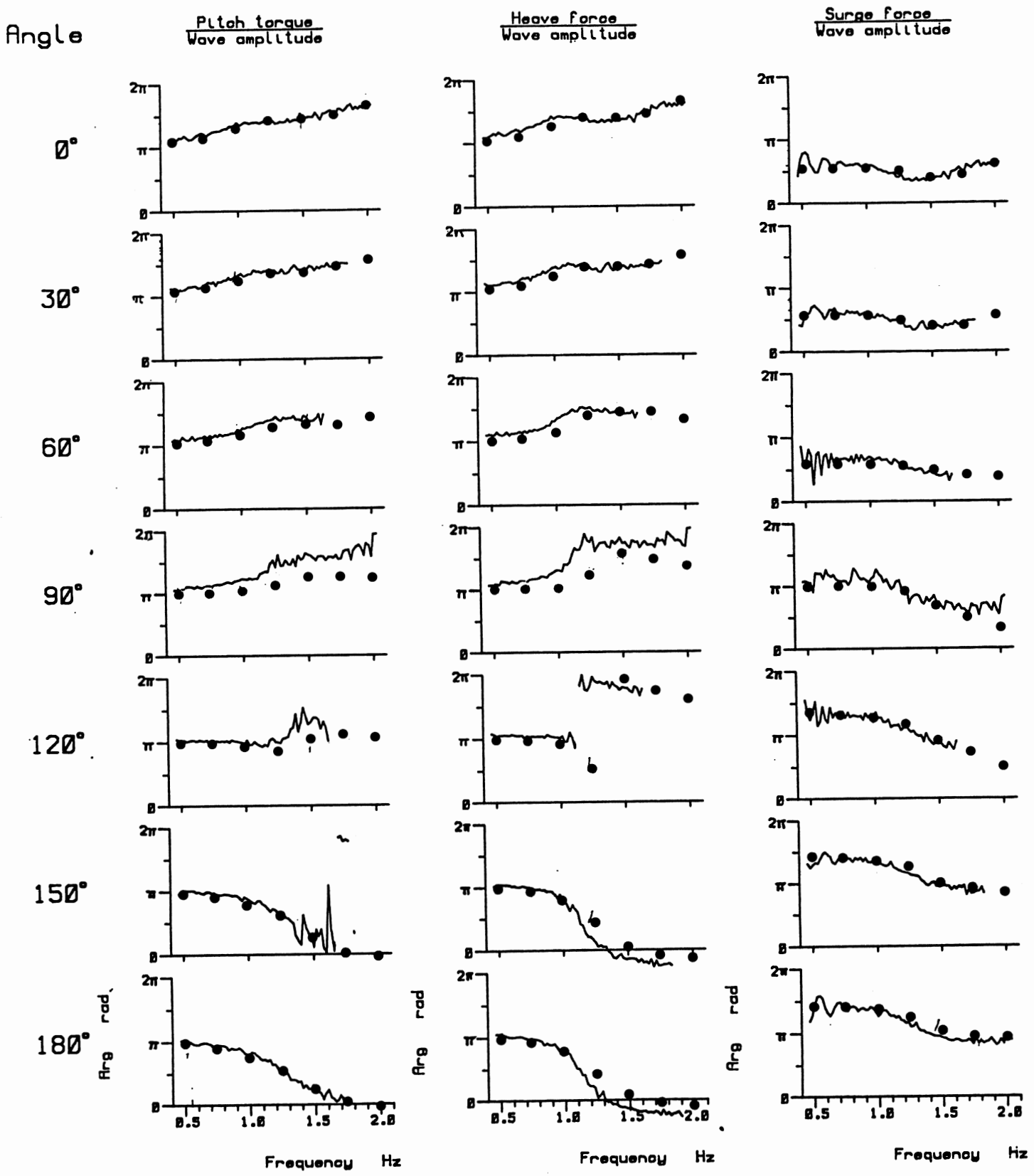

Figure 3: Excitation forces on the duck, phase. — experimental results, • numerical results

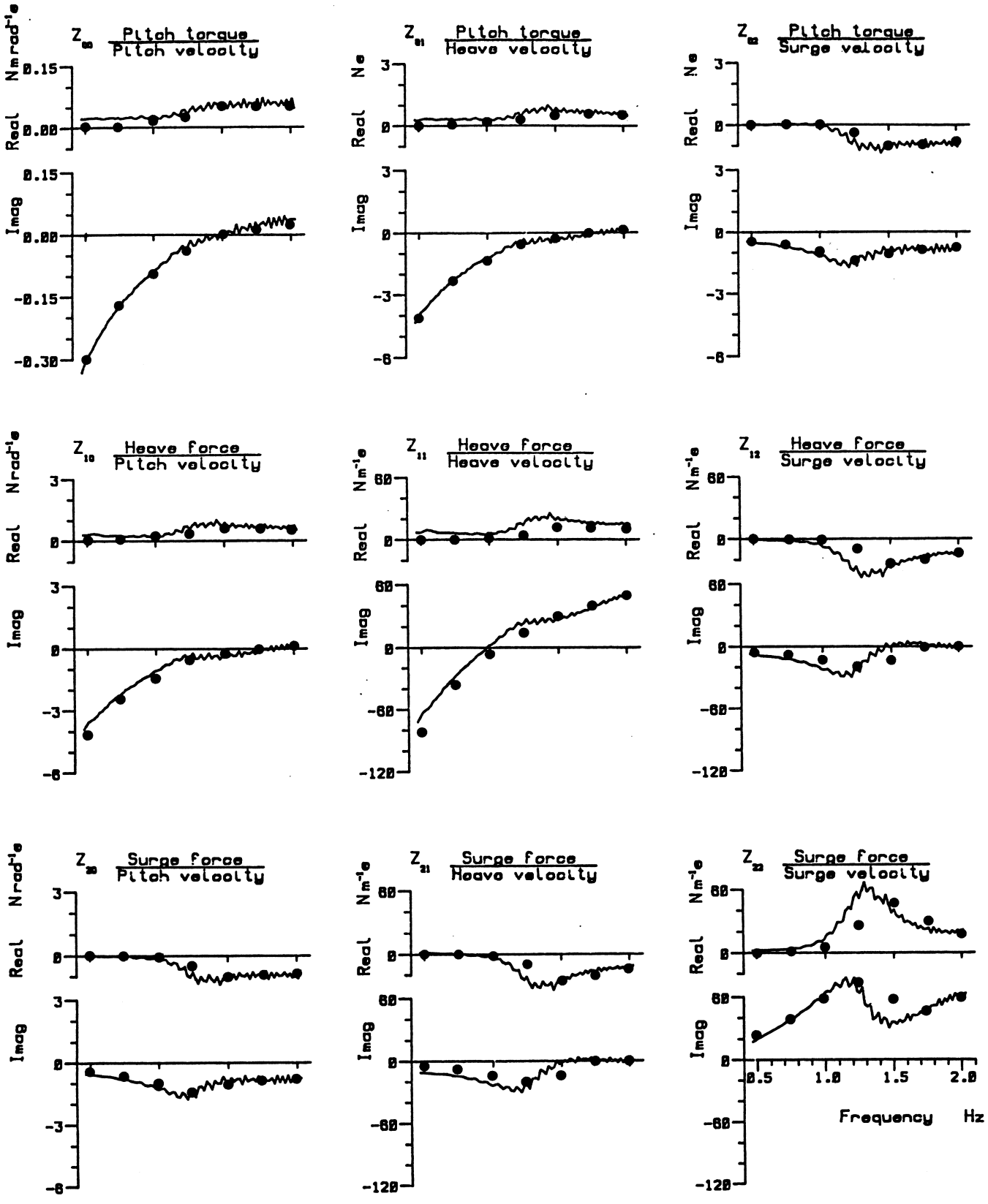

Figure 4: Complex impedance matrix of the duck. — experimental results, • numerical results

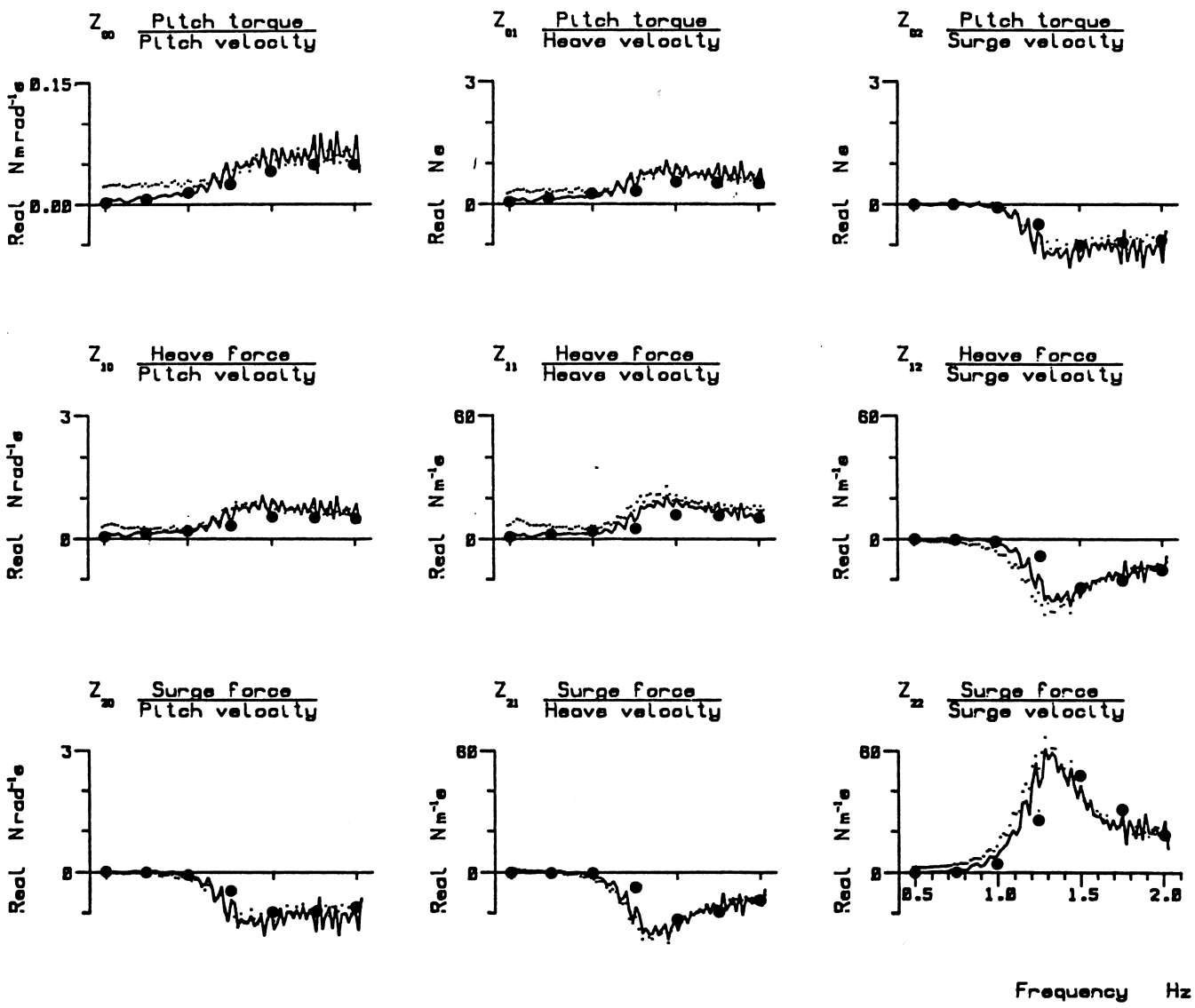

Figure 5: Damping matrix of the duck. $\cdots$ from experimental forces and velocities, — from experimental radiated waves, • numerical results.

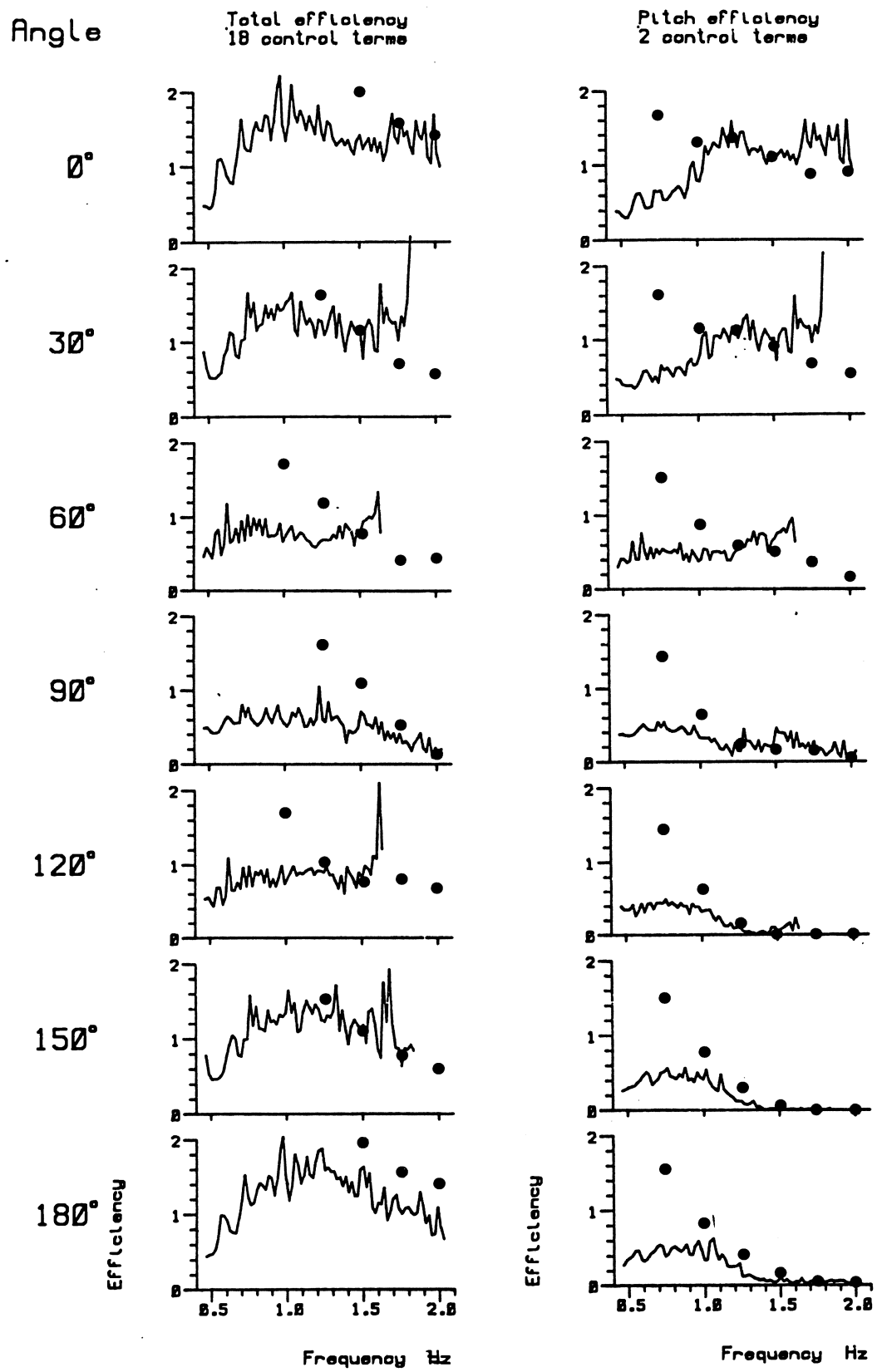

Figure 6: Efficiency of the duck. — experimental results, • numerical results.

6 Power Absorption Under Motion Constraints

At first sight, the large relative capture widths predicted by the point absorber theory in section 3, and the numerical calculations presented in section 5, indicate that a solo duck is likely to be many times more efficient than its spine based counterpart. However for realistic wave amplitudes the limitations of linear theory are soon reached since large displacements of the body are required in order to attain these maximum efficiencies. This is particularly apparent in multi-degree of freedom systems, in which a near-singular damping matrix results in large motions for very small incident waves.

Consideration of the maximum power absorption under a suitable motion constraint will ensure that the linear theory remains valid. In this context, relative capture widths significantly greater than one are worth serious investigation.

6.1 Theory of Constraints

Evans [8] presents expressions for the maximum power absorption of a multi-degree of freedom system under a *global* motion constraint on the velocities. He presents analytical results for the simple cases of a half immersed sphere in heave, and a circular cylinder in heave and surge.

For application to the duck, Evans' constraint is generalised to allow for different weightings for each degree of freedom. Here the constraint on the velocity, **U**, for an n-degree of freedom system is of the form:

$$\sum_{i=1}^{n} \frac{U_i}{\beta_i} \leq 1$$

.

In the case of heave, surge and sway this constraint confines the body velocity to an ellipsoid with semi-principal axes given by β_i $i = 1, 2, 3$. This implies that each component of the velocity, U_i, is always less than β_i.

Expressions for maximum power absorption are re-derived with the weighted constraint. The maximum power is determined by the introduction of a *lagrange multiplier*, μ, which may be found numerically from a matrix equation.

6.2 Modification to the Control Matrix

As described in section 3, the control matrix gives the damping inertia and spring which must be applied to the body in order to make it move with the optimal velocity. Forming the equations of motion with the optimal velocity gives the control matrix :

$$\mathbf{C} = \mathbf{Z}^* + \mathbf{C}_a$$

where $\mathbf{C}_a$ is the *added control*, and takes the diagonal form:

$$\mathbf{C}_a = \begin{pmatrix} C_{11} & & 0 \\ & \ddots & \\ 0 & & C_{nn} \end{pmatrix}$$

If maximum power absorption is possible without the velocities reaching their global limit, $\mathbf{C}_a = \mathbf{0}$ and complex conjugate control is achieved. Otherwise $\mathbf{C}_a \neq \mathbf{0}$ and it represents the modification to complex conjugate control required in order to limit the velocities.

6.3 Comparison with Analytical Results

For the simple case of a heaving sphere Evans [8] presents an analytical solution for the maximum absorption under a motion constraint. His solution requires knowledge of the damping, for which he uses Havelock's results [1]. Evans presents graphs of efficiency for different constraints on the amplitude ratio of the body motion, α, with respect to the incident wave amplitude, A. His constraint is therefore of the form: $\beta_1 = \omega A \alpha$. Comparison with efficiencies obtained with the presented numerical method are shown in figure 7.

6.4 Linearity Constraint

For the remainder of this report we consider a fixed constraint on the amplitude of the displacement in terms of the body dimensions, i.e. $\beta_1 = \omega\gamma$. Graphs are then given for different values of the incident wave amplitude. Since large amplitude ratios do not invalidate the linearity assumption if the incident wave amplitude is small, this way of presenting the results gives a clearer indication of how the restriction to the linear regime effects power absorption.

6.5 Heaving and Surging Sphere

6.5.1 Single degree of freedom

Considering again the case of a heaving sphere, the amplitude constraint applied is that the displacement of the sphere must be less than a quarter of its radius. Hence, for the

unit sphere $\gamma = 0.25$.

Figure 8 gives the displacements and efficiencies for single degree of freedom cases of heave and surge. It is seen that when the displacements reach their maximum, the efficiencies fall away from the point absorber results, see section 3.2.4. At low frequencies the damping in surge is considerably smaller than in heave since a surge motion displaces no net volume. This means that surge requires larger displacements to achieve maximum efficiency. Thus, although the point absorber efficiency for surge is double that of heave, with an amplitude constraint, heave is better at absorbing power in long waves.

6.5.2 Two degrees of freedom

The numerical procedure evaluates the optimal combination of heave and surge to yield the maximum power within the linearity constraint, see figure 9. At high frequencies and small wave amplitudes the point-absorber efficiencies are obtained since the displacements are within their constraint. At low frequencies, where heave is better than surge at absorbing power, the surge displacement becomes very small the heave-only efficiency is attained. At intermediate frequencies and wave amplitudes, a varying combination of heave and surge give larger efficiencies with broader bandwidths than the single degree of freedom cases.

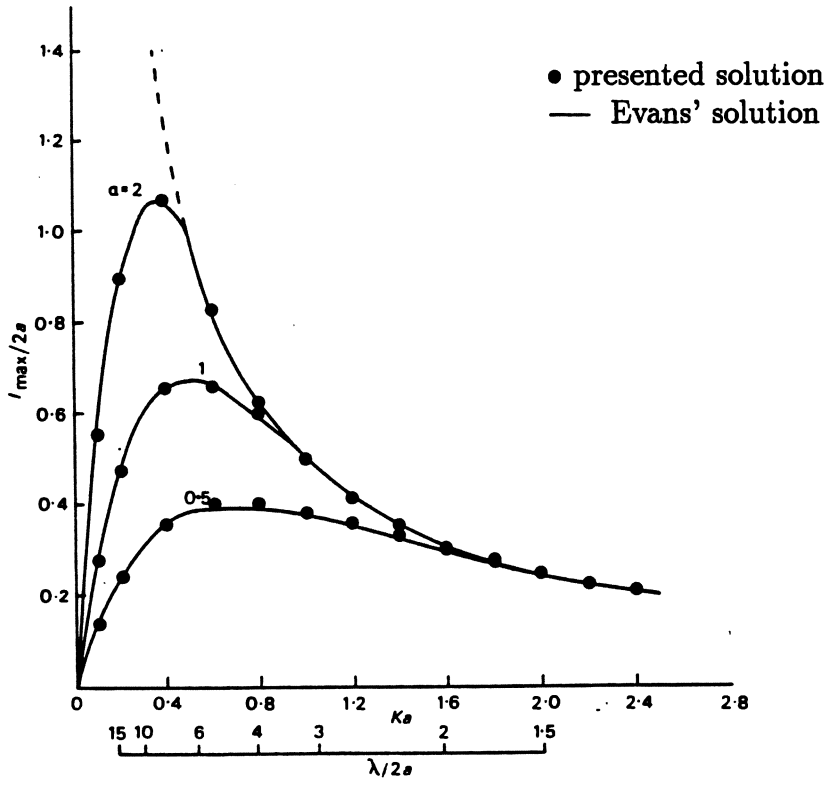

Figure 7: Efficiency of a heaving sphere with motion constraints. Comparison with Evans.

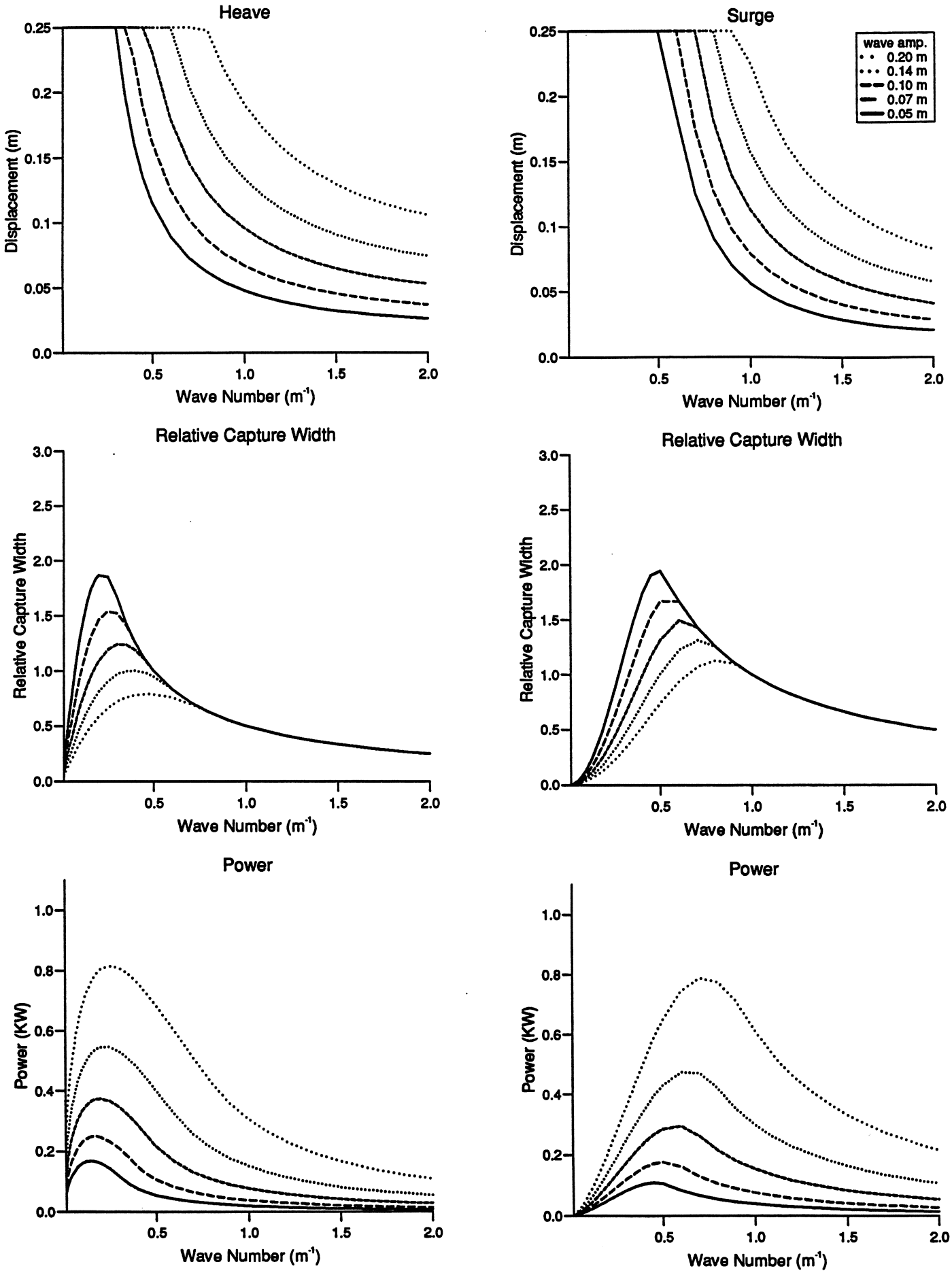

Figure 8: Velocity and efficiency of sphere in a single degrees of freedom with motion constraints. First column of graphs is for heave and the second is for surge.

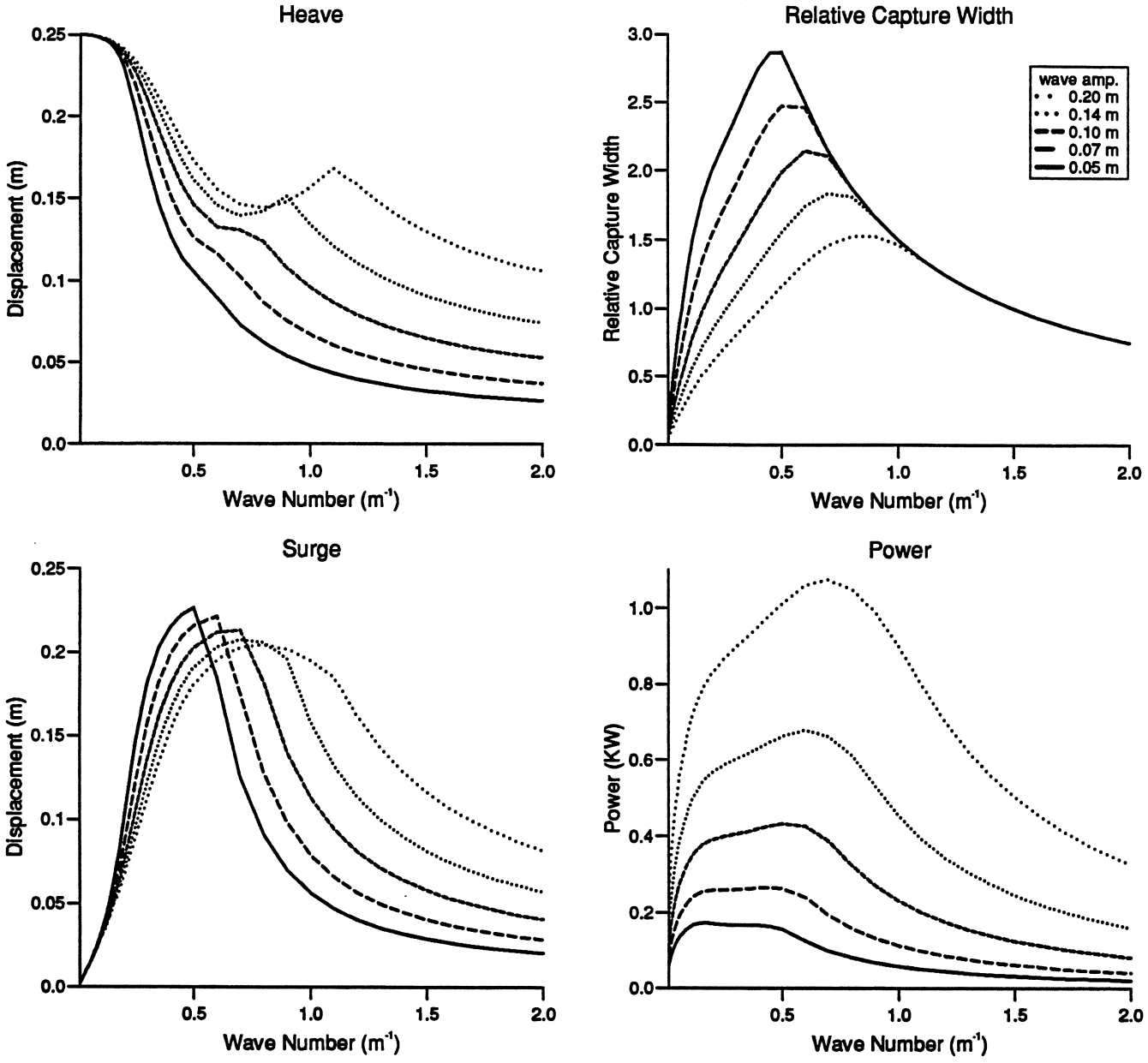

Figure 9: Velocity and efficiency of a heaving and surging sphere with motion constraints

7 Application to a Solo Duck

In this section the methods described above are applied to a solo duck in order to assess its performance. Graphs of displacements, forces, power absorbed and efficiencies are presented for a variety of power absorption configurations.

The practicality of utilising the point absorber effect (see section 3) is investigated by imposing a motion constraint (see section 6), and thus ensuring that the assumptions of linear theory are not invalidated.

7.1 Description of the duck

7.1.1 Geometry

The duck studied here is the same as that used by Skyner [2] in his 100^{th} scale experimental study. Its principal dimensions are given in figure 10 and in the table below.

Diameter	10.0	m
Beak length	8.0	m
Water level	5.5	m
Beak angle	36.0	deg
Width	29.0	m
Displacement	3500.0	m^3
Mass	1396.0	tonnes

In this study the duck is assumed to be in a water depth of 60 meters.

The linearity motion constraint is as described in section 6, with $\gamma_i = : 2.5$ metres for the translational motions; 0.5 radians for pitch; and 0.2 radians for roll and yaw. An experimental study on the onset of non-linearity is needed to justify or possibly relax this choice.

7.1.2 Power absorption configurations

The duck is a buoyant body, its mass being about 0.4 times its displacement. It is held in position by tension moorings and/or power absorbing legs. The mooring configuration is as-of-yet undetermined and several possibilities are investigated. In each case the duck is free to move (and absorb power) only in the prescribed degrees of freedom, and is assumed to be fixed in other directions. However, the duck may be free to move in the other, non-absorbing, degrees of freedom, and further study is required to investigate the effect of these motions on efficiency.

First, absorption in head-on waves is considered for combinations of the fore, aft and pitch degrees of freedom. Absorption in oblique waves is then investigated for three and six degrees of freedom configurations.

7.2 Power Absorption in Head-On Waves

The symmetry of power absorption in head-on waves simplifies the system to three degrees of freedom. The conventional pitch-heave-surge system is transformed into the pitch-fore-aft system. In figure 11 graphs of the displacements, efficiencies and power absorbed are given for various wave amplitudes. The control force and added control terms are given in figure 12 and the control matrix is given in figure 13. It is seen that the added control terms are of the same order of magnitude as would be used in unconstrained complex-conjugate control. The engineering demands are not greatly different.

In figures 14, 15 and 16 displacements efficiencies and power absorbed are given for each of the two degree of freedom systems. It is seen that the removal of a degree of freedom reduces power absorption only by about 10 %.

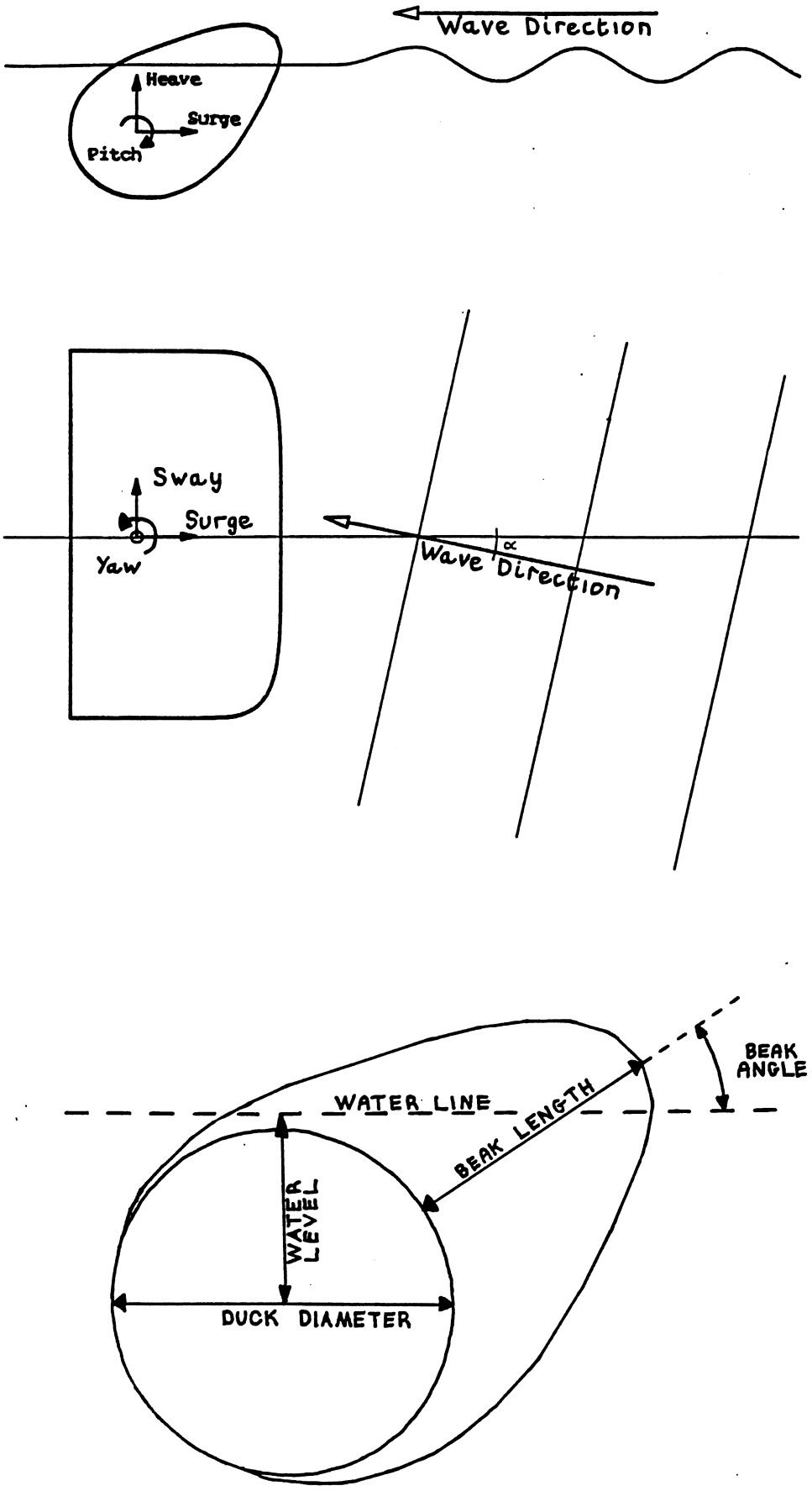

Figure 10: The solo duck geometry.

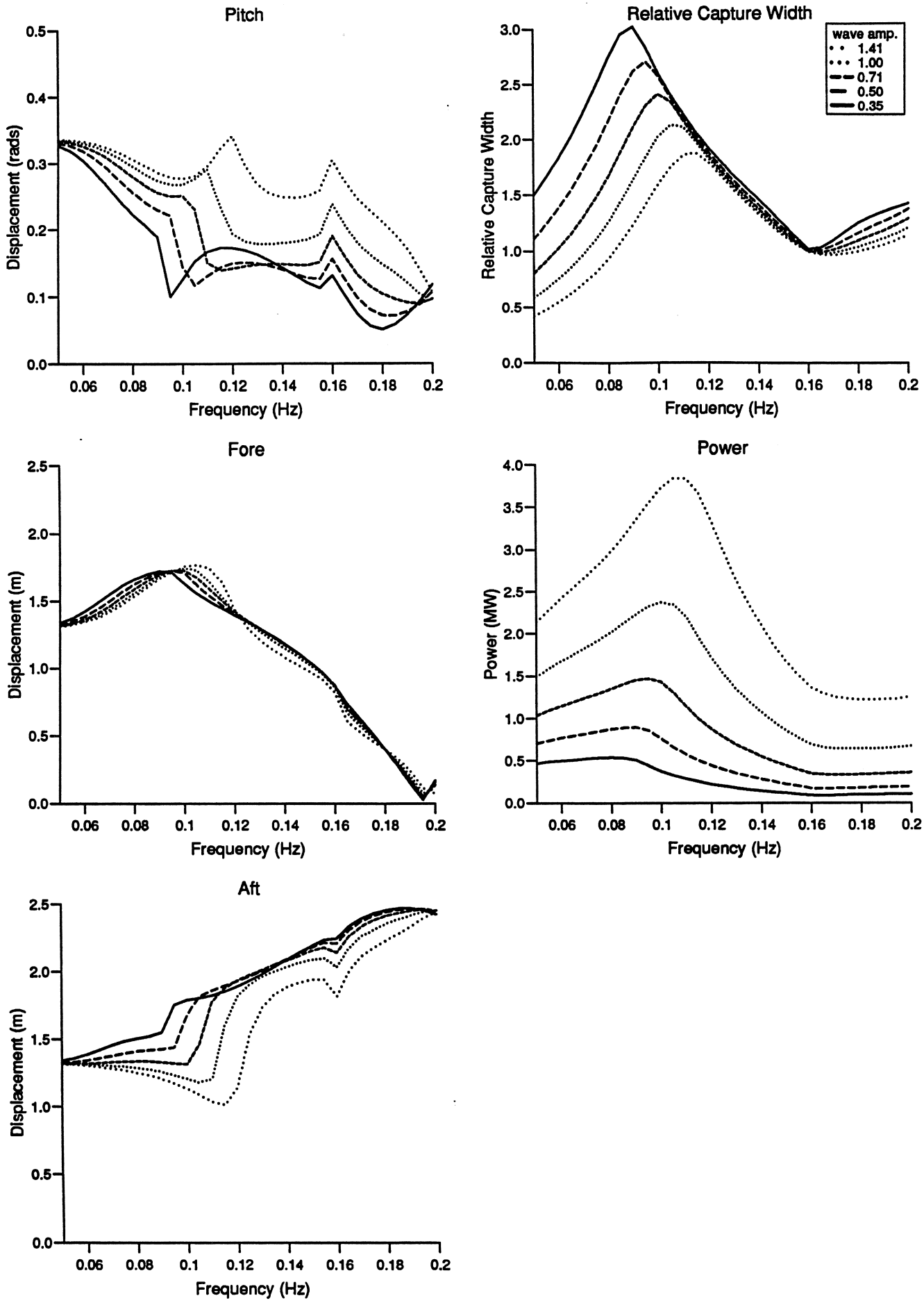

Figure 11: Displacements, efficiency and power absorption in head-on waves. Pitch, fore and aft system

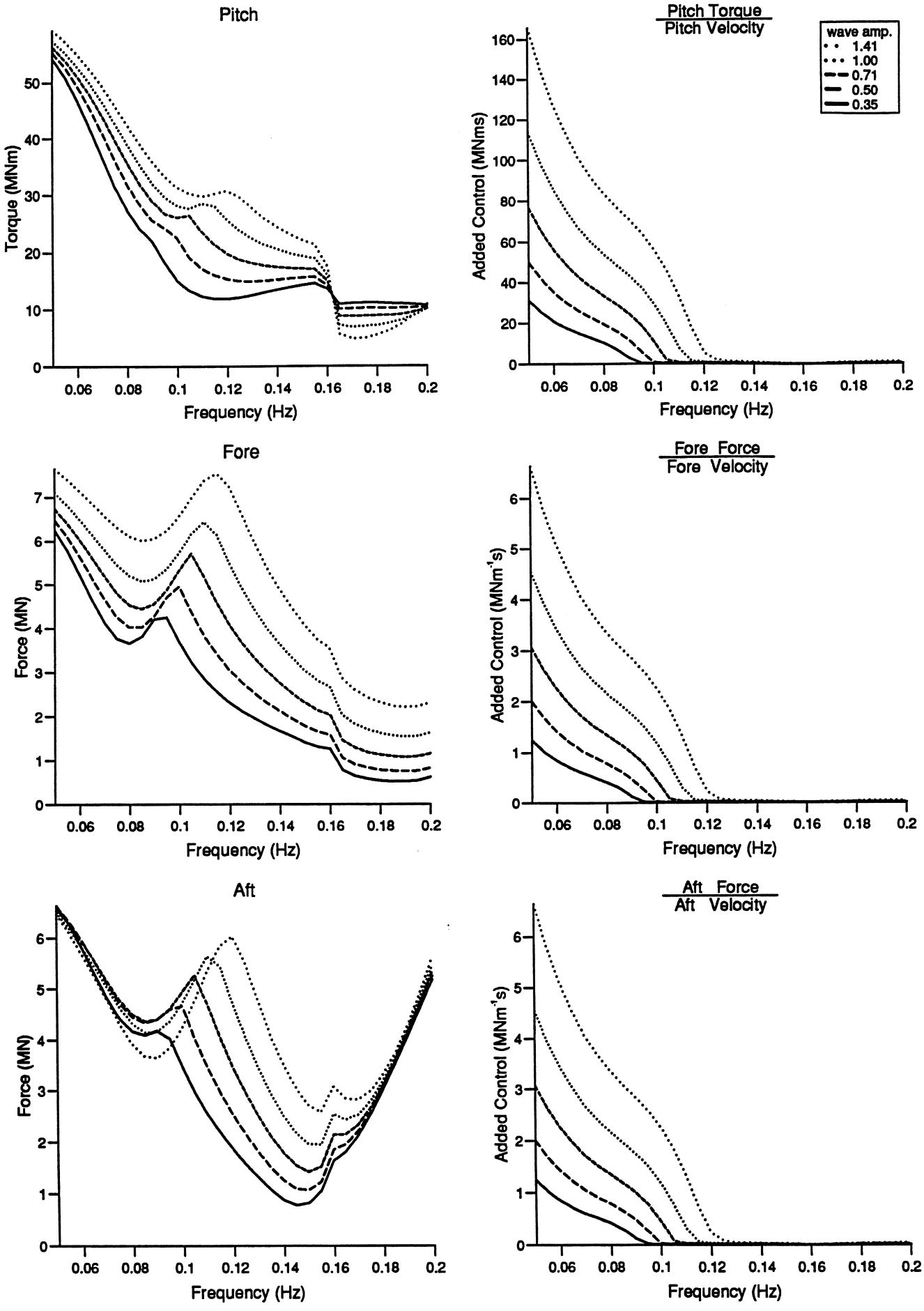

Figure 12: Control force and added control terms in head-on waves. Pitch, fore and aft system

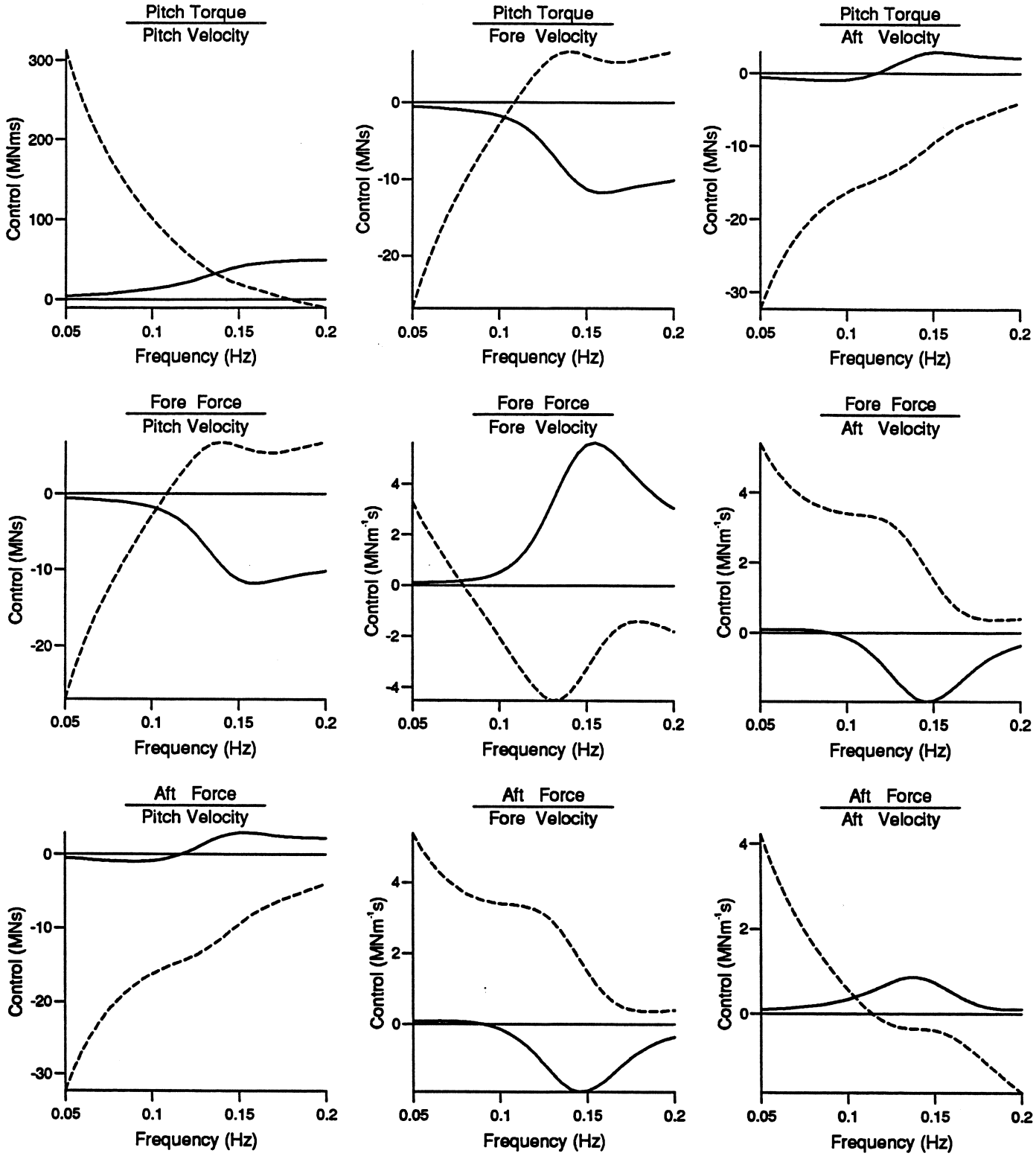

Figure 13: Control matrix, Pitch, fore and aft system. — real part,····· imaginary part

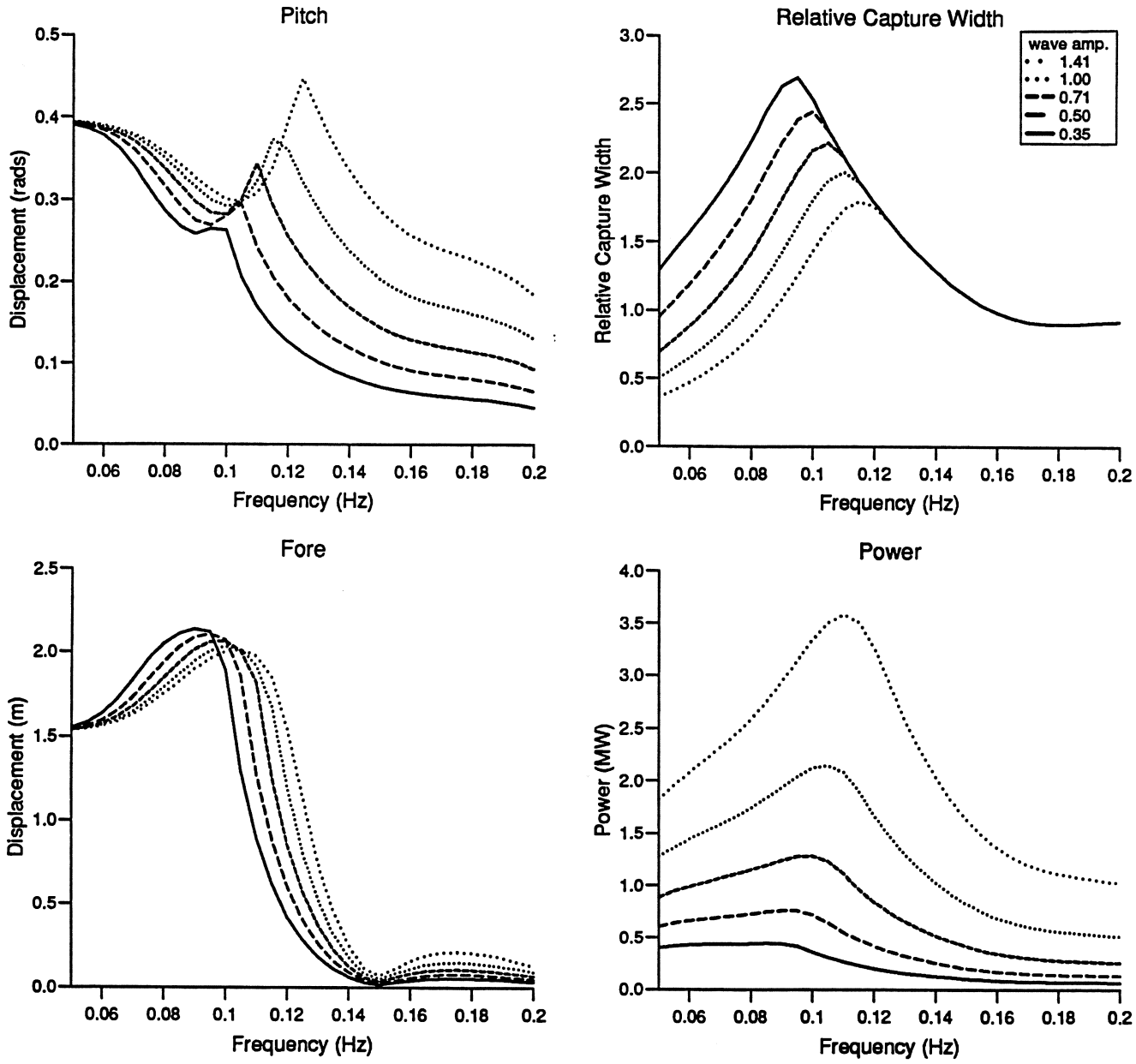

Figure 14: Displacements, efficiency and power absorption in head-on waves. Pitch and fore system

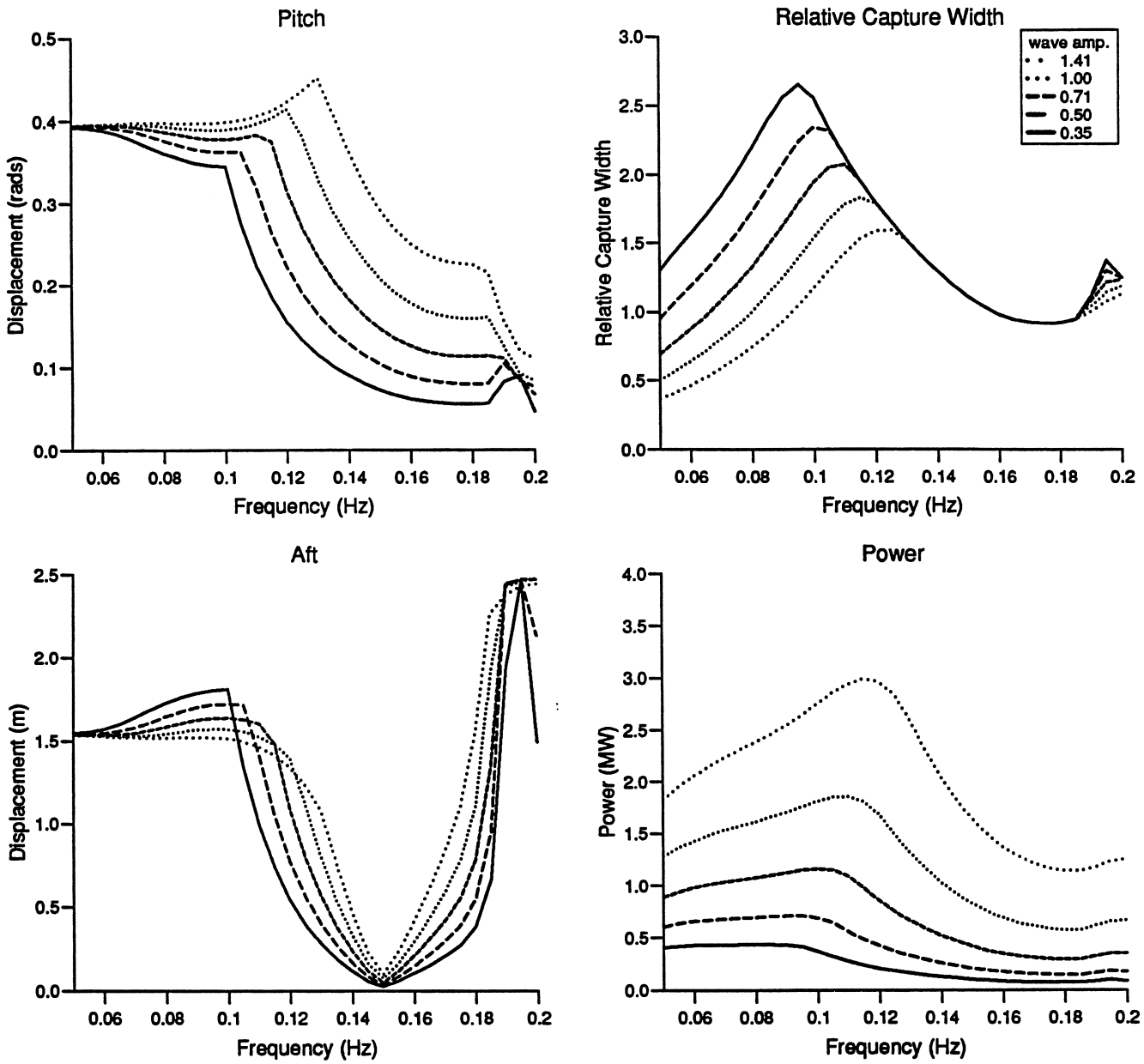

Figure 15: Displacements, efficiency and power absorption in head-on waves. Pitch and aft system

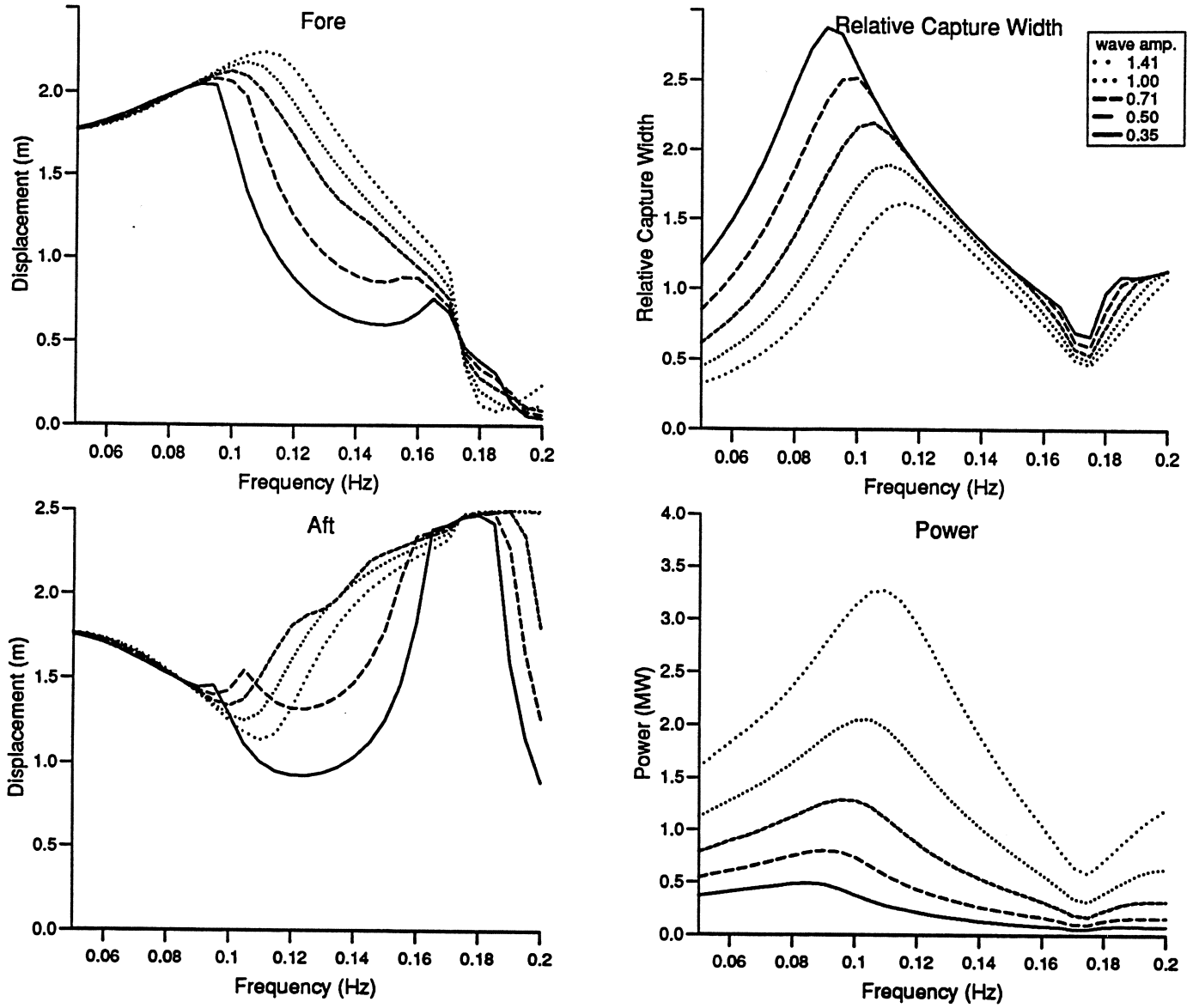

Figure 16: Displacements, efficiency and power absorption in head-on waves. Fore and aft system

7.3 Power Absorption in Oblique Waves

In figure 17 efficiency and power absorption in oblique waves is given for the pitch-fore-aft system. At low frequencies the efficiency is fairly independent on wave angle, but is halved in oblique waves for higher frequencies.

Efficiency and power absorption for the six degrees of freedom case is given in figure 18. Because of the symmetry, for head-on waves no extra power is absorbed due to the extra three degrees of freedom. At low frequencies the efficiency is again fairly independent of wave angle. However the six degree of freedom system attains higher efficiencies for short oblique waves than for short head-on waves. This is a surprising result and suggests that the solo duck may perform better if placed at an angle to the prominent wave direction. Another interpretation of this result is that the present geometry of the solo duck makes it a poor point absorber in head waves — perhaps because it is unable to utilise all three degrees of freedom due to the existence of a wave-free mode (see section 5).

It may not be necessary to have all six degrees of freedom to achieve these high efficiencies in oblique waves. As we have seen in the head-on wave case, suppressing a degree of freedom need not significantly reduce the efficiency. Further study is required optimise the solo duck geometry and power absorption configuration.

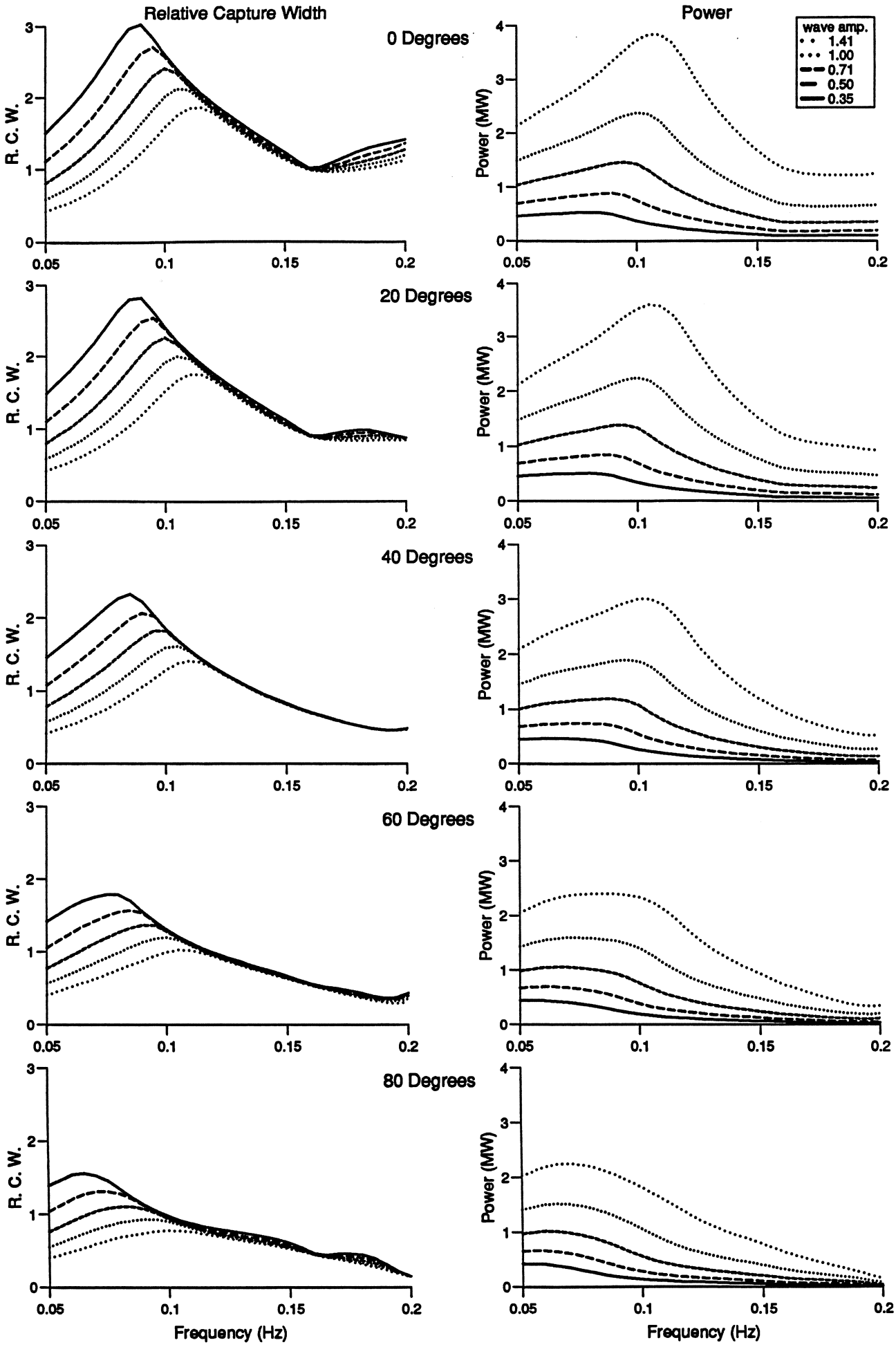

Figure 17: Efficiency and power absorption in oblique waves. Pitch-fore-aft system

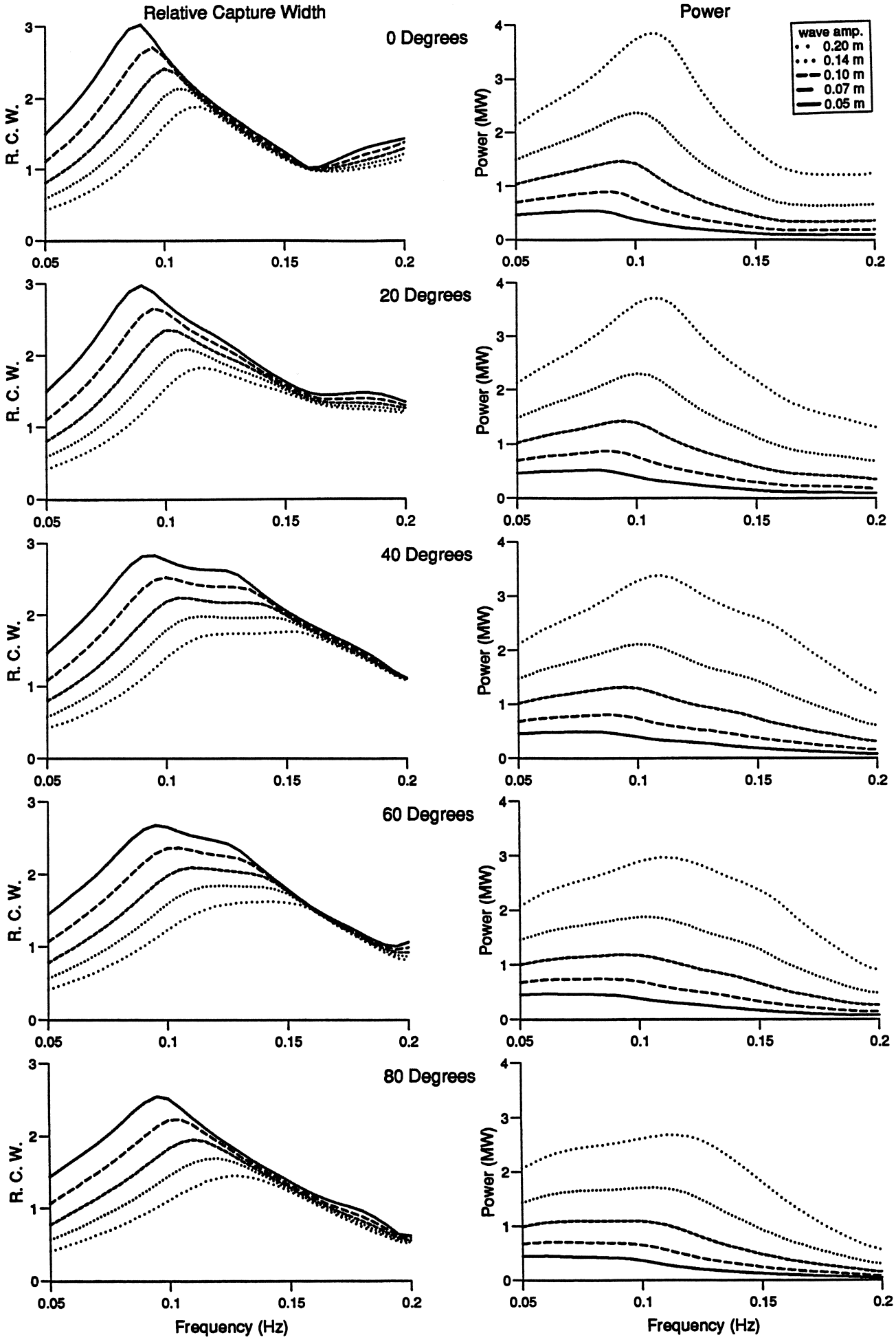

Figure 18: Efficiency and power absorption in oblique waves. six degree of freedom system

8 Recommendations for Further Study

1. Further experimental studies should be performed to investigate:
   (a) the non-linear effects at various larger wave amplitudes;
   (b) power absorption with amplitude constraints using the modified complex conjugate control with real-time digital control.
   (c) the suspected power losses in the rig used by Skyner and Nebel.
2. The current formulation permits any number of degrees of freedom, all of which may absorb power. A new formulation is required in order to permit non-absorbing degrees of freedom, and to investigate their effect on efficiency for various configurations.
3. Statistical predictions using realistic sea spectra are required in order to obtain accurate estimates of power output.
4. The current geometry of the solo duck is inherited from the spine based system. Further study is required in order to understand the three-dimensional effects and to obtain the optimal geometry.
5. The prediction of the performance of an array of ducks requires knowledge of the hydrodynamic interaction between ducks. The optimal spacings and geometries need to be investigated.

References

[1] Havelock, T. H. 'Waves due to a floating sphere making periodic heaving oscillations', Proc. R. Soc., 1955, (A), **231**, 1.

[2] Skyner, D. 'Solo duck linear analysis', Edinburgh Wave Power Project, University of Edinburgh, Department of Mechanical Engineering, 1987.

[3] Evans, D. V. 'A theory for wave-power absorption by oscillating bodies, J. Fluid Mech., 1976, **77**, 1

[4] Mei, C. C. 'Power extraction from water waves', J. Ship. Res., 1976, **20**, 63

[5] Newman, J. N. 'The interaction of stationary vessels with regular waves', Proc. 11th Symp. Naval Hydrodynamics, London, 1976, p 491.

[6] Ursell, F. 'On the heaving motion of a circular cylinder on the surface of a fluid', Quart. Journ. Mech. and Applied Math., **II**, Pt.2, 1949

[7] Garrison, C. J. and Chow, P. Y.,'Wave forces on submerged bodies', J. of Waterways, Harbors and Coastal Eng. Div., Proc. of A.S.C.E, August, 1972.

[8] Evans, D. V. 'Maximum wave-power absorption under motion constraints', Applied Ocean Research, 1981 **3** No. 4, 200.

[9] Nebel, P. 'Optimal control of a duck', Edinburgh Wave Power Project, University of Edinburgh, Department of Mechanical Engineering, 1992.